

**Non-equilibrium universality:  
slow drives, measurements  
and dephasing**

**Dissertation**  
**Björn Ladewig**  
**Köln 2023**

**Non-equilibrium universality:  
slow drives, measurements and  
dephasing**

Inaugural-Dissertation  
zur  
Erlangung des Doktorgrades  
der Mathematisch-Naturwissenschaftlichen  
Fakultät  
der Universität zu Köln  
vorgelegt von

Björn Ladewig  
aus Göttingen

Köln  
2023

Berichterstatter:  
(Gutachter)

Prof. Dr. Sebastian Diehl  
Prof. Dr. Achim Rosch

Tag der mündlichen Prüfung: 13.02.2023

Dissertation durch die Mathematisch-Naturwissenschaftliche Fakultät der Universität zu Köln 2023 angenommen.

**Abstract:**

The behavior of quantum mechanical systems can be influenced by factors ranging from ground state physics and unitary evolution to measurements or decoherence due to the coupling to a bath. For large composite quantum systems, these mechanisms can give rise to collective phenomena like phases, phase transitions and universality. One example are quantum phase transitions (at zero temperature) in the *ground states* of a Hamiltonian  $\mathbf{H}$ . Close to the phase transition, where the energy gap closes, scale invariant behavior emerges. It is characterized by a set of universal critical exponents and the leading scaling behavior is determined by only a few relevant parameters. Complementarily, many of the microscopic details are *irrelevant* for the physics at large distances - the origin of universality.

If the system is *driven* in the vicinity of the phase transition, the additional drive scale can lead to a breakdown of the equilibrium scaling behavior. The state gets excited away from the ground state - adiabaticity is broken. Nevertheless, the breakdown inherits universal properties: Driving the gap parameter gives access to the leading critical exponents (Kibble-Zurek mechanism). However, the *whole hierarchy* of critical exponents, relevant and irrelevant, is accessible by a slow drive. We establish this generalized mechanism and its observable consequences at the level of elementary, but experimentally relevant, spin and fermion models. In particular, we construct drives that turn equilibrium irrelevant couplings into *relevant* drive couplings with an observable scaling in the excitation density.

Criticality and universality also arise from the competition of unitary evolution and measurements. Entangling unitary dynamics can compete with local measurements, such that the stochastic evolution of pure states can undergo a measurement-induced (entanglement) transition. An example are (free) fermion models featuring a transition between an extended ‘critical’ phase and a ‘pinned’, weakly entangled phase. However, the inevitable coupling to an environment can result in mixed and dephased states. We investigate the role of this third mechanism of dephasing (or imperfect measurements) onto the aforementioned transition. For this we use (i) numerical approaches based on stochastic quantum trajectories, (ii) an effective bosonic replica field theory, paired with a renormalization group treatment and (iii) a perturbative treatment of the fermion dynamics. On the one hand, weak dephasing leaves the ‘critical’ phase and measurement-induced transition in tact. On the other hand, we observe the emergence of a new, temperature-like scale for strong dephasing and weak measurements, enabled by the interplay of all three mechanisms. Despite the presence of the finite scale, observables like density-dependent correlations still feature scale invariant behavior. Paired with a perturbative treatment for strong dephasing, this behavior hints at a diffusion-like dynamics on the diagonal of the density matrix in the occupation number basis.

**Zusammenfassung:**

Das Verhalten quantenmechanischer Systeme kann durch verschiedene Faktoren wie der Grundzustandsphysik, unitärer Entwicklung bis hin zu Messungen oder Dekohärenz durch die Kopplung an die Umwelt beeinflusst werden. Für ausgedehnte Quantensysteme können diese Mechanismen zu kollektivem Verhalten in Form von Phasen, Phasenübergängen und Universalität führen. Ein Beispiel sind Quantenphasenübergänge (bei verschwindender Temperatur) im Grundzustand von einem Hamiltonian  $H$ . In the Nähe des Phasenübergangs, angezeigt durch die sich schließende Energielücke, tritt skaleninvarianten Verhalten auf. Dieses Verhalten ist durch universelle kritische Exponenten charakterisiert, wobei das führende Skalenverhalten durch nur wenige Parameter bestimmt wird. Hingegen sind viele mikroskopische Details *irrelevant* für das Verhalten auf großen Skalen - die Ursache der Universalität.

Wenn das System getrieben wird, kann die zusätzliche Treibskala zur Einschränkung des skaleninvarianten Verhaltens im Gleichgewicht führen. Die Dynamik führt zu Anregungen im System, welches sich somit nicht mehr im Grundzustand befindet - Adiabaticität wird gebrochen. Jedoch trägt diese Dynamik immer noch universelle Informationen: durch das Treiben des Parameters, der die Energielücke kontrolliert, können die führenden kritischen Exponenten bestimmt werden (Kibble-Zurek Mechanismus). Jedoch kann im dynamischen Fall die *gesamte Hierarchie* von kritischen Exponenten, relevant wie irrelevant, bestimmt werden. Wir weisen diesen *verallgemeinerten* Mechanismus und seine beobachtbaren Implikationen für elementare, aber experimentell relevante, Spin Modelle nach. Insbesondere konstruieren wir Protokolle, die es ermöglichen, irrelevante Kopplungen im Gleichgewicht in *relevante* Kopplungen im dynamischen Fall zu übersetzen. Diese führen zu einem nachweisbaren Skalenverhalten in der Dichte von Anregungen.

Kritisches Verhalten und Universalität können auch durch den Wettbewerb von unitärer Dynamik und Messungen ermöglicht werden. Verschränkende unitäre Dynamik kann mit lokalen Messungen konkurrieren, sodass ein messinduzierter Phasenübergang in der stochastischen Entwicklung von reinen Zuständen möglich wird. Ein Beispiel sind (freie) Fermionen, die einen Phasenübergang zwischen einer 'kritischen' Phase und einer 'gepinnten', schwach verschränkten Phase zeigen. Jedoch kann die unausweichliche Kopplung an die Umwelt zu gemischten Zuständen führen. Wir untersuchen die Rolle dieses dritten Mechanismus der Dephasierung (bzw. unvollständiger Messungen) in Bezug auf diesen Phasenübergang. Dazu verwenden wir (i) numerische Methoden, basierend auf stochastischen Quantentrajektorien, (ii) eine effektive, bosonische Replika-Theorie, gepaart mit einer Renormierungsanalyse und (iii) eine Störungsrechnung der fermionischen Dynamik. Für schwaches Dephasieren ist die kritische Phase und der messinduzierte Phasenübergang stabil. Hingegen induziert starkes Dephasieren eine neue, temperaturähnliche Skala, die erst durch das Zusammenspiel aller drei Mechanismen ermöglicht wird. Trotz dieser neuen Skala bleibt skaleninvarianten Verhalten zum Beispiel für dichteabhängige Korrelationen erhalten. Zusammen mit der störungstechnischen Untersuchung deutet dieses Verhalten auf eine effektiv diffusive Dynamik auf der Diagonalen der Dichtematrix (in der Besetzungszahlbasis) hin.

# Contents

<b>1</b>	<b>Introduction</b>	<b>1</b>
<b>2</b>	<b>Minimal Models – From single Qubits to the Ising Model</b>	<b>7</b>
2.1	Minimal Models (1): Single Qubits . . . . .	7
2.1.1	Time dependent Hamiltonian: Landau-Zener Model – An Exercise in Scales . . . . .	7
2.1.2	Coupled Systems: Dephasing of a Qubit coupled to a Bath	10
2.2	Minimal Models (2): Quantum Ising Chain . . . . .	13
2.2.1	Exact Solution – Formal Treatment . . . . .	15
2.2.2	Coarse Graining, Field Theories and Emergence of Universality . . . . .	17
<b>3</b>	<b>Generalized Kibble-Zurek Mechanism in Spin and Fermion Models</b>	<b>27</b>
3.1	Driven transverse XY Chain - Mechanism of Adiabaticity Breaking . . . . .	32
3.1.1	Phenomenological Perspective . . . . .	33
3.1.2	Generalized Mechanism – RG Perspective . . . . .	34
3.1.3	Practical Implementation for Spin Models . . . . .	36
3.1.4	Interlude: Time Evolution of Gaussian States . . . . .	39
3.2	Linear Drive (1): Transverse XY Model and relevant Couplings	41
3.3	Linear Drive (2): Scaling and Crossover Scales in the generalized XY Model . . . . .	44
3.3.1	Key Results – Generalized Drives . . . . .	47
3.3.2	Generalized Drives – Analytical Investigation . . . . .	50
3.3.3	Limiting Case: Purely parallel Drive and Adiabaticity Restoring . . . . .	52
3.4	Generalized Drives in the transverse XY Model . . . . .	55
3.5	Outlook: Generalized Kibble–Zurek Mechanism (KZM), Universal and Non-Universal Aspects . . . . .	63
<b>4</b>	<b>Unitary Evolution, Measurements and Decoherence</b>	<b>69</b>
4.1	Fermion Models and the Role of Entanglement . . . . .	77
4.1.1	Definition of the fermionic hopping Model . . . . .	77
4.1.2	Phenomenology of the fermionic Model: Entanglement and Quasi-Particle Picture . . . . .	82
4.2	Coupling the System to an Environment . . . . .	84

4.3	Fermionic Model (1): Unitary Evolution and Dephasing – Evolution towards the maximally mixed State . . . . .	88
4.4	Measuring the Environment: How Measurements and Dephasing are connected . . . . .	92
4.5	Fermionic Model (2): Unitary Evolution and Measurements – Qualitative Picture of Measurement Dynamics . . . . .	96
4.5.1	Qualitative Identification of Observables . . . . .	96
4.5.2	Limiting Case: Unitary Evolution and Measurements . . . . .	99
4.6	Solving the conditional Master Equation for small Systems – Including Dephasing . . . . .	102
4.7	Analytical Approach: Observables from Replica Approach . . . . .	105
4.7.1	Measurements in the bosonic Theory – Model Definition . . . . .	105
4.7.2	Interlude: Exact Solution of Connected Correlation Functions in case of linear Measurement Operators . . . . .	106
4.7.3	General Construction of the Replica Theory . . . . .	109
4.7.4	Executive Summary – Replica Approach in the bosonic Theory . . . . .	110
4.7.5	Dynamics of Replicas – Part 1: Replica Master Equation . . . . .	112
4.7.6	Symmetries in the Replica Formulation . . . . .	115
4.7.7	Dynamics of Replicas – Part 2: Linear Measurement Operators . . . . .	117
4.7.8	Dynamics of Replicas – Part 3: Non-linear Measurement Operators . . . . .	123
4.8	Correlation Functions and renormalization group (RG) Analysis . . . . .	125
4.8.1	Momentum Shell RG– Part 1: First Order Analysis . . . . .	126
4.8.2	Momentum Shell RG– Part 2: Second Order Analysis . . . . .	129
4.9	Fermionic numerical Investigation: Ensemble of Quantum Trajectories . . . . .	133
4.9.1	Quantum Trajectory Picture in the Presence of a Bath . . . . .	136
4.9.2	Quantum Trajectory Picture in the Presence of imperfect Measurements . . . . .	137
4.10	Outlook: Effective (fermionic) Descriptions . . . . .	138
4.10.1	Dynamics in the dephasing-free Subspace . . . . .	138
4.10.2	Random Unitary Evolution as a Proxy for a Bath . . . . .	140
4.10.3	Effective Dynamics due to additional random unitary Evolution . . . . .	143
4.11	Summary, Limitations and Outlook . . . . .	147
<b>5</b>	<b>Conclusion</b>	<b>151</b>
<b>A</b>	<b>Gaussian States</b>	<b>155</b>
A.1	Jordan-Wigner Transformation . . . . .	158
A.2	Gaussian States in Measurement Scenarios . . . . .	158
A.3	Numerical Parameters . . . . .	162
<b>B</b>	<b>Keldysh Field Theory for a (bosonic) Master Equation</b>	<b>163</b>
<b>C</b>	<b>AIA vs. exact Results, Fitting and adiabatic non-perturbative Contributions</b>	<b>165</b>

---

<b>D</b>	<b>Bosonization</b>	<b>169</b>
<b>E</b>	<b>Heating Dynamics</b>	<b>175</b>
	E.1 Lindblad Dynamics from weak System-Bath Coupling . . . . .	175
	E.2 Heating under Lindblad Dynamics . . . . .	177
	E.3 Heating of the absolute Mode . . . . .	177
<b>F</b>	<b>Different Measurement Protocols</b>	<b>181</b>
<b>G</b>	<b>Perturbative Dynamics of the Diagonal of the Density Matrix</b>	<b>185</b>
<b>H</b>	<b>Integrating out the absolute Mode</b>	<b>189</b>
<b>I</b>	<b>Details about the Derivation of the Flow Equations</b>	<b>191</b>
	I.1 $\langle \Delta S \rangle_<$ – 1st Order Renormalization . . . . .	193
	I.2 2nd Order Renormalization . . . . .	193
	I.3 Scaling of the Integral Expressions . . . . .	197
	I.4 2nd Order Renormalization: Full Set of Flow Equations . . . . .	201
	I.5 First Order Flow Equations from treating Space and Time on equal Footing . . . . .	202
	I.6 Limiting Case: Flow Equations for $\gamma_B = 0$ . . . . .	202
	I.7 Effective Action for the relative Mode in the Presence of random unitary Evolution . . . . .	204
	I.8 Details about Solving the Flow Equations . . . . .	204

### Erklärung zur Dissertation

Hiermit versichere ich an Eides statt, dass ich die vorliegende Dissertation selbstständig und ohne die Benutzung anderer als der angegebenen Hilfsmittel und Literatur angefertigt habe. Alle Stellen, die wörtlich oder sinngemäß aus veröffentlichten und nicht veröffentlichten Werken dem Wortlaut oder dem Sinn nach entnommen wurden, sind als solche kenntlich gemacht. Ich versichere an Eides statt, dass diese Dissertation noch keiner anderen Fakultät oder Universität zur Prüfung vorgelegen hat; dass sie - abgesehen von unten angegebenen Teilpublikationen und eingebundenen Artikeln und Manuskripten - noch nicht veröffentlicht worden ist sowie, dass ich eine Veröffentlichung der Dissertation vor Abschluss der Promotion nicht ohne Genehmigung des Promotionsausschusses vornehmen werde. Die Bestimmungen dieser Ordnung sind mir bekannt. Darüber hinaus erkläre ich hiermit, dass ich die Ordnung zur Sicherung guter wissenschaftlicher Praxis und zum Umgang mit wissenschaftlichem Fehlverhalten der Universität zu Köln gelesen und sie bei der Durchführung der Dissertation zugrundeliegenden Arbeiten und der schriftlich verfassten Dissertation beachtet habe und verpflichte mich hiermit, die dort genannten Vorgaben bei allen wissenschaftlichen Tätigkeiten zu beachten und umzusetzen. Ich versichere, dass die eingereichte elektronische Fassung der eingereichten Druckfassung vollständig entspricht.

Teilpublikationen:

1. B. Ladewig, S. Mathey, and S. Diehl: "Kibble-Zurek mechanism from different angles: The transverse XY model and subleading scalings", Phys. Rev. B **102**, 104306 (2020), DOI: 10.1103/PhysRevB.102.104306
2. B. Ladewig, S. Diehl, and M. Buchhold: "Monitored open fermion dynamics: Exploring the interplay of measurement, decoherence, and free Hamiltonian evolution", Phys. Rev. Research **4**, 033001 (2022), DOI: 10.1103/PhysRevResearch.4.033001

18.12.2022

Björn Ladewig

Unterschrift

**Bemerkung:** Aus beiden Publikationen wurden Abbildungen in dieser Arbeit wiederverwendet bzw. adaptiert.

# 1 | Introduction

The properties of a quantum mechanical system can be shaped by quite different means, ranging from equilibrium settings with thermal states and unitary evolution, to the coupling to a bath or frequent measurements, resulting in a non-unitary (even non-linear) evolution. The four pillars, which we are going to investigate are: (i) an equilibrium setting with  $\rho \sim \exp(-\beta\mathbf{H})$  for a static Hamiltonian  $\mathbf{H}$  and inverse temperature  $\beta$  (e.g., ground states), (ii) driven setups with a time-dependent Hamiltonian  $\mathbf{H}(t)$ , (iii) dephasing due to the coupling to an additional quantum system (a bath), and (iv) frequent local measurements to reveal information.

A notable feature of all these ‘mechanisms’ is that in extended systems, they can give rise to collective phenomena like phases, phase transitions and emerging *universality* [1–4]. The concept of universality refers to the idea that the qualitative behavior at large, macroscopic length (and time) scales only depends on fundamental information like the *dimensionality* and *symmetries* of the system. Different systems with the same symmetries and dimensionality can have the same qualitative behavior, whereas other details of the systems are *irrelevant*. The concept of *phases* or phase transitions refers to a qualitative change of the properties of the quantum state between the one and the other phase (see, e.g., Ref. [2] for quantum phase transitions). Both concepts are intimately connected: an example for the first scenario mentioned above is given by a Hamiltonian  $\mathbf{H} = \mathbf{H}_0 + \lambda\mathbf{H}_1$  (e.g., a quantum Ising model) in one spatial dimension. The Hamiltonian consists of two incompatible parts:  $[\mathbf{H}_0, \mathbf{H}_1] \neq 0$  and hosts a symmetry  $[\mathbf{G}, \mathbf{H}] = 0$ . For  $\lambda \gg 1$  the ground state is approximately the ground state of  $\mathbf{H}_1$ , *sharing* the symmetry  $\mathbf{G}|\text{GS}\rangle \propto |\text{GS}\rangle$ . For  $\lambda \ll 1$ , the ground state  $|\text{GS}\rangle$  is approximately the ground state of  $\mathbf{H}_0$  with a *broken* symmetry  $\mathbf{G}|\text{GS}\rangle \not\propto |\text{GS}\rangle$  [2]. Since these ground states do not share the same symmetry, they are qualitatively different. At  $\lambda = \lambda_c$  the energy gap between the ground states and excited states closes and a continuous phase transition emerges. In its vicinity,  $|\lambda - \lambda_c| \ll 1$ , the interplay of both incompatible terms results in a *universal* and self similar behavior accompanied by a diverging correlation length.

Independent of the mechanisms, which play a part, the properties of an extended quantum system can be classified from different perspectives. On the one hand, states can be characterized in terms of *correlations* or *order parameters* in the system. They reveal typical length scales (e.g., the *correlation length*) or the presence of *symmetry breaking*. On the other hand, though connected to it,

states can be characterized by its *entanglement* properties. An example is the entanglement shared between different spatial regions of a system. Denoting these regions as  $A$  and  $B$  (the complement of  $A$ ), the Hilbert space under consideration can be written as a tensor product  $\mathcal{H} = \mathcal{H}_A \otimes \mathcal{H}_B$ . An entangled state *cannot* be written as a product state  $|\psi\rangle \neq |\psi_A\rangle \otimes |\psi_B\rangle$ . In this case, quantum information is scrambled over different parts of the system. The degree of entanglement can be quantified by, e.g., the von Neumann entanglement entropy  $S_{\text{vN}}(A) = -\text{tr}(\rho_A \log(\rho_A))$  of the reduced density matrix  $\rho_A = \text{tr}_B(|\psi\rangle\langle\psi|)$  [5]. Different thermodynamic phases can be indicated by different scalings with the subsystem size [6, 7].

**Role of a drive:** At criticality, the aforementioned ground state displays a ‘log law’ entanglement  $S_{\text{vN}}(A) \sim \log(|A|)$  with the size  $|A|$  of the subsystem (in one dimension) [8, 9]. In contrast, the ground states deep inside the phases display a weakly entangled area law:  $S_{\text{vN}}(A) \sim \text{const.}$ . An arising question is how such ‘critical’ states can be prepared. One possible approach is to prepare the ground state deep inside one of the phases and slowly drive the Hamiltonian towards the critical point:  $\lambda(t) \rightarrow \lambda_c$ . As long as the evolution is sufficiently slow, the pure state  $|\psi(t)\rangle$  remains in the proximity of the ground state at time  $t$  (adiabatic evolution). However, there is an arising dynamic competition between (i) the time scale on which the parameters are changed and (ii) the diverging correlation length (and time) of the ground state. Close to the transition, the drive inevitably becomes ‘fast’ compared to the diverging reaction time in the system. An adiabatic evolution is not possible anymore and  $|\psi(t)\rangle$  gets excited [10]- a non-equilibrium situation. Even at the transition  $\lambda(t) = \lambda_c$ , the correlation length  $\xi^*$  of  $|\psi(t)\rangle$  stays finite, reflected in a finite density of excitations. Similarly, correlations are exponentially decaying on length scales  $\gg \xi^*$  and the entanglement entropy is bounded:  $S_{\text{vN}}(A) \sim \log(\min(|A|, \xi^*))$  [11, 12]. Coming back to the original question: for a fixed drive velocity  $v$ , we can (only) adiabatically prepare (ground) states with a correlation length  $\xi \leq \xi^*(v)$ . However, for a slow drive, the length scale  $\xi^*(v)$  depends *universally* on the underlying equilibrium properties (Kibble-Zurek mechanism (KZM) [13–15]).

**Role of a bath:** The ground state and drive scenario considered above made use of pure states, their correlations and entanglement. The situation changes once the system is (inevitably) coupled to its surrounding environment (a bath - see Fig. 1.1). The interaction between the system and the bath often results in system-bath entanglement, where information spreads between system and bath [16]. This is reflected in a *mixed* state of the system, described by the reduced density matrix  $\rho_S = \text{tr}_B(|\psi_{SB}\rangle\langle\psi_{SB}|)$ . A competition between the system evolution and the system-bath coupling can arise again once the two Hamiltonians do not commute:  $[\mathbf{H}_S, \mathbf{H}_{SB}] \neq 0$ . However, even for commuting terms, effects like *dephasing* can occur, where the off-diagonal elements of  $\rho_S$  are strongly suppressed (e.g., in the particle number ba-

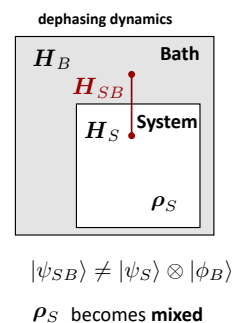


**Figure 1.1:** System ( $S$ , Hamiltonian  $\mathbf{H}_S$ ) coupled to a bath ( $B$ , Hamiltonian  $\mathbf{H}_B$ ) via the Hamiltonian  $\mathbf{H}_{SB}$ .

sis).

**Role of measurements:** The last dynamic ingredient are measurements. If local measurements are performed frequently on a system, they will influence the evolution of the system and can even compete with, e.g., the unitary evolution due to  $\mathbf{H}_S$  (see, e.g., Refs. [6, 7, 17–20]). The ‘direct’ version of a measurement is a *projective* measurement of an operator  $\mathbf{M}$ : the measurement outcome is an eigenvalue of  $\mathbf{M}$  and the state is projected onto the corresponding eigenspace. However, this is an idealized scenario for an extended system. An alternative version (generalized measurements [5]) are again based on entanglement: the system is coupled to a small ancillary system (e.g., a qubit [21]), such that the desired system information gets entangled with the ancilla. By projectively measuring the ancilla, we extract information about the system (see Fig. 1.2). In both scenarios, local (in space) measurements *reduce* the entanglement between subparts of the system. If the measurements are performed frequently, they give rise to a stochastic and non-linear dynamic evolution [21–23], competing with mechanisms that build up entanglement. An example is the interplay with a unitary evolution due to  $\mathbf{H}_S$  with  $[\mathbf{H}_S, \mathbf{M}] \neq 0$ .

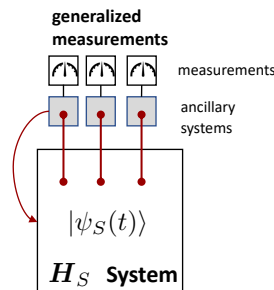


**Figure 1.2:** System coupled to ancillas, which are measured projectively (resulting in a conditional evolution of the state  $|\psi_S\rangle$ ).

All the above mentioned dynamic mechanisms play a part in the realm of quantum computation and simulations, in particular for noisy intermediate-scale quantum (NISQ) devices [24]. Ingredients of their operation are: (i) state *preparation*, (ii) state *manipulation* (e.g., via unitary transformations) and (iii) (read-out) *measurements*. In case of *digital* quantum computers, the existing devices are of intermediate scale with a number of qubits<sup>1</sup> at the order of  $L \sim \mathcal{O}(10^2)$  [25]. Their potential is rooted in, e.g., making use of controlled interference and entanglement in well-controlled quantum systems. In theory, these ingredients can lead to a computational speedup for problems that are believed to be hard to solve classically [24]. An example is the simulation of complex quantum systems itself. However, the existing devices are prone to errors - the systems are noisy. As an example, the inevitable coupling to an environment can induce decoherence in the system, based on the entanglement of system qubits with the environment. Decoherence, e.g., in the form of dephasing, leads to a suppression of the off-diagonal elements in the density matrix  $\rho_S$  (in the computational basis), with rates that can even scale with  $L$  [27]. However, the desired interference and entanglement *in the system* rely on the off-diagonal elements of  $\rho_S$ . Therefore, error *correction* might be necessary<sup>2</sup>, which can be based on entanglement *and measurements*. One possibility is to decode ‘logical’ qubits in a redundant fashion (e.g., using a repetition code [29]) in multiple entangled physical qubits. The decoherence of single *physical* qubits can then be corrected by (i) identifying the error by ‘stabilizer’ measurements and (ii) afterwards un-

<sup>1</sup>The numbers are platform dependent, see also Refs. [25, 26].

<sup>2</sup>For an introduction to error correction, see, e.g., Ref. [28]

doing the error. Therefore, measurements play a two-fold role in those systems: on the one hand, they can be harmful if we think of the environment as performing undesired measurements on the system. On the other hand, they can be used to protect/recover quantum information. The competition of a finite error rate and stabilizer measurements can lead to a *measurement-induced* phase transition, separating (i) a regime, where error correction is possible (the logical qubit can be decoded) and (ii) a regime where error correction is not possible anymore [30–32]<sup>3</sup>.

Closely related to quantum computers are quantum *simulators* (and *annealing* devices). In the analogue form of quantum simulators [26, 35], quantum models are analyzed by engineering the desired Hamiltonian  $\mathbf{H}(t)$  in a well-controlled quantum experiment like Rydberg atoms [26]. As an example, critical properties of quantum phase transitions can be accessed dynamically by making use of the Kibble–Zurek scaling [36]. A related platform are quantum *annealers* (see, e.g., Ref. [37]), where a time dependent Hamiltonian  $\mathbf{H}(t)$  is used to prepare a desired ground state (e.g., the solution to an optimization problem) (see, e.g., Refs. [38, 39]). Here, a relevant question is how the drive speed and drive protocol affect the final state. From the NISQ perspective, the KZM, in combination with exactly solvable (spin) models, provides a testbed to probe adiabaticity as well as decoherence and other sources of errors in the hardware [40].

In the following chapters, we investigate the interplay of different mechanisms: (i) critical ground state physics with slow drives and (ii) unitary evolution with measurements and dephasing.

**(i) Generalized slow drives:** In Chap. 3, we analyze the interplay of *generalized* slow drives with a quantum phase transition in the transverse XY model ( $\mathbb{Z}_2$  symmetry in one dimension) and its corresponding fermionic version. We demonstrate that even equilibrium *irrelevant* couplings, once they are driven, can give rise to a *universal* scaling behavior of  $\xi^*$ , complementing the RG predictions made in Ref. [41]. Therefore, the KZM is enriched by another competing scale. The observable scaling is determined by the smallest of up to three scales: (i) a drive scale associated with a relevant coupling, (ii) a drive scale associated with an irrelevant coupling and (iii) a (finite) equilibrium correlation length.

- This part is based on the publication: B. Ladewig, S. Mathey, and S. Diehl: "Kibble-Zurek mechanism from different angles: The transverse XY model and subleading scalings" Phys. Rev. B **102**, 104306 (2020).

**(ii) Measurements and dephasing:** In Chap. 4 we investigate the interplay of a fermionic hopping Hamiltonian ( $U(1)$  symmetry in one dimension) with measurements of the local particle number *and* dephasing. In the absence of dephasing, the model hosts an extended *critical phase* for weak measurements [18, 19], reminiscent of the ground state at the critical point discussed before. Such a critical behavior can be fragile against the introduction of new scales stemming, e.g., from drives (as we have seen before). We expand the stability analysis

---

<sup>3</sup>First experimental investigations are performed, e.g., on a trapped ion based quantum computer [33] (see also Ref. [34]).

including a dephasing bath. Besides being stable against weak dephasing, the interplay of strong dephasing and weak measurements indicates a new phase with scale invariant features, but strongly suppressed off-diagonal elements in the density matrix (in the measurement eigenbasis).

- This part is based on the publication: B. Ladewig, S. Diehl, and M. Buchhold: "Monitored open fermion dynamics: Exploring the interplay of measurement, decoherence, and free Hamiltonian evolution" Phys. Rev. Research **4**, 033001 (2022).

**About the structure of the thesis:** The thesis was written with the intent to be self-consistent (assuming only the knowledge of second quantization), therefore many details are provided throughout the text. Those details appear (i) in boxes in the main text (to indicate that they can be skipped if necessary) and (ii) in an extended appendix, where, e.g., fermionic Gaussian states are discussed in detail. The thesis has three main chapters apart from the introduction: In Chap. 2, minimal models for the aforementioned scenarios are introduced, ranging from linear drives and dephasing for single qubits to the renormalization group discussion of the transverse XY model. In Chap. 3 the generalized KZM is discussed and in Chap. 4 the interplay of measurements, dephasing and unitary evolution is analyzed.

**Notation:**

- Operators will be denoted with **bold** symbols, like a Hamiltonian  $\mathbf{H}$  and creation/annihilation operators  $\mathbf{c}^\dagger, \mathbf{c}$ .
- Dimensionless quantities will be denoted by a hat (or a bar).

**Box 1: Repetition code**

**Quantum error correction:** In a quantum computing setup, the coupling to an environment and imperfections in applying quantum gates can lead to local errors in qubits (e.g., bit flips, described by the Pauli operator  $\sigma_j^x$ ). To circumvent this issue, a logical qubit can be encoded in a redundant fashion in many physical qubits. An example is the repetition code [32]:

$$\text{logical bit: } a_0|0\rangle + a_1|1\rangle$$

↓

$$\text{physical encoding: } a_0|00\dots 0\rangle + a_1|11\dots 1\rangle.$$

Errors in the physical model, like bit flips  $\sigma_j^x$ , distort the state, but can be detected by performing a set of *stabilizer* measurements  $\{\sigma_j^z \sigma_{j+1}^z\}$ .



## 2 | Minimal Models – From single Qubits to the Ising Model

The main questions we are addressing in the following can be divided into a few categories: (i) ground state problems for time independent Hamiltonians; (ii) time evolved states  $|\psi(t)\rangle$  of time *dependent* Hamiltonians  $\mathbf{H}(t)$  starting from a ground state; (iii) global properties (like entanglement) of time evolved states for fixed Hamiltonians starting [from (a superposition of) highly excited states], and (iv) *stationary* states for non-unitary evolutions  $\rho(t \rightarrow \infty) = \rho_{\text{stationary}}$ .

*The discussion in Sec. 2.2 contains parts which are adapted (and partly extended) from the publication [42].*

### 2.1 Minimal Models (1): Single Qubits

All models we will discuss in the next chapters are based, in one form or another, on single qubits as their ‘atomic’ unit. Despite the simplicity of two level systems, many ingredients for the effects we study in the many body context are already rooted in this reduction. In the following, we consider: (i) a two level system in the presence of a time dependent Hamiltonian (which already renders the solution of the model quite intricately (and not exactly solvable in many cases)) and (ii) the effect of a bath (an ancillary system) onto the qubit, which will lead to dephasing.

#### 2.1.1 Time dependent Hamiltonian: Landau-Zener Model – An Exercise in Scales

The category we consider first are time-dependent Hamiltonians  $\mathbf{H}(t)$ . The question we address (belonging to the category (ii)) in the following is: Does a state, initially prepared in the ground state of  $\mathbf{H}(t = 0)$ , stay close to the ground state of  $\mathbf{H}(t)$ ? Here,  $\mathbf{H}(t)$  corresponds to slowly changing one of the systems parameter in time. The quantitative version of the question is how strongly the system gets excited during the drive.

The minimal version of this scenario is a driven two level system, which is not just an elementary version but also experimentally relevant, for example in

trapped ion experiments [43, 44]. We consider the time dependent Hamiltonian  $\mathbf{H}(t) = b\sigma_x + vt\sigma_z$ , written in terms of the Pauli operators<sup>1</sup> and the drive velocity  $v$ . The eigenenergies of  $\mathbf{H}(t)$  are shown in Fig. 2.1): due to the presence of  $\sigma_x$ , an avoided level crossing occurs. The state is parametrized as  $|\psi(t)\rangle = (U(t), V(t))^T$  with its time evolution given by

$$i\partial_t \begin{pmatrix} U(t) \\ V(t) \end{pmatrix} = \begin{pmatrix} vt & b \\ b & -vt \end{pmatrix} \begin{pmatrix} U(t) \\ V(t) \end{pmatrix}. \quad (2.1)$$

The evolution starts at  $t_i = -\infty$  in the ground state:  $|U(-\infty)| = 1$  and  $V(-\infty) = 0$ . The evolution equation (2.1) can be parametrized in terms of a single dimensionless effective parameter  $\hat{v}_{\text{eff}} := v/b^2$  and rescaled time  $\bar{t} = bt$ :

$$i\partial_{\bar{t}} \begin{pmatrix} U \\ V \end{pmatrix} = \begin{pmatrix} \hat{v}_{\text{eff}} \cdot \bar{t} & 1 \\ 1 & -\hat{v}_{\text{eff}} \cdot \bar{t} \end{pmatrix} \begin{pmatrix} U \\ V \end{pmatrix}. \quad (2.2)$$

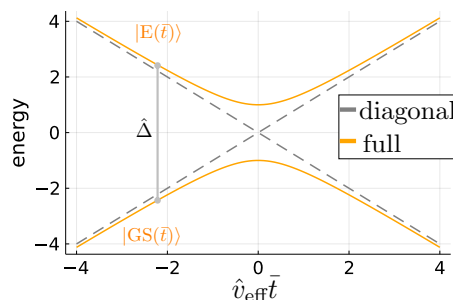


**Figure 2.1:** Energy levels of the ‘unperturbed’ dimensionless model (dashed, only  $\sigma_z$ ) and the full model (orange) in the driven two-level system, (2.2). The energy difference between the ground  $|\text{GS}(\bar{t})\rangle$  and excited state  $|\text{E}(\bar{t})\rangle$  is given by the (instantaneous) energy gap  $\hat{\Delta}(\bar{t})$ .

The evolution is *adiabatic*, if the state remains in the instantaneous ground state  $|\text{GS}(\bar{t})\rangle$  of  $\mathbf{H}(\bar{t})$  during the drive (corresponding to lower orange line in Fig. 2.1). The probability of  $|\psi(t_f)\rangle$  to be in the excited state for  $t_f = \infty$  is  $|U(\infty)|^2$  (corresponding to the upper branch in Fig. 2.1 with the excited state given by  $|\text{E}(\infty)\rangle = (1, 0)$ ). Calculating the final state  $|\psi(t_f)\rangle$  is already a challenging task since the Hamiltonians at different times do not commute  $[\mathbf{H}(t_1), \mathbf{H}(t_2)] \neq 0$ . Nevertheless, for such a *linear drive* an exact *asymptotic* solution is known<sup>2</sup> [46–48]:

$$\text{Landau-Zener: } p(t_f) := |\langle \text{E}(t_f) | \psi(t_f) \rangle|^2 = |U(\infty)|^2 = \exp(-\pi \hat{v}_{\text{eff}}^{-1}). \quad (2.3)$$

According to (2.3), a slow drive with  $\hat{v}_{\text{eff}} \ll 1$  results in a strongly suppressed excitation probability - the evolution is *adiabatic*. For a fast drive,  $\hat{v}_{\text{eff}} \gg 1$ , adiabaticity is broken and the excitation probability is close to 1. To get a more physical understanding, we identify/approximate the time range where adiabaticity is broken (in the vicinity of the avoided level crossing). We divide the dynamics into three regimes: adiabatic-impulse-adiabatic (AIA approximation [45, 49]). The excitation probability builds up in the ‘impulse’ regime, see Fig. 2.2(b). To extract the time of adiabaticity breaking, we identify the competing time scales. The first one,  $\xi_\tau(t)$ , is set by the (instantaneous) energy gap  $\Delta(t)$ , giving rise to a characteristic time scale  $\xi_\tau = \frac{1}{\Delta}$ :

$$\Delta(t) = 2\sqrt{(vt)^2 + b^2} = 2b\sqrt{(\hat{v}_{\text{eff}} \cdot \bar{t})^2 + 1} \Rightarrow \xi_\tau = \frac{1}{\Delta}. \quad (2.4)$$

<sup>1</sup>Using the basis  $\{|0\rangle, |1\rangle\}$ :  $\sigma_x = |0\rangle\langle 1| + |1\rangle\langle 0|$ ,  $\sigma_z = |0\rangle\langle 0| - |1\rangle\langle 1|$ .

<sup>2</sup>Even the full time evolution can be determined, see, e.g., Ref. [45].

The second one corresponds to the time scale on which the ‘coupling’  $g(t) = vt$  changes. This scale is given by  $g(t)/\dot{g}(t) = t$  (see also Ref. [10]) and corresponds to the time needed to reach the anti-crossing center. For an adiabatic evolution, this time  $t$  is larger than  $\xi_\tau(t)$ . Once both time scales become comparable at  $t^* \approx \xi_\tau(t^*)$ , adiabaticity is assumed to be broken:

$$\frac{1}{2\Delta(t^*)} = \alpha_1 t^*. \quad (2.5)$$

with a constant  $\alpha_1$ <sup>3</sup>. Starting at  $t_i = -\infty$ , the state up to time  $-t^*$  is well described by the instantaneous ground state  $|\psi(t)\rangle \approx |0(t)\rangle$ . Afterwards, in the range of adiabaticity breaking  $[-t^*, t^*]$  the state is essentially frozen:  $|\psi(t^*)\rangle \approx |\psi(-t^*)\rangle$  (also referred to as ‘impulse regime’). For  $t > t^*$ , the evolution is again adiabatic, although  $|\psi(t)\rangle$  is an excited state. Since the dynamics is adiabatic for  $t > t^*$ , the probability to be in the excited state will not change:  $|\langle E(t_f)|\psi(t_f)\rangle|^2 \approx |\langle E(t^*)|\psi(t^*)\rangle|^2$ . Therefore, once  $t_f > t^*$ , the overall excitation probability for the drive is estimated to be [49]:

$$\begin{aligned} \text{AIA approximation: } p &= |\langle E(t_f)|\psi(t_f)\rangle|^2 \approx |\langle E(t^*)|\psi(t^*)\rangle|^2 \\ &\approx |\langle E(t^*)|\psi(-t^*)\rangle|^2 \approx |\langle E(t^*)|\text{GS}(-t^*)\rangle|^2. \end{aligned}$$

The advantage of this expression is that its final form only requires the knowledge of (i) the eigenstates of  $\mathbf{H}(t)$  and (ii) the adiabaticity breaking time  $t^*$ . Looking back at the argumentation, we did specify the order of the drive, which means that this approximation can also be used for different drive protocols. An example of and a comparison to the exact result is shown in Fig. 2.2: the approximation works particularly well for fast drives.

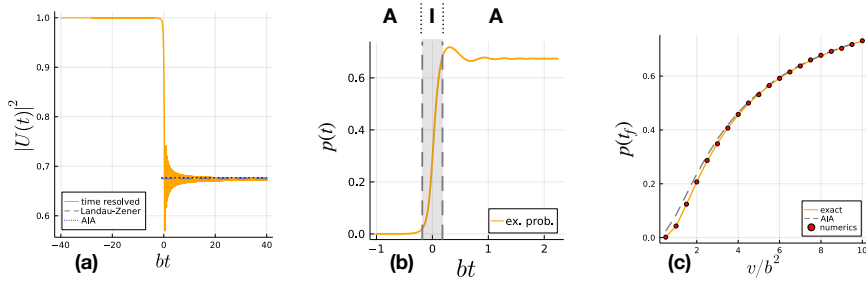


**Figure 2.2:** (a) Evolution of  $|U(t)|^2$ , which corresponds asymptotically ( $t \rightarrow \infty$ ) to the excitation probability and reaches the Landau-Zener result. (b) Time resolved excitation probability  $p(t)$ , starting from the ground state at some  $t_i \ll 0$  (here:  $v/b^2 = \hat{v}_{\text{eff}} = 8$  - fast drive). The area between the dashed lines marks the impulse regime. (c) Comparison of the AIA approximation, exact asymptotic results and numerical simulations (starting from the same Hamiltonian with  $vt_i/b = -200$ ) for  $p(t_f)$ . The approximation becomes very good for  $\hat{v}_{\text{eff}} \gg 1$ .

In summary, we can adiabatically prepare the ground state of  $\mathbf{H}(t)$ , starting from the ground state of  $\mathbf{H}(t_i)$ . However, this requires a sufficiently slow drive ( $\hat{v}_{\text{eff}} \ll 1$ ), related to the energy gap in the system. It is this requirement that will be violated close to a quantum phase transition.

<sup>3</sup>It can be determined by a comparison to a diabatic expansion [45].

### 2.1.2 Coupled Systems: Dephasing of a Qubit coupled to a Bath

The second dynamical scenario we consider is *dephasing* in a system due to the coupling to an additional system (bath). As a system, we consider again a qubit with Hilbert space  $\mathcal{H}_S$  spanned by  $\{|0\rangle, |1\rangle\}$ . The qubit is coupled to a bosonic bath, described in terms of creation/annihilation operators<sup>4</sup>  $\mathbf{b}_k^\dagger/\mathbf{b}_k$  for  $L$  modes, labelled by  $k$  (following Refs. [16, 27, 50]):

$$\mathbf{H} = \underbrace{\frac{\omega}{2}\sigma_z + \sum_k \epsilon_k \mathbf{b}_k^\dagger \mathbf{b}_k}_{=\mathbf{H}_0} + \underbrace{\sigma_z \sum_k (g_k \mathbf{b}_k^\dagger + g_k^* \mathbf{b}_k)}_{=\mathbf{H}_{\text{int}}}, \quad [\mathbf{H}_0, \mathbf{H}_{\text{int}}] = 0. \quad (2.6)$$

The summation over  $k$  can, e.g., correspond to the summation over quasi momenta of phonons. Qualitatively, we expect the time evolution  $\mathbf{U}(t)$  to *entangle* the system degrees of freedom and the bath degrees of freedom: an initial product state will evolve into  $|\psi_{SB}\rangle \neq |\phi_S\rangle \otimes |\chi_B\rangle$ . Therefore, the reduced density matrix of the system:

$$\rho_S(t) := \text{tr}_B[\mathbf{U}(t)\rho_S \otimes \rho_B \mathbf{U}^\dagger(t)], \quad (2.7)$$

will become mixed. In the following, we derive an expression for  $\rho_S(t)$  and afterwards specify the energies  $\epsilon_k$ 's and coupling strengths  $g_k$ . The time evolution of this model can be solved exactly by going to the interaction picture  $\tilde{\rho}(t) = e^{i\mathbf{H}_0 t} \rho(t) e^{-i\mathbf{H}_0 t}$  [50]:

$$\tilde{\mathbf{H}}(t) = e^{i\mathbf{H}_0 t} \mathbf{H}_{\text{int}} e^{-i\mathbf{H}_0 t} = \sigma_z \sum_k (g_k e^{i\epsilon_k t} \mathbf{b}_k^\dagger + \text{h.c.}). \quad (2.8)$$

In this new frame, the Hamiltonian  $\tilde{\mathbf{H}}(t)$  is still time dependent, but its commutator  $[\tilde{\mathbf{H}}(t_2), \tilde{\mathbf{H}}(t_1)]$  is merely a time-dependent scalar. The time evolution operator is [50]:

$$\begin{aligned} \tilde{\mathbf{U}}(t) &= \underbrace{e^{\frac{1}{2} \int^t dt_1 \int^{t_1} dt_2 [\tilde{\mathbf{H}}(t_2), \tilde{\mathbf{H}}(t_1)]}}_{\text{phase factor } \phi(t)} \cdot e^{-i \int_0^t dt' \tilde{\mathbf{H}}_{\text{int}}(t')} \\ &= e^{-i\varphi(t)} e^{\sigma_z \sum_k \left( \frac{\alpha_k(t)}{2} \mathbf{b}_k^\dagger - \frac{\alpha_k^*(t)}{2} \mathbf{b}_k \right)}, \quad \alpha_k(t) := 2g_k \frac{1 - e^{i\epsilon_k t}}{\epsilon_k}. \end{aligned} \quad (2.9)$$

This evolution will *entangle* an initial product state of the form (with  $|a_0|^2 + |a_1|^2 = 1$ ) [27]:

$$(a_0|0\rangle + a_1|1\rangle) \otimes \left( \prod_k |0_k\rangle \right) \rightarrow \underbrace{\prod_k (a_0|0\rangle \otimes |\alpha_k/2\rangle + a_1|1\rangle \otimes |-\alpha_k/2\rangle)}_{\neq |\phi_S\rangle \otimes |\chi_B\rangle}.$$

The states  $|\alpha_k/2\rangle$  are bosonic coherent states (see info box below), created by the displacement operator  $\mathbf{D}_k(\alpha_k/2)$  acting on the vacuum:

$$\begin{aligned} \mathbf{b}_k |\alpha_k/2\rangle &= \alpha_k/2 |\alpha_k/2\rangle, \\ \mathbf{D}_k(z) &:= \exp\left(z \mathbf{b}_k^\dagger - z^* \mathbf{b}_k\right), \quad |\alpha_k/2\rangle = \mathbf{D}_k(\alpha_k/2) |0_k\rangle. \end{aligned}$$

<sup>4</sup> $[\mathbf{b}_k, \mathbf{b}_{k'}^\dagger] = \delta_{k,k'}$  with vacuum states  $|0_k\rangle$ .

Calculating the reduced density matrix  $\tilde{\rho}_S(t)$  according to (2.7), we observe that the diagonal elements are not affected by the dynamics<sup>5</sup>. The off-diagonal elements are of the form:

$$\langle 0|\tilde{\rho}_S(t)|1\rangle = \langle 0|\tilde{\rho}_S(0)|1\rangle \cdot \text{tr}_B \left[ \prod_k \mathbf{D}_k(\alpha_k(t)) \rho_B \right]. \quad (2.11)$$

So far, the analysis is exact, but will depend on the initial state and the not yet specified coefficients (entering  $\alpha_k(t)$ ). To be definite, we consider a thermal (Gaussian) state of the bath:  $\rho_B \sim \exp(-\beta \sum_k \epsilon_k \mathbf{b}_k^\dagger \mathbf{b}_k)$ . The expression in (2.11) can be evaluated by inserting a completeness relation in terms of coherent states (see info box), which gives rise to [50]:

$$\text{tr}_B \left[ \prod_k \mathbf{D}_k(\alpha_k(t)) \rho_B \right] = \exp \left( - \sum_k \frac{|\alpha_k|^2}{2} \coth \left( \frac{\epsilon_k}{2k_B T} \right) \right). \quad (2.12)$$

To infer the implication of (2.12) onto the off-diagonal elements, we have to specify the model. First of all, we work in the thermodynamic limit (thinking of, e.g., an infinite lattice  $L \rightarrow \infty$ ), such that the energies  $\epsilon_k$  become dense. Therefore, we rewrite the summation of functions  $f(\epsilon_k)$  over  $k$  in terms of an integral (including some phenomenological cutoff  $\epsilon_c$ ):

$$\text{thermodynamic limit: } \sum_k f(\epsilon_k) \stackrel{L \rightarrow \infty}{\approx} \int_0^{\epsilon_c} d\epsilon \mu(\epsilon) f(\epsilon) \quad (2.13)$$

with the mode density  $\mu(\epsilon)$ . The bath contribution then reads:

$$\text{tr}_B \left[ \prod_k \mathbf{D}_k(\alpha_k(t)) \rho_B \right] \approx \exp \left( - \int_0^{\epsilon_c} d\epsilon \underbrace{\mu(\epsilon) 4|g(\epsilon)|^2}_{=: J(\epsilon)} \frac{1 - \cos(\epsilon t)}{\epsilon^2} \coth \left( \frac{\epsilon}{2k_B T} \right) \right),$$

where  $J(\epsilon)$  denotes the spectral density of the bosonic bath [50]. Here, we assume an ohmic version  $J(\epsilon) = c\epsilon$  with  $c > 0$ . The only scales are set by (i) the inverse temperature  $1/(k_B T)$  and (ii) the cutoff  $\epsilon_c$ . Dimensionless variables can therefore be defined as  $\bar{\epsilon} = \epsilon/(k_B T)$  and  $\bar{t} = k_B T t$ . In the limit  $\epsilon_c/(k_B T) \gg 1$ , the bath contribution can be calculated exactly<sup>6</sup>. For long times  $\bar{t} \gg 1$ , the off-diagonal elements decay exponentially [16, 50]:

$$\text{dephasing: } \langle 0|\tilde{\rho}_S(t)|1\rangle = \langle 0|\tilde{\rho}_S(0)|1\rangle e^{-\Gamma(t)} \quad \text{with: } \Gamma(t) \sim ck_B T \cdot t.$$

Therefore, the off-diagonal elements are suppressed and the state becomes more mixed:  $\text{tr}[\rho_S^2] < 1$ . The suppression of the off-diagonal elements  $\rho_{i \neq j}$  in the density matrix  $\rho_S = \sum_{i,j} \rho_{ij} |i\rangle\langle j|$  leads to the loss of, e.g., interferences in the system. For extended systems, also the entanglement in the system etc. will be suppressed (which also depends on  $\rho_{i \neq j}$ ). We consider an extended

<sup>5</sup> $\text{tr}_B[\tilde{U}(t)|\sigma\rangle\langle\sigma| \otimes \rho_B \tilde{U}^\dagger(t)] = |\sigma\rangle\langle\sigma| \cdot \text{tr}_B[\rho_B]$  for  $\sigma = 0, 1$ .

<sup>6</sup>See Ref. [16] on details on how to evaluate the integral.

fermionic system<sup>7</sup> in Sec. 4.3. Here, the interplay of non-commuting system and bath operators results in the featureless ‘infinite temperature’ state  $\rho_S \sim \mathbb{1}$  for long times. Information that are encoded in, e.g., (quantum) ‘coherences’ like  $|\langle c_i^\dagger c_j \rangle|^2$  will vanish for  $i \neq j$  for those heated states.

**Remark:** The fermionic model consists of a finite chain and a fixed number of fermions, where each lattice site is subject to dephasing. The dephasing might stem from, e.g., contributions of the drive laser used to create an optical lattice [51]. Alternatively, it might result from a phonon bath at high temperatures (see also Ref. [4]).

### Box 2: Coherent states & Co.

Coherent states are eigenstates of bosonic (or fermionic) annihilation operators:

$$\mathbf{b}_k |\alpha_k\rangle = \alpha_k |\alpha_k\rangle, \quad \alpha_k \in \mathbb{C}, \quad |\alpha_k\rangle = e^{-\frac{1}{2}|\alpha_k|^2} \sum_{n=0}^{\infty} \frac{\alpha_k^n}{\sqrt{n!}} |n_k\rangle$$

$$|\alpha_k\rangle = \exp\left(\alpha_k \mathbf{b}_k^\dagger - \alpha_k^* \mathbf{b}_k\right) |0_k\rangle = \exp(\alpha_k \mathbf{b}_k^\dagger) \exp(-\alpha_k^* \mathbf{b}_k) \exp\left(-\frac{1}{2}|\alpha_k|^2\right) |0\rangle,$$

where  $|n_k\rangle$  is a number eigenstate with  $n_k$  bosons. Different coherent states have a non-vanishing overlap, but nonetheless provide a completeness relation<sup>a</sup> (see also Ref. [52]):

$$\langle \alpha | \phi \rangle = \exp\left(-\frac{1}{2}(|\alpha|^2 + |\phi|^2) + \alpha^* \phi\right), \quad \mathbb{1} = \frac{1}{\pi} \int d^2\phi |\phi\rangle \langle \phi|.$$

The expression (2.12) in the main text can be evaluated as follows for  $\rho_B \propto \sum_{\{n_k\}} \exp(-\beta \sum_k \epsilon_k n_k) |\{n_k\}\rangle \langle \{n_k\}|$ , where  $|\{n_k\}\rangle$  are the Fock states with  $n_k$  bosons in mode  $k$ . Focusing on a single mode  $k$ , we insert the completeness relation to convert creation/annihilation operators into numbers:

$$\begin{aligned} & \sum_{n_k=0}^{\infty} \langle n_k | \mathbf{D}(\alpha_k) \exp(-\beta \epsilon_k n_k) | n_k \rangle \\ &= \sum_{n_k} \langle n_k | \exp(-\alpha_k^* \mathbf{b}_k) \mathbb{1} \exp(\alpha_k \mathbf{b}_k^\dagger) \exp\left(+\frac{|\alpha_k|^2}{2}\right) \exp(-\beta \epsilon_k n_k) | n_k \rangle \\ &= \frac{1}{\pi} \int d^2\phi \underbrace{\sum_{n_k} |\langle n_k | \phi \rangle|^2 \exp(-\beta \epsilon_k n_k) \exp(\alpha_k \phi^*) \exp(-\alpha_k^* \phi) \exp\left(+\frac{|\alpha_k|^2}{2}\right)}_{\exp(-(1-\exp(-\beta \epsilon_k))|\phi|^2)} \end{aligned}$$

The remaining integral is a complex Gaussian integral and evaluates to the result (2.12) in the main text. This idea of converting creation/annihilation operators into numbers (or fields) will be a recurrent theme in the following sections.

continued on next page

<sup>7</sup>Described by creation/annihilation operators  $c_j^\dagger, c_j$  on lattice sites  $j$ .

continued from page before

<sup>a</sup>Depending on the reference, there can be a difference in the normalization of the coherent states.

## 2.2 Minimal Models (2): Quantum Ising Chain

The third class of models we consider are *ground states* in extended many body quantum systems ( $L$  lattice sites and lattice spacing  $a$ ). Different phases can be distinguished by, e.g, the symmetry of the ground state. Importantly, the *ground state* of a Hamiltonian  $\mathbf{H}$  does not need to have the same symmetries as  $\mathbf{H}$  itself, a scenario referred to as (spontaneous) symmetry breaking [2].

A paradigmatic and exactly solvable model to study those transitions are quantum Ising and XY models, consisting of a chain of interacting spin- $\frac{1}{2}$  particles (or qubits). The competing terms are ferromagnetic nearest-neighbor interactions and a (non-commuting) transverse magnetic field<sup>8</sup>:

$$\mathbf{H} = -g \sum_{l=1}^L \sigma_l^z - J_x \sum_{l=1}^L \sigma_l^x \sigma_{l+1}^x - J_y \sum_{l=1}^L \sigma_l^y \sigma_{l+1}^y. \quad (2.14)$$

The chain consists of  $L$  sites with periodic boundary conditions ( $\sigma_{L+1} = \sigma_1$ ) and it has a  $\mathbb{Z}_2$ -symmetry, encoded in

$$[\mathbf{H}, \prod_l \sigma_l^z] = 0. \quad (2.15)$$

For ferromagnetic spin-spin couplings, we have  $J_x, J_y > 0$ . The special case  $J_y = 0$  corresponds to the *transverse Ising model*. For simplicity, we stick with  $J_y = 0$  for the moment. The competition is encoded in the incompatibility of the transverse field  $g \sum \sigma_l^z$  and the interaction term  $J_x \sum \sigma_l^x \sigma_{l+1}^x$ . The ground state of the first term would take the form  $|\uparrow\uparrow \dots\rangle$  (paramagnetic phase), whereas the ferromagnetic coupling favors  $|\rightarrow\rightarrow \dots\rangle$  or  $|\leftarrow\leftarrow \dots\rangle$  (ferromagnetic phase). The latter are *not* invariant under the symmetry operation and therefore correspond to the symmetry broken or ordered phase. The competition is encoded in the dimensionless ratio  $g/J$  and a phase transition takes place at  $g/J = 1$ , indicated by a vanishing energy gap.

Deep inside the phases ( $g/J \gg 1$  or  $g/J \ll 1$ ), the ground states are nearly product states with correlations bounded to nearby spins (in the following we rescale  $g \rightarrow g/J$ ). This property is quantified by a dimensionless correlation length of order one:  $\xi/a \sim \mathcal{O}(1)$ . It is the relevant scale for (connected) correlation functions [53] ( $a, b \in \{x, y, z\}$ ):

$$\langle \sigma_0^a \sigma_l^b \rangle - \langle \sigma_0^a \rangle \langle \sigma_l^b \rangle \sim \exp(-l/\xi). \quad (2.16)$$

<sup>8</sup> $\sigma_z |\uparrow\rangle = |\uparrow\rangle, \sigma_z |\downarrow\rangle = -|\downarrow\rangle$  and  $\sigma_x |\rightarrow\rangle = |\rightarrow\rangle$  etc. with  $|\rightarrow\rangle = \frac{1}{\sqrt{2}}(|\uparrow\rangle + |\downarrow\rangle)$

A very different behavior emerges at the critical point  $g = g_c$ , where the energy gap  $\Delta$  in the spectrum vanishes. At this point, the correlation length diverges and, instead of exponentially decaying correlations, an algebraic behavior emerges [53]:

$$\langle \sigma_0^a \sigma_l^b \rangle - \langle \sigma_0^a \rangle \langle \sigma_l^b \rangle \sim l^{-\alpha}. \quad (2.17)$$

The exponents  $\alpha$  reveal *universal* information about the transition and the model. In the vicinity of the transition, many quantities, like the correlation length or the inverse gap, scale *algebraically* with the distance to the critical point. The corresponding ‘critical’ exponents are defined as [2]

$$\begin{aligned} \text{energy gap:} \quad & \Delta \sim |g - g_c|^{z\nu}, \\ \text{correlation length:} \quad & \xi^{-1} \sim |g - g_c|^\nu, \\ & \Delta \sim \xi^{-z}. \end{aligned} \quad (2.18)$$

Besides correlations, a (pure) quantum mechanical states  $|\psi\rangle$  can also be classified according to the *entanglement* between a subregion  $A$  of the lattice and the rest of the system  $B$ . The amount of entanglement can be quantified by the von Neumann entanglement entropy  $S_{\text{vN}}$  of the reduced density matrix of the subregion:

$$S_{\text{vN}}(A) = -\text{tr}_A [\rho_A \log(\rho_A)], \quad \rho_A = \text{tr}_B [|\psi\rangle\langle\psi|]. \quad (2.19)$$

Considering first the limiting case  $J \rightarrow 0$ , the ground state is close to a product state. Therefore, we expect that the entanglement between a bipartite system should be (vanishingly) small. Similarly, for  $g \rightarrow 0$ , the ground state is again a product state, though there is one difference: the ground state is twofold degenerate, corresponding to an entanglement entropy of  $\log(2)$  [9]. In both cases, increasing the subsystem size  $|A|$  will not lead to an increase in the entanglement:  $S_{\text{vN}}(A) \sim |A|^0$  (area law), see Fig. 2.3(b). Quite in contrast, close to the critical point, large parts of the system become correlated and the entanglement becomes  $A$ -dependent. To be precise,  $S_{\text{vN}}(A)$  grows *logarithmically* as a function of the subsystem size [8]:  $S_{\text{vN}}(A) \sim \log(|A|)$  (log law), see Fig. 2.3(c).

**Outlook towards a field theory:** This critical behavior is a hallmark of a conformal field theory (CFT), where the scaling of the entanglement of a subregion of size  $|A|$  is known [9, 54]:

$$\text{finite system:} \quad S_{\text{vN}}(A) \approx \frac{c + \bar{c}}{6} \log_2 \left( \frac{L}{\pi} \sin \left( \frac{\pi|A|}{L} \right) \right), \quad (2.20)$$

$$\text{thermodynamic limit:} \quad S_{\text{vN}}(A) = \frac{c + \bar{c}}{6} \log_2(|A|). \quad (2.21)$$

The constants  $c, \bar{c}$  are the central extensions/charges of the CFT [54], encoding universal information. Whenever there is a finite length scale  $\xi$  in the system, either due to (i) a finite distance to the critical point (static case) or due to (ii) adiabaticity breaking (dynamical case) [12], we expect the entanglement entropy to be bounded:

$$S_{\text{vN}}(A) \sim \log_2(\min[|A|, \xi]). \quad (2.22)$$

Nevertheless, in Chap. 4 we will encounter a (fermionic) critical theory, *extended* in a finite parameter regime.

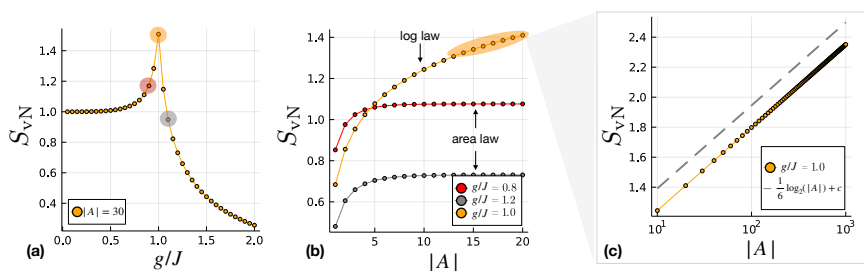


**Figure 2.3:** Entanglement entropy  $S_{vN}$  of a subsystem (size  $|A|$ ) with the rest of the system (infinite chain) for the ground state of the transverse Ising model (see, e.g. Ref. [8] how to calculate the entanglement). (a) Entanglement entropy for fixed subsystem size and different points in parameter space, signalling a transition at  $g/J = 1$ ; (b) Subsystem size resolved scaling, distinguishing 'area law' scaling (inside the phases) and 'log law' scaling at criticality; (c) Semi logarithmic plot of the entropy at the critical point up to  $|A| = 1000$ .

### 2.2.1 Exact Solution – Formal Treatment

The advantage of this class of models is that they can be mapped to *local* non-interacting fermion models via a non-local Jordan-Wigner transformation [2, 11, 55–59]). The fermionic models, in turn, are exactly solvable (see App. A.1 for more details). However, not all spin observables are local in the fermionic language. The spin model (2.14) in terms of fermions takes the form:

$$\mathbf{H}^+ = - \sum_{l=1}^L \left[ \underbrace{(J_x + J_y)}_{=:J} \mathbf{c}_l^\dagger \mathbf{c}_{l+1} + \underbrace{(J_x - J_y)}_{=: \gamma} \mathbf{c}_l^\dagger \mathbf{c}_{l+1}^\dagger - g \mathbf{c}_l^\dagger \mathbf{c}_l + \frac{g}{2} + \text{h.c.} \right], \quad (2.23)$$

which is valid in the sector with an even number of fermions, including the ground states [11]. This Hamiltonian is still a *local* Hamiltonian. Making use of the discrete translational invariance, the model takes the following form in Fourier space<sup>9</sup>

$$\begin{aligned} \mathbf{H}^+ &= \frac{1}{2} \sum_k \begin{pmatrix} \mathbf{c}_k^\dagger & \mathbf{c}_{-k} \end{pmatrix} h_k \begin{pmatrix} \mathbf{c}_k \\ \mathbf{c}_{-k}^\dagger \end{pmatrix} + \text{const.} \ , \\ h_k &= \begin{pmatrix} 2(g - J \cos(ka)) & 2\gamma \sin(ka) \\ 2\gamma \sin(ka) & -2(g - J \cos(ka)) \end{pmatrix}. \end{aligned} \quad (2.24)$$

The Hamiltonian is not yet diagonal, but can be diagonalized by introducing new quasi-particle operators:  $\{\mathbf{c}_k, \mathbf{c}_k^\dagger\} \rightarrow \{\boldsymbol{\chi}_k, \boldsymbol{\chi}_k^\dagger\}$  (Bogoliubov transformation

<sup>9</sup>Convention as in Ref. [11]:

$$\mathbf{c}_l = \frac{e^{-i\frac{\pi}{4}}}{\sqrt{L}} \sum_k \mathbf{c}_k e^{ik(la)}, \quad k_j = \frac{2\pi}{La} \left[ -\frac{L}{2} + \left( j - \frac{1}{2} \right) \right], \quad j \in \{1, \dots, L\}.$$

[11, 55, 56] - see info box):

$$\mathbf{H}^+ = \sum_k \epsilon_k \left( \chi_k^\dagger \chi_k - \frac{1}{2} \right), \quad (2.25)$$

$$\epsilon_k = 2\sqrt{(g - J \cos(ka))^2 + (\gamma \sin(ka))^2}.$$

Here,  $\pm\epsilon_k$  are the eigenvalues of  $h_k$ . Therefore, the interacting spin model is mapped to non-interacting fermionic quasi-particles, described by the creation/annihilation operators  $\chi_k^\dagger, \chi_k$ . To recapitulate: the possibility of (continuous) phase transitions in the spin model is encoded in the energy spectrum of  $\mathbf{H}$ .

In the fermionic formulation, we can determine the ground state (no quasi-particles), the excited states and their energies exactly. The energy gap between the ground state and lowest-lying excited state is:  $\Delta(g, J, \gamma) = \min_k[\epsilon_k]$ . It closes for  $k \rightarrow 0$  for  $g = J$  and for a finite system it scales as:

$$\epsilon_k \sim |k|, \quad \Delta(g = J, \gamma) \sim \frac{1}{L}. \quad (2.26)$$

The different gap closings are indicated in Fig. 2.4.

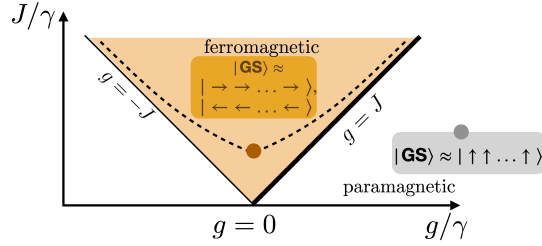


**Figure 2.4:** Phase diagram of the transverse XY model, extracted from the gap (closing) of  $\Delta(g, J, \gamma)$  for (i)  $ka \rightarrow 0$  (thick black line),  $|ka| = \pi$  (thin black line) and (ii) minimal gap at intermediate  $k$  (above dashed line) followed by a region of incommensurability [60, 61]. The (approximate) ground states for two parameter points are shown.

### Box 3: Bogoliubov transformation & ground states

The fermionic Hamiltonian can be written as a sum  $\mathbf{H} = \sum_{k>0} \mathbf{H}_{k,-k}$ , where each  $\mathbf{H}_{k,-k}$  only acts on the space spanned by  $\{|0\rangle_k, \mathbf{c}_k^\dagger \mathbf{c}_{-k}^\dagger |0\rangle_k\}$ . Here,  $|0\rangle_k$  is the vacuum state of the original operators  $\mathbf{c}_k$  (see also Refs. [11, 62]) and  $\mathbf{H}_{k,-k}$  takes the form:

$$\mathbf{H}_{k,-k} = \frac{1}{2} \begin{pmatrix} \mathbf{c}_k^\dagger & \mathbf{c}_{-k} \end{pmatrix} h_k \begin{pmatrix} \mathbf{c}_k \\ \mathbf{c}_{-k}^\dagger \end{pmatrix}. \quad (2.27)$$

The hermitian matrix  $h_k$  is a  $2 \times 2$  matrix that can be parametrized as  $h_k = \vec{\delta}_k \cdot \vec{\sigma}$  with  $\vec{\sigma}$  being the vector of Pauli matrices (not to be confused with the spin operators). Due to  $h_k^2 = |\vec{\delta}_k|^2 \mathbb{1}$ , the eigenvalues

continued on next page

continued from page before

are  $\pm\epsilon_k = \pm|\vec{\delta}_k|$  with eigenstates

$$|+\rangle_k = \begin{pmatrix} u_k \\ v_k \end{pmatrix}, \quad |-\rangle_k = \begin{pmatrix} -v_k^* \\ u_k^* \end{pmatrix}. \quad (2.28)$$

The diagonal form of  $h_k$  is given by (see also, e.g., Ref. [62])

$$U_k h_k U_k^\dagger = \epsilon_k \sigma_z, \quad U_k^\dagger = \left( (\vec{+})_k, (\vec{-})_k \right) = \begin{pmatrix} u_k & -v_k^* \\ v_k & u_k^* \end{pmatrix}. \quad (2.29)$$

Correspondingly, the operator  $\mathbf{H}_{k,-k}$  takes the form:

$$\mathbf{H}_{k,-k} = \frac{1}{2} \begin{pmatrix} \mathbf{c}_k^\dagger & \mathbf{c}_{-k} \end{pmatrix} U_k^\dagger (\epsilon_k \sigma_z) U_k \begin{pmatrix} \mathbf{c}_k \\ \mathbf{c}_{-k}^\dagger \end{pmatrix}, \quad (2.30)$$

with new creation and annihilation operators (see also Ref. [63] for more details on the properties such a Bogoliubov/fermionic transformation needs to fulfill):

$$U_k \begin{pmatrix} \mathbf{c}_k \\ \mathbf{c}_{-k}^\dagger \end{pmatrix} =: \begin{pmatrix} \boldsymbol{\chi}_k \\ \boldsymbol{\chi}_{-k}^\dagger \end{pmatrix}. \quad (2.31)$$

They fulfill, e.g.,  $\{\boldsymbol{\chi}_k, \boldsymbol{\chi}_k^\dagger\} = 1$  (using  $v_{-k} = -v_k$  and  $u_{-k} = u_k$ ). This reproduces the Hamiltonian in the quasi-particle representation given in (2.25). The ground state is the state without any quasi-particles  $\boldsymbol{\chi}_k|\text{GS}\rangle = 0 \ \forall k$ . The ground state correspondingly takes the form

$$|\text{GS}\rangle = \prod_{k>0} (u_k^* - v_k^* \mathbf{c}_k^\dagger \mathbf{c}_{-k}^\dagger) |0\rangle, \quad (2.32)$$

where the coefficients can be chosen to be real-valued:

$$\begin{pmatrix} u_k \\ v_k \end{pmatrix} = \begin{pmatrix} \cos(\theta_k/2) \\ \sin(\theta_k/2) \end{pmatrix}, \quad \tan(\theta_k) = \frac{\gamma \sin(ka)}{J \cos(ka) - g}. \quad (2.33)$$

## 2.2.2 Coarse Graining, Field Theories and Emergence of Universality

In the vicinity of a continuous phase transition, e.g., in the transverse XY model, a scaling behavior emerges *on large length scales*  $L'$  (on scales  $a \ll L' \leq \xi$ ). Additionally, the correlation length  $\xi$  itself diverges with a *universal*, critical exponent [52, 64, 65]. In the following, we argue why the phenomenon of universality emerges, which in turn is characterized by a set of critical exponents (which only depend on the dimensionality and symmetries of the system). To this end, we derive an effective description at the scale  $L'$  by integrating out degrees of freedom at shorter distances, also referred to as **coarse graining**. An intuitive version for a lattice spin system would correspond to first separating the lattice into two sublattices: every second spin corresponds to the sublattice

$B$ , whereas the remaining spins correspond to the sublattice  $A$ . Afterwards, the spins on sublattice  $B$  are traced out, giving rise to a reduced density matrix  $\rho_A = \text{tr}_B[\rho]$  on the remaining lattice  $A$  with  $L/2$  sites and lattice distance  $2a$ . With  $\rho_A$ , we can ‘only’ calculate correlations etc. for the remaining degrees of freedom (dof’s). Repeating this procedure  $n$  times, we get an effective density matrix for the remaining  $L/2^n$  lattice sites/spins. The remaining spins are defined on a lattice with a lattice distance of  $2^n a$ . Therefore, by repeating this procedure, we are describing the physics at larger and larger length scales. The general strategy for coarse graining<sup>10</sup> is to ‘sum out’ or ‘integrate out’ degrees of freedom, either at the level of the density matrix  $\rho$  (in and out of equilibrium), the partition sum  $Z = \text{tr}[\exp(-\beta\mathbf{H})]$  (in equilibrium with inverse temperature  $\beta = 1/(k_B T)$ ) or  $Z = \text{tr}[\rho]$  (in the context of Keldysh field theories) [4, 69]. In all these cases, a unifying approach is to rewrite the objects in terms of a *field theory* [4, 52, 69, 70], by inserting completeness relations of, e.g., coherent states. In the following, we consider one explicit example.

In the equilibrium setting, the partition sum is defined in terms of the trace over the Fock states (of symmetric (bosons)/anti-symmetric states (fermions)) [52]

$$Z = \sum_n \langle n | e^{-\beta\mathbf{H}} | n \rangle. \quad (2.34)$$

This is a challenge for a generic Hamiltonian with unknown eigenstates. In the following, we consider a reformulation of  $Z$  for fermion models (relevant for the transverse XY model) like the one in (2.24). However, the strategy also works for interacting theories. In both cases, the strategy is to convert the creation/annihilation operators into fields. To this end, fermionic coherent states, as eigenstates of annihilation operators  $c_l$  (or  $c_k$  in momentum space), are used. They are defined as  $c_l|\psi\rangle = \psi_l|\psi\rangle$ , where  $\psi_l$  are anti-commuting Grassmann numbers ( $\psi_l\psi_m = -\psi_m\psi_l$ ) [52]. They, again, give rise to a completeness relation, which can be inserted in (2.34) (similar to the treatment of the bosonic bath before). In this procedure, the summation over  $|n\rangle$  is exchanged for the integration over fields  $\psi_{\tau,k}$ . These fields depend on an ‘imaginary time’  $\tau$  and, e.g., the physical (quasi)momentum  $k$  (see info box). Each field configuration is weighted by an action  $S[\bar{\psi}, \psi]$ , which in case of our fermionic theory (2.24) takes the form (see also Ref. [52] for more details on this procedure):

$$S[\bar{\psi}, \psi] = \frac{1}{2} \int_0^\beta d\tau \sum_k [\bar{\Psi}_k [\partial_\tau + h_k] \Psi_k], \quad \Psi_k := \begin{pmatrix} \psi_{\tau,k} \\ \bar{\psi}_{\tau,-k} \end{pmatrix}. \quad (2.35)$$

The partition sum is given as a functional integral over all field configurations:

$$Z = \int \mathcal{D}(\bar{\psi}, \psi) e^{-S[\bar{\psi}, \psi]} \Big|_{\text{boundary condition}}. \quad (2.36)$$

---

<sup>10</sup>Such a coarse graining procedure, only considering a subset of degrees of freedom, is ubiquitous in statistical physics. As an example, the entropy of a closed quantum system will stay constant under unitary evolutions. However, the entanglement entropy between subsystems evolves and can, e.g., indicate the approach towards equilibrium [66–68].

The boundary condition is given by:  $\bar{\psi}_{0,k} = -\bar{\psi}_{\beta,k}$  and  $\psi_{0,k} = -\psi_{\beta,k}$ . It emerges from taking the trace in (2.34) and taking the Grassmann nature into account [52].

#### Box 4: Construction of the field theory

The idea behind inserting completeness relations in terms of coherent states is that objects like  $\langle \psi' | \mathbf{H} | \psi \rangle$  are straightforward to evaluate for normal ordered Hamiltonians. The completeness relation for fermionic coherent states takes the form [52]:

$$\mathbb{1}_\psi = \int \prod_l d\bar{\psi}_l d\psi_l e^{-\sum_l \bar{\psi}_l \psi_l} |\psi\rangle \langle \psi|, \quad \langle \psi' | \psi \rangle = \exp\left(\sum_l \bar{\psi}'_l \psi_l\right), \quad (2.37)$$

where the summation runs over all lattice sites (or momenta). Therefore, we can write [52]

$$Z = \sum_n \langle n | \mathbb{1}_\psi e^{-\beta \mathbf{H}} | n \rangle = \int \prod_l d\bar{\psi}_l d\psi_l e^{-\sum_l \bar{\psi}_l \psi_l} \sum_n \langle n | \psi \rangle \langle \psi | e^{-\beta \mathbf{H}} | n \rangle$$

$$\stackrel{\text{Grassmann}}{=} \int \prod_l d\bar{\psi}_l d\psi_l e^{-\sum_l \bar{\psi}_l \psi_l} \langle -\psi | e^{-\beta \mathbf{H}} | \psi \rangle. \quad (2.38)$$

To evaluate  $\langle -\psi | e^{-\beta \mathbf{H}} | \psi \rangle$ , the exponential is split into infinitesimal chunks ( $\delta = \frac{\beta}{N_\tau}$ ):

$$e^{-\beta \mathbf{H}} = \prod_{i=1}^{N_\tau} e^{-\frac{\beta}{N_\tau} \mathbf{H}} = \mathbb{1}_{\psi_{N_\tau}} e^{-\delta \mathbf{H}} \mathbb{1}_{\psi_{N_\tau-1}} e^{-\delta \mathbf{H}} \dots \mathbb{1}_{\psi_1} e^{-\delta \mathbf{H}}.$$

Each of these terms becomes simple, based on the identity (for  $\delta \rightarrow 0$ ):

$$e^{-\sum_l \bar{\psi}_{l,t} \psi_{l,t}} \langle \psi_{t+1} | e^{-\delta \mathbf{H}} | \psi_t \rangle \approx e^{\sum_l (\bar{\psi}_{l,t+1} - \bar{\psi}_{l,t}) \psi_{l,t}} e^{-\delta H(\{\bar{\psi}_{l,t+1}, \psi_{l,t}\})}. \quad (2.39)$$

Here,  $H(\{\bar{\psi}_{l,t+1}, \psi_{l,t}\})$  corresponds to  $\mathbf{H}$ , where the creation/annihilation operators have been replaced by the fields. Recombining this contribution from all chunks gives rise to the partition sum (2.36) with the action  $S$ , (2.35), in the exponential with  $\tau = t \cdot \frac{\beta}{N_\tau}$ .

#### Renormalization group:

**Abstract idea:** Given such a field theory, we can make the notion of coarse graining more precise. We consider a theory, described by couplings<sup>11</sup>  $\{g_i\}$  and fields  $\Psi_X$  ( $X = (\tau, x)$ ). We denote the short distance modes we like to integrate out as  $\Psi^<$  and the long distance modes as  $\Psi^>$ . An explicit example is the

<sup>11</sup>Containing (all) terms that are allowed by symmetry.

momentum-shell RG , where the modes are defined as [52, 64]

$$\Psi_X^< := \int_{\Lambda/b < |k| < \Lambda} \frac{dk}{2\pi} e^{ikx} \Psi_{\tau,k}, \quad \Psi_X^> := \int_{|k| < \Lambda/b} \frac{dk}{2\pi} e^{ikx} \Psi_{\tau,k},$$

relative to a momentum cutoff  $\Lambda$ . Formally, integrating out the short distance modes gives rise to a new action for the remaining degrees of freedom  $\Psi^>$ :

$$Z = \int \mathcal{D}[\Psi^<, \Psi^>] e^{-S[\Psi^<, \Psi^>, \{g_i\}]} = \int \mathcal{D}[\Psi^>] e^{-S[\Psi^>, \{g'_i\}]}. \quad (2.40)$$

The new action is formally defined as:

$$e^{-S[\Psi^>, \{g'_i\}]} := \int \mathcal{D}[\Psi^<] e^{-S[\Psi^<, \Psi^>, \{g_i\}]}, \quad (2.41)$$

whose calculation in many cases is a formidable task.

**Transverse XY:** The application to the transverse XY model in the fermionic version instead is straightforward, since the modes at different momentum scales are not coupled. We study the model in the vicinity of the gap closing ( $g \approx J$ ) for  $k \rightarrow 0$  and start from the operator perspective. In the thermodynamic limit  $L \rightarrow \infty$ , we define continuum field operators as  $\psi_k = \mathbf{c}_k \sqrt{La}$  for  $k \in [-\Lambda, \Lambda]$  and write the Hamiltonian as (for  $k \rightarrow 0$ ):

$$\mathbf{H}^+ \approx \int_{-\Lambda}^{\Lambda} \frac{dk}{2\pi} \left[ \Delta \psi_k^\dagger \psi_k + \frac{1}{2} D_1 k [\psi_k^\dagger \psi_{-k}^\dagger + \psi_{-k} \psi_k] + D_2 k^2 \psi_k^\dagger \psi_k + \mathcal{O}(k^3) \right], \quad (2.42)$$

couplings:  $\{g_0, g_1, g_2, \dots\} = \{\Delta = 2(g - J), D_1 = 2\gamma a, D_2 = Ja^2, \dots\}$ .

The corresponding field theoretic representation of the partition sum is constructed with the help of (2.35). Based on the coherent eigenstates  $\psi_Q$  of  $\psi_k$ , the action at zero temperature ( $\beta \rightarrow \infty$ ) reads ( $Q := (\tau, k)$ ) (see also Ref. [2]):

$$S = \int_{-\infty}^{\infty} d\tau \int_{-\Lambda}^{\Lambda} \frac{dk}{2\pi} \left[ \bar{\psi}_Q \partial_\tau \psi_Q + \Delta \bar{\psi}_Q \psi_Q + \frac{1}{2} D_1 k [\bar{\psi}_Q \bar{\psi}_{-Q} - \psi_Q \psi_{-Q}] \right. \\ \left. + D_2 k^2 \bar{\psi}_Q \psi_Q + \mathcal{O}(k^3) \right]. \quad (2.43)$$

Integrating out the short distance modes is feasible since  $S = S[\Psi^<] + S[\Psi^>]$ :

$$e^{-S[\Psi^>, \{g'_i\}]} := \left( \int \mathcal{D}[\Psi^<] e^{-S[\Psi^<]} \right) e^{-S[\Psi^>, \{g_i\}]}, \\ S[\Psi^>] = \int_{-\infty}^{\infty} d\tau \int_{-\Lambda/b}^{\Lambda/b} \frac{dk}{2\pi} \left[ \bar{\psi}_Q^> \partial_\tau \psi_Q^> + \Delta \bar{\psi}_Q^> \psi_Q^> + \frac{1}{2} D_1 k [\bar{\psi}_Q^> \bar{\psi}_{-Q}^> - \psi_Q^> \psi_{-Q}^>] \right. \\ \left. + D_2 k^2 \bar{\psi}_Q^> \psi_Q^> + \mathcal{O}(k^3) \right] + \text{const.}$$

The follow-up conceptual idea is to *compare* this coarse grained action with the original one. However, in its current form the length scales etc. are different (the ‘resolution’ has changed). Therefore, the action is rescaled according to

$$\begin{aligned} \text{rescaling of space/time: } & x \rightarrow b \cdot x, \quad \tau \rightarrow b^z \cdot \tau, \quad k \rightarrow b^{-1} \cdot k, \\ \text{rescaling of the field: } & \Psi_Q^> \rightarrow b^\chi \cdot \Psi_Q, \end{aligned}$$

with  $z$  the dynamical critical exponent relating space and time. The rescaling restores the original cutoff  $\Lambda$  and the coarse grained and rescaled action reads:

$$\begin{aligned} Z = & \underbrace{Z_{<}}_{\text{global prefactor from integrated out modes}} \times \\ & \int \mathcal{D}[\Psi] \exp \left( - \int_{-\infty}^{\infty} d\tau \int_{-\Lambda}^{\Lambda} \frac{dk}{2\pi} b^{2\chi-1} \bar{\psi}_Q \partial_\tau \psi_Q + b^{2\chi+z-2} \frac{1}{2} k D_1 [\bar{\psi}_Q \bar{\psi}_{-Q} - \psi_Q \psi_{-Q}] \right. \\ & \left. + b^{2\chi-1+z} \Delta \bar{\psi}_Q \psi_Q - k^2 D_2 b^{2\chi-3+z} \bar{\psi}_Q \psi_Q + \mathcal{O}(b^{2\chi+z-(n+1)} k^n) \right). \end{aligned}$$

**Abstract idea:** The smallest length scale of the coarse grained model is  $b \cdot a$ , where  $b > 1$  parametrizes the coarse graining. Therefore, the correlation length, measured in terms of this enlarged length scale, is reduced by  $b$ :  $\xi \rightarrow \xi/b$  (it is measured in rescaled units). To compare the model before and after this step, the coarse grained version is also rescaled. We denote the *renormalized* couplings and fields as  $\{\hat{g}_i^{(b)}\}$  and  $\Psi_b$ . Here we use *dimensionless* couplings (indicated by a hat), such that the process reads:

$$\begin{aligned} \text{microscopic model: } & (\Psi = \Psi^> + \Psi^<, \{\hat{g}_i\}, S[\Psi, \{\hat{g}_i\}] | \text{not coarse grained}) \\ & \downarrow \\ \text{renormalized model: } & (\Psi_b, \{\hat{g}_i^{(b)}\} = R_b[\{\hat{g}_i\}], S[\Psi_b, \{\hat{g}_i^{(b)}\}] | \text{coarse grained by factor } b). \end{aligned}$$

The computationally heavy part, related to calculating (2.41), is encoded in the ‘RG transformation’  $R_b$  [64]. Repeating the renormalization step for two rescaling factors  $b_1$  and  $b_2$  should give rise to a single rescaling with  $b_1 b_2$  (equivalently to calculating the reduced density matrix, where tracing out two subsystems successively is the same as tracing out both jointly). Therefore, the transformation has the property  $R_{b_1} R_{b_2} = R_{b_1 b_2}$  [64]. A special scenario arises once the effective description is not changing anymore under renormalization:

$$\{\hat{g}_i^*\} = R_b[\{\hat{g}_i^*\}]. \quad (2.44)$$

Such a *fixed point* of the RG can have different meanings: (i) the correlation length can be infinite, corresponding to a *critical point* (the special case we have mentioned before) or (ii) the correlation length is zero (corresponding to a ‘bulk’ phase) [64]. Note that these are the only two options since under the RG transformations, the correlation length always shrinks (in the new units) [64].

**Transverse XY:** The (possible) fixed points in this model depend on the choice of the rescaling factors  $\chi, z$ . For (i)  $2\chi - 1 = 0$  and (ii)  $z = 1$ , the temporal

and the leading spatial derivative term are invariant under rescaling (see also Ref. [2]). This results in a scale invariant fixed point theory once the gap vanishes  $\Delta = 0$ <sup>12</sup> [2]:

$$S_{\text{crit}}^* = \int d\tau \int \frac{dk}{2\pi} \bar{\psi}_Q \partial_\tau \psi_Q + \frac{1}{2} k D_1 [\bar{\psi}_Q \bar{\psi}_{-Q} - \psi_Q \psi_{-Q}]. \quad (2.45)$$

In particular, the only remaining coupling is  $D_1$ . Based on  $D_1$  and the cutoff  $\Lambda$ , we define *dimensionless* couplings in a two-step process:

1. Rescaled couplings (using  $D_1$ ):  $\Delta' = \frac{g-J}{\gamma a}$  and  $D'_j = \frac{D_j}{2\gamma a}$ .
2. Dimensionless couplings (using  $\Lambda$ ):  $\hat{\Delta} = \Delta' \Lambda^{-1}$  and  $\hat{D}_j = D'_j \Lambda^{-\dim[D_j]}$ .

The couplings and their dimensions (in terms of  $[k]$ ) are summarized in Tab. 2.1. In the vicinity of the critical point, the set of dimensionless couplings and cor-

microscopic	rescaled	(dimensionful)	scaling dim.	dimensionless
$t$	$t' = 2\gamma a t$	$[t'] = [k]^{-1}$		$\hat{t} = 2\gamma t$
$\psi_k = c_k \sqrt{L} a$	$\psi'_k = \psi_k$	$[\psi'_k] = [k]^{-1/2}$		$\hat{\psi}_k = c_k \sqrt{L}$
$D_1 = 2\gamma a$				
$\Delta = 2(g - J)$	$\Delta' = \frac{g-J}{\gamma a}$	$[\Delta'] = [k]$	+1	$\hat{\Delta} = \frac{2(g-J)}{2\gamma}$
$D_2 = J a^2$	$D'_2 = \frac{J}{2\gamma} a$	$[D'_2] = [k]^{-1}$	-1	$\hat{D}_2 = \frac{J}{2\gamma}$
$D_n = \dots$	$D'_n = \frac{D_n}{2\gamma a}$	$[D'_n] = [k]^{-(n-1)}$	$-(n-1)$	$\hat{D}_n = D'_n \Lambda^{n-1}$

**Table 2.1:** Overview of the operators and couplings in the fermionic theory for the microscopic model (2.42), its rescaled, and dimensionless version. The corresponding couplings and dimensions ( $a$ : lattice spacing) are given, where  $[k]$  denotes the dimension of momentum. Here we used  $\Lambda = 1/a$  as the scale to define the dimensionless couplings (e.g.,  $\hat{k} = ka$ ).

responding fixed point are:

$$\text{couplings: } \vec{\hat{g}} = \begin{pmatrix} \hat{\Delta} \\ \hat{D}_2 \\ \vdots \end{pmatrix}, \quad \text{fixed point: } \vec{\hat{g}}^* = \begin{pmatrix} 0 \\ 0 \\ \vdots \end{pmatrix}. \quad (2.46)$$

**Abstract idea:** The RG transformations in the vicinity of a critical point give rise to the universal scaling behavior. To see this, we consider the RG transformation in the vicinity of a critical point  $\vec{\hat{g}}^*$ , where the deviation  $\delta\vec{\hat{g}} := \vec{\hat{g}}^* - \vec{\hat{g}}$  is small [64]:

$$R_b[\{\hat{g}_n\}] = \{\hat{g}_n^{(b)}\} \quad \text{with: } \hat{g}_n^{(b)} \approx \hat{g}_n^* + \underbrace{\sum_l \frac{\partial \hat{g}_n^{(b)}}{\partial \hat{g}_l} \Big|_{\vec{\hat{g}}=\vec{\hat{g}}^*} \cdot \delta\hat{g}_l}_{=: (M_b \cdot \delta\vec{\hat{g}})_n}. \quad (2.47)$$

The behavior close to a critical point is therefore solely determined by the eigenvalues (and eigenvectors) of the matrix  $M_b$ . According to the same argument as

<sup>12</sup>For  $\Lambda \rightarrow \infty$  or  $a \rightarrow 0$ .

before, this matrix fulfills:  $M_{b_1} M_{b_2} = M_{b_1 b_2}$ . This behavior also holds true for the eigenvalues  $\{\lambda_b^{(\alpha)}\}$  of  $M_b$ , which in turn can be written as  $\{\lambda_b^{(\alpha)} = b^{y_\alpha}\}$ . In this form, the *critical exponents*  $y_\alpha$  are independent of  $b$  and, together with the eigenvectors, encode the behavior in the vicinity of the critical point. To clarify the implication for a microscopic model, we write each *microscopic* coupling (understood as a vector) as a linear combination of the effective couplings  $\tilde{g}_\alpha$  (the eigenvectors of  $M_b$ ). The behavior of  $\tilde{g}_\alpha$  depends on the *sign* of  $y_\alpha$ <sup>13</sup>:

- **relevant coupling** with  $y_\alpha > 0$ : the corresponding coupling will grow (relative to the fixed point) for larger  $b$ .
- **irrelevant coupling** with  $y_\alpha < 0$ : the corresponding coupling will shrink for larger  $b$ .

Physically, only very few couplings will be relevant and determine the leading behavior. In turn, much of the microscopic information is irrelevant for the behavior at large distances - the origin of universality. The set of irrelevant couplings spans a *basin of attraction*: each set of microscopic parameters inside the basin will flow to the *same* fixed point (same critical theory, see Fig. 2.5). In the following, we will denote  $y_\alpha$  as the *scaling dimension*  $\dim[\tilde{g}_j]$  of the operator/coupling  $\tilde{g}_j$ . The full set of all relevant and irrelevant scaling dimensions (and their corresponding operators) are defined as a *universality class*.

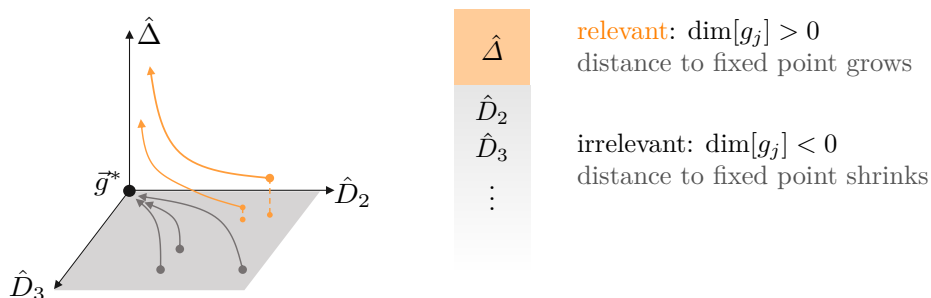


**Figure 2.5:** Concept of universality (here: Ising universality class) defined by the (infinite) set of relevant and irrelevant couplings and sketch of the RG ‘flow’ (for larger and larger  $b$ ) for different initial couplings. The gray ones lie in the basin of attraction of the fixed point.

**Transverse XY:** Looking back at Tab. 2.1, the RG transformations for the transverse XY model have the form:

$$R_b[\hat{\Delta}] = \hat{\Delta} \cdot b^{+1}, \quad R_b[\hat{D}_n] = \hat{D}_n \cdot b^{-(n-1)}. \quad (2.48)$$

The gap  $\hat{\Delta}$  is the relevant coupling in this setting, growing away from the fixed point (see Fig. 2.5). The remaining derivative couplings are irrelevant at large distances. Practically, this means that a different microscopic spin model with, e.g., additional next-nearest neighbor interactions etc. can have the *same* scaling

<sup>13</sup>There is also the possibility of marginal couplings with  $y_\alpha = 0$ , which will not be our main focus.

behavior in the vicinity of the critical point. An example would be an additional  $g_2$ -term, as given in Tab. 2.2. In Tab. 2.2, different spin terms and their scaling dimensions are given<sup>14</sup>.

scaling dim.	spin operator	fermionic action
$\dim[g_0] = 1$ :	$-g_0 \sum_l \sigma_l^z$	$\sim k^0 \bar{\psi}_{\tau,k} \psi_{\tau,k}$
$\dim[g_1] = -1$ :	$g_1 (\sum_l \sigma_l^z + \sum_l (\sigma_l^x \sigma_{l+1}^x + \sigma_l^y \sigma_{l+1}^y))$	$\sim k^2 \bar{\psi}_{\tau,k} \psi_{\tau,k}$
$\dim[g_2] = -1$ :	$g_2 (\sum_l \sigma_l^z + \sum_l \sigma_{l+1}^z (\sigma_l^x \sigma_{l+2}^x + \sigma_l^y \sigma_{l+2}^y))$	$\sim k^2 \bar{\psi}_{\tau,k} \psi_{\tau,k}$
kept fixed:	$\gamma \sum_l (\sigma_l^x \sigma_{l+1}^x - \sigma_l^y \sigma_{l+1}^y)$	$\sim k^1 \psi_{\tau,k} \psi_{\tau,-k} + \text{conj.}$
$\dim[g_x] = \frac{1}{8}$	$g_x \sum_l \sigma_l^x$	(non-local)
$\dim[J_z] = -2$	$J_z \sum_l \sigma_l^z \sigma_{l+1}^z$	$\sim \bar{\psi}_X (\partial_x \bar{\psi}_X) (\partial_x \psi_X) \psi_X$

**Table 2.2:** Spin operators and their scaling dimensions (with  $X = (\tau, x)$ ). The gray marked terms map to non-local and/or non-quadratic fermions [2].

Note that for this simple model, there is no need for linearization as the transformations are already linear:  $R_b[\hat{g}_j] = \hat{g}_j \cdot b^{\dim[g_j]}$  and we can directly read off the scaling dimensions (see Fig. 2.6). A reduced part of this coupling space is shown in Fig. 2.6 with the ‘transversal’ direction given by  $\hat{\Delta}$  and ‘longitudinal’ directions  $\hat{D}_2, \hat{D}_3, \dots$  (spanning the basin of attraction). In a last step, we can reformulate the RG transformation in a continuous way by rewriting  $b = e^s$  and sending  $s \rightarrow 0$ :

$$\underbrace{\hat{D}_n(b)}_{R_b[\hat{D}_n]} - \hat{D}_n \stackrel{s \rightarrow 0}{\approx} \hat{D}_n \cdot (1 - (n-1)s) - \hat{D}_n$$

RG flow equation:  $\partial_s \hat{D}_n(s) \approx -(n-1) \cdot \hat{D}_n = \dim[D_n] \cdot \hat{D}_n.$

The corresponding differential equation is referred to as a *flow equation*.

**Origin of scaling - transverse XY model:** In the transverse XY model, the transverse field  $g$  allows us to cross the phase transition - it is a relevant coupling associated with  $\hat{\Delta}$ . The leading behavior of the correlation length  $\xi_{\text{eq}}$  depends on this coupling:  $\xi_{\text{eq}}(\hat{\Delta})$ . Or to put it more precisely: it depends on the distance to the critical point  $\delta \hat{\Delta} = \hat{\Delta} - \hat{\Delta}^* = \hat{\Delta}$ . Physically,  $\xi_{\text{eq}}$  is the scale beyond which we do *not* expect a universal scaling behavior anymore. Therefore, we can extract  $\xi_{\text{eq}}$  from the breakdown of the linearized analysis above. The analysis is valid for  $|\delta \hat{\Delta}| \ll 1$ , but an initially finite coupling  $\hat{\Delta} \neq 0$  will grow  $R_b[\hat{\Delta}] = \hat{\Delta} \cdot b^{y_\Delta}$  with  $y_\Delta > 0$ . Once  $R_{b^*}[\hat{\Delta}] \approx 1$  (see Fig. 2.6(mid)), the analysis breaks down, translating into a scale:

$$\xi_{\text{eq}}(\hat{\Delta}) \sim \hat{\Delta}^{-\frac{1}{y_\Delta}} = \hat{\Delta}^{-1}. \quad (2.49)$$

From this analysis, the critical exponent for the quantum Ising transition in one dimension are given by (compare to (2.18) again) [2]:

$$\text{quantum Ising universality: } z = 1, \quad \nu = 1. \quad (2.50)$$

<sup>14</sup>The scaling of  $g_x \sum_l \sigma_l^x$  can be inferred from, e.g., the scaling of  $\langle \sigma_l^x \sigma_{l+n}^x \rangle$  [2].

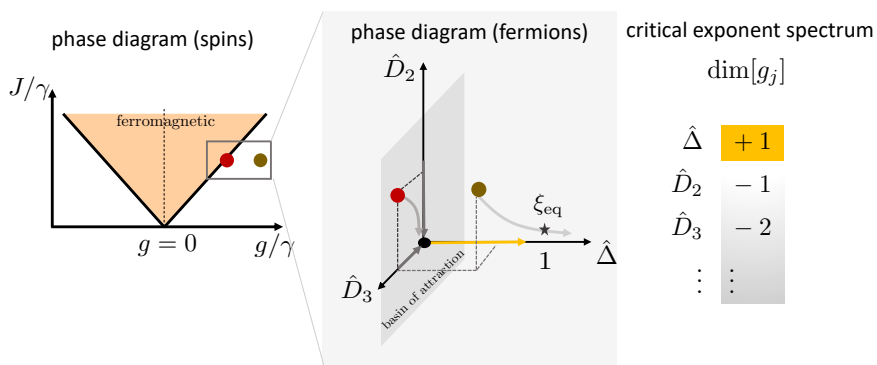


**Figure 2.6:** Sketch of the phase diagram of the transverse XY model, expressed in terms of the spin couplings (left) and a subset of the corresponding fermionic couplings (middle). In the fermionic version, the axes point in the eigendirections of the linearized flow. The scaling dimensions of the corresponding couplings are given to the right. The two marked points correspond to (i) a point close to criticality ( $\bullet$  brown) and (ii) a point at criticality ( $\bullet$  red; lying inside the basin of attraction). The corresponding RG flow is sketched in the middle.

**Connection to the spin couplings:** Since we understand the scaling of the fermionic couplings (which directly define the eigendirections of the linearized RG flow), we can expand the spin couplings in terms of the fermionic ones to obtain their leading scaling behavior. As we see from the phase diagram in Fig. 2.4, both spin couplings  $g$  and  $J$  can be used to tune over the transition (with  $\hat{\Delta} = (g-J)/\gamma$ ). Therefore, both are relevant. However,  $J$  corresponds to a combination of relevant and irrelevant couplings. The first subleading coupling  $\hat{D}_2$  (in the limit  $k \rightarrow 0$ ) can be varied by changing  $J/\gamma$  while keeping  $g - J$  constant:

$$\hat{\Delta} \approx \frac{g - J}{\gamma}, \quad \hat{D}_2 \approx \frac{J}{2\gamma}$$

(see also Tab. 2.2 again).

**Remark:** The RG analysis is done with respect to a chosen fixed point. The corresponding scaling dimensions and the dynamical critical exponent  $z$  are directly linked to the scaled out coupling of the critical theory. For the equilibrium transverse XY model, the Ising critical theory  $S^*$  contains the first order temporal and spatial derivative terms, where we scaled out  $D_1$ . Later on, we will also encounter two different scenarios: (i) by fine tuning, the couplings  $D_1, D_2$  will be absent and the leading derivative coupling is  $D_3$ . In turn, the critical theory is described by  $z = 3$ ; (ii) in a quenched scenario where  $D_1$  is driven ( $D_1 \rightarrow D_1(t)$ ), such that this coupling *cannot* be scaled out. The resulting theory has a dynamical critical exponent  $z = 2$ .



# 3 | Generalized Kibble-Zurek Mechanism in Spin and Fermion Models

The main results of this chapter have been published in the publication [42] (they are in large parts adapted in the following summary and in particular in Secs. 3.3, 3.4 and beginning of Sec. 3.5 and partly in Secs. 3.1-3.2). The following sections contain an adapted and partly extended discussion.

The KZM [13–15] describes the interplay of the universal equilibrium physics (determined by  $\mathbf{H}(\{g_i\})$  in the quantum setting) in the vicinity of a critical point and a slow drive of the system parameters  $\mathbf{H} \rightarrow \mathbf{H}(\{g_i(t)\})$  close to it. A typical scenario is a ‘transversal’ drive, starting in the ground state of the symmetric phase and running into the symmetry broken phase (see, e.g., Ref. [11]). In terms of couplings, such a drive can take the form  $g_j(t) - g_{j,c} = v_j t^n$  (‘order  $n$  drive’), where  $g_{j,c}$  is the coupling at the critical point. It is parametrized by a ‘generalized’ velocity  $v_j$ , which is slow in the sense of its dimensionless version being small:  $\hat{v}_j \ll 1$ . Outside the critical region, deep in a gapped phase ( $\hat{\Delta} \gg 1$ ), the evolution will be *adiabatic*: a state initially prepared in the ground state will stay in the ground state during the time evolution  $|\psi(t)\rangle \approx |\text{GS}(t)\rangle$ . In contrast, close to the phase transition and the gap closing, the equilibrium correlation length (and time) are diverging. Even a slow drive will inevitably break adiabaticity - being ‘fast’ compared to the equilibrium scales - with  $|\psi(t)\rangle \neq |\text{GS}(t)\rangle$ . Even though the time evolution cannot break the global symmetry, the breaking of adiabaticity is reflected in the emergence of *locally* symmetry-broken domains. The average size of these domains induce a finite, observable length scale  $\xi^*$  in the system. This scale can also be inferred from the density of ‘defects’, separating the domains [15, 71].

This *finite* length  $\xi^*$  signals that the drive was *diabatic* close to the transition, hindering the time evolved state from adapting the diverging correlation length of the ground state close to the transition. Nevertheless,  $\xi^*$  can be used to extract the universal equilibrium critical exponents. For a coupling  $g_0$ , relevant at equilibrium, the ground state correlation length scales as  $\xi_{\text{eq}} \sim |g_0 - g_{0,c}|^{-1/\nu}$ . Once  $g_0$  is driven with an order  $n$  drive and ‘velocity’  $v_0$ , the induced scale  $\xi^*$

depends algebraically on  $v_0$  with an exponent depending on  $z, \nu$  [72–75]:

$$\xi^* \sim v_0^{-\frac{1}{nz+1/\nu}}.$$

To estimate this scaling of  $\xi^*$ , we assume that the evolution is adiabatic initially, such that the state  $|\psi(t)\rangle$  follows the ground state. At some point in time  $t^*$ , adiabaticity will be broken. The system is essentially frozen in the state  $|\text{GS}(t^*)\rangle$ , which is characterized by the finite correlation length  $\xi^*$ . Therefore,  $\xi^*$  can be estimated by determining the adiabaticity breaking time  $t^*$ . To do so, we compare the two available time scales: (i) the rate of change of the coupling, given by  $|(g_0(t) - g_{0,c})/\dot{g}_0| \propto t$ , and (ii) the equilibrium correlation time  $\xi_\tau(t) \sim \Delta^{-1}(t)$ . As long as  $t \gg \xi_\tau(t)$ , the system is essentially adiabatic. The onset of adiabaticity breaking is signalled by  $\xi_\tau(t^*) \approx t^*$ , see Fig. 3.3(b). At this point in time, the spatial correlation length is estimated to be<sup>1</sup>

$$\xi^* = \xi_0 \sim v_0^{-\frac{1}{nz+1/\nu}}. \quad (3.1)$$

This heuristic perspective can be complemented by a RG consideration [41]. In the adiabatic regime, the physical properties are still encoded in the zero temperature partition sum  $Z(g, J, \gamma) \rightarrow Z(g(t), J(t), \gamma(t))$  (encoding the ground state properties for the transverse XY model). In the RG, the equilibrium couplings as well as the new velocity couplings are scale dependent. The adiabatic description breaks down once the velocity couplings grow large. The length scale of the breakdown corresponds to  $\xi^*$ . Furthermore, the RG indicates that even driven couplings that are *irrelevant* at equilibrium can lead to adiabaticity breaking [41], generalizing the aforementioned KZM scenario. The idea is that any coupling  $g_j$  with scaling dimension  $\text{dim}[g_j]$  that is driven according to  $v_j t^n$  gives rise to a length scale

$$\xi_j \sim v_j^{-\frac{1}{nz+\text{dim}[g_j]}}. \quad (3.2)$$

Once  $nz + \text{dim}[g_j] > 0$ , this scale grows large in the limit of slow drives and can become observable.

In this chapter, we complement the abstract RG prediction of the scales  $\xi_j$  with an analysis of paradigmatic spin/fermion models (in particular the transverse XY model). In these models, we extract the observable consequence of adiabaticity breaking - a finite excitation density - and its scaling with the drive velocities of relevant *and* irrelevant couplings. Depending on the drive protocol, we consider the competition of three scales: (i) the equilibrium length scale  $\xi_{\text{eq}}$ , (ii) the KZM length scale  $\xi_\perp$ , resulting from a drive *across* the transition, and (iii) the length scale due to a drive *parallel* to the phase boundary, corresponding to a drive of an irrelevant coupling (see also Fig. 3.2(a)). The *observable* length scale is determined by the smallest of those scales:

$$\xi^* \sim \min[\xi_{\text{eq}}, \xi_\perp, \xi_\parallel]. \quad (3.3)$$

In case of  $\xi^* \sim \xi_{\text{eq}}$  the drive is adiabatic and we refer to this scenario as adiabaticity restoring.

---

<sup>1</sup>Based on the scaling of the correlation time:  $\xi_\tau \sim |g_0 - g_{0,c}|^{-z\nu}$  and  $g_0 - g_{0,c} = v_0 t^n$ .

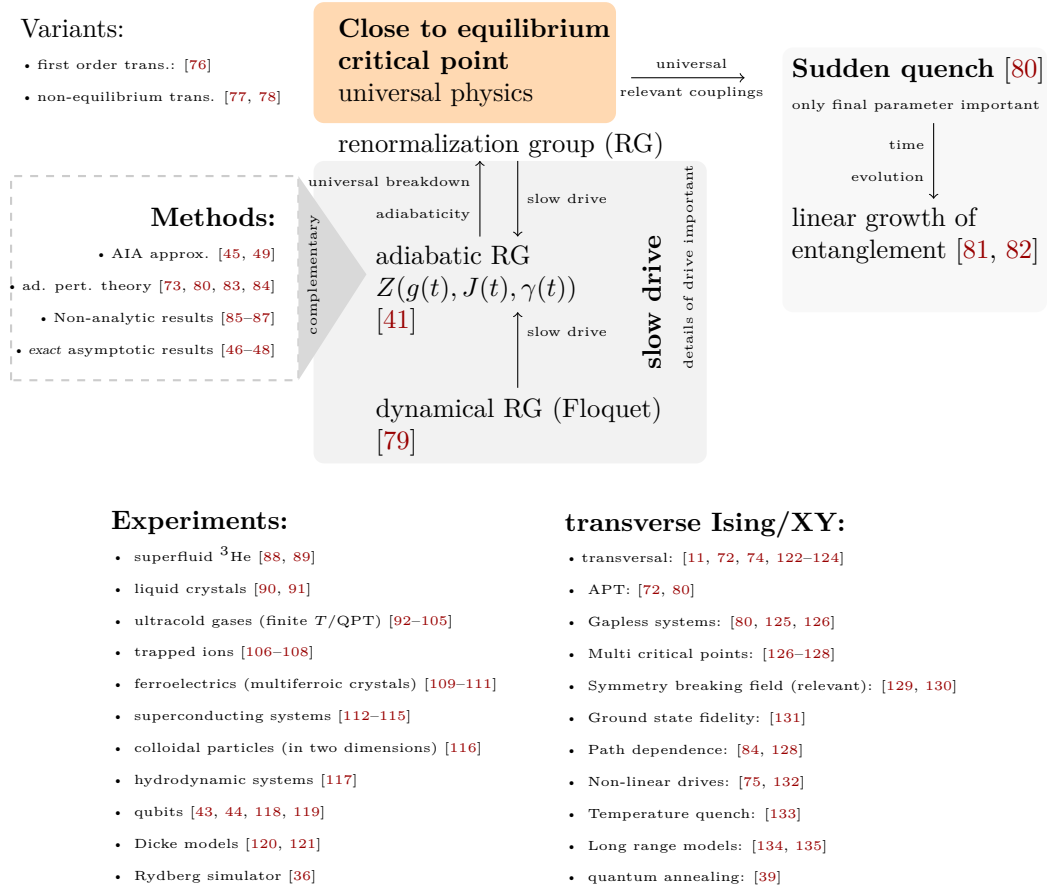


**Figure 3.1:** Fraction of the KZM (literature) landscape relevant for this chapter (APT: adiabatic perturbation theory).

We demonstrate the generalized KZM for two spin models: the transverse XY model ( $z = 1$ ) and an effective description of an *extended* XY model ( $z = 3$ ). In both cases an order  $n$  drive is used, where the driven couplings are one relevant coupling (with  $v_{\perp}$ ) and one irrelevant coupling (with  $v_{\parallel}$ ). The different kind of drives are shown in Fig. 3.2(a). The model class of transverse XY/Ising models is well-studied and many different drive scenarios have already been analyzed, see Fig. 3.1 for an overview. Nevertheless, on the one hand, the RG perspective gives a unified framework to explain many of the observations in those models. On the other hand, the observable scaling due to equilibrium *irrelevant* coupling is a novel aspect, completing existing drive protocols. Two approaches that are related to our investigation are:

- **Drives along critical lines** [61, 125, 126, 132]: depending on the driven coupling, such a drive either corresponds to (i) a special case of the drive (3) in Fig. 3.2(a), or (ii) the drive of the coupling of the equilibrium fixed point theory as in Ref. [125]. The scenario (i) is only realized *once the driven coupling corresponds to the drive of an equilibrium irrelevant coupling* and will be our focus.

- **Adiabaticity restoring** due to the presence of a small symmetry breaking field as studied in Ref. [129]. Such a field corresponds to another relevant coupling. Its presence keeps the correlation length  $\xi_{\text{eq}}$  *finite*, competing with the drive scale of a transversal drive  $\xi_{\perp}$ .

Summary of the main results:

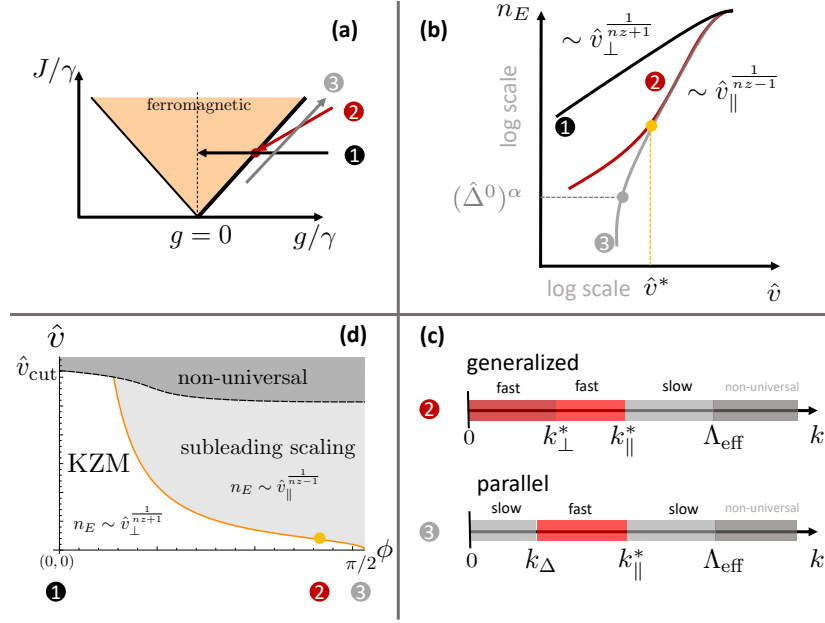


**Figure 3.2:** Conceptual overview of the generalized KZM: (a) Drive scenarios: (1) transversal drive crossing the transition (‘velocity’  $v_{\perp}$ ); (2) generalized drive ending/starting at the transition ( $v_{\perp}$  and  $v_{\parallel}$ ); (3) longitudinal/parallel drive ( $v_{\parallel}$ ) with a finite gap  $\hat{\Delta}^0$  during the drive. (b) Algebraic scaling behavior of the excitation density  $n_E$  as a function of the drive speed and for the different protocols. A transversal drive gives rise to the leading scaling, whereas a generalized drive has two scaling regimes (separated by  $\hat{v}^*$ ). The scaling regime of the parallel drive is limited to finite velocities by the finite gap  $\hat{\Delta}$ . (c) Depending on the momentum scale  $k$ , the different drives are either effectively slow or fast (indicating adiabaticity breaking, onset denoted by  $k^*$ ). For a parallel drive, the finite gap restores adiabaticity for  $k \ll k_{\Delta}$ . (d) Schematic scaling regimes of the excitation density  $n_E(\hat{v}, \phi)$ , parametrized by the drive angle (in the fermion model). For  $\hat{v} \rightarrow 0$ , the KZM scaling emerges, separated from the subleading scaling by the crossover velocity  $\hat{v}^*(\phi)$  (orange line). For velocities  $\hat{v} \gg \hat{v}_{\text{cut}}(\Lambda_{\text{eff}})$  no universal behavior is expected.

**Generalized drives - Competing drive scales:** The generalized drives of order  $n$  are based on  $v_{\perp}, v_{\parallel}$  and reach and/or cross the critical point in the spin models, scenario ② in Fig. 3.2(a). Therefore, adiabaticity is inevitably broken (with  $\xi_{\text{eq}} \gg \xi_{\perp}, \xi_{\parallel}$ ) even for slow drives. Here, the notion of slow ‘microscopical’

velocities refer to their dimensionless<sup>2</sup> versions as being small:  $\hat{v}_\perp, \hat{v}_\parallel \ll 1$ . The breaking of adiabaticity is signalled by a finite correlation length  $\xi^*$ . It manifests in a finite density of excitations  $n_E$ , like spin flips (paramagnetic phase) or domain walls (ferromagnetic phase):  $\xi^* \sim n_E^{-1}$ . To infer the long distance behavior, both spin models are mapped to non-interacting fermions via a Jordan-Wigner transformation. In both cases, the fermionic Hamiltonian takes the form  $\mathbf{H} = \sum_{k>0} \mathbf{H}_{k,-k}$  with time evolved states  $|\psi(t)\rangle = \bigotimes_{k>0} |\psi_{k,-k}(t)\rangle$ . Therefore, different momentum sectors decouple and we can study adiabaticity breaking at each length scale (or momentum scale  $k$ ) individually. The breaking of adiabaticity is signalled by a significant population of the excited states. The total excitation density is given by

$$n_E(v_\perp, v_\parallel) = \frac{1}{L} \sum_k p_k(v_\perp, v_\parallel), \quad p_k = |\langle \psi_{k,-k} | \mathbf{E}_{k,-k} \rangle|^2,$$

where  $p_k$  corresponds to the excitation probability at momentum  $k$ . Adiabaticity breaking at momentum  $k$  is signalled by  $p_k \sim \mathcal{O}(1)$  and is associated with an *effectively* fast drive. At each  $k$ , we can associate effective velocities  $\hat{v}_k^{(j)}$  ( $j \in \{\perp, \parallel\}$ ) with the bare velocities  $\hat{v}_\perp, \hat{v}_\parallel$ . The effective velocities will grow for  $k \rightarrow 0$ , indicating adiabaticity breaking once  $\hat{v}_k^{(j)} \approx 1$ :

$$\left. \begin{array}{l} \hat{v}_k^{(j)} \gg 1 \quad \Leftrightarrow \quad p_k \sim \mathcal{O}(1), \\ \hat{v}_k^{(j)} \ll 1 \quad \Leftrightarrow \quad p_k \ll 1 \end{array} \right\} \hat{v}_k^{(j)} \approx 1 \quad \Rightarrow \quad k_j^* \sim v_j^{\frac{1}{n_z + \dim[g_j]}}. \quad (3.4)$$

Therefore, the drive is effectively fast for sufficiently small momenta ( $|k| < k_j^*$ ), with the observable excitation density scalings as:

$$n_E(v_\perp, v_\parallel) = \frac{1}{L} \sum_k p_k \sim \max[k_\perp^*, k_\parallel^*] \sim (\min[\xi_\perp, \xi_\parallel])^{-1}. \quad (3.5)$$

In summary, the dynamics of the states  $|\psi_{k,-k}(t)\rangle$  can be classified as either: (i) non-universal for  $k \gg \Lambda_{\text{eff}}$ , (ii) universal ( $k \ll \Lambda_{\text{eff}}$ ) but slow ( $|\hat{v}_k| \ll 1$ ), and (iii) universal and fast ( $|\hat{v}_k| \gg 1$ ), see Fig. 3.2(c). The last two cases are separated by the onset of adiabaticity breaking at  $k \sim k^*$ . In case of two driven couplings, there are also two scales:  $k_\perp^*$  and  $k_\parallel^*$ . Only for  $k_\parallel^* \gg k_\perp^*$  the scaling due to the longitudinal drive becomes observable (see again (3.5) and Fig. 3.2(c)). A convenient way to parametrize the drive in terms of dimensionless couplings is:

$$\vec{\hat{v}} = \hat{v}_\perp \vec{e}_\Delta + \hat{v}_\parallel \vec{e}_{D_2} = \hat{v} \begin{pmatrix} \cos(\phi) \\ \sin(\phi) \end{pmatrix}. \quad (3.6)$$

In this setting, the choice of  $\phi$  (how steeply we approach the transition) sets a crossover velocity  $\hat{v}^*(\phi)$  defined by  $k_\parallel^* \approx k_\perp^*$ , such that the excitation density  $n_E(\hat{v}, \phi)$  is either dominated by (i) the drive of the subleading coupling for  $1 \gg \hat{v} \gg \hat{v}^*(\phi)$  or (ii) the leading coupling for  $\hat{v} \ll \hat{v}^*(\phi)$ . A schematic overview plot is shown in Fig. 3.2(d).

<sup>2</sup>The dimensionless velocities are determined from the two-step process: (i) rescaling with the leading derivative coupling  $D_z$  and (ii) forming dimensionless combination using the cutoff  $\Lambda$ .

**Parallel drive - Competing drive and equilibrium scales:** Since the drives above either cross or at least reach the critical point, the equilibrium scale  $\xi_{\text{eq}} \sim \hat{\Delta}^{-1}$  is not observable in the dynamic setting (in the thermodynamic limit). A different scenario is the drive *parallel* (with  $v_{\parallel}$ ) to the phase boundary, while keeping a constant distance to it (see ③ in Fig. 3.2(a)). In this case,  $\xi_{\text{eq}}$  is *finite* based on  $\hat{\Delta}(t) = \hat{\Delta}^0 = \text{const.}$ . Therefore, the finite correlation length  $\xi_{\text{eq}}$  can become smaller than  $\xi_{\parallel}$ , resulting in a competition. The role of  $\xi_{\text{eq}}$  is to *restore* adiabaticity at large distances, see Fig. 3.2(c). It provides an ideal testbed for the generalized KZM since the observable scaling of  $\xi^*$  as a function of  $v_{\parallel}$  is only provided by an equilibrium irrelevant coupling.

**Drive geometry - microscopic vs macroscopic couplings:** The construction of a drive is (naively) based on the phase diagram in terms of ‘microscopic’ couplings as in Fig. 3.2(a). From the geometry of the ‘microscopic’ phase diagram, a transversal drive would cross the phase boundary in a perpendicular fashion, whereas a parallel drive would run along the phase boundary. In contrast, the large distance behavior and the induced scales by the drive are inferred from the RG analysis. The geometry in the RG need not be ‘aligned’ with the geometry in terms of the microscopic couplings. The first is dictated by the *fixed point* of the flow equations. In its vicinity, effective couplings (the eigendirections of the linearized flow) can be defined with well-defined scaling dimensions. These effective couplings can be different from the microscopic couplings. In particular, they *need not be orthogonal to each other* (interpreting effective couplings as vectors in the coupling space). In this framework, a transversal drive corresponds to a drive of a relevant effective coupling. A longitudinal drive corresponds to a drive of an irrelevant effective coupling. Therefore, it is possible that a perpendicular drive in the ‘microscopic’ phase diagram can correspond to a generalized drive of a relevant *and* a subleading coupling. In contrast, driving parallel to the phase boundary is unambiguous and corresponds to a drive of a subleading coupling. We demonstrate this at the level of spin vs. fermion couplings (see also ① in Fig. 3.5, which corresponds to a purely transversal drive). Finally, we argue that the same issue arises for Wilson-Fisher fixed points in interacting theories.

### 3.1 Driven transverse XY Chain - Mechanism of Adiabaticity Breaking

In the following, we approach the KZM from different perspectives: (i) a phenomenological perspective, (ii) a RG perspective with a generalization for irrelevant couplings, and (iii) a practical implementation for spin models. A well-studied version, theoretically and experimentally, of the KZM in quantum models corresponds to the driving of the (relevant) transversal field  $g(t)$  in transverse XY and related models (see again Fig. 3.1). An example of an experimental realization in the same universality class are slow drives in Rydberg atom systems<sup>3</sup>, revealing a remarkable agreement with the theoretical predictions [36].

---

<sup>3</sup>Here, the correlation length was extracted from the density-density correlations  $C_{ij} = \langle \mathbf{n}_i \mathbf{n}_j \rangle - \langle \mathbf{n}_i \rangle \langle \mathbf{n}_j \rangle$  where  $\mathbf{n}_i$  is the projector onto the Rydberg state.

### 3.1.1 Phenomenological Perspective

We consider the aforementioned drive of the transversal field  $g(t) - g_c = v_0 t$  in the transverse XY model [11]. The drive starts at time  $t_i$  with  $g(t_i)/J \gg 1$  in the  $\mathbb{Z}_2$ -symmetric ground state and ends at  $t_f$  at  $g(t_f)/J = 0$  in the symmetry broken phase. Since the system is initialized in the ground state of  $\mathbf{H}(t_i)$ , it will stay (approximately) in the ground state as long as the drive with velocity  $v_0$  is slow compared to the time scale set by the gap  $\Delta(t)$  of the instantaneous Hamiltonian:  $\xi_\tau \sim \Delta^{-1}(t)$ . Close to the gap closing at the transition, adiabaticity will inevitably break down and the system gets excited. The symmetry of the ground state will not be broken during the unitary evolution. However, the non-adiabatic evolution results in a final state of the form<sup>4</sup>

$$|\psi(t_f)\rangle = \text{superposition}(|\rightarrow\rightarrow\rightarrow| \leftarrow\leftarrow\leftarrow | \rightarrow\rightarrow \dots\rangle). \quad (3.7)$$

The state contains locally ordered patches, separated by domain walls (marked orange) with a density:

$$n_E = \left\langle \frac{1}{L} \sum_l \underbrace{\frac{1}{2}(1 - \sigma_l^x \sigma_{l+1}^x)}_{\text{spin operators}} \right\rangle = \left\langle \frac{1}{L} \sum_k \underbrace{\chi_k^\dagger \chi_k}_{\text{fermion op.}} \right\rangle \neq 0. \quad (3.8)$$

In this limit, the density of spin defects is also equal to the quasi-particle density in the fermionic description. The average size of the domains is denoted as  $\xi^*$  and depends on the drive velocity. This length scale is directly related to the domain wall density (in one dimension<sup>5</sup>) [10]

$$\xi^* \sim n_E^{-1}.$$

The scaling of  $\xi^*$  with the drive velocity is dictated by the underlying *equilibrium* model, as argued before (see also Fig. 3.3(b)):

$$\xi^* = \xi_0 \sim v_0^{-\frac{1}{nz+1/\nu}}. \quad (3.9)$$

The finite length scale  $\xi^*$  depends on the equilibrium critical exponents  $z, \nu$  and the information of the drive (order  $n$  and the velocity  $v_0$ ).

#### Box 5: Adiabaticity breaking from a physical perspective

Physically, the system can be seen as being *frozen* in the non-adiabatic regime ('impulse regime'), unable to follow the fast time-evolved Hamiltonian. A second, more refined point of view takes the speed of quasi-particles/excitations into account. The excitations spread with a velocity, determined by their dispersion with a (maximal) velocity scale  $v \approx \xi^*/t^*$  [124, 137]. Therefore, the correlation length still grows during the "impulse" regime, which will nevertheless not change the overall scaling with the critical exponents. For an example of a fully time-resolved process see, e.g., Ref. [138].

<sup>4</sup>With  $\langle \frac{1}{L} \sum_l \sigma_l^x \rangle = 0$ .

<sup>5</sup>The generalization in  $d$  dimensions and 'defects' of dimension  $p$  is:  $n_E \sim \xi^{*(d-p)}$  [136].

**Generalized heuristics:** The aforementioned scaling behavior can be generalized as was shown in Ref. [41]: even equilibrium *irrelevant* couplings can lead to a ‘universal’ breaking of adiabaticity with an observable length scale. We can anticipate this effect from the earlier heuristic derivation, if we associate a length scale with each coupling  $g_j$  (and its dimensionless version  $\hat{g}_j$ ) according to

$$\xi \sim |\hat{g}_j - \hat{g}_j^*|^{-\frac{1}{\dim[g_j]}}. \quad (3.10)$$

Here,  $\hat{g}_j^*$  is the fixed point value of the coupling. This scale is only a relevant scale once it grows at larger distances, which is the case for relevant couplings. Nevertheless, this is *not* a necessary condition to break adiabaticity in the driven scenario. If a coupling  $\hat{g}_j$  is driven with  $\hat{v}_j \hat{t}^n$  relative to the fixed point ( $\hat{v}_j$ : generalized ‘velocity’), the same heuristic arguments as above lead to the prediction of a scaling behavior:

$$\xi_j \sim \hat{v}_j^{-\frac{1}{nz + \dim[g_j]}}. \quad (3.11)$$

Even for irrelevant couplings with  $\dim[g_j] < 0$ , a drive of sufficiently high order  $n$  can lead to a *diverging* length in the limit of a slow drive ( $\hat{v}_j \rightarrow 0$ ) once  $nz + \dim[g_j] > 0$ . Therefore, even couplings *irrelevant* at equilibrium can lead to universal breaking of adiabaticity.

### 3.1.2 Generalized Mechanism – RG Perspective

This heuristic derivation of the universal KZM scaling can also be obtained from an *adiabatic* RG analysis, summarized in Fig. 3.3. In this approach, the onset of adiabaticity breaking is signalled by the breakdown of the adiabatic description at the length scale  $\xi^*$  [41].

#### Adiabatic perspective:

A system prepared in the ground state of  $\mathbf{H}(t_i)$  will approximately stay in the ground state of  $\mathbf{H}(t)$  for an adiabatic evolution. Therefore, the thermodynamic quantities can still be obtained from the *equilibrium* partition sum, evaluated at a given point in time,  $Z(\{g_i\}) \rightarrow Z(\{g_i(t)\})$  [41]. The role of time  $t$  is comparable to an additional parameter in the equilibrium RG. Therefore, the equilibrium RG discussion, based on  $\{g_j\}$ , can be lifted to an adiabatic RG analysis *including a slow drive* with velocities  $v_j$ . The full set of couplings therefore is given by  $\{g_j, v_j\}$  (for drives of order  $n$ ). In analogy to the equilibrium case, the new couplings  $\{v_j\}$  can be classified as (i) relevant, (ii) marginal or (iii) irrelevant. The relevant ones will be responsible for adiabaticity breaking and the breakdown of the adiabatic description. As an example, we consider again the partition sum of the transverse XY model. This time, we include a slow drive of the relevant coupling  $\Delta$  with  $v_\perp t^n$  (*perpendicular* to the phase boundary) and a drive of the irrelevant coupling  $D_2$  with  $v_\parallel t^n$  (*parallel* to the phase boundary), see Fig. 3.4. To keep the notation light, we do not include the index  $n$  in the following. Repeating the three RG steps in the momentum-shell RG (including a rescaling of time as  $t \rightarrow b^z t$ ), the coarse grained description

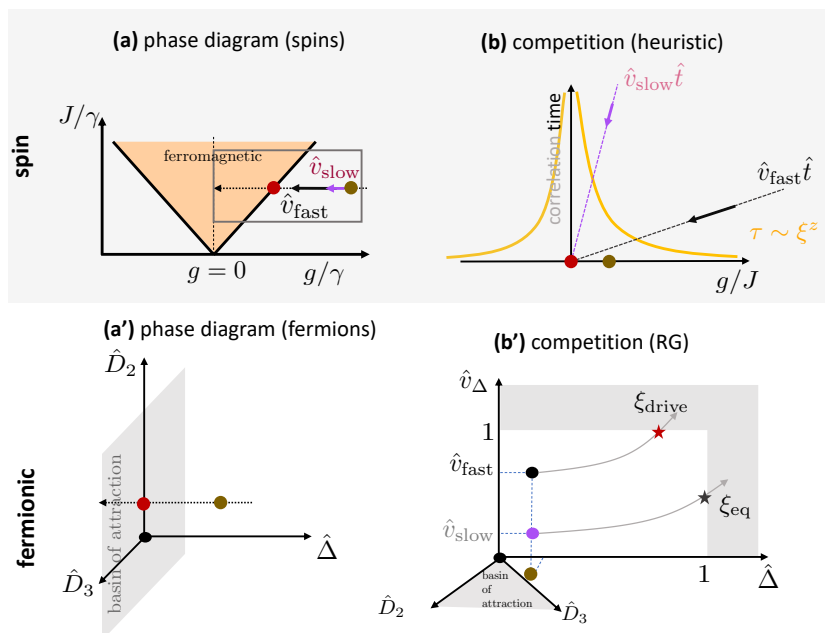


**Figure 3.3:** Overview of the Kibble-Zurek mechanism for transversal drives across a continuous phase transition ((a) spin couplings; (a') fermion couplings). (b) Two time scales compete: (i) the correlation time  $\xi_\tau$  (solid line), and (ii) the time scale of the drive (dashed in (b)). The slower the drive, the closer to the transition adiabaticity gets broken. In the fermionic version, this drive corresponds to changing a relevant coupling  $\hat{\Delta}$  in time. (b') In the adiabatic RG, this drive corresponds to a new relevant coupling  $\hat{v}_\perp = \hat{v}_\Delta$ . Depending on the value of  $\hat{\Delta}$  and the drive velocity, adiabaticity is broken (at larger scales) once  $|\hat{v}_\Delta(s)| \approx 1$  before  $|\hat{\Delta}(s)| \approx 1$ . In the reversed case, the evolution remains adiabatic. The brown dot corresponds to the undriven scenario, the black dot corresponds to  $(\hat{\Delta}, \hat{v}_{fast})$  (adiabaticity broken), and the purple dot to  $(\hat{\Delta}, \hat{v}_{slow})$  (adiabaticity unbroken).

reads:

$$\begin{aligned}
 Z(\{g_i(t)\}) = Z_{<} \times & \\
 \int \mathcal{D}[\Psi] \exp \left( - \int_{-\infty}^{\infty} d\tau \int_{-A}^A \frac{dk}{2\pi} \bar{\psi}_Q \partial_\tau \psi_Q \right. & \left. \begin{array}{l} \text{coupling} \\ \hat{\Delta} \\ \hat{v}_\perp \\ \hat{D}_2 \\ \hat{v}_\parallel \end{array} \right. \\
 + \frac{1}{2} k D_1 [\bar{\psi}_Q \bar{\psi}_{-Q} - \psi_Q \psi_{-Q}] & \left. \begin{array}{l} \text{scaling dim.} \\ +1 \\ +1 + nz \\ -1 \\ -1 + nz \end{array} \right. \\
 + (b^{+1} \Delta + b^{+1+nz} v_\perp t^n) \bar{\psi}_Q \psi_Q & \\
 - (b^{-1} k^2 D_2 + b^{-1+nz} v_\parallel t^n k^2) \bar{\psi}_Q \psi_Q & \\
 + \mathcal{O}(b^{2\chi+z-(n+1)} k^n). &
 \end{aligned}$$

The scaling dimensions and RG transformations of the drive couplings have a very similar structure compared to the equilibrium case in (2.48). Collecting the dimensionless equilibrium couplings in  $\vec{g}_{eq} = (\hat{\Delta}, \hat{D}_2, \dots)$  and the drive couplings

in  $\vec{g}_{\text{drive}} = (\hat{v}_{\Delta}, \hat{v}_{D_2}, \dots)$ , the flow equations are:

$$\partial_s \vec{g}_{\text{eq}} = M \vec{g}_{\text{eq}}, \quad \partial_s \vec{g}_{\text{drive}} = (M + nz\mathbb{1}) \vec{g}_{\text{drive}}. \quad (3.12)$$

Therefore, the (linearized) flow equations *for the drive couplings* have the same eigendirections (eigenvectors of  $M$ ) as their equilibrium counterparts but with shifted critical exponents:

$$\dim[v_j] = nz + \dim[g_j]. \quad (3.13)$$

This also applies to *interacting* models with a Wilson-Fisher fixed point [41].

---

### Adiabaticity breaking:

This adiabatic description is valid as long as the drive couplings stay small:  $|\vec{g}_{\text{drive}}| \ll 1$ . However, adiabaticity can be broken once  $|\vec{g}_{\text{drive}}(s^*)| \sim \mathcal{O}(1)$ . As an example, consider the flow of  $\hat{v}_{\perp}(s)$  based on (3.13):

$$\hat{v}_{\perp}(s^*) = \hat{v}_{\perp} e^{(nz + \dim[\Delta])s^*} = \hat{v}_{\perp} b^{*nz + \dim[\Delta]} \stackrel{!}{\approx} 1 \quad \Rightarrow \quad b^* \approx \hat{v}_{\perp}^{-\frac{1}{nz + \dim[\Delta]}}.$$

The corresponding length scale  $\xi^* \sim a \cdot b^*$  has the same scaling behavior as the heuristically derived one in (3.1). Nevertheless, for a finite distance to the critical point, the underlying equilibrium correlation length  $\xi_{\text{eq}}$  is also finite. It is determined by the growth of  $\hat{\Delta}$  at larger distances:  $|\hat{\Delta}(s^*)| \approx 1$ . For a given set of microscopic couplings  $\hat{\Delta}$ ,  $\hat{v}_{\perp}$  (two dots in Fig. 3.3(b')), two length scales emerge:

$$\begin{aligned} |\hat{\Delta}(s)| \approx 1 &\quad \Rightarrow \quad \xi_{\text{eq}} \sim \hat{\Delta}^{-\frac{1}{\dim[\Delta]}}, \\ |\hat{v}_{\perp}(s)| \approx 1 &\quad \Rightarrow \quad \xi_{\text{drive}} \sim \hat{v}_{\perp}^{-\frac{1}{nz + \dim[\Delta]}}. \end{aligned} \quad (3.14)$$

The observable behavior is determined by the smaller scale. At a given point in the phase diagram the drive is either (i) adiabatic with a correlation length  $\xi^* \sim \xi_{\text{eq}}$  or (ii) non-adiabatic with  $\xi^* \sim \xi_{\text{drive}}$ , see Fig. 3.3(b'). If more than one coupling is driven,  $\xi_{\text{drive}}$  is replaced by the individual drive scales  $\xi_j$  (see (3.2)) for each driven coupling  $g_j$ :

$$\xi^* \sim \min[\xi_{\text{eq}}, \xi_0, \xi_1, \dots]. \quad (3.15)$$

### 3.1.3 Practical Implementation for Spin Models

Our main goal in the following sections is to demonstrate (i) a competition of scales due to multiple driven couplings and (ii) the emergence of a finite length scale from driven *irrelevant* couplings in the transverse XY and related models. Therefore, we combine the phenomenological perspective (spin observables) with the RG considerations for the fermion model. Possible options to extract the correlation length  $\xi^*$  from spin observables are: (i) extract  $\xi^*$  from correlation functions like  $C_{ij}^{zz}$  or  $C_{ij}^{xx}$ , (ii) extract  $\xi^*$  from order local expectation values like the domain wall density (ferromagnetic) or spins flip density (paramagnetic) or (iii) extract  $\xi^*$  from the entanglement entropy (see, e.g., Refs. [11, 12]). The

second option is directly linked to the *fermionic* excitation density. If the drive is stopped at a vanishing transverse field  $g = 0$  (deep in the ferromagnetic phase), the fermionic excitation density corresponds to the density of domain walls, see again (3.8). If the drive is stopped deep in the paramagnetic phase ( $g - J \gg \gamma$  or  $J(g - J) \gg \gamma^2$ ), the excitation density corresponds to the density of spin flips [11]. In this regime, the quasi-particle operators are  $\chi_k \approx \mathbf{c}_k$ , such that<sup>6</sup>

$$n_E = \frac{1}{L} \left\langle \sum_k \chi_k^\dagger \chi_k \right\rangle \approx \frac{1}{L} \left\langle \sum_k \mathbf{c}_k^\dagger \mathbf{c}_k \right\rangle = \frac{1}{L} \left\langle \sum_l \frac{1}{2} (1 - \sigma_l^z) \right\rangle. \quad (3.16)$$

Therefore, we can directly relate the fermionic excitations with observable spin excitations and extract  $\xi^* \sim n_E^{-1}$  in the limiting cases. This leads to a simplification: to extract  $\xi^*$  we can entirely work with local operators in the fermionic description. Nevertheless, the drives have to be built around tuning the spin couplings  $J(t) = J_0 + v_J t^n$  and  $g(t) = g_0 + v_g t^n$  for the transverse XY model. We have already argued that driving  $g(t)$  will lead to the known KZM scaling, associated with the relevant coupling  $\hat{\Delta}$ . In contrast, driving *parallel* to the phase boundary with  $g(t) - J(t) = \text{const.}$  corresponds to a drive of the irrelevant coupling  $\hat{D}_2$ . In the limit  $k \rightarrow 0$  the drives are related as

eff. fermion couplings	eff. velocities
$\frac{g(t)-J(t)}{\gamma} \stackrel{k \rightarrow 0}{\approx} \hat{\Delta}(\hat{t}) = \hat{\Delta}^0 + \hat{v}_\perp \hat{t}^n,$	$\hat{v}_\perp \approx \frac{2(v_g - v_J)}{(2\gamma)^{n+1}},$
$\frac{J(t)}{2\gamma} \stackrel{k \rightarrow 0}{\approx} \hat{D}_2(\hat{t}) = \hat{D}_2^0 + \hat{v}_\parallel \hat{t}^n,$	$\hat{v}_\parallel \approx \frac{v_J}{(2\gamma)^{n+1}}.$

In the fermionic language, the desired drive of a relevant and an irrelevant coupling corresponds to the time dependent dimensionless Hamiltonians for each momentum sector ( $k, -k$ ) (see again (2.24)):

$$\hat{h}_k(\hat{t}) = \left[ \underbrace{\hat{\Delta}^0 + \hat{v}_\perp \hat{t}^n}_{=(g(t)-J(t))/\gamma} + 2 \underbrace{(\hat{D}_2^0 + \hat{v}_\parallel \hat{t}^n)}_{=J(t)/\gamma} (1 - \cos(ka)) \right] \sigma_z + \sin(ka) \sigma_x.$$

Exemplary drives are shown in Fig. 3.5. The involved static and driven couplings give rise to three competing length scales

$$\xi_{\text{eq}} \sim \hat{\Delta}_0^{-1}, \quad \xi_\perp \sim \hat{v}_\perp^{-\frac{1}{1+nz}}, \quad \xi_\parallel \sim \hat{v}_\parallel^{-\frac{1}{-1+nz}}. \quad (3.17)$$

For the transverse XY model with  $z = 1$ , *both* drive scales diverge for  $\hat{v} \rightarrow 0$  once the drive is at least quadratic  $n \geq 2$ . Depending on the microscopic coupling strengths, either one of the three length scales becomes observable as shown in Fig. 3.4(b). A microscopic velocity  $1 \gg \hat{v}_\perp \gg \hat{v}_\parallel$  favors the emergence of  $\xi^* \sim \xi_\perp$  (case 3 in Fig. 3.4). For  $1 \gg \hat{v}_\parallel \gg \hat{v}_\perp$ , the subleading scaling can become observable  $\xi^* \sim \xi_\parallel$  (case (1) in Fig. 3.4). Therefore, the observable scale  $\xi^*$  depends on the ratio of  $\hat{v}_\parallel$  and  $\hat{v}_\perp$ . However, we will specify the conditions

<sup>6</sup>The Hamiltonian at the end of the drive is:

$$\text{transverse XX: } \mathbf{H}(|t| \rightarrow \infty) \propto - \left( \frac{\hat{v}_\perp}{2} + \hat{v}_\parallel \right) \sum_l \sigma_l^z - \frac{\hat{v}_\parallel}{2} \sum_l (\sigma_l^x \sigma_{l+1}^x + \sigma_l^y \sigma_{l+1}^y)$$

with the ground state  $|\uparrow\uparrow \dots\rangle$ . The fermionic version is diagonal in momentum space with  $\chi_k = \mathbf{c}_k$ .

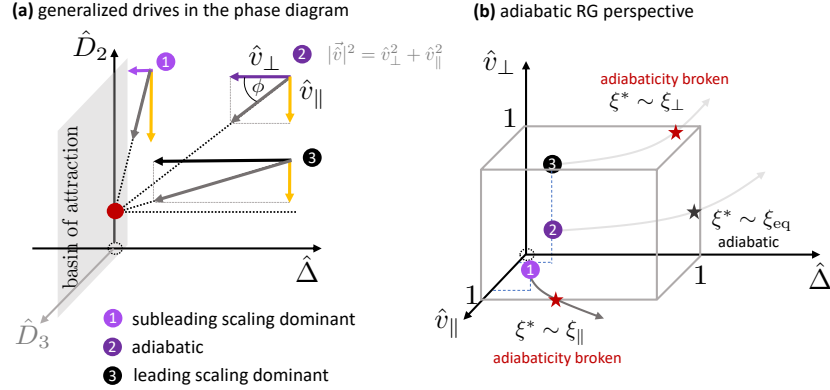


**Figure 3.4:** (a) A generalized drive in the transverse  $XY$  model with a component along the relevant direction  $\hat{v}_\perp$  and along the subleading (irrelevant) direction  $\hat{v}_\parallel$ . (b) At a given point in time, the relevant information is encoded in  $(\hat{\Delta}, \hat{v}_\perp, \hat{v}_\parallel)$ , which changes under the RG at larger distances. Depending on the position parameters at that time, the drive is either adiabatic (case 2) or non-adiabatic due to the drive of  $\hat{\Delta}$  (case 3) or the drive of  $\hat{D}_2$  (case 1).

more precisely in the following sections.

**Parametrization:** The scaling behavior of  $\xi^*$  (and  $n_E$ ) is inferred from the fermionic RG flow in the vicinity of the fixed point. As mentioned before, the drive couplings have the same eigendirections compared to the equilibrium RG. Therefore, the simple structure of the equilibrium RG flow allows us to decompose a drive coupling vector  $\vec{v}$  in terms of the orthogonal (equilibrium) directions  $\hat{\Delta}$  and  $\hat{D}_2$ . In terms of dimensionless couplings the decomposition reads:

$$\vec{v} = v_\perp \vec{e}_{\hat{\Delta}} + v_\parallel \vec{e}_{\hat{D}_2} = v \begin{pmatrix} \cos(\phi) \\ \sin(\phi) \end{pmatrix}, \quad (3.18)$$

as shown in Fig. 3.4(a). The angle  $\pi/2 - \phi$  is defined as the angle enclosed with the equilibrium irrelevant direction ( $\hat{D}_2$ -direction) [notation as in Ref. [41]]. We will typically consider drives for a fixed angle and vary  $\hat{v}$  to extract  $\xi^*(\hat{v})$ . An example is sketched in Fig. 3.2(b). For  $\hat{v} \rightarrow 0$ , the scaling due to  $\xi_\perp$  will be observable, since the transversal drive is the *leading* relevant coupling. Nevertheless, for an intermediate range of velocities  $\hat{v}$  ( $1 \gg \hat{v} \gg \hat{v}^* = \hat{v}^*(\phi)$ ) the subleading scaling will be observable as well, sketched in Fig. 3.2(b). The leading and subleading scaling regime are separated by a crossover velocity  $\hat{v}^*(\phi)$ . For angles closer to  $\pi/2$ ,  $\hat{v}^*(\phi)$  becomes smaller and the subleading scaling regime increases.

### Box 6: Spin vs. fermionic coupling space

The definition of the angle is based on the linearized fermionic RG and the eigendirections of  $M$  at the fixed point  $\vec{g}^*$ . A drive of the transversal field corresponds to  $\phi_1 = 0$  (see Fig. 3.5(b)). By definition, this is a *transversal* drive (driving an equilibrium relevant coupling). A *longitudinal* (or *parallel*) drive (3) lies in the basin of attraction spanned by all the *irrelevant* coupling directions. A feature of these drive protocols is that the notion of ‘transversal’ is less obvious in the spin language, where the same protocol corresponds to path (1) in Fig. 3.5(a) with  $\phi'_1 \neq 0$ . Formally speaking, the mapping between the spin and fermion couplings ((3.19) for  $k \rightarrow 0$ ) is not angle preserving. Practically, this means that the nature of a drive (transversal or longitudinal) cannot always be inferred from the ‘microscopic’ phase diagram. Mathematically, for  $k \rightarrow 0$  and in the vicinity of the critical point, the fermionic and spin couplings are related by:

$$\mathcal{M} \begin{pmatrix} g/\gamma \\ J/\gamma \end{pmatrix} \approx \begin{pmatrix} \hat{\Delta} \\ \hat{D}_2 \end{pmatrix}, \quad \mathcal{M} = \begin{pmatrix} 1 & -1 \\ 0 & \frac{1}{2} \end{pmatrix}, \quad (3.19)$$

with  $\mathcal{M}^{-1} \neq \mathcal{M}^T$ . Given a drive  $\vec{v}$ , the corresponding angles can be expressed in terms of  $\mathcal{M}$  and the unit vectors  $\vec{e}_j$  in coupling direction  $j$ :

$$\text{fermions: } \sin(\phi) = \frac{\langle \hat{v}, \vec{e}_{\hat{D}_2} \rangle}{|\hat{v}| |\vec{e}_{\hat{D}_2}|}, \quad \text{spin: } \sin(\phi') = \frac{\langle \mathcal{M}^{-1} \hat{v}, \mathcal{M}^{-1} \vec{e}_{\hat{D}_2} \rangle}{|\mathcal{M}^{-1} \hat{v}| |\mathcal{M}^{-1} \vec{e}_{\hat{D}_2}|}.$$

Even though the angles will deviate for a composite drive, a ‘longitudinal’ drive is longitudinal in both systems (see Sec. 3.4 for an example).

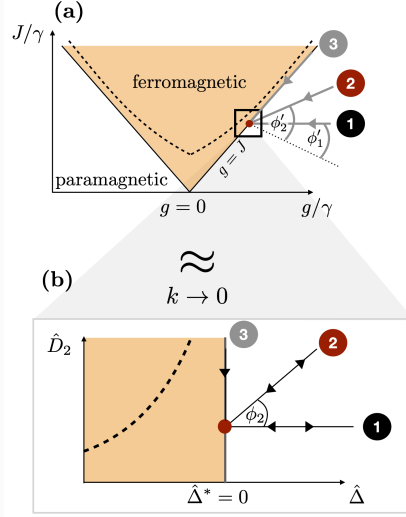


**Figure 3.5:** Transversal (1), generalized (2) and (3) parallel drive for the transverse XY model, reaching the same critical point (top: spin couplings, bottom: fermionic couplings). The angles in the spin and fermion setting are  $\phi'_{1,2}$  and  $\phi_{1,2}$  respectively. Importantly,  $\phi_1 = 0$  corresponds to  $\phi'_1 \neq 0$ .

### 3.1.4 Interlude: Time Evolution of Gaussian States

The time evolution of interacting models becomes intractable for large system sizes due to the exponentially (in  $L$ ) large number of needed parameters to de-

scribe the state. The advantage of quadratic non-interacting fermion models is that the ground states (as well as thermal states) are Gaussian states. In particular, the ground state is described by the set of complex coefficients  $(u_k, v_k)$  (polynomial in  $L$ ) with  $|\text{GS}_{t_i}\rangle = \prod_{k>0} (u_k^* - v_k^* \mathbf{c}_k^\dagger \mathbf{c}_{-k}^\dagger) |0\rangle$ . This Gaussian form is preserved under the time evolution of a quadratic Hamiltonian  $\mathbf{H}(t) = \sum_{k>0} \mathbf{H}_{k,-k}(t)$ , where the different momentum sectors completely decouple. Therefore, we seek for a description in terms of time dependent parameters  $(U_k(t), V_k(t))$ 's (where the capital letters are used to distinguish them from the ground state values). There are two equivalent approaches to find the evolution of the coefficients: (1) Schrödinger picture approach and (2) Heisenberg picture approach.

**Schrödinger picture:** The direct approach is to solve the Schrödinger equation in each momentum sector spanned by  $\{|0\rangle_k, \mathbf{c}_k^\dagger \mathbf{c}_{-k}^\dagger |0\rangle_k\} =: \{|0\rangle, |1\rangle\}$  (forming a two level system). The  $(k, -k)$  part of the initial ground state in this basis is given by  $|\text{GS}_k\rangle = (-v_k^*, u_k^*)^T$  and the Hamiltonian takes the form

$$\begin{pmatrix} \langle 0 | \mathbf{H}_{k,-k}(t) | 0 \rangle & \langle 0 | \mathbf{H}_{k,-k}(t) | 1 \rangle \\ \langle 1 | \mathbf{H}_{k,-k}(t) | 0 \rangle & \langle 1 | \mathbf{H}_{k,-k}(t) | 1 \rangle \end{pmatrix} := \tilde{h}_k(t) = \sigma_x h_k(t) \sigma_x, \quad (3.20)$$

$$i\partial_t \begin{pmatrix} -V_k^*(t) \\ U_k^*(t) \end{pmatrix} = \tilde{h}_k(t) \begin{pmatrix} -V_k^*(t) \\ U_k^*(t) \end{pmatrix}. \quad (3.21)$$

Therefore, each momentum sector corresponds to a Landau-Zener like model in disguise and can be solved individually.

**Heisenberg picture:** The second equivalent approach, often used in the literature [10, 11], takes the operator perspective in the Heisenberg picture. As an ansatz, the time-dependent annihilation operators  $\mathbf{c}_k(t)$  are written in terms of the *initial* quasi-particle creation and annihilation operators  $\{\chi_k(t_i), \chi_k^\dagger(t_i)\}$ :

$$\begin{aligned} \text{ansatz: } \quad \mathbf{c}_k(t) &= U_k(t) \chi_k(t_i) + V_{-k}^*(t) \chi_{-k}^\dagger(t_i) \\ \text{evolution: } \quad i\partial_t \mathbf{c}_k(t) &= [\mathbf{c}_k(t), \mathbf{H}^+(t)]. \end{aligned} \quad (3.22)$$

The time evolution of  $\mathbf{c}_k(t)$  translates into the time evolution of the coefficients  $(U_k(t), V_k(t))$ , which evolve according to [11] (see again (2.28)):

$$\begin{aligned} |A(t)\rangle_k &:= \begin{pmatrix} U_k(t) \\ V_k(t) \end{pmatrix}, \quad |A(t_i)\rangle_k = |+(t_i)\rangle_k, \\ i\partial_t |A(t)\rangle_k &= h_k(t) |A(t)\rangle_k. \end{aligned} \quad (3.23)$$

Note that in this second approach, the initial ground state of the fermion model corresponds to the *excited* state of  $h_k$ .

In both approaches, the time evolved state (in the Schrödinger picture) takes the form:

$$\text{adiabatic representation: } |\Psi(t)\rangle = \prod_{k>0} (U_k^*(t) - V_k^*(t) \mathbf{c}_k^\dagger \mathbf{c}_{-k}^\dagger) |0\rangle. \quad (3.24)$$

The state has a similar appearance as the ground state, but it can host excitations. Rewriting the state in terms of the instantaneous ground state  $|\text{GS}_t\rangle$  and

quasi-particle operators  $\chi_{k,t}$  gives:

$$\text{adiabatic representation: } |\Psi(t)\rangle = \prod_{k>0} (a_k(t) + b_k(t)\chi_{k,t}^\dagger\chi_{-k,t}^\dagger)|\text{GS}_t\rangle. \quad (3.25)$$

The coefficients in the two representations are related as:

$$\begin{pmatrix} a_k \\ b_k \end{pmatrix} = \begin{pmatrix} u_k & v_k \\ v_k^* & -u_k^* \end{pmatrix} \begin{pmatrix} U_k^* \\ V_k^* \end{pmatrix}. \quad (3.26)$$

The advantage of the adiabatic representation (3.25) is that we can directly deduce the excitation density:

$$n_E(t) = \frac{1}{L} \sum_k \langle \Psi(t) | \chi_{k,t}^\dagger \chi_{k,t} | \Psi(t) \rangle = \frac{1}{L} \sum_k p_k = \frac{1}{L} \sum_k |b_k|^2. \quad (3.27)$$

#### Box 7: Relation of the coefficients

To relate the coefficients  $a_k, b_k$  in the adiabatic representation to the diabatic representation, we express  $|\Psi(t)\rangle$  in terms of the ground state and excited states (for momenta  $\pm k$ ):

$$\begin{aligned} |\text{GS}_{t,k}\rangle &= (u_k^* - v_k^* c_k^\dagger c_{-k}^\dagger) |0_k\rangle, & |\text{E}_{t,k}\rangle &= \chi_k^\dagger \chi_{-k}^\dagger |\text{GS}_{t,k}\rangle, \\ \text{many-body state: } |\Psi(t)\rangle &= \prod_{k>0} (a_k |\text{GS}_{t,k}\rangle + b_k |\text{E}_{t,k}\rangle). \end{aligned} \quad (3.28)$$

The adiabatic representation of the corresponding two level description ( $|A(t)\rangle_k$ ) is obtained by using the instantaneous eigenstates  $\{|+(t)\rangle_k, |-(t)\rangle_k\}$  of  $h_k(t)$ :

$$\text{two-level state: } |A(t)\rangle_k = a_k^*(t) |+(t)\rangle_k - b_k^*(t) |-(t)\rangle_k. \quad (3.29)$$

The overall relation between the coefficients is given in (3.26).

To summarize: starting from the ground state in the transverse XY model, the evolution of the different momentum sectors ( $k, -k$ ) decouples. Each sector is described by a two level system with time dependent Hamiltonian  $h_k(t)$ . Nonetheless, the time evolution for  $h_k(t)$  is *not* necessarily exactly solvable. A notable exception is a *linear drive*, corresponding to the Landau-Zener model discussed in Sec. 2.1.1 (and, e.g., Ref. [11]).

## 3.2 Linear Drive (1): Transverse XY Model and relevant Couplings

In the following, we will supplement the heuristic and RG derivation of the KZM scaling of  $\xi^*$  (and therefore  $n_E$ ) with an exact calculation for a linear drive of the transversal field - a purely transversal drive [11]. The derivation in the context of a quantum phase transition and the quantum Ising model was first performed by Dziarmaga [11]. Besides its simplicity, it also lays out the

strategy we will follow in the next sections.

For such a *linear* drive, the excitation density  $n_E$  can be exactly calculated based on the asymptotic Landau-Zener result (2.3). The drive starts from the paramagnetic phase and ends deep in the ferromagnetic phase with  $g(t)/\gamma = -v_0 t$  for  $t_i = -\infty$  and  $t_f = 0$ . The coupling  $J/\gamma = J_0/\gamma$  is held fixed and the transition is crossed at  $g_c = J_0$ , see Fig. 3.3(a). In the paramagnetic phase, the physical observable is the domain wall density  $n_E(\hat{v}_0)$ , depending on the dimensionless velocity  $\hat{v}_0$ . Using the KZM argument, the domain wall density should scale universally with  $\hat{v}_0$  in the vicinity of the transition ( $z = \nu = 1$ ):

$$n_E(\hat{v}_0) \sim \xi^{*-1} \quad \Rightarrow \quad \text{KZM prediction: } \xi^* \sim \hat{v}_0^{-\frac{1}{2}}.$$

In the fermionic formulation, the excitation density  $n_E$  is given by summing up the excitation probabilities  $p_k$  for each two level system labelled by  $(k, -k)$ , see again (3.27). In case of a linear drive, the  $p_k$ 's can be determined exactly based on the Landau-Zener result (2.3). In Sec. 2.1.1, the two level model was recast in a *canonical* dimensionless form:

$$i\partial_{\bar{t}} \begin{pmatrix} U \\ V \end{pmatrix} = \begin{pmatrix} \hat{v}_{\text{eff}} \cdot \bar{t} & 1 \\ 1 & -\hat{v}_{\text{eff}} \cdot \bar{t} \end{pmatrix} \begin{pmatrix} U \\ V \end{pmatrix}. \quad (3.30)$$

The asymptotic excitation probability will only depend on the dimensionless velocity  $\hat{v}_{\text{eff}}$ . A fast drive with  $\hat{v}_{\text{eff}} \gg 1$  will lead to a probability close to 1. In the following, we adapt this strategy for the two level systems  $h_k(t)$  for the transverse XY model. In this case, the effective velocity will be  $k$ -dependent (scale dependent). Adiabaticity breaking is indicated by a diverging effective velocity for  $k \rightarrow 0$ , as we will analyze in the following.

**Canonical parametrization:** In analogy to (3.30), the state in each sector is described by  $(U_k(t), V_k(t))$ . The time evolution is encoded in the hermitian matrix  $h_k(t)$ , see again (3.23). Similar to the RG discussion, we will use dimensionless quantities in the following. Scaling out  $\gamma$ , the drive is parametrized by dimensionless time  $\hat{t} = 2\gamma t$  and velocity  $\hat{v}_0 = 2v_0/(2\gamma)^2$ . Similarly, the dimensionless fermion couplings are:

$$\hat{\Delta}(t) = \hat{\Delta}^0 - \hat{v}_\perp \hat{t} \approx (g(t) - J_0)/\gamma, \quad \hat{D}_2(t) = \hat{D}_2^0 \approx J_0/(2\gamma). \quad (3.31)$$

To extract the excitation density, we bring the two level models  $h_k(t)$  into the aforementioned canonical form (3.30), which we will use extensively throughout the whole chapter. The advantage of this form is that it reveals the scaling of equilibrium and non-equilibrium couplings in the limit  $k \rightarrow 0$  on equal footing. Generalizing for later use to a drive of order  $n$ , we define<sup>7</sup>:

$$\begin{aligned} \text{canonical form: } \quad \bar{h}_k &= (\hat{v}_k \hat{t}_k^n + \hat{\mu}_k) \sigma_z + \sigma_x, \\ \text{eigenvalues: } \quad \mathcal{E}(k, \hat{t}_k) &= \pm \sqrt{(\hat{v}_k \hat{t}_k^n + \hat{\mu}_k)^2 + 1}, \end{aligned} \quad (3.32)$$

(where  $n = 1$  for the linear drive here) with rescaled time  $\hat{t}_k = 2\gamma t \cdot \sin(ka)$  and

---

<sup>7</sup>See also Refs. [139, 140] for a linear and quadratic drive.

effective parameters:

$$\text{effective parameters: } \hat{v}_k = (-1)^n \frac{\hat{v}_0}{\sin^{n+1}(ka)} \quad \xrightarrow{k \rightarrow 0} \sim (ka)^{-(n+1)}, \quad (3.33)$$

$$\hat{\mu}_k = 2\hat{D}_2^0 \frac{(1 - \cos(ka))}{\sin(ka)} \quad \xrightarrow{k \rightarrow 0} \sim (ka). \quad (3.34)$$

The effective parameters encode the effective velocity  $\hat{v}_k$  at momentum  $k$  and the effective static (equilibrium) scale  $\hat{\mu}_k$ . The effective velocity  $\hat{v}_k$  scales as  $\sim (ka)^{-(n+1)}$  and is comparable to the scale dependent velocity coupling  $\hat{v}_0(s)$  in the RG (diverging for  $s \rightarrow \infty$ , see (3.12)). Therefore, the effective velocity  $\hat{v}_k$  will become dominant at large distances even though the microscopic velocity is small  $\hat{v}_0 \ll 1$ . The second parameter,  $\hat{\mu}_k$ , instead becomes vanishingly small ( $\sim (ka)$ ). It incorporates equilibrium irrelevant couplings, which similarly become irrelevant at large scales<sup>8</sup>.

**Linear drive:** Rewritten in the form (3.32) and  $n = 1$ , the excitation probability  $p_k = \exp(-\pi|\hat{v}_k|^{-1})$ , and therefore  $n_E$ , for asymptotically large times can be predicted exactly. For sufficiently small  $k$ , the formal limit of asymptotically large times and the usage of the Landau-Zener formula is justified (as we discuss in the info box). The overall excitation density (3.27) is obtained by summing up all excitation probabilities  $p_k$ . The expression can be turned into a Gaussian integral and the density of fermionic excitations, being equal to the density of domain walls, scales in the predicted fashion [11]:

$$n_E = \frac{1}{L} \sum_k p_k \approx \int_{-\pi}^{\pi} p_k \frac{d(ka)}{2\pi} \approx \int_{-\pi}^{\pi} e^{-\pi \frac{(ka)^2}{\hat{v}_0}} \frac{d(ka)}{2\pi} \sim \hat{v}_0^{\frac{1}{2}}. \quad (3.35)$$

Note that for  $\hat{v}_0 \ll 1$ , the excitation probabilities  $p_k$  is strongly suppressed for those momenta where the asymptotic result would not hold (making it self-consistent).

#### Box 8: Applicability of the asymptotic result

For small enough  $k$ , the asymptotic result can be used even though the final time is finite ( $\hat{t}_{f,k} \neq \infty$ ). In the following, we make use of the intuition developed around the AIA approximation (see again (2.5) in Sec. 2.1.1) to argue that the asymptotic Landau-Zener result is applicable once the drive starts and ends in an adiabatic (A) regime. In particular, it should cross the entire impulse (I) regime (where the excitations are generated). The onset of the impulse regime is marked by the adiabaticity breaking time<sup>a</sup>  $\hat{t}_k^*$ :

$$\frac{1}{2\mathcal{E}(k, \hat{t}_k^*)} = \frac{1}{2\sqrt{(\hat{v}_k \hat{t}_k^{*n} + \hat{\mu}_k)^2 + 1}} \stackrel{!}{=} \alpha_1 \hat{t}_k^*,$$

where  $\hat{\mu}_k$  is negligible in the limit  $k \rightarrow 0$ . The condition of starting and

continued on next page

<sup>8</sup>Nevertheless, once  $\hat{\Delta}_0 \neq 0$  (staying at a finite distance to the critical point),  $\hat{\mu}_k$  will become the leading scale and allows for the restoring of adiabaticity.

continued from page before

ending outside of the impulse regime in terms of initial and final times  $\hat{t}_{i,k}, \hat{t}_{f,k}$  reads:

$$\hat{t}_{i,k} \ll -\hat{t}_k^* < \hat{t}_k^* \ll \hat{t}_{f,k}.$$

The drive ends at  $\hat{t}_{f,k}$ , defined by  $g(t_f) = 0 \Leftrightarrow \hat{\Delta}(\hat{t}_f) = -2\hat{D}_2^0$ :

$$\hat{t}_{f,k} = \frac{2\hat{D}_2^0}{\hat{v}_0} \sin(ka). \quad (3.36)$$

In the limit  $k \rightarrow 0$ , the effective velocity becomes large  $\hat{v}_k \gg 1$  and the adiabaticity breaking time scales as  $\hat{t}_k^* \sim \hat{v}_0^{-\frac{1}{2}} \cdot (ka)$ . Therefore, the requirement (3.36) for the final time translates into

$$\hat{v}_0 \ll \left(2\hat{D}_2^0\right)^2, \quad \text{given a fast eff. velocity: } \hat{v}_k = \frac{\hat{v}_0}{\sin^2(ka)} \gg 1. \quad (3.37)$$

This requirement is always fulfilled for sufficiently small momenta and a microscopically slow drive.

<sup>a</sup>Making use of (2.5) for the canonical Hamiltonian (3.32).

### 3.3 Linear Drive (2): Scaling and Crossover Scales in the generalized XY Model

In the last sections, we have laid out the formalism to treat and understand the generalized KZM, in particular from a RG perspective. Though the treatment of the XY model in the fermionic formalism is straight forward, an *exact* analytical calculation is hindered by the numerical values of the critical exponents. With  $z = \nu = 1$  and the scaling dimension of the first subleading coupling  $\dim[D_2] = -1$ , at least a quadratic drive ( $n = 2$ ) of  $\hat{D}_2$  is required, to make the subleading scaling observable. However, quadratic drives are not exactly solvable anymore. To make use of the exact solutions for a linear drive, we start with a full analysis of the related *extended* XY model (also used in, e.g., Ref. [137]; see also Refs. [141, 142]) and discuss the transverse XY model afterwards. The extended model includes spin interactions between up to second nearest neighbors:

$$\begin{aligned} \mathbf{H} = & -g \sum_l \sigma_l^z - J_x \sum_l \sigma_l^x \sigma_{l+1}^x - J_y \sum_l \sigma_l^y \sigma_{l+1}^y \\ & - J_{xx} \sum_l \sigma_l^x \sigma_{l+2}^x \sigma_{l+1}^z - J_{yy} \sum_l \sigma_l^y \sigma_{l+2}^y \sigma_{l+1}^z. \end{aligned} \quad (3.38)$$

In contrast to the transverse XY model, the additional couplings can be fine tuned such that the model hosts a critical theory with  $z = 3$ . In this case, a linear drive is sufficient to ‘activate’ equilibrium irrelevant exponents. By construction, the model can still be mapped to fermions, where each momentum

sector is described by (see also App. A.1)

$$h_k = 2[g - J \cos(ka) - J_2 \cos(2ka)]\sigma_z + [2\gamma \sin(ka) + 2\gamma_2 \sin(2ka)]\sigma_x,$$

$$\text{couplings: } \begin{aligned} J &= J_x + J_y, & J_2 &= J_{xx} + J_{yy}, \\ \gamma &= J_x - J_y, & \gamma_2 &= J_{xx} - J_{yy}. \end{aligned}$$

By choosing  $\gamma_2 = -1/2 \cdot \gamma$  and  $J_2 = -1/4 \cdot J$ , the lowest momentum terms are of order  $\mathcal{O}(k^3)$  and therefore the dynamical critical exponent is  $z = 3$ :

$$h_k = 2[g - J \cos(ka) + \frac{1}{4}J \cos(2ka)]\sigma_z + [2\gamma \sin(ka) - \gamma \sin(2ka)]\sigma_x,$$

$${}^{k \ll \Lambda_{\text{eff}}} \approx 2 \left[ g - \frac{3}{4}J + \frac{1}{8}J(ka)^4 \right] \sigma_z + [\gamma(ka)^3] \sigma_x. \quad (3.39)$$

The gap  $\Delta(g, J, \gamma) = \min_k[\epsilon_k]$  closes at  $k \rightarrow 0$  for  $g = \frac{3}{4}J$ . In the vicinity of the gap closing and at large distances ( $k < \Lambda_{\text{eff}}$ ), higher order momentum terms can be ignored (defining  $\Lambda_{\text{eff}}$ ). At those large scales and in the thermodynamic limit  $L \rightarrow \infty$ , the effective Hamiltonian is given by (see also again the discussion around (2.42))

$$\mathbf{H} \approx \int_{-\Lambda_{\text{eff}}}^{\Lambda_{\text{eff}}} \frac{dk}{2\pi} \left[ \Delta \psi_k^\dagger \psi_k + \frac{1}{2} D_3 k^3 [\psi_k^\dagger \psi_{-k}^\dagger + \psi_{-k} \psi_k] + D_4 k^4 \psi_k^\dagger \psi_k \right]. \quad (3.40)$$

**Static setup:** The model (3.40) is similar to the transverse XY model but with the couplings  $D_1$  and  $D_2$  absent. In a first step, we derive the scaling dimensions of the equilibrium couplings from the RG perspective. Therefore, we identify the equilibrium RG fixed point and the scaling dimensions from the flow in its vicinity. Using a similar rescaling as before but with  $z = 3$ , the RG fixed point theory is described by the leading derivative term  $D_3$ . Scaling out  $D_3$  and using  $\Lambda_{\text{eff}}$ , the dimensionless couplings  $\vec{g}_{\text{eq}}$  (with fixed point  $\vec{g}^* = (0, 0, \dots)^T$ ) are given by:

$$\vec{g}_{\text{eq}} = \begin{pmatrix} \hat{\Delta} \\ \hat{D}_4 \\ \hat{D}_5 \\ \vdots \end{pmatrix} = \begin{pmatrix} \frac{\Delta}{D_3} \Lambda_{\text{eff}}^{-3} \\ \frac{D_4}{D_3} \Lambda_{\text{eff}}^1 \\ \vdots \end{pmatrix} \quad \begin{array}{l} \dim[\Delta] \\ \dim[D_4] \\ \dim[D_5] \\ \vdots \end{array} \begin{array}{l} +3 \\ -1 \\ -2 \\ \vdots \end{array}. \quad (3.41)$$

**Drive setup:** Due to the larger dynamical critical exponent  $z = 3$ , even a linear drive ( $n = 1$ ) of the irrelevant coupling  $\hat{D}_4$  with  $\hat{v}_\parallel \hat{t}$  will induce a diverging length scale. To study the competition of scales induced by driving the relevant gap  $\hat{\Delta}$  with  $\hat{v}_\perp \hat{t}$  and  $\hat{D}_4$  with  $\hat{v}_\parallel \hat{t}$ , we consider two scenarios: (i) a combined (generalized) drive, and (ii) a linear drive of the irrelevant coupling  $\hat{D}_4$  only while keeping a constant distance ( $\hat{\Delta}(t) = \hat{\Delta}^0$ ) to the phase boundary (parallel drive). Both scenarios are described by the dimensionless hermitian matrix for

each momentum sector with  $\hat{k} = k/\Lambda_{\text{eff}}$ :

$$\hat{h}_k(\hat{t}) \approx \begin{pmatrix} \underbrace{(\hat{\Delta}^0 + \hat{v}_\perp \hat{t})}_{\hat{\Delta}(t)} + \underbrace{(\hat{D}_4^0 + \hat{v}_\parallel \hat{t})}_{\hat{D}_4(t)} \hat{k}^4 & \hat{k}^3 \\ \hat{k}^3 & -(\hat{\Delta}^0 + \hat{v}_\perp \hat{t}) - (\hat{D}_4^0 + \hat{v}_\parallel \hat{t}) \hat{k}^4 \end{pmatrix}. \quad (3.42)$$

From the point of view of the adiabatic RG (and dimensional analysis), the drive couplings have scaling dimensions that are shifted by  $z$  (for a linear drive):

$$\vec{g}_{\text{drive}} = \begin{pmatrix} \hat{v}_\perp \\ \hat{v}_\parallel \\ \vdots \end{pmatrix} = \begin{pmatrix} \frac{v_\perp}{D_3^2} \Lambda_{\text{eff}}^{-6} \\ \frac{v_\parallel}{D_3^2} \Lambda_{\text{eff}}^{-2} \\ \vdots \end{pmatrix} \quad \begin{array}{l} \dim[v_\perp] \\ \dim[v_\parallel] \\ \vdots \end{array} \begin{array}{l} +6 \\ +2 \\ \vdots \end{array}. \quad (3.43)$$

From the spin perspective, a purely transversal drive would correspond to driving  $g(t)$  and keeping  $J(t) = J_0$  constant. Similar to the linear drive in the transverse XY model, a protocol can be to start from  $t_i = -\infty$  with  $g(t_i) = \infty$  and ending at  $g(t_f) = 0$ . A parallel drive corresponds to driving  $J(t) > 0$  (and  $J_2(t)$ ) while keeping  $g(t) - \frac{3}{4}J(t)$  constant.

**Fermionic perspective:** In the following, we rather think of this model as a ‘minimal’ fermion model, putting aside the aforementioned details of the drive protocols. An idealized drive with  $t_i = -\infty$  and  $t_f = +\infty$  would take the form:

$$\left. \begin{array}{l} \hat{\Delta}(\hat{t}) = \hat{\Delta}^0 + \hat{v}_\perp \hat{t} \\ \hat{D}_4(\hat{t}) = \hat{D}_4^0 + \hat{v}_\parallel \hat{t} \end{array} \right\} \vec{v} = \begin{pmatrix} \hat{v}_\perp \\ \hat{v}_\parallel \end{pmatrix} = \hat{v} \begin{pmatrix} \cos(\phi) \\ \sin(\phi) \end{pmatrix}. \quad (3.44)$$

For each  $(k, -k)$  two level system, the Hamiltonian (3.42) can be brought into its canonical form (3.32). The effective parameters for the  $z = 3$  model are:

$$\begin{array}{l} \text{drive: } \hat{v}_k \approx \hat{v}_\perp \hat{k}^{-6} + \hat{v}_\parallel \hat{k}^{-2} \\ \text{static: } \hat{\mu}_k \approx \underbrace{\hat{\Delta}^0 \hat{k}^{-3}}_{\text{relevant}} + \underbrace{\hat{D}_2^0 \hat{k}^{+1}}_{\text{irrelevant}}. \end{array} \quad (3.45)$$

Focusing on this asymptotic limit, we extract the contribution to the excitation density  $n_E(\hat{v}, \phi)$  for  $k < \Lambda_{\text{eff}}$ . We separate the contributions to  $n_E$  into two parts: (i) a non-universal part for  $k > \Lambda_{\text{eff}}$  and (ii) a universal part for  $k < \Lambda_{\text{eff}}$ :

$$n_E = \frac{a\Lambda_{\text{eff}}}{\pi} \int_0^{\pi/a\Lambda_{\text{eff}}^{-1}} p_k d\hat{k} = \underbrace{\frac{a\Lambda_{\text{eff}}}{\pi} \int_0^1 p_k d\hat{k}}_{\text{universal}} + \underbrace{\frac{a\Lambda_{\text{eff}}}{\pi} \int_1^{\pi/a\Lambda_{\text{eff}}^{-1}} p_k d\hat{k}}_{\text{non-universal}}, \quad (3.46)$$

assuming  $p_k = p_{-k}$ . By restricting our discussion to the long distance model (3.40), we only consider the universal part. As a reminder: this is also the regime where the asymptotic results are applicable.

### 3.3.1 Key Results – Generalized Drives

The first class of drives we will consider are generalized drives, where  $\hat{\Delta}$  and  $\hat{D}_4$  are linearly driven across the critical point. Here we choose  $\hat{\Delta}^0 = \hat{D}_4^0 = 0$ . Driving these two couplings gives rise to two competing scales according to the previous RG considerations (3.43):

$$\xi_{\perp} \sim \hat{v}_{\perp}^{-\frac{1}{6}}, \quad \xi_{\parallel} \sim \hat{v}_{\parallel}^{-\frac{1}{2}} \quad \Rightarrow \quad \xi^* \sim \min[\xi_{\perp}, \xi_{\parallel}].$$

The excitation density  $n_E(\hat{v}, \phi)$  should have two universal scaling regimes: (i)  $n_E \sim \xi_{\perp}^{-1}$  for the smallest velocities  $\hat{v} \ll \hat{v}^*(\phi)$ , and (ii)  $n_E \sim \xi_{\parallel}^{-1}$  for  $1 \gg \hat{v} \gg \hat{v}^*(\phi)$ . The two regimes are separated by the crossover velocity  $\hat{v}^*(\phi)$ . A prototypical dependence of  $n_E$  with respect to  $\hat{v}$  with a fixed angle  $\phi$  is shown in Fig. 3.6(a). It is obtained from summing up the exact expressions for  $p_k$ , as discussed in further detail down below. For a fixed angle  $\phi$ , the behavior of  $n_E(\hat{v}; \phi)$  as a function of  $\hat{v}$  indicates two scaling regimes in the excitation density  $n_E(\hat{v}; \phi)$ , as well as a regime of saturation:

- For  $\hat{v} \rightarrow 0$  we observe the KZM scaling behavior  $n_E \sim \xi_{\perp}^{-1} \sim \hat{v}_{\perp}^{\frac{1}{6}}$ .
- For intermediate velocities  $\hat{v}^*(\phi) \ll \hat{v} \ll 1$ , the scaling stems from the driven subleading coupling  $n_E \sim \hat{v}_{\parallel}^{\frac{1}{2}}$ .
- For velocities  $\hat{v} \sim \mathcal{O}(1)$ , the excitation density saturates.

The two scaling regimes are separated by the crossover velocity  $\hat{v}^*(\phi)$ , indicated by orange dots in Fig. 3.6(b). It is estimated by a direct fit as detailed in Fig. 3.6(c).

**Universal scalings:** For drives nearly parallel to the phase boundary ( $|\pi/2 - \phi| \ll 1$ ), the crossover velocity  $\hat{v}^*(\phi)$  itself scales algebraically:  $\hat{v}^*(\phi) \sim |\pi/2 - \phi|^{1/2}$  as shown in Fig. 3.6(b),(f). The extracted universal scaling exponents of  $n_E(\hat{v}; \phi)$  (with  $\hat{v}$ ) are shown in Fig. 3.6(e). For a reasonable quantitative estimate of the subleading scaling, we require the subleading scaling to cover at least on order of magnitude in  $\hat{v}$ .

**Observability:** The possibility of observing the subleading scaling strongly depends on the crossover velocity  $\hat{v}^*(\phi)$ . Excitations are dominantly generated by the subleading drive in the velocity range  $\hat{v} \in [\hat{v}^*(\phi), 1]$ . For a broader range of  $\phi$ , the crossover velocity (orange line) and the extent of this velocity range in the  $(\phi, \hat{v})$  plane<sup>9</sup> are shown in Fig. 3.6(d). As we anticipate from Fig. 3.6(d)-(f), the velocity range  $[\hat{v}^*(\phi), 1]$ , relevant for the drive of the subleading coupling, gets very narrow for intermediate values of  $\phi$ . To extract a quantitatively reliable subleading scaling exponent, the angle  $\phi$  has to be large enough:  $\phi > \phi_{\min}$ . Here,  $\phi_{\min}$  is marked by red dots in Fig. 3.6(d),(f).

In the following, we pair this overview (based on the exact excitation density for an asymptotic drive) with an analytical investigation to extract the crossover scales. This analysis, based on the excitation density, complements the abstract RG analysis from before. Finally, we investigate drives *parallel* to the phase boundary with  $\hat{\Delta}^0 \neq 0$ .

<sup>9</sup>Corresponding to a quantitative version of Fig. 3.2(d).

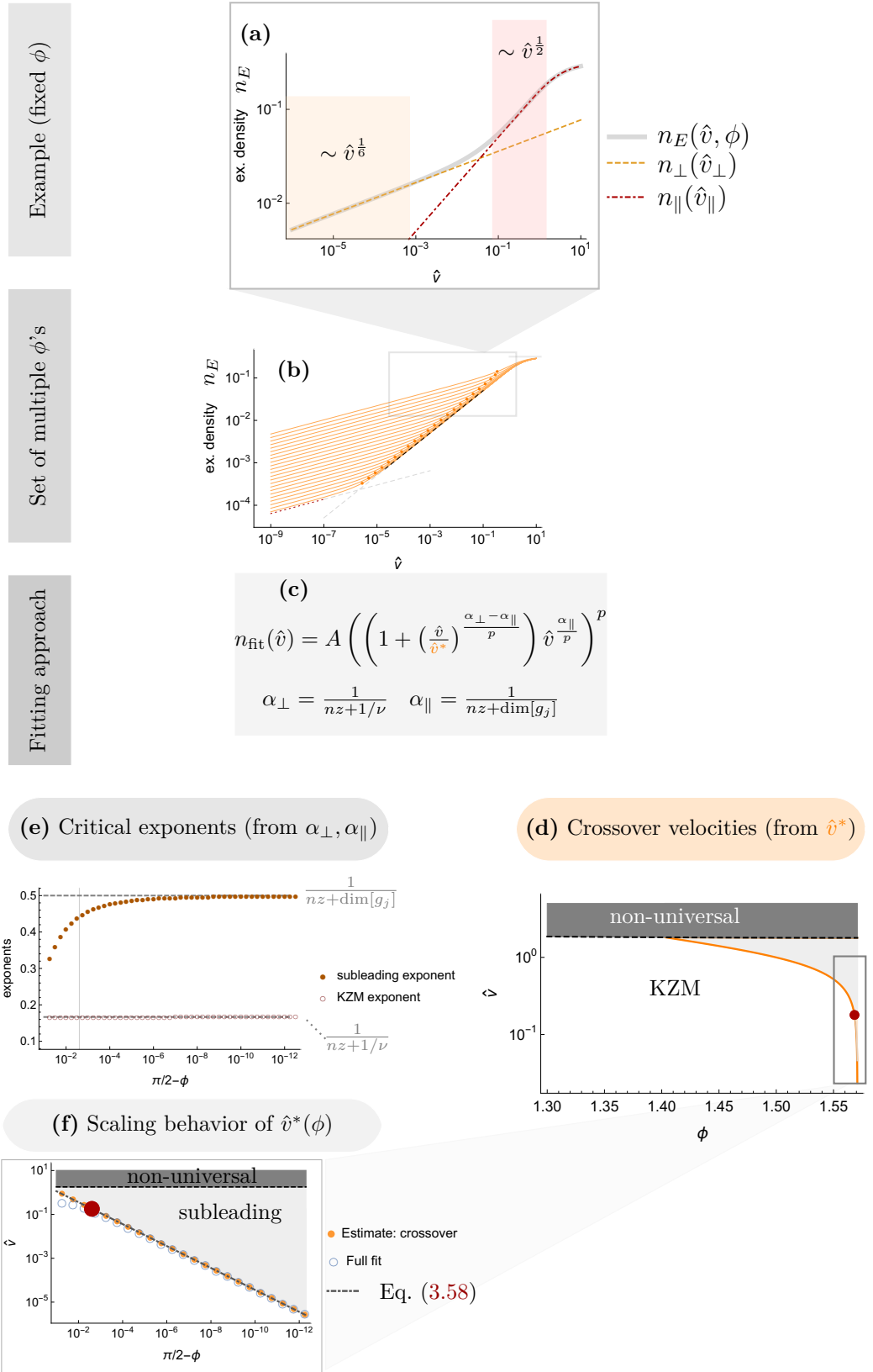


**Figure 3.6:** (from top to bottom): **(a)** Example of the excitation density  $n_E(\hat{v}, \phi)$  as a function of  $\hat{v}$  and fixed  $\phi = \pi/2 - 10^{-4}$  (log-log scale). It features two scaling regimes: KZM scaling at low velocities, separated from the subleading scaling at intermediate velocities and a non-universal regime at velocities  $\hat{v} \sim \mathcal{O}(1)$ . Deep inside a scaling regime,  $n_E$  is dominated by either  $n_\perp$  or  $n_\parallel$ . **(b)** Multiple  $n_E$  curves for different  $\phi$ 's are shown; for  $\phi \rightarrow \pi/2$  the onset of the KZM scaling is shifted to lower velocities, where the crossover velocity  $\hat{v}^*(\phi)$  also scales in a power law fashion (for  $\hat{v} \ll 1$ ). **(d)** Zooming out, the KZM regime (white), subleading scaling regime (light gray) and the non-universal regime (estimated from the saturation of  $n_E$ ) are indicated for an extended range of  $\phi$ . The extracted universal scaling exponents (e) and crossover velocities (f) are extracted by fitting  $n_E(\hat{v}; \phi)$  as detailed in (c). **(e)** The critical exponents for different  $\phi$ 's are plotted (log-linear scale) with the RG predictions (dashed lines). The vertical line indicates the smallest  $\phi$  ( $\phi_{min}$ ) which enables a good extraction of the exponents. **(f)** For  $\phi \rightarrow \pi/2$ , the crossover velocity also scales universally, which is estimated using (i) Eq. (3.56) (orange dots) and (ii) a full fit (blue circles) of the curves in (b). Both approaches are consistent with the analytical expression Eq. (3.56) (gray dash-dotted line).

### 3.3.2 Generalized Drives – Analytical Investigation

We are considering linear drives in the asymptotic limit of the  $z = 3$  model. Therefore, the Landau-Zener result is applicable to determine  $p_k$ . With the effective velocity  $\hat{v}_k$  in (3.45),  $p_k$  reads:

$$p(\hat{k}, \vec{v}) = \exp\left(-\pi \frac{1}{\hat{v}_\perp \hat{k}^{-6} + \hat{v}_\parallel \hat{k}^{-2}}\right) =: \exp(-\pi \hat{v}_k^{-1}). \quad (3.47)$$

Depending on the size of  $\hat{v}_k$ , the drive is either slow ( $\hat{v}_k \ll 1$ ) or effectively fast ( $\hat{v}_k \gg 1$ ) at momentum  $k$ . If we consider the two contributions in (3.45) and (3.47) as two different effective velocities ( $\hat{v}_k^{(\perp)}$  and  $\hat{v}_k^{(\parallel)}$ ), we can associate fast drives with an excitation probability close to 1:

	excitation density	effective velocities
$\hat{v}_k^{(j)} \gg 1$	$\Leftrightarrow p_k \sim \mathcal{O}(1)$ diabatic	$\hat{v}_k^{(\perp)} \sim \hat{v}_\perp \hat{k}^{-6}$
$\hat{v}_k^{(j)} \ll 1$	$\Leftrightarrow p_k \ll 1$ adiabatic	$\hat{v}_k^{(\parallel)} \sim \hat{v}_\parallel \hat{k}^{-2}$ .

The limiting cases correspond to a transversal drive ( $\phi = 0, \hat{v}_\parallel = 0$ ) and a parallel drive ( $\phi = \pi/2, \hat{v}_\perp = 0$ ). In both cases, we can associate an excitation density  $n_\perp(\hat{v}_\perp)$  or  $n_\parallel(\hat{v}_\parallel)$  to the drive (3.48). The excitation density for intermediate angles  $n_E(\hat{v}, \phi)$  is approximately given by the larger of those individual excitation densities:

$$\left. \begin{aligned} n_\perp(\hat{v}_\perp) &\approx \frac{a\Lambda_{\text{eff}}}{\pi} \int_0^1 \exp\left(-\pi \frac{\hat{k}^6}{\hat{v}_\perp}\right) d\hat{k} \sim \hat{v}_\perp^{\frac{1}{6}}, \\ n_\parallel(\hat{v}_\parallel) &\approx \frac{a\Lambda_{\text{eff}}}{\pi} \int_0^1 \exp\left(-\pi \frac{\hat{k}^2}{\hat{v}_\parallel}\right) d\hat{k} \sim \hat{v}_\parallel^{\frac{1}{2}}, \end{aligned} \right\} n_E(\hat{v}, \phi) \approx \max[n_\perp(\hat{v}_\perp), n_\parallel(\hat{v}_\parallel)]. \quad (3.48)$$

The expressions  $n_\perp(\hat{v}_\perp)$  and  $n_\parallel(\hat{v}_\parallel)$  are plotted in Fig. 3.6(a) as well. The different scaling regimes of  $n_E(\hat{v}, \phi)$  are rooted in the two different velocity contributions in  $\hat{v}_k$ . Based on them, the excitation probability  $p_k$  features two different regimes as a function of  $\hat{k}$ , separated by the crossover scale  $\hat{\kappa} := (\hat{v}_\perp/\hat{v}_\parallel)^{1/4}$ :

$$p\left(\hat{k} \ll \hat{\kappa}, \vec{v}\right) \sim \exp\left(-\pi \frac{\hat{k}^6}{\hat{v}_\perp}\right), \quad p\left(\hat{k} \gg \hat{\kappa}, \vec{v}\right) \sim \exp\left(-\pi \frac{\hat{k}^2}{\hat{v}_\parallel}\right). \quad (3.49)$$

The momentum range is separated by  $\hat{\kappa}$  into (i) a range, where excitations are generated due to the transversal drive ( $\hat{k} \ll \hat{\kappa}$ ) and (ii) a range, where excitations are generated due to the longitudinal drive ( $\hat{k} \gg \hat{\kappa}$ ). Therefore, the contributions to the full excitation density  $n_E(\hat{v}, \phi)$  can also be split into two parts:

$$n_E(\hat{v}, \phi) = \underbrace{\frac{a\Lambda_{\text{eff}}}{\pi} \int_0^{\hat{\kappa}} p(\hat{k}, \vec{v}) d\hat{k}}_{\approx n_\perp(\hat{v}_\perp)} + \underbrace{\frac{a\Lambda_{\text{eff}}}{\pi} \int_{\hat{\kappa}}^1 p(\hat{k}, \vec{v}) d\hat{k}}_{\approx n_\parallel(\hat{v}_\parallel)}. \quad (3.50)$$

Apart from a crossover regime,  $n_E(\hat{v}, \phi)$  in (3.50) is dominated by only one of the terms, see again Fig. 3.6(a). The lowest order approximation of both terms is given in (3.48). It corresponds to setting  $\hat{\kappa} \rightarrow 1$  or  $\hat{\kappa} \rightarrow 0$  in (3.50).

**Crossover velocity - Scaling behavior:** In the last section, we have identified the scaling of  $n_E$  for the limiting cases of  $\hat{v}_\parallel \rightarrow 0$  or  $\hat{v}_\perp \rightarrow 0$ . The important question regarding *observability* is: Where is the crossover velocity  $\hat{v}^*(\phi)$  located and how does it depend on the universal information of the transition? In the following, we derive under which conditions the subleading scaling, and therefore the contribution  $n_\parallel(\hat{v}_\parallel)$ , becomes dominant/observable. Furthermore, we extract the universal scaling of the crossover velocity  $\hat{v}^*(\phi)$  in the limit  $\phi \rightarrow \pi/2$  (which can be similarly derived from the RG considerations [41]).

Starting from (3.50), the contribution  $n_\parallel$  is approximated as

$$n_\parallel \approx \int_{\hat{\kappa}}^1 p(\hat{\kappa}, \hat{v}_\parallel) d\hat{\kappa} \stackrel{\bar{k} := \hat{\kappa}/\hat{v}_\parallel^{\frac{1}{2}}}{=} \hat{v}_\parallel^{\frac{1}{2}} \cdot \int_{\hat{\kappa}/\hat{v}_\parallel^{\frac{1}{2}}}^{1/\hat{v}_\parallel^{\frac{1}{2}}} p(\bar{k}, 1) d\bar{k}. \quad (3.51)$$

The expression scales algebraically with  $\hat{v}_\parallel$  once the remaining integral is a  $\hat{v}_\parallel$ -independent constant to a good approximation. Therefore, we require the integration domain to be sufficiently large such that the integral itself does not depend on  $\hat{v}_\parallel$  anymore:

- ①  $\hat{\kappa}/\hat{v}_\parallel^{\frac{1}{2}} \ll 1$ : Corresponds to  $\hat{v}_\perp \ll \hat{v}_\parallel^3$ . The transversal drive velocity needs to be small enough compared to the longitudinal one. Otherwise, the transversal drive and scaling would overwrite the subleading scaling.
- ②  $1/\hat{v}_\parallel^{\frac{1}{2}} \gg 1$ : Corresponds to the requirement of a slow drive (small enough to not enter the non-universal regime:  $\hat{v}_\parallel \ll \hat{v}_{\text{cut}} \approx 1$ ).

Since we are only concerned with (microscopically) slow drives ( $\hat{v}_\parallel \ll 1$ ), the *observability* of the subleading scaling depends on ①. Parametrizing the drive in terms of  $\hat{v}$  and  $\phi$  instead of  $\hat{v}_\parallel$  and  $\hat{v}_\perp$ , the crossover velocity  $\hat{v}^*(\phi)$  indicates the velocity scale, where the condition is violated. For  $\phi \rightarrow \pi/2$ , the crossover velocity, determined from  $\hat{\kappa}/\hat{v}_\parallel^{\frac{1}{2}} \approx 1$ , scales as:

$$\text{extended transverse XY: } \hat{v}^*(\phi) \sim \left| \frac{\pi}{2} - \phi \right|^{1/2} = \left| \frac{\pi}{2} - \phi \right|^{\frac{z + \dim[D_4]}{\dim[\Delta] - \dim[D_4]}}.$$

This scaling behavior is in full agreement with the RG predictions [41]. The generalization to other (Gaussian) models is straightforward (see info box). In all cases, the scaling of  $\hat{v}^*(\phi)$  depends universally on the equilibrium critical exponents.

#### Box 9: Generalization to other Gaussian models

This discussion can be generalized to variants of this fermionic Gaussian model with a dynamical critical exponent  $z$ , where a relevant coupling ( $\dim[g_0] > 0$ ) and an irrelevant coupling ( $\dim[g_j] < 0$ ) are driven linearly.

continued on next page

continued from page before

Firstly, the crossover scale  $\hat{\kappa}$  is determined by the difference in the scaling dimensions:

$$\hat{\kappa} \sim (\hat{v}_\perp / \hat{v}_\parallel)^{\frac{1}{\text{dim}[g_0] - \text{dim}[g_1]}} = (\tan(\theta))^{\frac{-1}{\text{dim}[g_0] - \text{dim}[g_1]}}. \quad (3.52)$$

The order of the drive does not enter the expression, as long as the couplings are driven with the same order  $n$ . Secondly, the conditions for  $n_\parallel$  to take a scaling form are given by:

$$\textcircled{1} : \hat{\kappa} / \hat{v}_\parallel^{\frac{1}{z + \text{dim}[g_j]}} \ll 1, \quad \textcircled{2} : 1 / \hat{v}_\parallel^{\frac{1}{z + \text{dim}[g_j]}} \gg 1. \quad (3.53)$$

Correspondingly, the crossover velocity  $\hat{v}^*(\phi)$  takes a scaling form as a function of  $|\pi/2 - \phi|$  in the limit  $|\pi/2 - \phi| \ll 1$ :

$$\hat{v}^*(\phi) \sim |\pi/2 - \phi|^{\frac{z + \text{dim}[g_j]}{\text{dim}[g_0] - \text{dim}[g_j]}} \quad (3.54)$$

(compare to Eq. (17) in Ref. [41]). For an order  $n$  drive, we only have to update  $z \rightarrow nz$ , resulting in

$$\hat{v}^*(\phi) \sim |\pi/2 - \phi|^{\frac{nz + \text{dim}[g_j]}{\text{dim}[g_0] - \text{dim}[g_j]}}. \quad (3.55)$$

**Crossover velocity - prefactor:** The analysis so far was based on scaling considerations. However, we are also interested in the prefactor, which will depend on the specifics of the model at hand. To estimate  $\hat{v}^*(\phi)$  *including the prefactor*, we compare our first approximations for  $n_\perp$  and  $n_\parallel$ , (3.48), with each other. We identify the crossover scale as the point where both contributions become comparable:

$$n_\perp(\hat{v}_\perp^*) \stackrel{!}{\approx} n_\parallel(\hat{v}_\parallel^*). \quad (3.56)$$

In the limit, where the width of the probability distribution  $p_k$  as a function of  $k$  becomes narrow, we can analytically evaluate the integrals in (3.48) by extending the integration to infinity. The two expressions are ( $b := \frac{\Gamma(\tau/6)}{(\pi)^{1/6}}$ ):

$$n_\perp(\hat{v}_\perp) \approx b \frac{a\Lambda_{\text{eff}}}{\pi} \cos(\phi)^{\frac{1}{6}} \cdot \hat{v}_\perp^{\frac{1}{6}}, \quad n_\parallel(\hat{v}_\parallel) \approx \frac{1}{2} \frac{a\Lambda_{\text{eff}}}{\pi} \sin(\phi)^{\frac{1}{2}} \cdot \hat{v}_\parallel^{\frac{1}{2}}. \quad (3.57)$$

The crossover condition (3.56) translates into:

$$\hat{v}^*(\phi) \approx (2b)^3 |\pi/2 - \phi|^{1/2}. \quad (3.58)$$

The exponent  $\alpha = 1/2$  fits exactly to the estimate in (3.54). In Fig. 3.6(f), we compare this limiting expression for  $\hat{v}^*(\phi)$  with the crossover velocities extracted from a full fit of  $n_E(\hat{v}; \phi)$ .

### 3.3.3 Limiting Case: Purely parallel Drive and Adiabaticity Restoring

For generalized drives that reach the critical point (with  $\hat{\Delta}^0 = 0$ ), the observable length scale  $\xi^*$  is determined by one of the drive scales  $\xi_\perp$  or  $\xi_\parallel$  (due to

the diverging equilibrium correlation length). A related scenario is a purely longitudinal drive, parallel to the phase boundary. In contrast to the generalized drives discussed before, a constant distance to the transition is kept, encoded in  $\hat{\Delta}^0 \neq 0$ . Therefore, the equilibrium correlation length is *finite* in this setting, competing with the drive scale  $\xi_{\parallel}$ . For sufficiently small drive velocities, the finite distance to the transition will *restore* adiabaticity with  $\xi^* \sim \xi_{\text{eq}}$ .

In this scenario, the effective parameters  $\hat{v}_k$  and  $\hat{\mu}_k$  in (3.45) are competing. For  $k \rightarrow 0$ ,  $\hat{\mu}_k$  will grow as well, indicating the growth of the relevant coupling  $\hat{\Delta}$ . At those scales, the asymptotic results ( $\Leftrightarrow t_i, t_f = \pm\infty$ ) will not be applicable. Therefore, the excitation density adapted from (3.49):

$$p(\hat{k}, \hat{v}_{\parallel}) = \exp\left(-\pi \frac{\hat{k}^6}{\hat{v}_{\parallel} \hat{k}^4}\right), \quad n_E(\hat{v}_{\parallel} \ll 1) \approx \frac{a\Lambda_{\text{eff}}}{2\pi} \sqrt{\hat{v}_{\parallel}}, \quad (3.59)$$

will only be applicable for an intermediate  $k$  range.

**Breakdown of asymptotic description:** From the spin perspective, it is reasonable to assume that a parallel drive starts at couplings  $J(t_i)/\gamma \rightarrow \infty$ <sup>10</sup> with  $(g(t) - 3/4J(t))/\gamma = \text{const.}$ . The drive ends at  $J(t_f)/\gamma \sim \mathcal{O}(1)$  (to stay in a parameter regime dominated by the Ising transition) with  $t_f \sim -1/\hat{v}_{\parallel}$ . In the following, we check under which conditions the drive ends outside the impulse regime such that the asymptotic analysis stays valid. In a first step, we bring the model into the canonical form (the same as in Sec. 2.1.1):

$$\bar{h}_k = -\hat{v}_k \tilde{t}_k \sigma_z + \sigma_x, \quad \tilde{t}_k = \hat{t}_k - \frac{\hat{\mu}_k}{\hat{v}_k}. \quad (3.60)$$

Here, the static part on the diagonal,  $\hat{\mu}_k$  (dictated by  $\hat{\Delta}^0$ ), was absorbed in the redefinition of time. For a fast effective drive velocity  $|\hat{v}_k| \gg 1$ , the onset of the impulse regime at time  $\tilde{t}_k^*$  is estimated by:

$$\frac{1}{2\mathcal{E}(k, \tilde{t}_k^*)} = \frac{1}{2\sqrt{(\hat{v}_k \tilde{t}_k^*)^2 + 1}} \stackrel{!}{\approx} \alpha \tilde{t}_k^* \Rightarrow \tilde{t}_k^* \sim \left(\frac{1}{\hat{v}_k}\right)^{1/2}. \quad (3.61)$$

Therefore, the evolution in the time range  $(-\tilde{t}_k^*, \tilde{t}_k^*)$  is assumed to be non-adiabatic (impulse). In the original (unshifted) time frame, the impulse regime at momentum  $k$  is given by  $(\hat{t}_{\text{start},k}^*, \hat{t}_{\text{end},k}^*)$ . To check if adiabaticity will be broken, we compare this time range with the time  $t_{f,k}$ , where the drive stops. There are three conditions:

- 0  $\hat{v}_k \gg 1$ : Fast effective drive, allowing for adiabaticity breaking.
- 1  $\hat{t}_{\text{start},k}^* < \hat{t}_{f,k}$ : Adiabaticity breaking requires the drive to *enter* the non-adiabatic regime.
- 2  $\hat{t}_{f,k} > \hat{t}_{\text{end},k}^*$ : For the asymptotic results to apply, the full impulse regime needs to be exploited.

<sup>10</sup>This is not entirely unproblematic: It might happen that for some finite  $t_i$ , the drive already starts in the impulse regime for some momenta  $k$ .

Condition ① reads:

$$\hat{t}_{\text{start},k}^* = \underbrace{-\tilde{t}_k^*}_{\sim \hat{k}} + \underbrace{\frac{\hat{\mu}_k}{\hat{v}_k}}_{\sim \hat{k}^{-1}} \stackrel{!}{<} \underbrace{\hat{t}_{k,f}}_{\sim \hat{k}^3}. \quad (3.62)$$

Depending on the momentum under consideration, there are two relevant scenarios for (3.62):

- Intermediate  $\hat{k}$ :  $|\tilde{t}_k^*| \gg \frac{\hat{\mu}_k}{\hat{v}_k}, \hat{t}_{k,f}$  (the drive enters the impulse regime at least partly).
- $\hat{k} \rightarrow 0$ :  $|\tilde{t}_k^*| \ll \frac{\hat{\mu}_k}{\hat{v}_k}$  (the drive cannot enter the impulse regime).

Due to the second scenario, the finite gap  $\hat{\Delta}^0$  suppresses adiabaticity breaking for sufficiently small momenta. The conditions ① to have a fast effective drive and ① to enter the impulse regime give rise to a momentum range, where adiabaticity breaking is possible:

$$\begin{array}{l} \text{effectively fast drive} \\ \text{entering impulse regime} \end{array} \quad \begin{array}{l} \hat{v}_k \gg 1 : \hat{k} \ll (\hat{v}_k)^{1/2} =: \hat{k}^*, \\ |\tilde{t}_k^*| \gg \hat{t}_{k,f} : \hat{k} \ll (\hat{v}_k)^{1/4} =: \hat{k}_v, \\ |\tilde{t}_k^*| \gg \hat{\mu}_k/\hat{v}_k : \hat{k} \gg \frac{(\hat{\Delta}^0)^{1/2}}{\hat{v}_k^{1/4}} =: \hat{k}_\Delta. \end{array} \quad (3.63)$$

Depending on  $\hat{k}$ , the dynamics of the two level systems is either adiabatic for the whole drive or partly non-adiabatic, see Fig. 3.7. For microscopically slow drives ( $\hat{v}_k \ll 1$ ), we have  $\hat{k}^* \ll \hat{k}_v$  and therefore the momentum splits into ‘adiabatic’ and ‘diabatic’ parts, see Fig. 3.7.

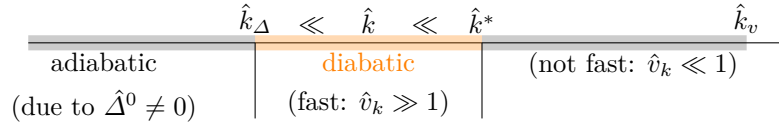


**Figure 3.7:** For a parallel drive with  $\hat{v}_k$  at a finite distance  $\hat{\Delta}^0$  to the critical point, excitations are only generated in a finite momentum range. At the largest distances,  $\hat{k} \ll \hat{k}_\Delta$  the drive is adiabatic due to the finite gap  $\hat{\Delta}^0$  in the system. For intermediate momenta, the drive is fast  $\hat{k}_\Delta \ll \hat{k} \ll \hat{k}^*$ . For larger momenta  $\hat{k} \gg \hat{k}^*$ , the drive is not fast and generates no significant excitations.

**Observability of subleading scaling:** For  $n_E(\hat{v}_k)$  to follow a scaling form, the evolution for a sufficiently large portion of momenta has to be diabatic. For a fixed velocity  $\hat{v}_k$ , a sufficiently large gap will restore adiabaticity once  $\hat{k}_\Delta \sim \hat{k}^*$ . In this case, the drive stays adiabatic up to  $t_f$  at all momentum scales. Therefore, only a sufficiently small gap  $\hat{\Delta}^0 \ll \hat{\Delta}^{0*}$ , with

$$\hat{\Delta}^{0*} \sim \hat{v}_k^{3/2}, \quad (3.64)$$

allows for non-adiabatic evolution and the subleading scaling can become observable. To estimate  $n_E(\hat{v}_k)$ , we determine the momenta, which also fulfill

condition 2. With a similar line of argumentation, the asymptotic results are roughly applicable for  $\hat{k}_\Delta \ll \hat{k}$  ( $\ll \hat{k}_v$ ):

$$n_E(\hat{v}_\parallel) \approx \frac{a\Lambda_{\text{eff}}}{\pi} \int_{\hat{k}_\Delta}^1 \exp\left(-\pi \frac{\hat{k}^2}{\hat{v}_\parallel}\right) d\hat{k}. \quad (3.65)$$

Here, the exact numerical value of the upper bound is not crucial, because excitations at those momenta are suppressed. Parallel to the discussion around (3.51), the excitation density (3.65) algebraically scales with  $\hat{v}_\parallel$  under the conditions: (1)  $\hat{\Delta}^0 \ll \hat{v}_\parallel^{3/2}$  and (2)  $\hat{v}_\parallel \ll 1$ .

In summary, a parallel drive with  $\hat{\Delta}(t) = \hat{\Delta}^0$  can reveal the universal scaling due to an equilibrium irrelevant coupling. However, the observability is limited by the size of  $\hat{\Delta}^0$ , which restores adiabaticity for  $k \rightarrow 0$ .

### 3.4 Generalized Drives in the transverse XY Model

The extended XY model and its (effective) fermionic version we have discussed before, require fine tuned parameters to guarantee  $z = 3$ . Without fine tuning, the extended XY model is in the Ising universality class with  $z = \nu = 1$ . In this case, to study the interplay of different drive scales, *including* the ones induced by driven irrelevant couplings, we need a drive of at least order  $n = 2$ . Those higher order drives are not exactly solvable anymore. Therefore, we rely on two different methods to extract the excitation density  $n_E$  for the transverse XY model: (1) AIA approximation (excitation density) and (2) numerical solution of the time dependent Schrödinger equation (full information). We extract the scaling exponents  $n_E(\hat{v}; \phi) \sim \hat{v}^\alpha$ , crossover velocities  $\hat{v}^*(\phi)$  and the extent of the overall scaling regime. The line of reasoning follows the discussion of the linearly driven extended XY model in Sec. 3.3.

**Setup:** The transverse XY model (in the vicinity of the fixed point) is described by the dimensionless (fermionic) couplings  $\{\hat{\Delta}, \hat{D}_2, \hat{D}_3, \dots\}$  (see again Sec. 2.2.2). The leading (relevant) coupling  $\hat{\Delta}$  and the first subleading (irrelevant) coupling  $\hat{D}_2$  are driven, which corresponds to a drive of the transversal field  $g(t)$  and the ferromagnetic coupling  $J(t)$ :

$$\hat{\Delta}(\hat{t}) = \hat{\Delta}^0 + \hat{v}_\perp \hat{t}^n \approx \frac{2(g(t) - J(t))}{2\gamma}, \quad \hat{D}_2(\hat{t}) = \hat{D}_2^0 + \hat{v}_\parallel \hat{t}^n \approx \frac{J(t)}{2\gamma}. \quad (3.66)$$

In contrast to the effective model discussed before, we will mostly consider drives that either start or end at the transition. The advantage of this protocol is that even for different drive angles, the start (or end) point in the phase diagram is always the same, e.g.,  $J(t_i) = g(t_i)$ . To be explicit, we set  $J/\gamma = 2$  at the transition if not stated differently. This corresponds to  $\hat{D}_2^0 \neq 0$  with  $\hat{D}_2^0 = 1$ . Building upon the discussions so far, we distinguish four different cases:

1. **Driving a relevant coupling towards the critical point** (corresponding to  $\hat{\Delta}^0 = 0$  in (3.66)). This scenario was discussed in Sec. 3.2. The finite

observable length scale is only determined by the drive:

$$\xi^* \sim \xi_{\perp} \Leftrightarrow n_E \sim \hat{v}_{\perp}^{-\frac{1}{nz+1/\nu}}.$$

2. **Driving a relevant and an irrelevant coupling  $g_j$  towards the critical point.** Such a generalized drive induces two competing scales:

$$\begin{aligned} \xi^* \sim \min[\xi_{\perp}, \xi_{\parallel}] &\Leftrightarrow n_E \sim \max[n_{\perp}, n_{\parallel}], \\ \text{with: } \xi_{\perp} \sim \hat{v}_{\perp}^{-\frac{1}{nz+1/\nu}}, \quad \xi_{\parallel} \sim \hat{v}_{\parallel}^{-\frac{1}{nz+\dim[g_j]}}. \end{aligned}$$

3. **Driving an irrelevant coupling** parallel to the phase boundary with  $\hat{\Delta}^0 \neq 0$ . In this case, the *finite* equilibrium correlation length  $\xi_{\text{eq}}$  stays in competition with the drive scale  $\xi_{\parallel}$ :

$$\xi_{\text{eq}} \sim (\hat{\Delta}^0)^{-\nu}, \quad \xi_{\parallel} \sim \hat{v}_{\parallel}^{-\frac{1}{nz+\dim[g_j]}}.$$

4. **Driving a coupling along a gapless line** (corresponding to  $\hat{\Delta}^0 = 0$ ). A special case corresponds to driving  $\gamma(t)$  (which nevertheless does not correspond to an irrelevant coupling in this setting).

The dynamic competition in the different momentum sectors  $(k, -k)$  is encoded in the effective velocity  $\hat{v}_k$  (drive scales) and static  $\hat{\mu}_k$  (equilibrium scales). In the limit  $k \rightarrow 0$ , the competition of  $\xi_{\perp}$  and  $\xi_{\parallel}$  is encoded in competing terms in  $\hat{v}_k$ , whereas the role of  $\xi_{\text{eq}}$  is reflected in  $\hat{\mu}_k$ . For small momenta, the terms scale as

$$\begin{aligned} \text{drive: } \hat{v}_k &\approx \hat{v}_{\perp} (ka)^{-(n+1)} + \hat{v}_{\parallel} (ka)^{-(n-1)}, \\ \text{static: } \hat{\mu}_k &\approx \underbrace{\hat{\Delta}^0 (ka)^{-1/\nu}}_{\text{relevant}} + \underbrace{\hat{D}_2^0 (ka)^{+1}}_{\text{irrelevant}}. \end{aligned} \quad (3.67)$$

In the following, we extract the observable scaling and crossover velocities for the different scenarios. Different methods to extract the excitation density are also discussed in the info box below.

**Box 10: Adiabatic-impulse approximation for drives starting/ending at the transition**

For drives that start or end at the transition (and end/start deep in the paramagnetic phase), the AIA approximation [45, 49] introduced in Sec. 2.1.1 has to be slightly adapted. From the perspective of the excitation density  $n_E$ , a drive starting or ending at the transition will give rise to the same expression [45]. For concreteness, we set  $t_i = -\infty$  and  $t_f = 0$ , in such a way that the drive term is always non-negative:  $\hat{v}_k \hat{t}_k^n \geq 0$ . Therefore, the gap for each  $(k, -k)$  two level system is smallest at  $t = 0$ . As before, the evolution starts in the adiabatic regime. Once the drive time scale and equilibrium correlation time scale are comparable (at  $\hat{t}_k^*$ ), adiabaticity is broken. Since the drive stops in the impulse regime,

continued on next page

continued from page before

the AI approximation is based on

$$p_k \approx |\langle -(0) | + (\hat{t}_k^*) \rangle_k|^2 = |\langle -( \hat{t}_k^*) | + (0) \rangle_k|^2, \quad (3.68)$$

$$\frac{1}{2\mathcal{E}(k, \hat{t}_k^*)} = \frac{1}{2\sqrt{(\hat{v}_k \hat{t}_k^{*n} + \hat{\mu}_k)^2 + 1}} \stackrel{!}{=} \alpha_n \hat{t}_k^*,$$

where  $\alpha_n$  is a coefficient we still need to fix. Depending on the scaling behavior of  $\hat{\mu}_k$ , we have two limiting cases for the time of adiabaticity breaking:

$$\hat{t}_k^* \approx \begin{cases} (\alpha_n |\hat{v}_k|)^{-\frac{1}{n+1}} & : \frac{|\hat{v}_k|}{\alpha_n^n \text{Max}[1, \hat{\mu}_k]^{n+1}} \gg 1 \\ (\alpha_n \text{Max}[1, \hat{\mu}_k])^{-1} & : \frac{|\hat{v}_k|}{\alpha_n^n \text{Max}[1, \hat{\mu}_k]^{n+1}} \ll 1 \end{cases}. \quad (3.69)$$

**Diabatic limit:** The first case in (3.69) is relevant for  $\hat{\Delta}^0 = 0$ . In this case,  $\hat{\mu}_k$  is vanishingly small for  $k \rightarrow 0$ , such that  $\hat{t}_k = 0$  corresponds to the ‘anti-crossing’ (or ‘touching’) center of the two level systems. The coefficient  $\alpha_n$  can be fixed by comparing the AI approximation of  $n_E$  with a *diabatic* expansion (assuming strong occupation, see Ref. [45]):

$$\alpha_n = (1 - \Delta n) \Gamma(1 - \Delta n)^{1/\Delta n} \cos\left(\frac{\pi}{2} \Delta n\right)^{1/\Delta n}, \quad \Delta n := \frac{n}{1+n}.$$

**Adiabatic limit:** Once  $\hat{\Delta}^0 \neq 0$ ,  $\hat{\mu}_k$  will become the dominant scale for  $k \rightarrow 0$  and the second case in (3.69) applies. In this limit, the AI approximation (3.68) indicates a *suppression* of the excitation probability:

$$p_k^{(\text{AI})} \approx \frac{1}{4} \left( \frac{\hat{v}_k}{\alpha_n^n \text{Max}[1, \hat{\mu}_k]^{n+2}} \right)^2 \ll 1. \quad (3.70)$$

This expression can be compared to a **first order adiabatic approximation** (see Refs. [73, 80, 83] for in depth discussions). In this approximation, the excitation density is expanded around the *adiabatic* limit  $a_k(\hat{t}_{k,f}) = 1$  (see again the adiabatic representation (3.25)) for small velocities  $\hat{v}_k \ll 1$ . For  $\hat{t}_{k,i} = -\infty$  and  $\hat{t}_{k,f} = 0$ , the leading contribution for an order  $n$  drive in powers of  $\hat{v}_k$  is [73, 80]

$$p_k \approx \left( \frac{n!}{2^{n+1}} \right)^2 \left( \frac{\hat{v}_k}{(\mathcal{E}_k(0))^{(n+2)}} \right)^2 \sim \begin{cases} (\hat{v}_k)^2 & : \hat{\mu}_k \ll 1 \\ \left( \frac{\hat{v}_k}{\hat{\mu}_k^{n+2}} \right)^2 & : \hat{\mu}_k \gg 1 \end{cases}. \quad (3.71)$$

The two cases underline the role of  $\hat{\mu}_k$ : on the one hand, for  $\hat{v}_k, \hat{\mu}_k \ll 1$ , the excitation density is small in accordance with a (quasi) adiabatic drive. Adiabaticity breaking is indicated by  $\hat{v}_k \approx 1$ , reflecting the breakdown of the approximation (see also Ref. [10]). On the other hand,  $\hat{\mu}_k \gg 1$  can *restore* adiabaticity: even for an effectively fast

continued on next page

continued from page before

drive,  $p_k$  is suppressed by  $\hat{\mu}_k$ . This adiabatic approach complements the exact asymptotic approach and the adiabatic-impulse approximation. Whereas the adiabatic approach is controlled for  $\hat{v}_k \ll 1$  (breaking down for  $k < k^*$ ), the adiabatic-impulse approximation works well for  $\hat{v}_k \gg 1$ .

In the asymptotic limit  $t_f \rightarrow \infty$ , another method can be used (see App. C): the leading contribution to  $p_k$  for  $t_f \rightarrow \infty$  is non-analytic and can be determined from the complex zeros of  $\mathcal{E}(k, \hat{t}_k)$  [85, 86].

**Cases (1) and (2) - generalized drives:** We consider a quadratic drive ( $n = 2$ ) that reaches the equilibrium critical point, where the underlying correlation time diverges. Therefore, a microscopically slow drive will inevitably break adiabaticity. For case (2), the onset of a fast effective drive  $\hat{v}_{k^*} \approx 1$  at momentum  $k^*$  can either result from the driven relevant coupling (with  $\hat{v}_\perp$ ) or the driven irrelevant coupling (with  $\hat{v}_\parallel$ ). Parallel to the discussion in Sec. 3.3, we can define a momentum scale  $\hat{\kappa} := (\hat{v}_\perp/\hat{v}_\parallel)^{1/2}$ . For  $\hat{k}^* \ll \hat{\kappa}$ , excitations are dominantly generated from the driven equilibrium relevant coupling. For  $1 \gg \hat{k}^* \gg \hat{\kappa}$ , excitations are generated from the driven equilibrium irrelevant coupling:

$$\hat{v}_{k^*} \approx 1 : \begin{cases} \hat{k}^* \ll \hat{\kappa} \text{ (KZM)} : & \hat{k}^* \sim \hat{v}_\perp^{\frac{1}{n+1}}, \\ \hat{\kappa} \ll \hat{k}^* \ll 1 \text{ (subleading)} : & \hat{k}^* \sim \hat{v}_\parallel^{\frac{1}{n-1}}. \end{cases} \quad (3.72)$$

An overview of the analysis for the generalized case (2) is shown in Fig. 3.8. Parametrizing the drive in terms of the angle  $\phi$  and magnitude  $\hat{v}$ :

$$\begin{pmatrix} \hat{v}_\perp \\ \hat{v}_\parallel \end{pmatrix} = \hat{v} \begin{pmatrix} \cos(\theta) \\ \sin(\theta) \end{pmatrix},$$

sets of  $n_E(\hat{v}; \phi)$  are shown in Fig. 3.8(a),(b). For intermediate angles, numerical integrations of the Schrödinger equation<sup>11</sup> (+) are compared with the AI approximation (orange lines). Afterwards, the AI approximation is used for a wider range of  $\hat{v}$  and  $\phi$ . For  $\phi$  sufficiently close to  $\pi/2$ , the subleading scaling regime becomes observable for  $1 \gg \hat{v} \gg \hat{v}^*(\phi)$ . The corresponding extent of the scaling regimes are shown in Fig. 3.8(d).

**Universal scalings:** Based on (3.67), the two scaling regimes of  $n_E$  are  $n_E \sim \hat{v}_\perp^{\frac{1}{3}}$  and  $n_E \sim \hat{v}_\perp^1$ , see Fig. 3.8(c). The scaling of the crossover velocity is expected to be

$$\text{transverse XY: } \hat{v}^*(\phi) \sim \left| \frac{\pi}{2} - \phi \right|^{1/2} = \left| \frac{\pi}{2} - \phi \right|^{\frac{z + \dim[D_2]}{\dim[\Delta] - \dim[D_2]}},$$

which fits to the findings in Fig. 3.8(d). Here, the crossover velocity was extracted from (i) a direct fit as well as (ii) the approximation (3.56).

<sup>11</sup>Using the adiabatic basis to solve the dynamics, stopping at  $J(t_f)/(2\gamma) \approx 600$ .

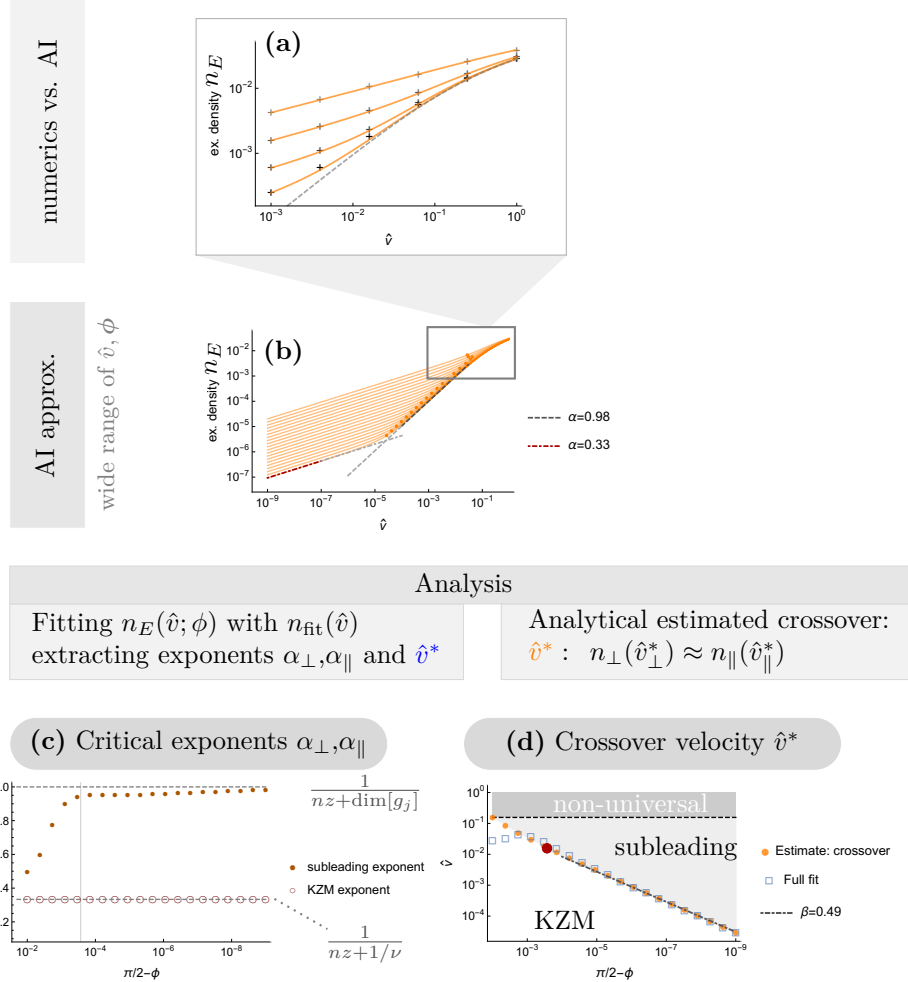


**Figure 3.8:** Summary of generalized drives in the transverse XY model ( $n = 2$ ) starting/stopping at the transition: **(a)** Set of curves  $n_E(\hat{v}; \phi)$  (log-log) for fixed angles ( $\pi/2 - \phi = 10^{-1}, 5 \times 10^{-3}, 2 \times 10^{-4}, 10^{-5}$ ) using (i) the AI approximation (orange lines; dashed line describes limiting case  $\phi \rightarrow \pi/2$ ) and (ii) numerical solutions (+, starting at the transition). **(b)** To analyze an extended velocity range, the AI approximation is used to approximate  $n_E$  (log-log). Two scaling regimes are observable ( $n_E \sim \hat{v}^{\alpha}$  fits are shown as well) with crossover velocities indicated by orange dots. **(c)** Scaling exponents extracted from the same fitting model as in the minimal model. The extracted exponents approach the RG predictions (dashed lines), where  $\phi > \phi_{\text{min}}$  (vertical line) allows for a quantitatively reasonable estimate. **(d)** Different scaling regimes in the  $(\pi/2 - \phi, \hat{v})$  plane with the crossover velocities estimated by Eq. (3.56) (orange dots) and a full fit (blue squares) of the curves in (b). In the limit  $|\pi/2 - \phi| \ll 1$ , the crossover velocities obey a scaling law with  $\beta = 0.49$  (fitting to the RG prediction of  $1/2$ ).

**Case (3) - Longitudinal drive:** Building upon the intuition from the extended XY model, we consider a slow quadratic drive of  $\hat{D}_2$  (with  $\hat{v}_\parallel$ ) parallel to the phase boundary with  $\hat{\Delta}(t) = \hat{\Delta}^0 \geq 0$ , see Fig. 3.9(a). For  $n = 2$ , the drive coupling is a relevant coupling with  $\dim[\hat{v}_\parallel] = 2z + \dim[D_2] > 0$  and can lead to adiabaticity breaking. However, a sufficiently large gap can restore adiabaticity. Only for small enough gaps, a parallel drive with  $\hat{v}_\parallel$  induces adiabaticity breaking for a finite range of momenta  $k$ .

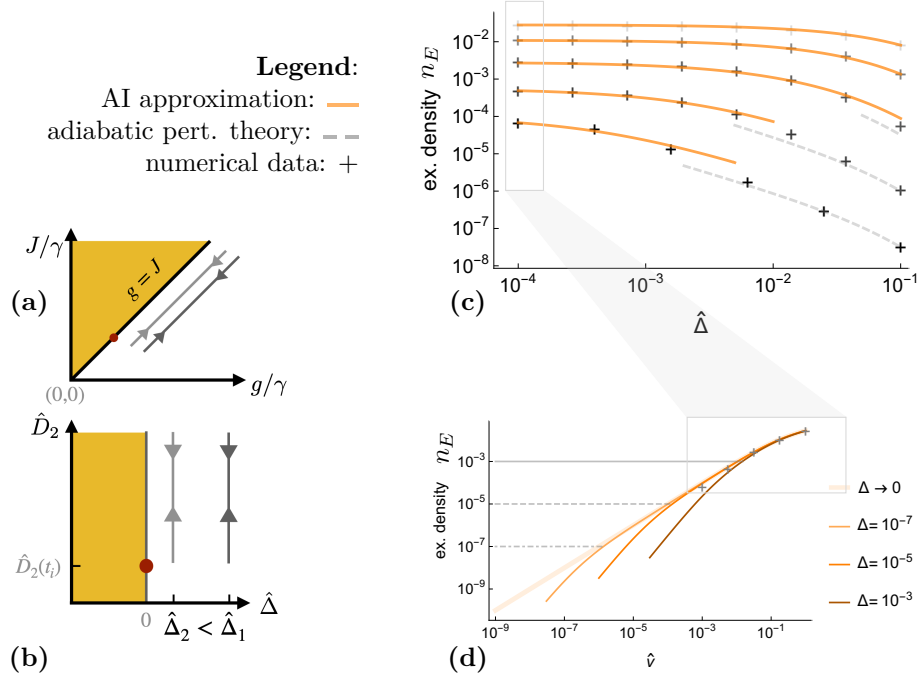


**Figure 3.9:** Parallel drive in the transverse XY model ( $n = 2$ ): drive protocol in (a) spin coupling space and (b) fermionic coupling space for finite gaps  $\hat{\Delta} = \hat{\Delta}^0$ . (c) Excitation density  $n_E(\hat{\Delta}; \hat{v})$  (log-log) for fixed velocities, extracted from (i) numerics (+), (ii) AI approximation (orange line), and (iii) (first order) adiabatic perturbation theory (gray dotted line). The velocities from top to bottom are:  $\hat{v} = 1.0 \times 10^0, 1.8 \times 10^{-1}, 3.2 \times 10^{-2}, 5.6 \times 10^{-3}, 1.0 \times 10^{-3}$  with system size  $L = 2 \times 10^3$  ( $L = 10^4$  for the smallest velocity). (d)  $n_E(\hat{v}; \hat{\Delta})$  for different fixed gaps  $\hat{\Delta}$  (AI approximation). The numerical data (+) from (b) for the smallest gap ( $\hat{\Delta} = 10^{-4}$ ) are also plotted. The subleading scaling regime ( $n_E \sim \hat{v}^1$ ) is only observable for  $\hat{\Delta} \ll \hat{v} \ll 1$  ( $\hat{v} \sim \hat{\Delta}$  indicated by the gray horizontal lines).

We consider a drive starting at  $\hat{D}_2(t_i) \approx J(t_i)/(2\gamma) = 1$  and running up to  $J(t_f)/(2\gamma) \gg 1$ , see Fig. 3.9(a),(b). We compare (i) direct numerical integrations with (ii) the AI approximation, see Fig. 3.9(c),(d). By construction, the AI approximation is quantitatively valid for fast drives  $\hat{v}_k \gg 1$ . Therefore, using the AI approximation for all momenta becomes reasonable once adiabaticity is broken for a sufficiently large range of momenta. In contrast, the finite gap can restore adiabaticity even for all  $k$ . In this case, the excitation density should

be better described by the *adiabatic* perturbation theory (3.71). In Fig. 3.9(c) a comparison between the AI approximation for all momenta (orange line) and the adiabatic approximation for all momenta (gray dashed line) is shown.

To reveal the competition between the drive and the finite gap, we extract  $n_E(\hat{\Delta}^0; \hat{v})$  as a function of the gap size  $\hat{\Delta}^0$  and different fixed velocities, see Fig. 3.9(c). Lowering the gap leads to an increased excitation density, saturating for  $n_E(\hat{\Delta}^0 \rightarrow 0; \hat{v})$ . In the limiting case  $\hat{\Delta}^0 \rightarrow 0$ , adiabaticity is broken on all momentum scales with  $\hat{k} \ll \hat{k}^*$ . These asymptotic values of  $n_E$  can be plotted as a function of  $\hat{v}$ , see Fig. 3.9(d). In this limit,  $n_E$  is an *algebraic* function of  $\hat{v}$  again, revealing the subleading scaling behavior  $n_E \sim \xi_{\parallel}^{-1}$  with  $n_E \sim \hat{v}_{\parallel}^1$ . Complementarily, the excitation density  $n_E(\hat{v}; \hat{\Delta}^0)$  as a function of  $\hat{v}$  but finite fixed gaps  $\hat{\Delta}^0$  is shown in Fig. 3.9(d). An algebraic scaling regime is restricted to  $\hat{\Delta}^0 \ll \hat{v} \ll 1$ . For smaller velocities, the excitation density vanishes more quickly and the observable scale  $\xi^*$  in the system is dictated by the equilibrium correlation length (analytically known for the XY model [59, 60]), see Fig. 3.10(b).

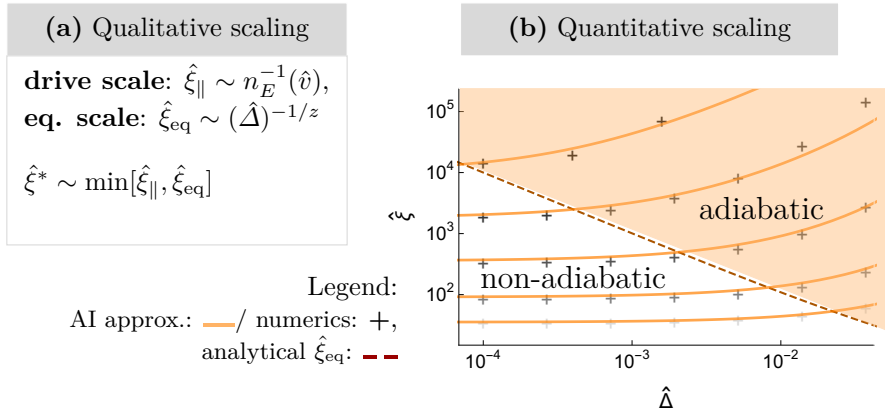


**Figure 3.10:** *Parallel drive in the transverse XY model ( $n = 2$ ): (a) Qualitative consideration: For a parallel drive, the competing length scales are set by the finite gap, dictating  $\hat{\xi}_{\text{eq}}$ , and the drive velocity, dictating  $\hat{\xi}_{\parallel}(\hat{v})$ . Only the smaller one is observable. (b) Comparison of  $n_E^{-1}(\hat{\Delta}; \hat{v}) \sim \hat{\xi}_{\parallel}$  (solid lines (AI) as in Fig. 3.9; +: (inverted) numerical data from Fig. 3.9) and  $\hat{\xi}_{\text{eq}}$  (red dashed line; evaluated for fixed  $J/\gamma$  close to  $\hat{D}_2^0 = 1$ ). Once  $\hat{\xi}_{\parallel}(\hat{v}) \ll \hat{\xi}_{\text{eq}}$ , a non-adiabatic regime is entered.*

**Comparison of scales:** The onset of a fast drive in the generalized setting is indicated by  $\hat{v}_{k^*} \approx 1$ . However, this condition is not sufficient for adiabaticity breaking once the static scales, encoded in  $\hat{\mu}_k$ , grow large as well. We can associate individual onset scales to  $\hat{v}_k$  and  $\hat{\mu}_k$  according to:  $\hat{v}_{k^*} \approx 1$  and  $\hat{\mu}_{k_\mu} \approx 1$ . Non-adiabatic dynamics is expected for  $k_\mu \ll k \ll k^*$ . Therefore, for a given velocity  $\hat{v}_{\parallel}$  adiabaticity breaking, and there observable algebraic scaling of  $n_E$ ,

is only possible for a sufficiently small gap  $\hat{\Delta}^0 \ll \hat{\Delta}^{0*}$ :

$$\hat{\Delta}^{0*} \sim \hat{v}_{\parallel}^{\frac{1/\nu}{nz + \dim[g_j]}} \stackrel{\text{here}}{=} \hat{v}_{\parallel}^1. \quad (3.73)$$

The condition  $\hat{\Delta}^0 \ll \hat{\Delta}^{0*}$  is also required for  $n_E(\hat{v}; \hat{\Delta}^0)$  to have an algebraic scaling form (in analogy to the discussion of the extended XY model in Sec. 3.3.3).

**Case (4) - Driving along a gapless line:** The limiting case of  $\hat{\Delta}^0 \rightarrow 0$  corresponds to a drive *along* the gapless line (related drives were already used in the transverse XY model, an overview is given in [61, 125, 126]). In this limit,  $n_E(\hat{v})$  becomes an algebraic function of  $\hat{v}$ . A simpler to realize scenario instead is a drive of the coupling  $\gamma$  (see again (2.24)), analyzed in Ref. [125]. In the limit  $k \rightarrow 0$ , this corresponds to driving  $D_1$ , which requires a reevaluation of the RG approach. In the approach used in Sec. 2.2.2, we *scaled out* the coupling  $D_1$ . It corresponded to the lowest momentum term, defining the fixed point theory  $S_{\text{crit}}^*$ . Once  $D_1$  is driven, we cannot scale out  $D_1$  anymore and the leading *non-driven* derivative term corresponds to  $D_2$ . In turn, the fixed point theory we are analyzing *in the driven scenario* has changed. The resulting critical exponents are  $z' = 2$  and  $\nu' = 1/2$ . This implies that  $D_1$  is a *relevant* coupling with  $\dim[D_1] = +1$ . Therefore, even a linear drive induces an observable scaling as predicted from the RG:

$$n_E(\hat{v}_{\parallel}) \sim \hat{v}_{\parallel}^{\frac{1}{2+1}}, \quad (3.74)$$

consistent with the findings in Ref. [125].

#### Box 11: Drives along gapless lines in Gaussian models

To cover a more general fermionic Gaussian case, consider an equilibrium model with dynamical critical exponent  $z$ . This corresponds to a fixed point theory with a term  $\propto D_z k^z$ . The next subleading term is of the form  $\propto D_l k^l$ . If the coupling  $D_z$  is driven with an order  $n$  drive, we scale out the next subleading coupling  $D_l$  and the critical exponents and scaling of  $n_E$  are given by:

$$z' = l, \quad \dim[D_z] = l - z : \quad n_E(\hat{v}_{\parallel}) \sim \hat{v}_{\parallel}^{\frac{1}{(n+1)l-z}}, \quad (3.75)$$

consistent with the findings in Refs. [125, 132].

### 3.5 Outlook: Generalized KZM, Universal and Non-Universal Aspects

In the following, we discuss some further aspects: (i) the role of the cutoff, (ii) geometries at a Wilson-Fisher fixed point (complementing the non-interacting fermionic model), (iii) measures of adiabaticity breaking beyond the excitation density and (iv) the scaling of the entanglement entropy.

**Role of the cutoff:** The scaling behavior of  $\xi^*$  (or here  $n_E$ ) is universal. It only depends on the equilibrium critical exponents and the order of the drive. From an abstract point of view, it results from the RG flow in the vicinity of a fixed point. Many microscopic details are *irrelevant* in its vicinity. As an example, spin models with additional interaction terms (e.g. between site  $l$  and  $l + 3$  etc.) can have the same critical behavior compared to the (extended) transverse XY model. At large length scales, the differences are washed out. However, they enter the description of a model at hand in the form of, e.g., an effective cutoff scale  $\Lambda_{\text{eff}}$ . For the extended XY model, we have used the description (3.40), where  $\Lambda_{\text{eff}}$  is sensitive to the introduction of further couplings. In case of a drive, the cutoff is related to the range of dimensional, microscopic velocities  $v_{\perp}, v_{\parallel}$ , for which the different universal scalings become observable. From the sketch in Fig. 3.2(c), we can already infer that a larger cutoff is favorable to observe the subleading scaling regime. To quantify this range, consider the extended XY model with  $z = 3$ :

- To observe the subleading scaling, we need:  $v_{\perp}^{1/3} \ll v_{\parallel} \ll \Lambda_{\text{eff}}^2$ .
- To not enter the non-universal regime, we need:  $v_{\perp} \ll \Lambda_{\text{eff}}^6$  and  $v_{\parallel} \ll \Lambda_{\text{eff}}^2$ .

The three regimes (i) leading scaling, (ii) subleading scaling and (ii) non-universal are summarized in a  $(v_{\perp}, v_{\parallel})$ -plot of *microscopic* velocities in Fig. 3.11. For  $v_{\perp}^{1/3} \ll v_{\parallel}$ , the subleading scaling with  $v_{\parallel}$  becomes observable (orange region). Otherwise, the leading KZM scaling with  $v_{\perp}$  is observable (white region). Two exemplary drive protocols<sup>12</sup>, are shown in Fig. 3.11 as dashed lines: only once the angle  $\phi_{\Lambda}$  is sufficiently close to  $\pi/2$ , the subleading scaling regime is entered.

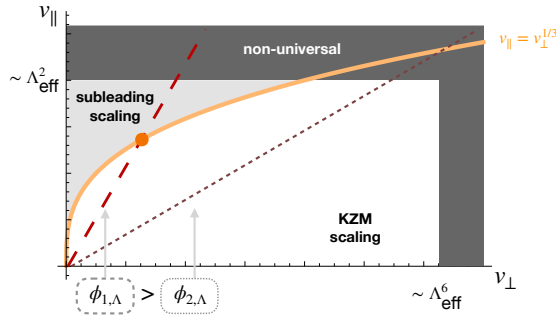


**Figure 3.11:** Schematic scaling regimes of the generalized KZM for dimensional velocities: the orange line separates the leading scaling (white region) from the subleading one (light gray region). The cutoff  $\Lambda_{\text{eff}}$  sets a scale, below which drives can be considered slow. The dashed lines correspond to tracking  $n_E(\hat{v}; \phi)$  for two different angles  $\phi_{1|2, \Lambda}$ . Only for sufficiently large angles (here:  $\phi_{1, \Lambda}$ ) both scalings are observable with the crossover velocity indicated by the darker orange dot.

<sup>12</sup>Corresponding to the setup we have discussed before (in terms of  $\hat{v}$  and  $\phi = \phi_{\Lambda}$ ).

**Box 12: Cutoff-dependence of the angles  $\phi_\Lambda$** 

The dimensionless velocities and the angles in the extended transverse XY model are defined as:

$$\left. \begin{aligned} \hat{v}_\perp(\Lambda_{\text{eff}}) &= (v_\perp/D_3^2) \Lambda_{\text{eff}}^{-6} \\ \hat{v}_\parallel(\Lambda_{\text{eff}}) &= (v_\parallel/D_3^2) \Lambda_{\text{eff}}^{-2} \end{aligned} \right\} \tan(\phi_\Lambda) = \frac{\hat{v}_\parallel(\Lambda_{\text{eff}})}{\hat{v}_\perp(\Lambda_{\text{eff}})} = \frac{v_\parallel}{v_\perp} \cdot \Lambda_{\text{eff}}^{-4}. \quad (3.76)$$

Changing the cutoff from  $\Lambda_{\text{eff}} \rightarrow \Lambda'_{\text{eff}}$ , the new angle is related to the previous one by:

$$\tan(\phi_{\Lambda'}) = \tan(\phi_\Lambda) \left( \frac{\Lambda_{\text{eff}}}{\Lambda'_{\text{eff}}} \right)^{-4} \Rightarrow \phi_{\Lambda'} \stackrel{\phi \rightarrow \pi/2}{\approx} \frac{\pi}{2} - \left( \frac{\Lambda'_{\text{eff}}}{\Lambda_{\text{eff}}} \right)^{-4} \left( \frac{\pi}{2} - \phi_\Lambda \right). \quad (3.77)$$

A larger cutoff ( $\Lambda'_{\text{eff}} > \Lambda_{\text{eff}}$ ) therefore has two manifestations: (i) it pushes the angles closer to  $\pi/2$  (see (3.77)), and (ii) the range of microscopic velocities, where subleading scaling is observable, is enlarged (the gray area in Fig. 3.11 is pushed outwards).

**Geometry at an interacting (Wilson-Fisher) fixed point and the generalized KZM:**

So far, we have studied a non-interacting fermion theory and its RG analysis. In this case, the eigenvectors of the linearized RG flow (described by the matrix  $M$ ) are orthogonal to each other (corresponding to  $\hat{\Delta}, \hat{D}_2, \dots$ ). Therefore, the (de)construction of a generalized drive in terms of those couplings is straightforward. Nevertheless, the notion of a ‘transversal’ drive is already altered once *spin* couplings are considered (see again Sec. 3.1.3): in this case, a transversal drive is not necessarily oriented orthogonally to the phase boundary. Another instance of this ‘orthogonality issue’ arises in interacting theories, e.g. a  $\phi^4$  theory (field theoretic relative of the lattice Ising model, defined below). It features a Wilson-Fisher fixed point [143], describing the transition (with, e.g., a finite value of the mass and interaction coupling). In this case, the matrix  $M$  is non-symmetric and has non-orthogonal eigenvectors. The equilibrium  $\phi^4$  theory in  $d$  dimensions is defined as:

$$S_{\text{eff}} = \int d^d x \left( \frac{1}{2} \nabla \phi \cdot \nabla \phi - \frac{\hat{g}_2}{2} \Lambda^2 \phi^2 - \frac{\hat{g}_4}{4!} \Lambda^{4-d} \phi^4 \right),$$

where  $\phi$  is a real-valued field. Here, the cutoff scale  $\Lambda$  is used to define dimensionless couplings [144]. Without going into the details, the linearized flow for the  $\phi^4$  theory in  $d = 4 - \epsilon$  dimensions [143] and relative to the non-Gaussian Wilson-Fisher fixed point  $\vec{g}^* = (\hat{g}_2^*, \hat{g}_4^*) \neq (0, 0)$  reads (see, e.g., Ref. [52, 144]):

$$\partial_s \begin{pmatrix} \delta \hat{g}_2 \\ \delta \hat{g}_4 \end{pmatrix} = \underbrace{\begin{pmatrix} 2 - \epsilon/3 & a(1 + \frac{\epsilon}{6}) \\ 0 & -\epsilon \end{pmatrix}}_{=: M} \begin{pmatrix} \delta \hat{g}_2 \\ \delta \hat{g}_4 \end{pmatrix}, \quad (3.78)$$

where  $a$  is a constant. Note that  $M$  is non-symmetric and we have to distinguish between left and right eigenvectors (which nonetheless have the same

eigenvalues) [64]:

$$M \cdot \mathbf{e}_R^{(j)} = \lambda_j \mathbf{e}_R^{(j)}, \quad \mathbf{e}_L^{(j)} \cdot M = \mathbf{e}_L \lambda_j. \quad (3.79)$$

The set of right eigenvectors are not orthogonal to each other, but the left and right eigenvectors corresponding to different eigenvalues are orthogonal. The eigendirections define the effective couplings with unique scaling dimensions:

$$\begin{array}{ll} \text{relevant} & \text{irrelevant} \\ \hat{\sigma}_2 = \delta \hat{g}_2, & \hat{\sigma}_4 = \delta \hat{g}_4 - \frac{a(1 + \epsilon/6)}{2(1 + \epsilon/3)} \delta \hat{g}_2, \end{array} \quad (3.80)$$

$$\dim[\sigma_2] = 2 - \epsilon/3, \quad \dim[\sigma_4] = -\epsilon. \quad (3.81)$$

Therefore, a slow transversal drive in the  $\phi^4$  theory has to point in the direction of  $\hat{\sigma}_2$  and a parallel drive in the direction of  $\hat{\sigma}_4$ . A general drive can then be decomposed into these two directions (with the help of the left eigenvectors). In terms of angles, a longitudinal drive corresponds to  $\phi = \pi/2$ , whereas a transversal drive corresponds to  $\phi \neq 0$  (in analogy to the drives in the spin coupling space we have discussed before).

### Box 13: Outlook - Beyond quasi-particle excitation densities

The analysis so far was based on the excitation density. For the models under investigation, excitations are well-defined, either as the quasi-particles in the fermionic system or domain walls/spin flips in the spin system. If such a notion is not possible anymore, other measures like the entanglement entropy, diagonal entropy density or excess energy density can be used [80] (see also, e.g., Refs. [130, 145]). The last two are based on the overlap of the state with the (instantaneous) energy eigenstates  $|\epsilon_m\rangle$  (in one dimension):

$$\text{diagonal entropy density: } S_{\text{diag}} = -\frac{1}{L} \sum_m p_m \log(p_m), \quad p_m = |\langle \psi | \epsilon_m \rangle|^2,$$

$$\text{excess energy density: } Q = \frac{1}{L} \sum_m (E_m - E_0) p_m.$$

Here,  $E_0$  is the ground state energy. Making use of, e.g., the adiabatic perturbation theory, these quantities also depend universally on the underlying critical exponents [80, 83]. As an example, consider the excess energy density for a generalized order  $n$  drive that ends at the transition:

$$Q \sim \frac{1}{L} \sum_k \epsilon_k(t_f) p_k(t_f) \sim (k^*)^{z+1} \sim \begin{cases} \hat{v}_{\parallel}^{\frac{z+1}{nz+\dim[g_j]}} & \text{subleading,} \\ \hat{v}_{\perp}^{\frac{z+1}{nz+1/\nu}} & \text{leading.} \end{cases}$$

**Sudden quenches and the role of time:** Complementary to the slow drives we have considered here, the limit of very fast drives (sudden quenches) have been studied in the literature (see, e.g., Ref. [73]). Here, the system is prepared in the ground state and a parameter of the system (e.g., the transversal field)

is changed instantaneously. The original ground state corresponds to a (superposition of) excited state(s) of the new Hamiltonian. Also in this scenario, observables like the excitation density scale universally with the equilibrium critical exponents as a function of the parameter change [73, 80]. Therefore, a slow quench and a sudden quench are qualitatively related. This can be traced back to the adiabatic impulse scenario: a slow drive (ending at the transition) can be understood as a sudden quench from the point in parameter space where adiabaticity is broken to the final point:  $(g(t^*), J(t^*)) \rightarrow (g(t_f), J(t_f))$  (where  $t^*$  is the time of adiabaticity breaking) [80]. To compare sudden quenches with *generalized* slow drives (including irrelevant couplings), we take reconsider the role of the adiabaticity breaking time. In the realm of the AIA approximation, we extracted it from equating (i) the time to reach the smallest gap and (ii) the time scale set by the gap, (3.68), for each two level system labelled by  $k$ . In this context, we used the rescaled,  $k$ -dependent time  $\hat{t}_k \sim \hat{k}^z t$ . For a transversal drive, where only the relevant coupling  $\hat{\Delta}$  is driven, we find:

$$\hat{t}_k^* \sim \hat{v}_\perp^{-1/(n+1)} \hat{k}^z \Leftrightarrow t^* \sim \hat{v}_\perp^{-1/(n+1)}. \quad (3.82)$$

This implies that there is a unique time of adiabaticity breaking  $t^*$  for *all* low lying momenta (no  $k$ -dependence of  $t^*$ ). In contrast, adiabaticity breaking due to a driven *irrelevant* coupling gives rise to

$$\hat{t}_k^* \sim \hat{v}_\parallel^{-1/(n+1)} \hat{k}^{(nz + \dim[g_j])/(n+1)} \Leftrightarrow t^*(k) \sim \hat{v}_\parallel^{-1/(n+1)} \hat{k}^{-\alpha}, \quad (3.83)$$

$$\alpha := z - \frac{nz + \dim[g_j]}{n+1} > 0.$$

This relation has two implications: (i) the *unrescaled* adiabaticity breaking time  $t^*(k)$  is  $k$ -dependent and (ii)  $t^*(k)$  is *diverging* for  $k \rightarrow 0$ . Therefore, we cannot associate a unique adiabaticity breaking time  $t^*$  to the drive of *irrelevant* couplings.

Accordingly, the association of slowly driven couplings with a sudden quench of the form  $(g(t^*), J(t^*)) \rightarrow (g(t_f), J(t_f))$  does *not* hold directly for the generalized case<sup>13</sup>. The implication (ii) mentioned above can limit the observability of the subleading scaling behavior. Depending on the other involved scales (stemming from  $\hat{v}_\perp$  and  $\hat{\Delta}^0$ ), the diverging behavior of  $t^*(k)$  indicates that the microscopic parameters  $(g(t^*(k)), J(t^*(k)))$ , below which the drive is non-adiabatic, will become large. If a drive is supposed to start in an adiabatic regime *for all*  $k$ , the aforementioned growth of  $(g(t^*(k)), J(t^*(k)))$  can be an obstacle.

**Remark:** In the last sections, we have made massive use of drives with (formally)  $t_i = \infty$  and therefore  $g(t_i), J(t_i) \rightarrow \infty$ . This is reasonable as long as finite values of  $g(t_i), J(t_i)$  will reproduce similar results. This is the case for drives of relevant couplings. In light of the discussion above, this can be a problematic assumption for longitudinal drives with  $\hat{\Delta}^0 = 0$  and  $\hat{v}_\perp = 0$ . These scales, once present, dominate the dynamics for  $k \rightarrow 0$ .

**Quantum information perspective - bridge to the second project:** As we have already mentioned partly in Sec. 2.2, close to the critical point of the

<sup>13</sup>We can still make use of this conceptual idea, but we have to consider the different states  $|\psi(t_k^*)\rangle_k$  individually:  $|\text{GS}(g(t^*(k)), J(t^*(k)))\rangle_k \rightarrow |\text{GS}(g(t_f), J(t_f))\rangle_k$ .

Ising transition, the entanglement entropy between a subregion  $A$  in space and the rest of the system scales as:

$$S_{vN}(A) \approx \frac{1}{6} \log_2(\min[\xi, |A|]). \quad (3.84)$$

Therefore, it is a witness of the correlation length scaling. For a slow transversal drive, the created excitations reduce the correlation length and therefore also the entanglement between two subsystems<sup>14</sup>. Combining this scaling behavior of the entropy with the KZM scaling of  $\xi^*$ , we expect that the entanglement between one half of the system and the other half scales as (see also Ref. [12]):

$$S_{vN}(L/2) \sim \frac{1}{6} \log_2(\hat{\xi}_\perp) \sim -\frac{1}{6 \cdot (nz + 1/\nu)} \log_2(\hat{v}_\perp) \quad (3.85)$$

(for an order  $n$  drive and  $\hat{\xi}_\perp \ll L/2$ ). As an example, we consider a linear (or quadratic) drive with velocity  $v_\perp$  of the transverse field. The drive starts at some finite value  $(g - J)/\gamma$  in the paramagnetic phase and ends at the transition (the linear drive scenario was considered in Ref. [12]). The resulting entanglement entropy scaling is shown in Fig. 3.12(a) (linear drive) and Fig. 3.12(b) (quadratic drive).

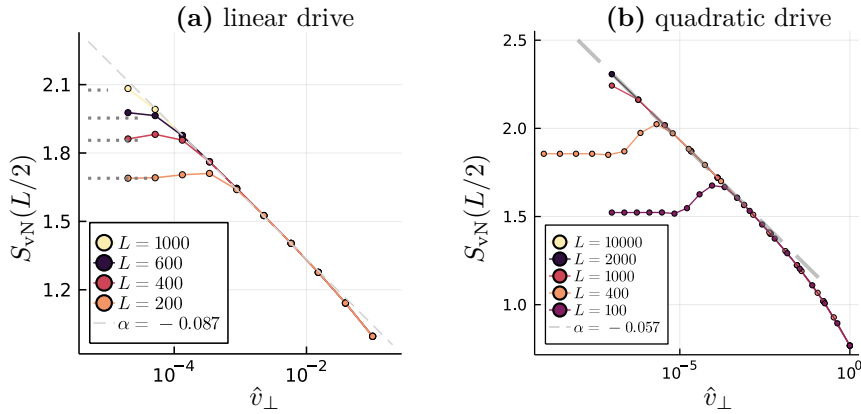


**Figure 3.12:** Half system entanglement entropy of the transverse XY model for different system sizes  $L$  and **(a)** a linear drive, starting at  $g(t_i)/\gamma = 5$ ,  $J/\gamma = 1/2$  and ending at the transition, and **(b)** a quadratic drive, starting at  $g(t_i)/\gamma = 20$ ,  $J/\gamma = 1/2$  and ending at the transition (semi-log scale). For a finite system, a sufficiently slow drive is still adiabatic. In the limit  $\hat{v}_\perp \rightarrow 0$  ( $n_E^{-1} \gg L$ ), the entanglement entropy is given by the ground state entanglement entropy (dotted lines in (a)). For intermediate velocities, we observe a scaling according to  $S_{vN} \sim \alpha \log_2(\hat{v}_\perp)$ . The values of  $\alpha$  from a fit (dashed lines) are close to the expected values  $-1/12$  (linear drive) and  $-1/18$  (quadratic drive).

**Remark:** Here we consider excitations on top of the translationally invariant ground state close to the critical point. In the next chapter, we will consider a quite different (energy) regime of a similar gapless fermionic model, starting

<sup>14</sup>The mutual information, which is directly related to the entanglement entropy, also provides an upper bound to possible correlations [146].

from an initial state that is a superposition of highly excited states. In this case, the evolution drives the state into a *volume-law* state  $S_{\text{vN}}(L/2) \sim L/2$ .

# 4 | Unitary Evolution, Measurements and Decoherence

In the previous chapter, we have encountered two important pillars of quantum dynamics:

- **Unitary evolution for a time-independent Hamiltonian:** On the one hand, the ground state of the Hamiltonian can undergo a quantum phase transition, displaying universal behavior in its vicinity [2]. On the other hand, states composed out of highly excited states can feature information scrambling leading to strong entanglement between subsystems.
- **(Slowly) Driven Hamiltonian:** Unitary time evolution due to a time-dependent Hamiltonian can excite the state, departing from an initial ground state. Even a slow drive can eventually break adiabaticity in the vicinity of a critical point.

In the following, we investigate two further fundamental aspects shaping the time evolution of a quantum state, resulting in *non-unitary* evolution:

- **Local measurements:** Measurements of local observables, like the particle number  $n_l$  at lattice site  $l$ , lead to the (local) projection onto an eigenstate of the measured operator. The projected state displays a reduced spatial entanglement.
- **Coupling to an environment:** If the system is coupled to an additional (quantum) system ('bath'), the interaction between system and bath can induce system-bath entanglement. In return, the reduced description of the system becomes mixed, which can manifest in, e.g., *dephasing*.

In the following, we discuss the competition between unitary evolution in various forms that *builds up* entanglement and local measurements that reduce entanglement. We briefly recapitulate some of the model classes which have been considered in literature. The interplay of unitary evolution due to a local (or non-local) Hamiltonian or due to random unitaries and different forms of measurements gives rise to a broad landscape of models and aspects of measurement induced dynamics, which is partly displayed in Fig. 4.1.

The main results of this chapter have been published in the publication [147]. In particular the key results, implications and Secs. 4.4-4.9 contain large parts which are adapted and extended from the publication [147].

**Quadratic models:** So far, we have considered fermionic hopping Hamiltonians in a closed system, featuring a quantum phase transition in its ground state. At the critical point, the ground state has features log law entanglement between subparts of the system. However, the time evolution due to the same Hamiltonians can also generate *volume law entanglement*. Initial states which are superpositions of highly excited states (from the middle of the energy spectrum of  $\mathbf{H}$ ) feature an extensive entanglement entropy between subsystems (see also, e.g., Refs. [148, 149] and Sec. 4.1). In contrast to the ground states and slow drives considered before, this scenario can arise in sudden quenches (see, e.g., Refs. [81, 82]).

**Interacting models:** Similarly, and beyond Gaussian models, volume law entanglement emerges in non-integrable, thermalizing closed quantum systems, which nonetheless are described by a unitary time evolution operator  $\mathbf{U}_t = \exp(-i\mathbf{H}t)$ . A related scenario are random unitary circuits, where instead of a fixed time evolution operator random unitary gates are applied at each discrete time step. They are randomly drawn from a specified distribution and act on, e.g., two neighboring lattice sites. In this setup, even the energy is not conserved, but the dynamics of quantities like the entanglement  $S_{\text{vN}}(t)$  show remarkable universal behavior [150, 151].

In all the models above, the growth of entanglement can be counteracted by measurements of *local* observables, favoring a spatial product state with locally well-defined eigenvalues of the measurement operators. Once these measurements take place with a certain probability  $p$  at each time step (and location), they constitute an additional dynamical *stochastic* process competing with the unitary evolution. This competition may result in a sharp continuous phase transition at a critical  $p_c$ , separating a volume law phase ( $p < p_c$ ) and an area law phase  $p > p_c$  [6, 152, 153]. As we will see later, quadratic fermion models are different: they do not support a volume law in the presence of local measurements [154], but can still feature a log to area law transition [18].

**Observables:** To extract and describe such phase transitions, we have to deal with the stochastic nature of individual measurement trajectories (due to the stochastic nature of the measurement outcomes). In a first step, we consider properties of the evolved states once a stationary value has been reached. As before, two possible approaches are based on: (i) extracting the entanglement properties or (ii) extracting correlations and/or order parameters of individual trajectories. In both cases, statistical non-stochastic statements can be obtained by averaging over the stochastic trajectories. However, it can be shown that averaged observables of the form  $\overline{\langle \mathcal{O} \rangle}$  (where  $\overline{(\dots)}$  denotes the average of different measurement outcomes) are trivial in the sense that they are *independent* of the details of the model like the measurement rate [6]. To obtain non-trivial statistical averages, higher moments, e.g., correlations of the form  $\overline{\langle \mathcal{O} \rangle^2}$  or the entanglement entropy  $\overline{S_{\text{vN}}}$ , have to be considered.

**Replica theory:** The fact that the transition is only encoded in higher moments also influences the relevant symmetries in the model. The transitions cannot be extracted from the averaged density matrix  $\bar{\rho}$ , but rather from averaged *replicated* density matrices of the form:  $\overline{\rho \otimes \rho \otimes \dots \otimes \rho}$  [9, 19, 20, 54, 155–162]. As discussed before, phase transitions can result from spontaneous symmetry breaking and a qualitative change in the correlations. In the stochastic measurement setup, the relevant symmetries consist of two parts: (i) the physical symmetry of the time evolution of single trajectories *and* (ii) replica exchange symmetries. Therefore, the interplay of unitary evolution and measurements gives rise to an *extended* set of symmetries, which possibly can be broken (spontaneously) (for examples see, e.g., Refs. [158, 160, 163, 164]). The coupling to an additional bath will explicitly break some of those symmetries.

**Role of mixed states:** The aforementioned aspects refer to *static* properties of the evolved states once a stationary value has been reached. By using the entanglement entropy, we implicitly assumed that the measurement trajectories were pure. A complementary perspective is to study the *dynamical* purification of an initially mixed state: under monitoring, an initially mixed state will *purify*. Depending on the underlying stationary phase (e.g, volume or area law), the purification is qualitatively different [31, 154, 158, 165, 166]. As an example, the typical purification time can scale differently with the system size  $L$ . The advantage of this approach is that it is also applicable to long range or all to all coupled models [31, 158], where the notion of entanglement between subsystems is not clearly defined.

Mixed states can also arise from the coupling to an environment/bath (e.g, another quantum system). Once system and bath build up entanglement, the reduced description<sup>1</sup> of the system  $\rho_S = \text{tr}_B[\rho_{SB}]$  becomes mixed. This is comparable to the scrambling dynamics in an extended, isolated system, where entanglement builds up between different subsystems. The interplay of measurement induced phase transitions and the presence of a (dephasing) bath is still a very open field and the main topic of this chapter. Recent works regarding this topic are:

- In Refs. [20, 172] a  $\mathbb{Z}_2$  symmetric circuit model was analyzed, based on competing measurements and a dephasing channel, each applied with a certain probability. The competing measurements are  $Z_i Z_{i+1}$  and  $X_i$ , featuring a measurement induced phase transition. The dephasing channel is based on  $X_j$ . The resulting phase diagram entails three different phases. Two of these phases feature different finite (non-linear) order parameters, indicating a symmetry breaking transitions (also present without dephasing). The third phase is a ‘trivial’ phase, where none of the order parameters is finite. Qualitatively, the same physics is obtained by coupling the model to an explicit bath (in a  $\mathbb{Z}_2$ -preserving fashion). The bath consists of a similar model, which is *not* monitored but evolves under random unitary dynamics.
- In Ref. [160] the influence of quantum errors (loss of measurement outcomes with a certain probability) onto a monitored Sachdev-Ye-Kitaev

<sup>1</sup>Determined by taking the partial trace of the full density matrix  $\rho_{SB}$  with respect to the bath.

(SYK) model with a measurement induced transition was analyzed. The finding is that the presence of those errors can smear out the transition. A related scenario for a (non-symmetric) stabilizer circuit model with a measurement induced transition was studied in Ref. [175]. In the presence of imperfections, the transition is broadened into a crossover. In both models, the original transition is based on the *spontaneous* breaking of a replica exchange symmetry, which is *explicitly* broken in the presence of imperfections.

- In Ref. [193], the influence of imperfect measurements on a bosonic CFT was studied, indicating that such conformal theories are robust against the imperfections. However, suitable observables like the logarithmic entanglement negativity (defined in (4.40)) have to be used to obtain non-trivial scaling information (in contrast to  $S_{vN}$ ).
- A partly related scenario corresponds to dephasing *at the boundary* in a random unitary circuit, discussed in Ref. [173]. In this case, measurements counteract the ‘trivializing’ dynamics of the dephasing. The interplay allows for the logarithmic negativity to scale as  $\sim |A|^{1/3}$  (with  $|A|$  the subsystem size) for weak measurements. An increasing measurement strength induces a phase transition into an area law phase. In contrast, bulk dephasing in this model would result in a featureless maximally mixed state. Related to that, boundary driven fermions have been studied in Ref. [174], featuring a transition from log law negativity to area law negativity (a transition that is not visible in, e.g., the purity).

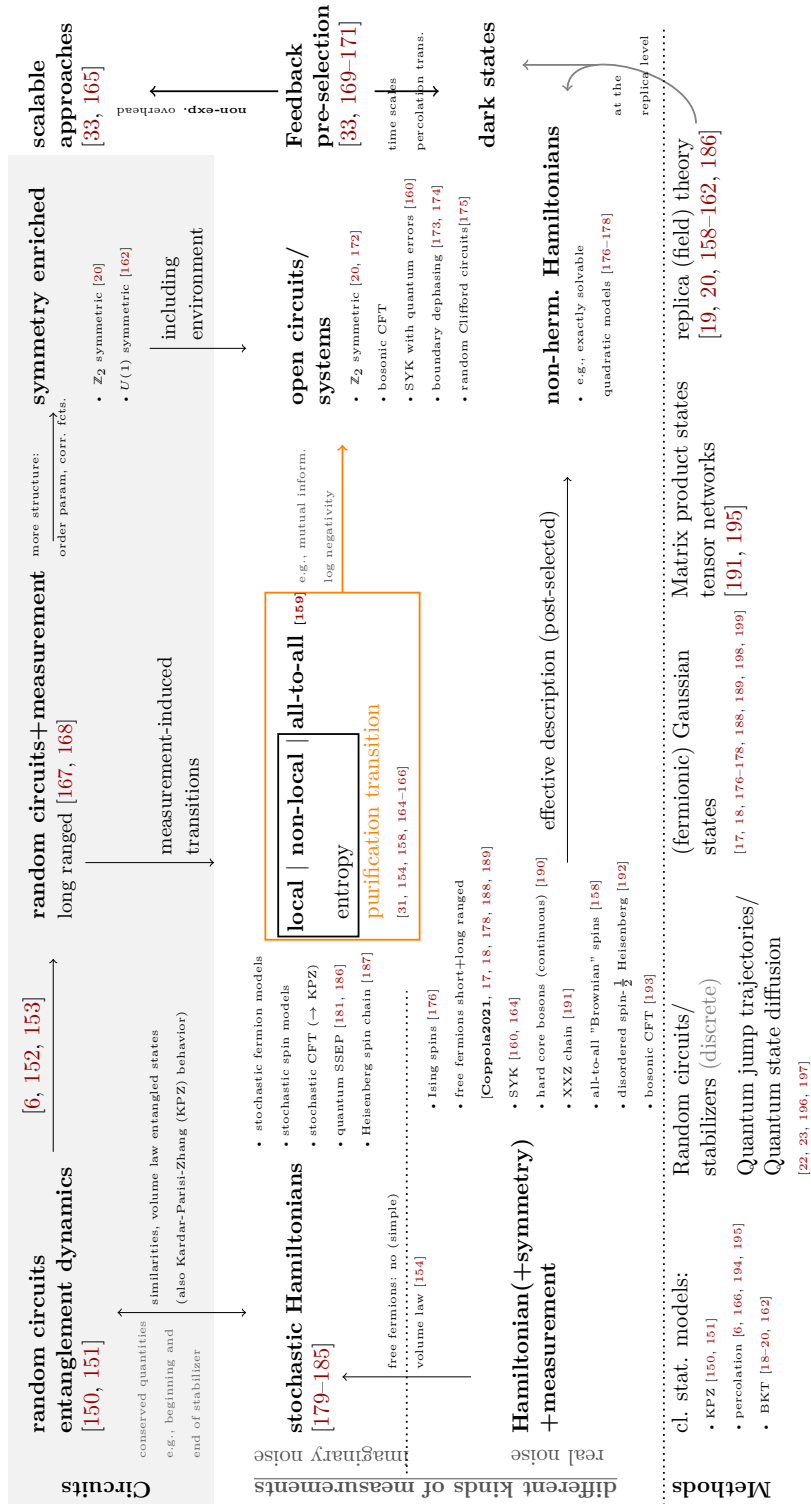


Figure 4.1: Overview of the topical landscape of measurement-induced dynamics.

**Key results:** In this chapter, we approach the question of the stability of measurement induced transitions against dephasing in an elementary fermionic model. At the level of measurements and unitary evolution, it features a continuous  $U(1)$  symmetry with a Berezinskii-Kosterlitz-Thouless (BKT) phase transition. For weak measurements, the model hosts an extended *critical phase* ( $C$ ) with log law entanglement and algebraically scaling correlation functions, comparable to the critical physics at the quantum Ising phase transition. For strong measurements, an area law phase ‘measurement’ ( $M$ ) with exponentially decaying correlations is found [18–20].

The competing contributions in the model are (i) unitary evolution due to a hopping Hamiltonian (with strength  $J$ ), (ii) continuous measurements of the local particle number (with strength  $\gamma_M$ ), and (iii) a dephasing bath (with strength  $\gamma_B$ ). In the absence of dephasing and weak measurements,  $\gamma_M/J \ll 1$ , the unitary scrambling dynamics is still dominant, resulting in ‘delocalized’ states. In contrast, strong measurements ‘pin’ the states close to number eigenstates (close to product states). We probe these phases against dephasing in the form of a Markovian Lindblad equation with Lindblad operators  $\mathbf{L}_l = \mathbf{n}_l$  for each lattice site  $l$ . Even though the validity of such a description will depend on the physical details of the system-bath coupling, it has the major advantage that it is equivalent to *imperfect* measurements. Imperfect measurements correspond to the scenario, where only a subset of the measurement outcomes are known to the observer. To analyze the interplay of the three dynamical contributions, we combine four different methods: (1) numerical simulations of the full conditional fermionic density matrix  $\rho^{(c)}$  for small system sizes ( $L = 8 - 10$ ); (2) numerical simulations of an approximation of  $\rho^{(c)}$  in terms of quantum trajectories; (3) perturbative treatment of the fermion dynamics in the limit of  $\gamma_B/J \gg 1$  in the dephasing-free subspace; (4) replica theory for an effective bosonic model in the thermodynamic limit (where the unitary part is parametrized by  $\nu$ ), formulated as a Keldysh field theory. All approaches are summarized in Fig. 4.2.

**Effective theory approach:** The long distance behavior can be effectively described by a bosonic replica theory [19, 188]. In the bosonic language, measurements of the particle density translate into a derivative term in the action, as well as a *non-linear* sine-Gordon term. For weak measurements and a weak bath ( $\gamma_M/J, \gamma_B/J \ll 1$ ), the non-linearities are irrelevant at large distances. Therefore, the description can be reduced to a massless bosonic CFT with a Green’s function  $G_{ab}^{-1} \sim \eta_{ab}^2 \partial_x^2 - \epsilon_{ab}^2 \partial_t^2$  (phase ‘scale invariant’ ( $C$ )). Once the non-linearities are relevant, we can still describe the model effectively in terms of a Green’s function *with additional mass terms*, which are non-vanishing in the limit  $k \rightarrow 0$ , see Fig. 4.2. The absence or presence of different mass terms or scales gives rise to a partition of the phase diagram into three parts, which we qualitatively summarize as:

- ( $C$ ): massless, featuring algebraic correlations.
- ( $M$ ): massive with exponential decay of correlations; states are close to eigenstates of the measurement operators.
- ( $C_D$ ): massive with a mass scale that resembles an effective temperature like scale, still featuring algebraic correlations; dynamics is strongly confined to the diagonal of the density matrix.

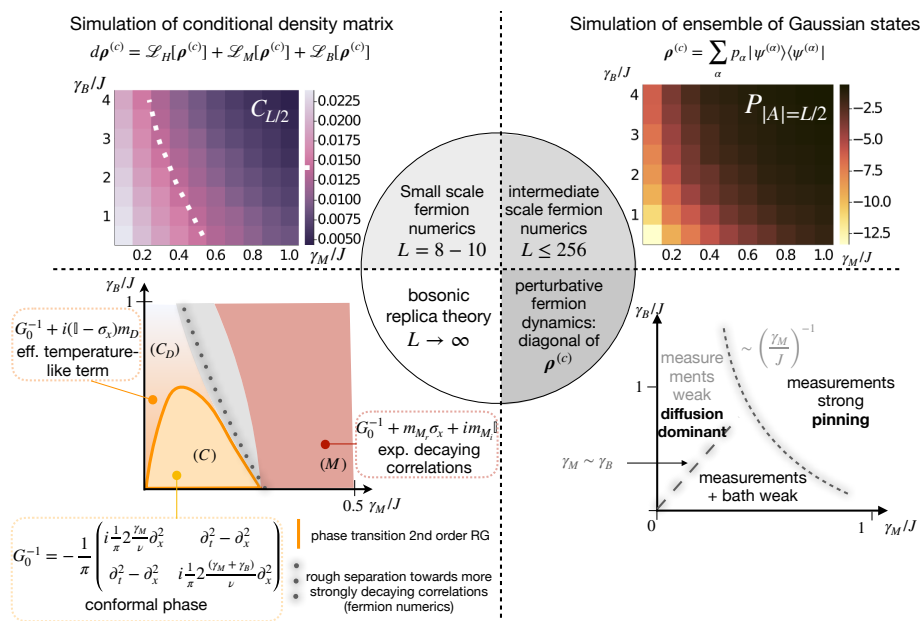


**Figure 4.2:** Overview of the four different methods used to study the effect of dephasing ( $\mathcal{L}_B$ ) onto the dynamics of  $L/2$  fermions on a lattice of size  $L$  subject to coherent hopping (unitary) ( $\mathcal{L}_H$ ) and local measurements of the particle number ( $\mathcal{L}_M$ ). In the lower left corner a sketch of the phase diagram, as synthesized from the different approaches, is shown.  $C_{L/2}$  and  $P_{L/2}$  are the density-density correlations and subsystem parity variance at largest distances (dashed line: guide to the eye).

In particular, the critical phase (C) is stable against weak dephasing albeit describing mixed states (see also Ref. [193]). The stability is inferred from a RG analysis, indicating the irrelevance of non-linearities at large scales in phase (C). The same analysis suggests that additional dephasing *enhances* the measurement induced phase (M). It also enables a new phase (C<sub>D</sub>), which still features algebraic particle number correlations. However, it includes a mass term that can be associated with the suppression of off-diagonal terms in the density matrix<sup>2</sup>, similar to a (high) temperature term.

**Numerical approach:** Measurement-induced transitions are encoded in observables that are non-linear in the density matrix. To extract *averaged* observables like  $\langle \mathcal{O} \rangle^2$  requires to perform several runs of the stochastic dynamics to average over different measurement outcomes. In the presence of a bath, each individual trajectory becomes mixed (and non-Gaussian), which limits an exact treatment to small system sizes (here  $L = 8 - 10$ ). Nonetheless, this approach grants full access to quantities like the purity and entanglement measures like the logarithmic negativity<sup>3</sup>. Qualitatively, three regimes can be identified with the regime ‘scale invariant dephasing’ (C<sub>D</sub>) featuring the lowest purity  $\text{tr}[\rho^{(c)2}]$

<sup>2</sup>It suppresses fluctuations of fields in a Keldysh field theory description that can be associated with off-diagonal terms in the density matrix.

<sup>3</sup>We discuss this object in, e.g., Sec. 4.3.

(for  $L = 8 - 10$ ), whereas regime ( $C$ ) is characterized by the largest logarithmic negativity. For larger system sizes (here  $L \leq 256$ ), a different approach is needed and we approximate the mixed states  $\rho^{(c)}$  in terms of a weighted set of quantum trajectories:  $\rho^{(c)} = \sum_{\alpha} p_{\alpha} |\psi^{(\alpha)}\rangle\langle\psi^{(\alpha)}|$ , with the probability weights  $p_{\alpha}$ . In this representation, the individual states  $|\psi^{(\alpha)}\rangle$  are Gaussian, such that quantities like the density-density correlations are straightforward to evaluate. In phases ( $C$ ) and ( $C_D$ ), these correlations are algebraic in the range of accessible system sizes, supporting the ‘scale free’ nature of both phases. However, the method does not give efficient nor reliable access to quantities like the purity. In summary, the results support the RG picture provided by the effective bosonic model, but the accessible system sizes are too small to make a definite statement about the sharpness of the transition.

**Qualitative picture:** Physically, we can make these findings plausible by considering the dynamics of the fermionic density matrix  $\rho^{(c)}$  in the occupation number basis  $\{|n_l\rangle\}$  for a fixed number of particles. On the one hand, strong dephasing decreases the magnitude of off-diagonal elements with the diagonal elements being decoherence-free. On the other hand, strong measurements tend to localize the diagonal to a few finite entries, corresponding to a product state with well defined local particle numbers. Complementary, the unitary dynamics connects the diagonal and off-diagonal elements and causes the scrambling of information. The contribution of the unitary evolution onto the dynamics on the diagonal is suppressed by strong dephasing. In this limit, the effective contribution of the unitary evolution takes the form of a weak *diffusion* with strength  $\sim (\gamma_B/J)^{-1}$ . For strong measurements and dephasing, this suppressed role of  $H$  favors the larger extent of phase ( $M$ ).

For weak measurements but strong dephasing, the same line of argument gives rise to a competition: the suppressed diffusion with  $\sim (\gamma_B/J)^{-1}$  can become the same size as the weak measurement evolution  $(\gamma_M/J)$ . Comparing these scales lends itself to a rough estimate of the two regimes, see Fig. 4.2. Therefore, phase ( $C_D$ ) is described by (incoherent) diffusion, only weakly stirred by the stochastic measurements. Once  $\gamma_M \gg \gamma_B$ , the critical behavior of phase ( $C$ ) is expected to dominate with a separation roughly given by  $\gamma_M \sim \gamma_B$ .

**Organization of the chapter:** We introduce the individual parts of the fermionic model in Sec. 4.1 (unitary part), Sec. 4.2 (coupling to an environment) and Sec. 4.4 (continuous measurements) in detail. In case of familiarity, the reader can also directly start with Sec. 4.5, where the qualitative aspects for our model are discussed, followed by the analysis of the full density matrix evolution for small system sizes in Sec. 4.6. The complementary replica approach is introduced in Sec. 4.7 and finalized by a RG discussion in Sec. 4.8. The numerical approach based on quantum trajectories is discussed in Sec. 4.9. Finally, the perturbative approach to the fermion dynamics is discussed in Sec. 4.10.

## 4.1 Fermion Models and the Role of Entanglement

In this section, we study the unitary entanglement (evolution) in fermionic models reaching a stationary volume law scaling. For those models, the entanglement evolution can be explained by a (heuristic) quasi-particle picture. However, this entanglement mechanism will not be robust against local measurements [17, 154] (in contrast to other models that support a volume law phase even in the presence of measurements).

### 4.1.1 Definition of the fermionic hopping Model

The model system we will investigate consists of  $N$  (free) fermions subject to three ingredients: (i) hopping on a lattice of  $L$  sites and lattice distance  $a$  in one dimension:

$$\mathbf{H} = -J \sum_{i=1}^L \mathbf{c}_i^\dagger \mathbf{c}_{i+1} + \mathbf{c}_{i+1}^\dagger \mathbf{c}_i = \sum_k \underbrace{-2J \cos(ka)}_{=: \epsilon_k} \mathbf{c}_k^\dagger \mathbf{c}_k \quad (4.1)$$

with (ii) local (continuous) measurements of the particle number  $\mathbf{n}_l = \mathbf{c}_l^\dagger \mathbf{c}_l$  at each lattice site  $l$ , and (iii) the coupling to a dephasing bath. The unitary evolution tends to build up entanglement between distant parts of the system, whereas local measurements reduce the entanglement by enforcing a definite particle number at a given site. The last aspect, coupling to an environment, is also tightly connected to the build up of entanglement, but this time between the system and another system (the environment). Loosely said, the interaction between system and environment will often lead to an overall state  $|\psi\rangle_{SB}$ , which is *not* a product state between system and bath<sup>4</sup>. In turn, the system itself is described by a reduced density matrix:  $\rho_S = \text{tr}_B[|\psi\rangle\langle\psi|]$  that is *mixed*. In our case, this is accompanied by *dephasing*: off-diagonal elements in the  $\rho_S$  are suppressed.

In the following, we ‘disentangle’ the different dynamical contributions, starting from identifying the relevant excitations in the system and how they influence, e.g., the entanglement. In contrast to the transverse XY model, this fermion model conserves the particle number  $[\sum_l \mathbf{n}_l, \mathbf{H}] = 0$ . For a given number of fermions  $N \leq L$ , the ground state  $|\psi\rangle_0$  is the state with the lowest  $N$  energy eigenstates occupied (up to some ‘Fermi momentum’  $k_F$  (or ‘Fermi energy’  $\epsilon_F$ )):

$$|\psi\rangle_0 = \left( \prod_{|k| < k_F} \mathbf{c}_k^\dagger \right) |0\rangle. \quad (4.2)$$

This is again a Gaussian state, which can also be represented in real space

<sup>4</sup>There are purposefully designed scenarios, where this is not the case, see, e.g., Ref. [200, 201].

according to

$$|\psi_t\rangle = \prod_{i=1}^N \underbrace{\left( \sum_{j=1}^L U_{ji}(t) \mathbf{c}_j^\dagger \right)}_{=: \mathbf{x}_i^\dagger} |0\rangle, \quad U^\dagger(t)U(t) = \mathbb{1}. \quad (4.3)$$

This is a flexible representation of particle number conserving Gaussian states, used in many parts later on. The state is parametrized in terms of the  $L \times N$  matrix  $U$  and is fully characterized by the correlation matrix

$$D_{ij}(t) = \langle \mathbf{c}_i^\dagger \mathbf{c}_j \rangle = (U(t)U^\dagger(t))_{ij} \quad (4.4)$$

(see again App. A). Since the particle number is conserved by the dynamics, excitations on top of this ground state have to preserve this number. In momentum space, excitations can be generated by destroying a particle at quasi momentum  $k$  and create one at  $k + q$ :  $\mathbf{c}_{k+q}^\dagger \mathbf{c}_k$  (*particle-hole excitations*). For a monotone dispersion relation, a larger momentum difference  $q$  comes with a larger excitation energy. In the following, we are going to focus on the long distance properties of this model (and its interplay with measurements and dephasing). Therefore, we can restrict the analysis to the lowest energy excitations  $q \rightarrow 0$ . In this light, it is reasonable to confine our attention to momenta close to  $\pm k_F$ , where we can *linearize* the dispersion, see Fig. 4.3. In this approximation, we can describe the fermionic theory equivalently in terms of *bosons*, which we will use as an effective description in later parts of the chapter.

#### Box 14: Linear dispersion: To be more precise ...

Consider some dispersion  $\epsilon_k = \epsilon_{-k}$  (e.g. from our microscopic model  $1 - \cos(ka)$ ) on an infinite lattice with lattice spacing  $a$ . The ground state for a given number of fermions corresponds to the state with all low-energy states filled up to  $|k| = k_F$ . Around these two points  $\pm k_f$ , we approximate the dispersion by linear ones with the corresponding velocity  $v_F = \partial_k \epsilon_k|_{k_f}$ . We refer to the two branches as "−" species ( $-k_F$ ) and "+" species ( $+k_F$ )<sup>a</sup>:

$$\mathbf{H}_{\text{lattice}} \approx \sum_{k < 0} v_F \underbrace{(-k - k_F)}_{=: k_-} \mathbf{c}_k^\dagger \mathbf{c}_k + \sum_{k > 0} v_F \underbrace{(k - k_F)}_{=: k_+} \mathbf{c}_k^\dagger \mathbf{c}_k \quad (4.5)$$

$$= \sum_{k_- > k_F} v_F k_- \mathbf{c}_{-,k}^\dagger \mathbf{c}_{-,k} + \sum_{k_+ > k_F} v_F k_+ \mathbf{c}_{+,k}^\dagger \mathbf{c}_{+,k} \quad (4.6)$$

$$= \sum_{\sigma = \pm} \sum_{k > -k_F} v_F k \mathbf{c}_{\sigma,k}^\dagger \mathbf{c}_{\sigma,k}. \quad (4.7)$$

Here, we redefined the momentum  $k$  as relative to the Fermi momentum, such that  $k > 0$  corresponds to  $\epsilon_k > 0$  for both species [202]. The full field operator for fermions in real space is given by the sum  $\psi_x =$

continued on next page

continued from page before

$e^{-ik_F x} \psi_{-,x} + e^{+ik_F x} \psi_{+,x}$ , which reads:

$$\psi_x \approx e^{-ik_F x} \frac{1}{\sqrt{La}} \sum_{k=-\infty}^{\infty} e^{ikx} c_{-,k} + e^{+ik_F x} \frac{1}{\sqrt{La}} \sum_{k=-\infty}^{\infty} e^{-ikx} c_{+,k}. \quad (4.8)$$

Here, we already made an essential approximation: the different species would physically only be defined for  $k > -k_F$ , but we extended both summations to  $\pm\infty$ , fulfilling the requirement for *bosonization* [202] (where fermionic operators are expressed in terms of bosonic ones). The ground state is given by the state with all (infinitely many) ( $k < 0$ )-states filled.

<sup>a</sup>Also denoted as right and left movers [202].

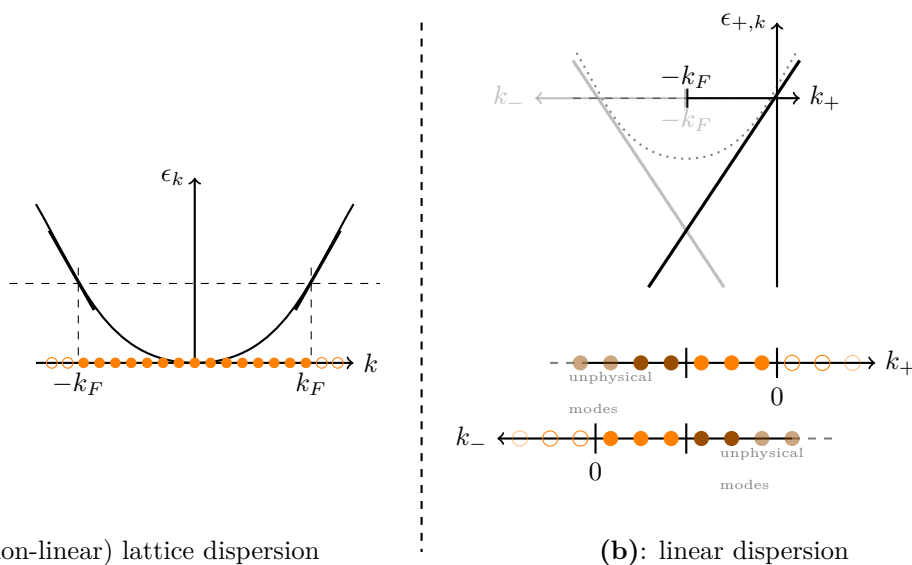


**Figure 4.3:** (a) *Non-linear lattice dispersion, where filled (empty) dots indicate occupied (unoccupied) modes. The horizontal dashed line indicates the Fermi energy.* (b) *Extended linearized dispersion with two branches ( $\pm$ ), including unphysical modes (darker color).*

In this linearized setting, we can already anticipate that besides the single particle-hole excitation  $c_{k+q}^\dagger c_k$  also the superposition of these excitations:

$$b_{\sigma,q>0}^\dagger \sim \sum_k c_{\sigma,k+q}^\dagger c_{\sigma,k}, \quad (4.9)$$

will describe a collective excitation, see also Fig. 4.4. This operator will turn out to be a proper *bosonic* operator, corresponding to an excitation with an

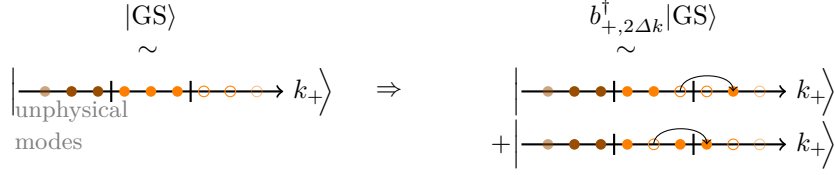


**Figure 4.4:** Bosonic excitation generated by  $b_{+,2\Delta k}^\dagger$  acting onto the ground state (only showing the  $+$ -particle part). Here,  $\Delta k$  is the distance between neighboring discrete momenta.

additional energy  $v_F q$ . To see this, consider the commutator [202]

$$[\mathbf{H}, \sum_k c_{\sigma,k+q}^\dagger c_{\sigma,k}] = v_F q \sum_k c_{\sigma,k+q}^\dagger c_{\sigma,k},$$

which implies that  $\mathbf{b}_{\sigma,q}^\dagger$  describes an excitation on top of any eigenstate  $|\epsilon\rangle$  of the Hamiltonian:

$$\mathbf{H} \sum_k c_{\sigma,k+q}^\dagger c_{\sigma,k} |\epsilon\rangle = (\epsilon + v_F q) \sum_k c_{\sigma,k+q}^\dagger c_{\sigma,k} |\epsilon\rangle. \quad (4.10)$$

By carefully choosing the prefactors of the operators  $\mathbf{b}, \mathbf{b}^\dagger$ , we see that they are indeed *bosonic* in nature (see also Fig. 4.4):

$$\left. \begin{aligned} \mathbf{b}_{\sigma,q>0}^\dagger &= i \left( \frac{2\pi}{La|q|} \right)^{1/2} \sum_{k=-\infty}^{\infty} c_{\sigma,k+q}^\dagger c_{\sigma,k}, \\ \mathbf{b}_{\sigma,q} &= -i \left( \frac{2\pi}{La|q|} \right)^{1/2} \sum_{k=-\infty}^{\infty} c_{\sigma,k-q}^\dagger c_{\sigma,k} \end{aligned} \right\} [\mathbf{b}_{\sigma,q}, \mathbf{b}_{\sigma',q'}^\dagger] = \delta_{qq'} \delta_{\sigma,\sigma'}. \quad (4.11)$$

The construction of fermionic operators in terms of bosonic ones, under certain conditions, is an exact operator identity (which is also valid for finite system sizes  $La$  as long as the conditions are fulfilled), see e.g. Ref. [202]. Instead of following a rigorous construction, we give the main plausibility arguments to derive the relation of fermionic and bosonic operators and sketch a more formal approach in the App. D.

Starting point of the heuristic derivation is to rewrite the bosonic creation and annihilation operators (for a single species) in terms of a density operator  $\rho_x$  and phase field  $\theta_x$  (for extended discussion see, e.g., Refs. [70, 202–206]):

$$\mathbf{b}_x = \sqrt{\rho_x} e^{i\theta_x}, \quad (4.12)$$

where the commutation relations  $[\mathbf{b}_x, \mathbf{b}_{x'}^\dagger] = \delta(x-x')$  can be fulfilled by requiring

$$[\theta_x, \rho_{x'}] = -i\delta(x-x'). \quad (4.13)$$

This identifies the density and phase as conjugate variables. A further useful quantity is the (cumulated) deviation from the mean density (as we will see in the following), defined by

$$\rho_x =: \rho_0 - \frac{1}{\pi} \partial_x \phi_x. \quad (4.14)$$

With (4.14), the bosonic creation/annihilation operators can be described in terms of the fields  $\phi$  and  $\theta$ . To construct a fermionic creation and annihilation operators based on  $\phi$  and  $\theta$ , we need three ingredients:

1. **Creating a particle:** Since  $\theta, \rho$  are conjugate variables, we can make use of the analogy to the harmonic oscillator with  $\rho_x, \theta_x \rightarrow \mathbf{X}, \mathbf{P}$ . In case of the harmonic oscillator, the translation operator  $e^{ia\mathbf{P}}$  shifts the operator  $\mathbf{X}$ :  $\mathbf{X}e^{ia\mathbf{P}} = e^{ia\mathbf{P}}(\mathbf{X} - a\mathbb{1})$ . In analogy, the exponential of the phase operator,  $e^{i\theta_x}$ , changes the local density  $\rho_x$ . In particular,  $e^{i\theta_x}$  decreases the density by 1.
2. **Anti-commutation relations:** To implement anti-commutation relations, we introduce a Jordan-Wigner string at position  $x$  by counting the number of particles to the left:

$$\exp \left[ \pm i\pi \int_{-\infty}^x \rho_{x'} dx' \right] \sim \exp [\pm i\pi \rho_0 x \mp i\phi_x], \quad (4.15)$$

where the sign is a priori not fixed.

3. **Anti-commutation relations for multiple species:** In the presence of multiple species (here:  $\pm$ ) of fermions, we need an additional anti-commuting factor:  $U_{\pm}$  (denoted as *Klein factors*). It might be roughly approximated by a Majorana fermion (for  $L \rightarrow \infty$ ) [206] (though it can be constructed rigorously [202]).

Using these ingredients, the full fermionic field operator  $\psi_x = e^{-ik_F x} \psi_{-,x} + e^{+ik_F x} \psi_{+,x}$  can be constructed as follows: the operators  $\psi_{\sigma,x}$  consist of two exponential contributions from (1) – (2) and the Klein factor. Therefore,  $\psi_x$  reads:

$$\psi_x \sim \sum_{\sigma=\pm} e^{\sigma i\pi \rho_0 x} \psi_{\sigma,x} \quad \text{with} \quad \psi_{\sigma,x} \sim U_{\sigma} \exp[-\sigma i\phi_x + i\theta_x]. \quad (4.16)$$

With this translation add, we can reformulate a fermionic theory in terms of a bosonic<sup>5</sup> one with the fundamental operators being  $\phi_x$  and  $\theta_x$ . Using these operator identifications, the fermion theory with a linear dispersion can be expressed in terms of bosonic operators as (see also Ref. [202])

$$\mathbf{H} = \frac{\nu}{2\pi} \int_x [(\partial_x \theta_x)^2 + (\partial_x \phi_x)^2]. \quad (4.17)$$

The strength of this approach is twofold: Firstly, some *linear* bosonic operators like  $\partial_x \phi_x$  corresponds to *quadratic* fermionic operators  $\psi_{\sigma,x}^{\dagger} \psi_{\sigma,x}$  [205], which maps certain *interacting* fermion theories to non-interacting bosonic ones. Secondly, the physical fermion density (which will be used as measurement operators or as a dephasing operators), is given by ( $\rho_0 = \frac{1}{2}, x = j \cdot a$ ) [19]

$$\psi_x^{\dagger} \psi_x = \psi_{-}^{\dagger} \psi_{-} + \psi_{+}^{\dagger} \psi_{+} + \left( e^{2i\pi \rho_0 x} \psi_{-}^{\dagger} \psi_{+} + \text{h.c.} \right). \quad (4.18)$$

<sup>5</sup>Strictly speaking, this requires for the Klein factors to drop out or at least play no role (since these are *not* bosonic operators).

Therefore, we associate two bosonic operators to the density<sup>6</sup>:

$$\begin{array}{ll} \text{fermionic} & \text{bosonic} \\ \mathcal{O}_{1,x} = \psi_-^\dagger \psi_- + \psi_+^\dagger \psi_+ & \rightarrow -\frac{1}{\pi} \partial_x \phi_x, \end{array} \quad (4.19)$$

$$\mathcal{O}_{2,x} = \psi_-^\dagger \psi_+ + \psi_+^\dagger \psi_- \rightarrow m \cos(2\phi_x), \quad (4.20)$$

where  $m$  is a constant depending on the details of the bosonization (see App. D). Measurements and/or dephasing based on the first operator still describe a quadratic, exactly solvable theory. The role of the second operator can then be studied (perturbatively) on top of the quadratic theory, which is the approach we choose in this chapter (following a strategy introduced in Ref. [19]).

**Summary:** The fundamental excitations in the fermionic model, confined to the vicinity of  $\pm k_F$ , are bosonic in nature. Under certain assumptions, we can reformulate the fermionic theory in terms of bosonic one, which can be technically advantageous. Nevertheless, our viewpoint on the relation of the bosonic to the fermionic model is the one of an *effective theory* (with the same long distance behavior) to a microscopic model. Depending on which properties we like to study, we will either use the fermionic model or the effective bosonic one (for the long distance behavior).

#### 4.1.2 Phenomenology of the fermionic Model: Entanglement and Quasi-Particle Picture

In the following, we consider the different dynamic mechanisms individually and their interplay. Firstly, we analyze the properties of the unitarily evolving quadratic fermion model and afterwards take a look at the modifications due to local measurements or a dephasing bath. Starting from an unentangled (Gaussian) Néel state  $|10101\dots\rangle$ , the entanglement entropy between two subsystems  $S_{vN}(L/2)$  of size  $L/2$  grows linearly in time up to a value  $\propto L$  (volume law), see Fig. 4.5.

To understand this behavior, we take a closer look at the initial state: it is globally very different from the ground state. It rather corresponds to a superposition of (highly) excited states, a situation that is similar to sudden quenches<sup>7</sup>. The linear growth and stationary volume law can be understood from the evolution of quasi-particle pairs (see, e.g., Ref. [81]),

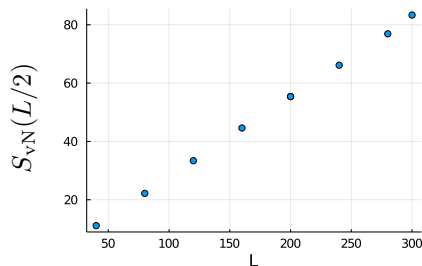


**Figure 4.5:** Unitary evolution in a fermionic chain: Stationary entanglement entropy  $S_{vN}(L/2)$  between two subsystems of size  $L/2$ , starting from  $|1010\dots\rangle$ . The entropy scales linearly with the subsystem size.

<sup>6</sup>Here, we neglect the role of the Klein factors.

<sup>7</sup>See, e.g., Ref. [82], where the entanglement in a transverse XY model (parameters:  $\gamma, g$ ) is tracked, starting from the ground state of the XY model at different parameters ( $\gamma', g'$ ). For an overview, see also Ref. [207].

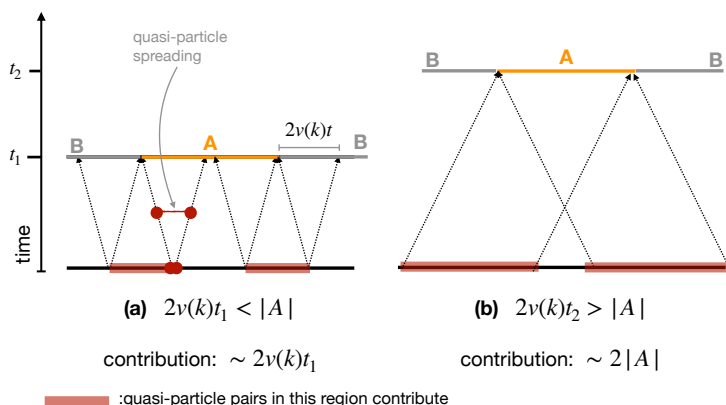


**Figure 4.6:** Qualitative picture of the spreading of quasi-particles (‘velocity’  $v(k)$ ), which lead to the growth of entanglement (starting from some highly excited state/ quench) between subsystem  $A$  (size  $|A|$ ) and its complement  $B$ . (a) Initially, the entanglement grows linearly (more pairs contribute). (b) For long times it saturates. The horizontal lines correspond to the lattice/system (at different times).

which spread with a velocity  $v(k) := 2J \sin(k)$ . The ‘excited’ initial state serves as a reservoir of quasi-particle excitations (at momentum  $k$ ), which will spread with the velocity  $v(k)$ <sup>8</sup>. Formally, this spreading can be described at the level of a (coarse grained) density<sup>9</sup> of quasi-particles  $n(x, k, t)$ , which evolves as:

$$\partial_t n(x, k, t) = -v(k) \partial_x n(x, k, t), \quad (4.21)$$

describing the ballistic spreading. Quasi-particle pairs, which start from the same position  $x$  (or are separated by a distance closer than the correlation length) are and stay entangled during the evolution. The entanglement between two subregions  $A$  and  $B$  is determined by the number of pairs, where one partner is found in  $A$  and the other in  $B$ , see Fig. 4.6. Taking all initial pairs into account (with some distribution<sup>10</sup>  $f(k)$ ), the entanglement between subsystem  $A$  and the rest is described by [81]:

$$S_{\text{vN}}(A, t) \sim t \underbrace{\int_{2v(k)t < |A|} f(k) 2v(k) dk}_{\text{‘early time’ contribution}} + |A| \underbrace{\int_{2v(k)t > |A|} f(k) dk}_{\text{‘late time’ contribution}}. \quad (4.22)$$

The first contribution describes the linear growth of  $S_{\text{vN}}$ , saturating once a volume law scaling  $S_{\text{vN}}(A, t \rightarrow \infty) \sim |A|$  is reached.

Such a volume law scaling in the stationary limit appears in a broad range of models (where a quasi-particle picture will not always be valid). Once the dynamics is enriched by local measurements, the volume law might not persist,

<sup>8</sup>Ignoring for the moment that the initial state is actually not translationally invariant, but see also Ref. [208].

<sup>9</sup>Based on the correlation matrix  $D$  [17, 209] and formally defined as  $n(x, k, t) := \sum_s e^{iks} D_{x-s/2, x+s/2}(t)$  [17].

<sup>10</sup>Assuming a translational invariant initial state for sake of simplicity.

depending on the mechanism behind the volume law. To make a rough distinction, we separate models into non-stochastic and stochastic ones. A few examples are given in the following:

- (Non-stochastic) Thermalizing quantum models (see, e.g., Ref. [68]) with an entanglement entropy given by the thermodynamic entropy. Related example: non-integrable spin chains with a ballistic growth of entanglement [210] (for an overview see also Ref. [211]).
- (Stochastic) Random unitary circuits, where the averaged entanglement entropy  $\overline{S_{vN}}$  grows linearly, though fluctuations grow as  $\sim t^{\frac{1}{3}}$  (KPZ universality) [150, 151].
- (Stochastic) Stochastic Hamiltonian models ( $\mathbf{H} = \mathbf{H}(t)$ , e.g., fluctuating chemical potentials), examples are: (i) free fermion models with a  $\sqrt{t}$  growth of  $S_{vN}$  [17, 212] (and references therein), and (ii) noisy interacting spin systems with a linear entanglement growth, but fluctuations scaling as  $\sim t^{\frac{1}{3}}$  (KPZ universality) [187].

The effect of local measurements on the entanglement in these different model classes can be quite different: the volume law entanglement for free fermions discussed above is actually *not* stable against arbitrary weak measurements for free fermions [154]. It will be reduced to either a log law or an area law [17–20], in contrast to, e.g., monitored random unitary circuits with an extended volume law phase (see, e.g., Ref. [6]). This behavior for free fermions is also not changed once we include an additional, local stochastic Hamiltonian. We will study this scenario at the end of this chapter (as a proxy for a bath) in Sec. 4.10.2.

## 4.2 Coupling the System to an Environment

Before we analyze the role of measurements on the dynamics, we clarify the role of the coupling to a bath (a second quantum system) and its subsequent entanglement with the system. Here we consider:

- Derivation of the Markovian Lindblad equation in a toy model of fermions coupled to ancillas.
- Application to the case of an occupation number sensitive interaction, resulting in *dephasing*.

In the last section, we have seen that starting from a highly excited (though unentangled) state, the unitary evolution leads to a strong entanglement between subsystems. Following the same line of thought: if the system  $S$  is coupled to an auxiliary system (bath/environment/...)  $B$ , the joined dynamics can entangle both systems. Denoting the joint system as  $SB$ , this would mean:  $|\psi\rangle_{SB} \neq |\psi\rangle_S \otimes |\phi\rangle_B$ . Consequently, the system itself is not described by a pure state anymore:

$$\rho_S = \text{tr}_B[\rho_{SB}], \quad \text{tr}[\rho_S^2] < 1. \quad (4.23)$$

Depending on the complexity of the interaction, we might not be able to evaluate the full unitary dynamics  $\mathbf{U}_t$  of system *and* bath exactly (in contrast to the

model discussed in Sec. 2.1.2). However, here we are only interested in the effective dynamics of  $\rho_S$  itself (formally written as (4.24)). Even if we are not able to determine the dynamics exactly, under certain assumptions (e.g., weak system-bath coupling), approximations for the evolution of  $\rho_S(t)$  can be found [16, 50]. A simplification arises once the time scale of the bath,  $t_B$ , where information of the system is still relevant, is small compared to (i) our time scales in the system, which can be resolved and (ii) to the time scales, where we like to observe the physical effect like decoherence. In this case, the dynamics of  $\rho_S(t)$  takes the form of a Markovian quantum master equation or Lindblad master equation, where  $\rho_S(t + \delta t)$  only depends on  $\rho_S(t)$ .

#### Box 15: Tracing out the bath

There are different methods to approximate the dynamics of the system, many based on a ‘weak’ interaction between system and bath [16, 50] or differently put: a clean separation of scales. If we consider an initial state of the form  $\rho_{SB} = \rho_S \otimes |0\rangle\langle 0|$ , where  $|0\rangle$  is the vacuum or ground state of the bath, the evolution of  $\rho_S$  is given by

$$\begin{aligned} \partial_t \rho_S &= \sum_j \underbrace{\langle j | U_t | 0 \rangle}_{=: M_j} \rho_S \langle 0 | U_t^\dagger | j \rangle = \sum_j M_j \rho_S M_j^\dagger, \\ \sum_j M_j^\dagger M_j &= \mathbb{1}_S. \end{aligned} \quad (4.24)$$

The operators  $M_j$  are denoted as *Kraus operators* [5]. Though very general, we still need a practical way to approximate the  $M_j$ ’s.

An elementary though very instructive workhorse to study the interplay of a system and an environment are finite dimensional (qubit) models (following Ref. [21]). If the system only briefly interacts with one qubit at a time (which afterwards stays in a fixed state), the operators  $M_j$  can be determined (we also give a weak coupling derivation in App. E.1, paralleling this discussion). Initially, we assume the system  $S$  and the environment  $B$  to be in a product state:

$$|\psi\rangle_{SB} = |\psi\rangle_S \otimes |\phi\rangle_B \Leftrightarrow \rho_{SB} = \rho_S \otimes \rho_B. \quad (4.25)$$

With  $S_j$  and  $B_j$  being hermitian operators, acting on the individual Hilbert spaces  $\mathcal{H}_S$  and  $\mathcal{H}_B$ , an arbitrary time evolution for a time step  $\delta t$  can be written as

$$U = \exp\left(-i\epsilon \sum_j S_j \otimes B_j\right), \quad \rho'_S = \text{tr}_B [U \rho_{SB} U^\dagger]. \quad (4.26)$$

Here,  $\epsilon$  is a small parameter (similar to a weak coupling assumption). The coupling between system and bath can generate entanglement between both. For a time evolution operator that cannot be written as a tensor product,  $U \neq U_S \otimes U_B$ , an initial product state becomes entangled under the evolution. Expanding  $U$  up to second order in  $\epsilon$ , we get the time evolution for one time

step  $\delta t$  [21]:

$$\rho'_S = \rho_S - i\epsilon \underbrace{\left[ \sum_j \text{tr}_B[\mathbf{B}_j \rho_B] \cdot \mathbf{S}_j, \rho_S \right]}_{= 0 \text{ (assumption)}} \quad (4.27)$$

$$+ \frac{\epsilon^2}{2} \sum_{j,l} \underbrace{\text{tr}_B[\mathbf{B}_j \mathbf{B}_l \rho_B]}_{:= \gamma_{jl}} (2\mathbf{S}_l \rho_S \mathbf{S}_j - \mathbf{S}_j \mathbf{S}_l \rho_S - \rho_S \mathbf{S}_j \mathbf{S}_l) + \mathcal{O}(\epsilon^3). \quad (4.28)$$

The matrix  $\gamma_{jl}$  can be diagonalized with eigenvalues  $\lambda_l$  and eigenvectors  $\vec{v}^{(l)}$ . Assuming that  $\epsilon \sim \sqrt{\delta t}$ , we get the *Markovian* Lindblad equation:

$$\rho'_S - \rho_S = \delta t \sum_j \left( \mathbf{L}_j \rho_S \mathbf{L}_j^\dagger - \frac{1}{2} \{ \mathbf{L}_j^\dagger \mathbf{L}_j, \rho_S \} \right) := \sum_j \mathbf{M}_j \rho_S \mathbf{M}_j^\dagger, \quad (4.29)$$

with the Lindblad operators being defined as

$$\mathbf{L}_l := \sqrt{\frac{\epsilon^2 \lambda_l}{\delta t}} \sum_j v_j^{(l)} \mathbf{S}_j. \quad (4.30)$$

This describes the evolution in a single discrete time step. We can turn this into a time discrete process under the following assumption: firstly, we leave the final state of the environment (ancilla) as it is. Secondly, we couple the system to a freshly prepared new ancillary system with the same initial state  $\rho_B$  and let system and bath interact for time  $\delta t$  again. The effect onto the system is comparable to the coupling to a large bath (with its own dynamics), which itself stays (nearly) in a stationary state (see again App. E.1). Another example is given in Ref. [21].

**Summary:** The ancilla approach therefore captures much of the system-bath coupling physics. The continuous version for  $\delta t \rightarrow 0$  reads:

$$\text{general:} \quad \partial_t \rho_S = \sum_j \left( \mathbf{L}_j \rho_S \mathbf{L}_j^\dagger - \frac{1}{2} \{ \mathbf{L}_j^\dagger \mathbf{L}_j, \rho_S \} \right), \quad (4.31)$$

$$\mathbf{L}_j \text{ hermitian:} \quad \partial_t \rho_S = -\frac{1}{2} \sum_j [\mathbf{L}_j, [\mathbf{L}_j, \rho_S]]. \quad (4.32)$$

**Example (lattice sites coupled to ancilla):** In the following, we consider an explicit example of a system-bath coupling following the argumentation above. The system consists of fermionic lattice sites  $j$ , which are individually coupled to an ancilla qubit ( $\mathcal{H}_B = \mathbb{C}^2$ ). The coupling is sensitive to the occupation of the fermionic lattice sites and will give rise to *dephasing* in the form of an effective non-unitary Lindblad evolution with  $\mathbf{L}_j \propto \mathbf{n}_j$ .

To entangle an initially unentangled system and bath, the time evolution operator should not be a tensor product. A possible choice is a variant of a controlled-NOT (CNOT) operation, based on the Hamiltonian  $\mathbf{H}_j$  (the following example follows Ref. [21]):

$$\begin{aligned} \mathbf{H}_j &= (\mathbb{1} - \mathbf{n}_j) \otimes \mathbb{1}_B + \mathbf{n}_j \otimes \sigma_x, \\ \mathbf{U}_j(\theta) &= \exp(-i\theta \mathbf{H}_j) = \cos(\theta) \mathbb{1}_{SB} - i \sin(\theta) \mathbf{H}_j. \end{aligned} \quad (4.33)$$

Here,  $\mathbf{n}_j$  is the number operator acting on a single lattice site  $j$ . The role of  $\mathbf{H}_j$  is to flip the ancilla qubit state only if the system state is occupied (analogous to a CNOT gate). Note that  $\mathbf{H}_j$  is unitary as well and fulfills  $\mathbf{H}_j^2 = \mathbb{1}_{SB}$ . For simplifying reasons (compensating same residual phase factors), we work with a slightly modified version of  $\mathbf{U}_j(\theta) \rightarrow \mathbf{U}'_j(\theta) = \mathbf{Z}_j \mathbf{U}_j(\theta)$  with

$$\mathbf{Z}_j = \exp\left(-i\frac{\theta}{2}(\mathbb{1} - 2\mathbf{n}_j)\right) \otimes \mathbb{1}_B.$$

The state  $|\psi_S\rangle \otimes |\sigma_B\rangle$  ( $\sigma = 0, 1$ ) evolves under this time evolution operator as

$$\mathbf{U}'_j |\psi_S\rangle \otimes |\sigma_B\rangle = e^{-i\frac{\theta}{2}} [(\mathbb{1} - \mathbf{n}_j) + \cos(\theta)\mathbf{n}_j] |\psi_S\rangle \otimes |\sigma_B\rangle - i \sin(\theta)\mathbf{n}_j |\psi_S\rangle \otimes |\neg\sigma_B\rangle, \quad (4.34)$$

where  $\neg\sigma$  is the negation of  $\sigma$ . Starting from the initial product state  $\rho_{SB} = |\psi_S\rangle\langle\psi_S| \otimes |0_B\rangle\langle 0_B|$  and working with  $\theta \ll 1$ , the reduced density matrix of the system evolves according to

$$\rho'_S = \text{tr}_B [\mathbf{U}'_j \rho_{SB} (\mathbf{U}'_j)^\dagger] = \rho_S - \frac{\theta^2}{2} [\mathbf{n}_j, [\mathbf{n}_j, \rho_S]] + \mathcal{O}(\theta^3). \quad (4.35)$$

The time evolution in the limit  $\delta t \rightarrow 0$ , assuming  $\theta = \sqrt{\gamma\delta t}$ , is of Lindblad form:

$$\rho'_S - \rho_S = -\frac{\gamma\delta t}{2} [\mathbf{n}_j, [\mathbf{n}_j, \rho_S]] + \mathcal{O}(\delta t^{3/2}) \xrightarrow{\delta t \rightarrow 0} \partial_t \rho_S = -\frac{\gamma}{2} [\mathbf{n}_j, [\mathbf{n}_j, \rho_S]].$$

As an example, consider a single fermion on two lattice sites, each coupled to an ancilla qubit. The basis states are given as  $\{|01\rangle, |10\rangle\}$ , such that the time evolved density matrix takes the form

$$\rho_S(t) = \sum_{i,j=0}^1 \rho_{ij}(t) |i\rangle\langle j| \quad \begin{cases} \partial_t \rho_{ii}(t) = 0, \\ \rho_{i \neq j}(t) = \exp(-\frac{\gamma}{2}t) \cdot \rho_{i \neq j}(0). \end{cases}$$

Similar to the exactly solvable case, the off-diagonal elements decay exponentially.

#### Box 16: Dependence on the initial state

In the above example, we have chosen  $\rho_{SB} = |\psi_S\rangle\langle\psi_S| \otimes |0_B\rangle\langle 0_B|$ . However, the resulting dynamics can depend on the choice of the initial state of the ancilla. Though there are other initial conditions like<sup>a</sup>  $\rho_B = |y_-\rangle\langle y_-|$ , featuring the same dynamics, an initial state like  $\rho_B = |x_-\rangle\langle x_-|$  will give rise to a different result. If we look back at the abstract derivation, (4.28), we assumed that the first order term would vanish. This assumption will depend on the initial state and to check this, we rewrite  $\mathbf{Z}_j \mathbf{U}_j$ , using a combined Hamiltonian:

$$\mathbf{H}'_j = \mathbf{H}_j - \frac{1}{2}(\mathbb{1} - 2\mathbf{n}_j) \otimes \mathbb{1}, \quad \mathbf{Z}_j \mathbf{U}_j = \exp(-i\theta \mathbf{H}'_j). \quad (4.36)$$

continued on next page

continued from page before

Therefore, the condition in (4.28) translates into:

$$\left[ \frac{1}{2} \underbrace{\text{tr}[\rho_B]}_{=1} |0\rangle\langle 0| + \left( \text{tr}_B[\sigma_x \rho_B] + \frac{1}{2} \underbrace{\text{tr}[\rho_B]}_{=1} \right) |1\rangle\langle 1|, \rho_A \right] \stackrel{!}{=} 0, \quad (4.37)$$

 which is fulfilled for any  $\rho_B$  with  $\text{tr}[\sigma_x \rho_B] = 0$  (graphically: lying in the  $z - y$  plane of the Bloch sphere).

<sup>a</sup>The states  $|y_{\pm}\rangle, |x_{\pm}\rangle$  denote the eigenstates of  $\sigma_y, \sigma_x$  with eigenvalues  $\pm 1$ .

### 4.3 Fermionic Model (1): Unitary Evolution and Dephasing – Evolution towards the maximally mixed State

The aforementioned model describes an interaction between individual fermionic lattice sites and ancillary qubits. The extended version corresponds to a fermionic (hopping) model with Hamiltonian  $\mathbf{H}_S$ , where each lattice site  $j$  is coupled to an ancillary qubit (e.g., prepared in  $|0_{j,B}\rangle$  before each interaction step) and the coupling between them results in local dephasing<sup>11</sup>:  $\mathbf{L}_i = \mathbf{n}_i$ . The corresponding model reads<sup>12</sup>:

$$\partial_t \rho_S = -i[\mathbf{H}_S, \rho_S] - \frac{\gamma_B}{2} \sum_i [\mathbf{n}_i, [\mathbf{n}_i, \rho_S]]. \quad (4.38)$$

For  $\mathbf{H}_S = 0$ , only the off-diagonal elements (in the occupation number basis) of the density matrix  $\rho_S$  are affected by dephasing, in analogy to the two sites considered before. In contrast, the unitary evolution due to  $\mathbf{H}_S$  will induce transitions or mixing between diagonal and off-diagonal elements. Since the Hamiltonian  $\mathbf{H}_S$  and the Lindblad operators  $\mathbf{L}_j$  do not commute, we expect some non-trivial interplay in the dynamics. Roughly speaking, the interplay leads to a diffusional dynamics of the diagonal elements of  $\rho_S$ , whereas the off-diagonal elements are suppressed. In the limit  $\gamma_B/J \gg 1$ , the dynamics on the diagonal can be approximated perturbatively and results in the diffusional spreading of  $\mathbf{n}_l$  in the Heisenberg picture (see Sec. 4.10.2 for further details<sup>13</sup>):

$$\partial_t \mathbf{n}_l \approx 2 \left( \frac{\gamma_B}{J} \right)^{-1} (\mathbf{n}_{l-1} - 2\mathbf{n}_l + \mathbf{n}_{l+1}).$$

For long times, all diagonal entries ‘equilibrate’ to a common value. Formally, this is encoded in the (only/unique<sup>14</sup>) stationary state of the evolution being  $\rho_S(t \rightarrow \infty) \propto \mathbb{1}_S$  (also referred to as *infinite temperature state*).

<sup>11</sup>For a derivation of dephasing in the context of optical lattices, see, e.g., Ref. [51].

<sup>12</sup>Dephasing of fermions, XX-models and hard-core bosons has been studied in, e.g., Refs. [185, 213–220].

<sup>13</sup>Perturbative treatments of Lindblad operators have been discussed in, e.g., Refs. [221–223] (in Ref. [224] an alternative method is used). Physically related models have been discussed in, e.g., Refs. [179–182] (quantum diffusive XX model, open quantum symmetric simple exclusion process) are relevant.

<sup>14</sup>Under certain conditions, see, e.g., Refs. [225–227].

From the entanglement perspective and at long times, system ( $S$ ) and bath ( $B$ ) are in a pure but strongly entangled state  $|\psi\rangle_{SB}$  ( $S_{vN}(S) \sim \mathcal{O}(L)$ ), such that  $\rho_S$  is strongly mixed. In the closed system setup (without ancillary systems), we studied the entanglement between two subparts of the system ( $A$  and its complement  $\bar{A}$ ), quantified by the von Neumann entanglement entropy  $S_{vN}(A)$ . In the presence of a bath, the same object  $S_{vN}(A)$  has a different meaning: it describes the entanglement of the subsystem  $A$  with the rest of the system and the bath, since  $\rho_A = \text{tr}_{\bar{A}}[\text{tr}_B[\rho_{SB}]]$  (see also the pictogram in Fig. 4.7). It does *not* describe the entanglement between the regions  $A$  and  $\bar{A}$  in the system alone. In Fig. 4.7, the von Neumann entropy of  $\rho_A$  and the full system  $\rho_{A\bar{A}} = \rho_S$  are shown, both being of the order of  $L$ . However, we know that the system itself evolves into the trivial state  $\mathbb{1}_S$  with no entanglement between  $A$  and  $\bar{A}$ . To quantify this lack of entanglement, we need (i) a notion of ‘product states’ in the context of mixed states and (ii) a measure to probe this property. The analog of pure product states are *separable states* defined as:

$$\rho_S \stackrel{!}{=} \sum_i \alpha_i \rho_A^{(i)} \otimes \rho_{\bar{A}}^{(i)}.$$

The infinite temperature state is separable since  $\mathbb{1}_S = \mathbb{1}_A \otimes \mathbb{1}_{\bar{A}}$ . One possible approach<sup>15</sup> to detect such states is the logarithmic entanglement negativity  $\mathcal{E}(A, \bar{A})$ , defined in the info box below. It is also shown in Fig. 4.7 and goes to zero for long times in accord with the separable nature of  $\rho_S$ .

#### Box 17: Entanglement negativity

Mathematically, one idea to detect separability is to use the partial transpose  $(\dots)^{TA}$  (only transposing the indices in subsystem  $A$ )<sup>a</sup>, which for a separable state reads

$$\rho_S = \sum_i \alpha_i \rho_A^{(i)} \otimes \rho_{\bar{A}}^{(i)} \quad \rightarrow \quad \rho_S^{TA} = \sum_i \alpha_i \rho_A^{(i)T} \otimes \rho_{\bar{A}}^{(i)}.$$

For separable states, this operation maps a valid density matrix to (different) valid density matrix with non-negative eigenvalues. In contrast, this need not be the case for entangled states and can result in negative eigenvalues of  $\rho_S^{TA}$ . To detect these, we can make use of the operator

continued on next page

<sup>15</sup>Unfortunately, these measures do not guarantee that the state is not entangled (they are necessary but not sufficient), see, e.g., Ref. [228, 229].

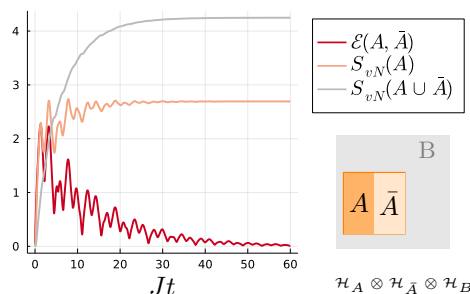


**Figure 4.7:** Evolution of the von Neumann entropy  $S_{vN}$  as well as the logarithmic entanglement negativity  $\mathcal{E}$  for a fermionic system with Hilbert space  $\mathcal{H}_A \otimes \mathcal{H}_{\bar{A}}$  (with  $|A| = |\bar{A}| = L/2$  and  $L = 8$ ) coupled to a dephasing bath with Hilbert space  $\mathcal{H}_B$ .

continued from page before

norm

$$\|\mathcal{O}\| := \text{tr} \left[ \sqrt{\mathcal{O}^\dagger \mathcal{O}} \right], \quad (4.39)$$

which is equal to one for  $\mathcal{O} = \rho_S$ . Including the partial transpose, the norm is  $\|\rho_S^{TA}\| \geq 1$ . Once  $\rho_S^{TA}$  is still a valid density matrix we have  $\|\rho_S^{TA}\| = 1$ . A corresponding entanglement measure [233] is defined as:

$$\text{log negativity:} \quad \mathcal{E}(A) = \log \left( \|\rho_S^{TA}\| \right). \quad (4.40)$$

**Remark:** In the limiting case of a pure density matrix  $\rho_S = |\psi\rangle\langle\psi|$ , the log negativity reduces to the Renyi- $\frac{1}{2}$  entropy:  $\mathcal{E}(A) = S_{\frac{1}{2}}(A)$  [231] with  $S_\alpha(A) := \frac{1}{1-\alpha} \log(\text{tr}(\rho_A^\alpha))$ .

<sup>a</sup>In fermionic systems, there some subtleties, see, e.g., Ref. [230, 231]. Nevertheless, for fermionic Gaussian states the calculation is straightforward, see, e.g., Ref. [232].

Furthermore, the complexity of this evolution has increased: though  $\mathbf{H}_S$  and the terms like  $\mathbf{n}_i^2 \rho_S = \mathbf{n}_i \rho_S$ , acting on  $\rho_S$  are still quadratic in the fermionic creation and annihilation operators, the term  $\mathbf{n}_i \rho_S \mathbf{n}_i$  is not. Therefore, the time evolution will result in a non-Gaussian state. Such theories are in many cases hard to deal with, since correlation functions with two and more operators/fields often depend on each other in a hierarchical fashion. Nevertheless, the case of a quadratic Hamiltonian and pure dephasing is special<sup>16</sup>: two-point correlations have a closed expression<sup>17</sup> (even though the state is non-Gaussian) [17] :

$$D_{ij} = \langle \mathbf{c}_i^\dagger \mathbf{c}_j \rangle, \quad dD = -i[h, D]dt - \gamma_B(D - D_{\text{diag}})dt. \quad (4.41)$$

Here,  $D_{\text{diag}}$  is the diagonal part of the correlation matrix and  $h$  is the hermitian matrix describing  $\mathbf{H}_S$ . The first term in the time evolution encodes the mixing dynamics due to the Hamiltonian and the second term encodes the exponential decay of *off-diagonal* correlations (or *coherences*). This equation can numerically be solved without any approximations, though we do not get access to higher-order correlations.

## Heating in the bosonized Description

In the beginning of this chapter, we have introduced the relation of the fermionic model to an (effective) bosonic model, encoding the fundamental excitations around  $\pm k_F$ . In the following, we investigate the heating dynamics in the effective bosonic description. To set the stage, we write the linearized fermionic dispersion with the added unphysical modes as a Dirac Hamiltonian with some

<sup>16</sup>It is still ‘exactly’ solvable in a sense. Some explicit results have been obtained in, e.g., Refs. [185, 215, 220] (see also Ref. [17, 179]).

<sup>17</sup>The matrix  $h$  is defined as  $h_{ij} = -J(\delta_{i,j-1} + \delta_{i,j+1})$ .

effective parameter  $\nu$  (see also Ref. [70] for more details on such a construction)

$$\mathbf{H}_{\text{lattice}} \xrightarrow{\text{eff. model}} \mathbf{H} = i\nu \int_x dx \vec{\psi}_x^\dagger \sigma_z \partial_x \vec{\psi}_x, \quad (4.42)$$

with  $\vec{\psi} = (\psi_+, \psi_-)^T$ . Physically, the coupling to a dephasing bath leads to the generation of those excitations, as we will see in the following. As we have already discussed, we can bosonize the fermion density (being cavalier about Klein factors and some other technical points (like normal ordering) here and refer to App. D for a more refined discussion) according to

$$\vec{\psi}_x^\dagger \vec{\psi}_x \stackrel{\text{boson.}}{\approx} -\frac{1}{\pi} \partial_x \phi_x + (-1)^x m \cos(2\phi_x) \quad (4.43)$$

for half-filling  $\rho_0 = \frac{1}{2}$ . If we want to study dephasing according to  $\mathbf{L}_x \sim \vec{\psi}_x^\dagger \vec{\psi}_x$ , the corresponding bosonic operators for this theory are:

$$\text{Hamiltonian: } \mathbf{H} = \frac{\nu}{2\pi} \int_x dx [(\partial_x \theta_x)^2 + (\partial_x \phi)^2], \quad (4.44)$$

$$\text{Lindblad operators: } \mathbf{L}_{1,x} = -\frac{1}{\pi} \partial_x \phi_x, \quad \mathbf{L}_{2,x} = m \cos(2\phi_x).$$

Here,  $m = 1/(\pi A)$  depends on a regularization in the bosonization procedure (see App. D) and the operators fulfill:  $[\partial_x \theta_x, \phi_y] = -i\pi \delta(x-y)$ . As a reminder: this reformulation of the theory has the major advantage that  $\mathbf{L}_{1,x}$  is *linear* in  $\phi_x$  and together with the quadratic Hamiltonian forms an exactly solvable, overall quadratic theory. On top of this solvable theory, the influence of  $\mathbf{L}_{2,x}$  can be studied.

Focusing on the linear (Lindblad) operators  $\mathbf{L}_{1,x}$ , the bosonic occupation number operator in momentum space,  $\mathbf{n}_{\sigma,q}$  (with  $\sigma = \pm$ ), and in the Heisenberg picture evolves as<sup>18</sup> (see App. E.2 for more details)

$$\partial_t \mathbf{n}_{\sigma,q} = \gamma_B q, \quad (4.45)$$

implying a linear growth in time. Similarly, the (normal ordered<sup>19</sup>) square of  $\phi_{\sigma,x}$  grows linearly in time:

$$\frac{1}{L} \int dx \mathop{*} \phi_{\sigma,x}^2(t) \mathop{*} \sim \gamma_B t, \quad (4.46)$$

indicating an (unbounded) growth of fluctuations.

**Remark:** This description can only capture the dynamics (i) as long as we can ignore the contribution of the non-linear parts in the bosonic version of  $\mathbf{n}_x$ , and (ii) no unphysical modes get excited.

<sup>18</sup>Ignoring the terms  $\mathbf{n}/L$  in the full bosonic Hamiltonian.

<sup>19</sup>Strictly speaking, we have to take care of the infinite set of occupied modes for  $k < 0$ , therefore we can subtract the expectation value with respect to the fermionic vacuum state (corresponding to state with no bosons).

**Summary:** The coupling of the fermionic system (or the bosonic system) to a dephasing bath leads to entanglement between the system and the bath. In turn, the reduced density matrix of the system  $\rho_S$  approaches a maximally mixed (featureless) state  $\sim \mathbb{1}_S$ . Formally, the dephasing is described by hermitian Lindblad operators  $\mathbf{L}_j = \mathbf{n}_j$ . In the simplified bosonic version ( $\mathbf{L}_x \sim -\partial_x \phi_x$ ), this heating towards an infinite temperature state is signalled by indefinitely growing fluctuations, e.g.,  $\langle \phi_{x,t}^2 \rangle \sim \gamma_B t \rightarrow \infty$ .

## 4.4 Measuring the Environment: How Measurements and Dephasing are connected

The coupling to a bath (in the aforementioned setting) results in system-bath entanglement. Information about the system becomes delocalized over the system and bath and therefore inaccessible from observing the system itself. To counteract this tendency, we can perform measurements on the ancillas, our toy model of a bath. In the following, we clarify the direct connection of dephasing and performing measurements.

First of all, such measurements of the ancillas correspond to a generalized measurement process: the ancillas can be seen as an ‘occupation number meter’ for the different lattice sites. Letting system and ancillas interact (with an occupation number sensitive interaction), measurements of the ancillas partially reveal information about the occupation number. Focusing on a single ancilla coupled to lattice site  $j$ , the process takes the form (see, e.g., Ref. [21]):

$$|\psi\rangle \otimes |0\rangle \xrightarrow{\text{interaction}} \mathbf{M}_0^{(j)}|\psi\rangle \otimes |0\rangle + \mathbf{M}_1^{(j)}|\psi\rangle \otimes |1\rangle \xrightarrow{\text{measurement}} \begin{cases} \mathbf{M}_0^{(j)}|\psi\rangle \otimes |0\rangle \\ \mathbf{M}_1^{(j)}|\psi\rangle \otimes |1\rangle \end{cases}.$$

In the last step, the measurement reveals one of the two possible measurement outcomes ((0) or (1)) and one of the two possible post-measurement states are realized. Since we know the measurement outcome, the evolution, reduced to the system and conditioned (c) to the measurement outcome, takes the form

$$|\psi^{(c)'}\rangle = \begin{cases} \frac{\mathbf{M}_0^{(j)}|\psi^{(c)}\rangle}{\sqrt{p_0}} & \text{with prob. } p_0, \\ \frac{\mathbf{M}_1^{(j)}|\psi^{(c)}\rangle}{\sqrt{p_1}} & \text{with prob. } p_1. \end{cases} \quad (4.47)$$

This is a pure state: the measurement cuts the entanglement between the ancilla and the system.

### Box 18: Generalized measurements

This indirect measurement and gain of information about the system is also referred to as a *generalized measurement*. The probability of a generalized measurement outcome and the corresponding post-measurement state are expressed in terms of  $\mathbf{M}_\nu$ . The role of  $\mathbf{M}_\nu$  is similar to the role of the projection operators  $\mathbf{P}_\nu$  in case of projective measurements

continued on next page

continued from page before

(see, e.g., Ref. [5] for more details):

	projective	generalized
post-measurement state:	$\mathbf{P}_\nu \psi\rangle$	$\mathbf{M}_\nu \psi\rangle$ ,
probability:	$p_\nu = \text{tr}[\rho\mathbf{P}_\nu]$	$p_\nu = \text{tr}[\rho\mathbf{M}_\nu^\dagger\mathbf{M}_\nu]$ ,
completeness relation:	$\sum_\nu \mathbf{P}_\nu = \mathbb{1}$	$\sum_\nu \mathbf{M}_\nu^\dagger\mathbf{M}_\nu = \mathbb{1}$ .

We can turn these generalized measurements into a *continuous* measurement process by repeatedly coupling the fermionic sites to ancillas for a time  $\delta t$  and measuring the ancillas afterwards. The result are stochastic trajectories  $\rho_S(t)$ , also denoted as a *quantum trajectories*. Focusing on the same model as before, the process takes four steps: (i) apply  $\mathbf{Z}_j\mathbf{U}_j|\psi\rangle \otimes |a\rangle$ , (ii) perform a projective measurement on the ancilla, (iii) reset the ancilla into the initial state  $|a\rangle$ , and (iv) repeat this process multiple times. With these, we can derive a continuous time evolution equation for the state  $\rho_S$ . If the initial state is a pure state, the time evolved state  $|\psi_S(t)\rangle$  is also pure.

**Example:** Starting from the initial state  $|a\rangle = \frac{1}{\sqrt{2}}(|0\rangle - i|1\rangle) = |y_-\rangle$ , the operators  $\mathbf{M}_k^{(j)}$  are given by (see again Ref. [21]):

$$\begin{aligned} \mathbf{M}_0^{(j)} &= \frac{e^{-i\theta/2}}{\sqrt{2}} [(\mathbb{1} - \mathbf{n}_j) + (\cos(\theta) - \sin(\theta))\mathbf{n}_j] \approx \frac{e^{-i\theta/2}}{\sqrt{2}} [(\mathbb{1} - \mathbf{n}_j) + \sqrt{1 - 2\theta\mathbf{n}_j}], \\ \mathbf{M}_1^{(j)} &= \frac{e^{-i\theta/2}}{\sqrt{2}} [(\mathbb{1} - \mathbf{n}_j) + (\cos(\theta) + \sin(\theta))\mathbf{n}_j] \approx \frac{e^{-i\theta/2}}{\sqrt{2}} [(\mathbb{1} - \mathbf{n}_j) + \sqrt{1 + 2\theta\mathbf{n}_j}]. \end{aligned}$$

For  $\theta \ll 1$ , the two operators  $\mathbf{M}_{0,1}^{(j)}$  are close to the identity and therefore the post-measurement states are only slightly changed. The probabilities for the different measurement outcomes are close  $\frac{1}{2}$ :

$$p_0 = \frac{1}{2}(1 - 2\theta\langle\mathbf{n}_j\rangle), \quad p_1 = \frac{1}{2}(1 + 2\theta\langle\mathbf{n}_j\rangle), \quad (4.48)$$

such that we measure (1) slightly more often once the fermionic site is occupied. The continuous process in the limit  $\delta t \rightarrow 0$ , as described above, is obtained by identifying  $\theta = \sqrt{\gamma\delta t}$  and expanding up to order  $\theta^2$  with  $\theta = \sqrt{\gamma\delta t}$ :

$$\begin{aligned} |\psi^{(c)'}\rangle - |\psi^{(c)}\rangle &\approx \left[ -\frac{\gamma}{2}\delta t(\mathbf{n}_j - \langle\mathbf{n}_j\rangle)^2 + \sqrt{\gamma}\Delta W_j(\mathbf{n}_j - \langle\mathbf{n}_j\rangle) \right] |\psi^{(c)}\rangle, \\ \Delta W_j &= \pm\sqrt{\delta t}, \quad \overline{\Delta W_j} = 0. \end{aligned} \quad (4.49)$$

Such a dynamics is also denoted as Quantum State Diffusion (QSD) [196]. This is a stochastic ( $\Delta W_j$ ) and non-linear ( $\langle\mathbf{n}_j\rangle$ ) equation, where both features stem from the measurement process: the outcomes are random and the post-measurement states need to be renormalized (non-linearity required). This non-unitary evolution also allows for dynamical *fixed points*:  $\partial_t|\psi^{(c)}\rangle = 0$  for  $|\psi^{(c)}\rangle = |0_j\rangle$  or  $|1_j\rangle$ .

**Relation to dephasing:** In a final step, we clarify how these measurements are related to the physics of a dephasing bath. To this end, we study the effect of *unknown* measurement outcomes. If an observer, confined to  $S$ , has no access to the measurement outcome, the observer's state of knowledge is the incoherent sum of both possibilities in (4.47) (see, e.g., Ref. [21, 22]). The reduced density matrix for such an 'uninformed' observer reads

$$\rho'_S = p_0 \cdot \frac{\mathbf{M}_0 \rho_S \mathbf{M}_0^\dagger}{\text{tr}[\mathbf{M}_0 \rho_S \mathbf{M}_0^\dagger]} + p_1 \cdot \frac{\mathbf{M}_1 \rho_S \mathbf{M}_1^\dagger}{\text{tr}[\mathbf{M}_1 \rho_S \mathbf{M}_1^\dagger]} = \sum_j \mathbf{M}_j \rho_S \mathbf{M}_j^\dagger. \quad (4.50)$$

To rephrase once more: Being limited to  $S$ , the observer can only obtain the information encoded in  $\rho_S$  (e.g., by quantum state tomography). However, the same expression describes the dynamics of the system being coupled to a bath, see again (4.29). For such an observer, there is no detectible difference. The state  $\rho_S$  evolves into the maximally mixed state, in contrast to the pure state evolution once the measurement outcomes are known. To connect the limiting cases of (i) performing measurements at all times and (ii) not performing measurements at all (being the same as not knowing the measurement outcomes), we consider the scenario, where the ancillas are only measured with a certain probability [21–23]. This scenario is captured by the generalized measurement operators *for the ancillas* [21]

$$\mathbf{M}_0^{(a)} = \sqrt{\eta}|0\rangle\langle 0|, \quad \mathbf{M}_1^{(a)} = \sqrt{\eta}|1\rangle\langle 1|, \quad \mathbf{M}_2^{(a)} = \sqrt{(1-\eta)}\mathbb{1}. \quad (4.51)$$

Here,  $\eta \leq 1$  is the probability that the ancilla is measured projectively. Following the same formal procedure to construct a continuous process, the time evolution takes the form (adding a Hamiltonian for completeness)

$$\begin{aligned} \rho_S^{(c)'} - \rho_S^{(c)} &= -i[\mathbf{H}_S, \rho_S^{(c)}]\delta t - \sum_i \frac{\gamma \delta t}{2} [\mathbf{n}_i, [\mathbf{n}_i, \rho_S^{(c)}]] + \sqrt{\gamma} \Delta W_i \{\mathbf{n}_i - \langle \mathbf{n}_i \rangle, \rho_S^{(c)}\}, \\ \overline{\Delta W_i} &= 0, \quad \overline{\Delta W_i \Delta W_j} = \eta \delta t \delta_{ij}. \end{aligned} \quad (4.52)$$

	coupling to a bath	imp. measurement
Lindblad prefactor	$\gamma_M + \gamma_B$	$\gamma$
Noise strength	$\gamma_M$	$\eta\gamma$
Conversion	$\eta = \frac{\gamma_M}{\gamma_M + \gamma_B}$	

**Table 4.1:** (*Conversion*) Imperfect knowledge of measurement outcomes, characterized by  $(\eta, \gamma)$ , and measurements in the presence of a dephasing bath  $(\gamma_M, \gamma_B)$  are different, but related, points of view to describe the evolution of a monitored system.

Crucially, the noise strength is modified by  $\eta$ . This description is equivalent to performing measurements and being coupled to a dephasing bath, see Tab. 4.1. For  $\eta = 1$ , we recover the measurement scenario from before: (i) the evolution of an initially pure state stays pure and (ii) an initially mixed state purifies (under certain conditions, see, e.g., Ref. [234]). An example is shown in Fig. 4.8(b). For  $\eta < 1$ , not all ancillas are measured and some residual entan-

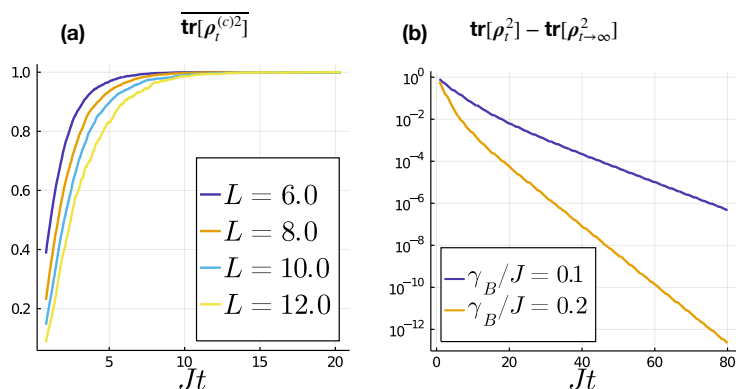


**Figure 4.8:** Purity in the limiting cases: (a) Purification for  $\gamma_B = 0$  with measurements and a Hamiltonian ( $\gamma_M/J = 1$ ), starting from  $\rho_{t=0}^{(c)} \sim \mathbb{1}$ . (b) Mixing in the absence of measurements ( $\gamma_M = 0$ ) with a dephasing bath and Hamiltonian for  $L = 10$  (decay towards the (maximally low) purity of the infinite temperature state  $\text{tr}[\rho_{t \rightarrow \infty}^2]$  with  $\rho_{t \rightarrow \infty} \sim \mathbb{1}$ ).

glement remains between those ancillas and the system, resulting in  $\rho_S^{(c)}$  being mixed. The last case,  $\eta = 0$  (not knowing any of the outcomes) corresponds to the dephasing bath scenario, where the stochastic term is absent and the state evolves into a strongly mixed state, see Fig. 4.8(b).

**Summary:** The coupling between the system and ancillas leads to the dephasing and mixing dynamics of  $\rho_S$ . If we intervene this process by performing measurements on the ancillas,  $\rho_S$  rather evolves stochastically and purifies (or stays pure). However, if we do *not* have access to the measurement outcomes, our knowledge of the state of the system,  $\rho_S$ , is again equal to the dephasing scenario since we have to sum up all possible outcomes.

## 4.5 Fermionic Model (2): Unitary Evolution and Measurements – Qualitative Picture of Measurement Dynamics

If we have access to the ancillas and can measure them, the state of the system follows a conditional evolution described by<sup>20</sup>  $\rho^{(c)}$ , conditioned on the measurement outcomes. The stationary states of this evolution are the eigenstates of the measurement operators  $\mathbf{n}_l$  (product states in real space). If we do not have access to the outcomes, our state of knowledge is described by the incoherent sum of the possible outcomes,  $\overline{\rho^{(c)}}$ . This has the same effect as being coupled to a dephasing bath with Lindblad operators  $\mathbf{n}_l$  and a stationary state  $\sim \mathbb{1}$ . Both mechanisms compete with the hopping Hamiltonian, already encoded in  $[\mathbf{H}, \mathbf{n}_l] \neq 0$ . At the level of states, the stationary states of the measurement operators correspond to a superposition of many excited states of the Hamiltonian. In contrast, the unitary evolution would evolve those states into strongly entangled states. Therefore, there is a (dynamical) competition between the two processes with the possibility of a phase transition. The situation is partly reminiscent of ground state quantum phase transitions. Here, the Hamiltonian consists of competing, non-commuting terms:  $\mathbf{H} = \mathbf{H}_0 + \lambda \mathbf{H}_1$  with  $\mathbf{H}_0$  and  $\mathbf{H}_1$  themselves featuring qualitatively different ground states.

The main question we are addressing in the following is the interplay of unitary evolution, measurements, and a bath (where both do not commute with the Hamiltonian): *How is the measurement-induced dynamics influenced by an additional coupling to a bath?* Or differently put: *How is the measurement-induced dynamics influenced if we have an incomplete record of the measurement outcomes?*

### 4.5.1 Qualitative Identification of Observables

To identify physically suitable ‘observables’ to study the interplay<sup>21</sup>, we start from the simplest incarnation of our model: one fermion on a lattice with two sites ( $L = 2$ ) and a Hilbert space spanned by  $\{|1, 0\rangle, |0, 1\rangle\}$ . In the absence of measurements, the model is described by:

$$\begin{aligned} \mathbf{H} &= -J(\mathbf{c}_1^\dagger \mathbf{c}_2 + \mathbf{c}_2^\dagger \mathbf{c}_1) = -J(|1, 0\rangle\langle 0, 1| + |0, 1\rangle\langle 1, 0|), \\ d\rho^{(c)} &= -i[\mathbf{H}, \rho^{(c)}]dt - \frac{\gamma_M}{2} \left( [\mathbf{n}_1, [\mathbf{n}_1, \rho^{(c)}]] + [\mathbf{n}_2, [\mathbf{n}_2, \rho^{(c)}]] \right) dt \\ &\quad + \sqrt{\gamma_M} \left( dW_1(t) \{ \mathbf{n}_1 - \langle \mathbf{n}_1 \rangle, \rho^{(c)} \} + dW_2(t) \{ \mathbf{n}_2 - \langle \mathbf{n}_2 \rangle, \rho^{(c)} \} \right). \end{aligned} \quad (4.53)$$

To get a first impression of the interplay, we extract the occupation of the first site,  $\langle \mathbf{n}_1 \rangle$ , for a single quantum trajectory, see Fig. 4.9. In the absence of measurements, the particle oscillates between the lattice sites (Rabi oscillations), whereas for  $\gamma_M/J \gg 1$ , the fermion has the tendency to be pinned onto one

<sup>20</sup>We will drop the subscript  $S$  in the following.

<sup>21</sup>We are a bit sloppy with the wording here, these are not quantum mechanical observables in the strict sense.

lattice site  $\langle \mathbf{n}_1 \rangle \approx 0, 1$  (which becomes a stationary state for  $J = 0$ ). This is the toy version for larger systems: starting from an initially pure state  $|\phi^{(c)}\rangle$ , the unitary evolution tends to delocalize the particles and spread correlations (and entanglement) over the system, as we have seen in Sec. 4.3. In contrast, measurements of the local particle number favor a state with well-defined local particle numbers, corresponding to a product state  $|n_1\rangle \otimes |n_2\rangle \dots \otimes |n_L\rangle$ .

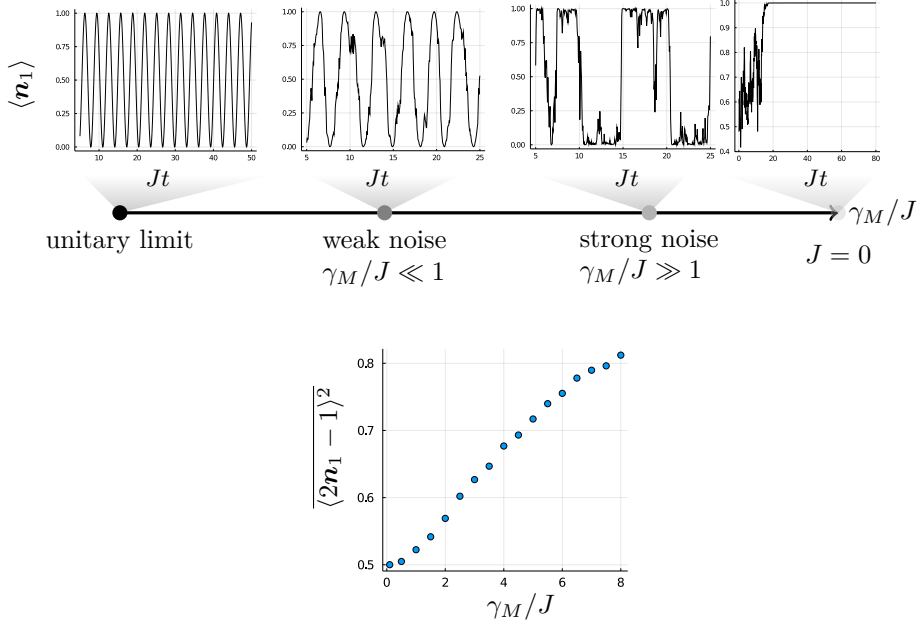


**Figure 4.9:** *Top:* Time evolution of the expected particle number  $\langle \mathbf{n}_1 \rangle$  at site 1 for a system of two sites ( $L = 2$ ) and one fermion. In the absence of noise, there are Rabi oscillations, which are only slightly disturbed for  $\gamma_M/J \ll 1$ . For  $\gamma_M/J \gg 1$ , the particle number is temporally pinned to the value 0 or 1, describing a ‘localized’ state. Without a Hamiltonian, the system relaxes into one of the number eigenstates. **Bottom:** Fluctuations around the mean occupation number as a non-trivial quantity under averaging.

The full model for an arbitrary lattice size  $L$ , combining the dynamics of stochastic, measurement-induced evolution, dephasing and unitary evolution reads:

$$\begin{aligned}
 d\rho^{(c)} = & -i[\mathbf{H}, \rho^{(c)}]dt - \underbrace{\frac{\gamma_B}{2} \sum_{i=1}^L [\mathbf{n}_i, [\mathbf{n}_i, \rho^{(c)}]]dt}_{\text{bath contribution}} \\
 & - \underbrace{\frac{\gamma_M}{2} \sum_{i=1}^L [\mathbf{n}_i, [\mathbf{n}_i, \rho^{(c)}]]dt + \sqrt{\gamma_M} \sum_{i=1}^L dW_i(t) \{\mathbf{n}_i - \langle \mathbf{n}_i \rangle, \rho^{(c)}\}}_{\text{measurement contribution}}.
 \end{aligned} \tag{4.54}$$

It describes the evolution of  $\rho^{(c)}$ , conditioned to the measurement outcomes  $\{m_{j,t}\}$  for each lattice site  $j$  and time  $t$ . As in the KZM discussion, we want to

extract the typical behavior of, e.g., order parameters, correlation functions or the entanglement entropy on large distances, examples being:

$$\begin{aligned}
 \text{order parameter} \quad \langle \mathcal{O} \rangle &= \text{tr}[\mathcal{O}\rho^{(c)}], \\
 \text{correlation} \quad \langle \mathbf{n}_i \rangle \langle \mathbf{n}_j \rangle - \langle \mathbf{n}_i \mathbf{n}_j \rangle &= \text{tr}[\mathbf{n}_i \rho^{(c)}] \cdot \text{tr}[\mathbf{n}_j \rho^{(c)}] - \text{tr}[\mathbf{n}_i \mathbf{n}_j \rho^{(c)}], \\
 \text{entropy} \quad S_{\text{vN}}(A) &= -\text{tr}[\rho_A^{(c)} \cdot \log(\rho_A^{(c)})].
 \end{aligned}$$

Before going into the details, there are multiple important points to raise: (i)  $\rho^{(c)}$  will depend on the particular measurement outcome and therefore vary for each experimental run, and (ii) extracting the expectation values experimentally is subtle. To calculate/approximate the expectation value, we would need to repeat the measurement on the *same* state multiple times. However, we cannot copy the state and it is very unlikely to experimentally obtain the same set of measurement outcomes  $\{m_{j,t}\}$  (and state) again (due to the exponentially growing number of possible measurement trajectories in time). The second issue is not so easy to address and we leave it for now, but the first issue can be addressed by working with averages over the measurement outcomes, which we denote as  $\overline{(\dots)}$ . Therefore, we are dealing with quantities like:

$$\overline{\langle \mathcal{O} \rangle} \approx \frac{1}{\mathcal{N}} \sum_{a=1}^{\mathcal{N}} \text{tr}[\mathcal{O}\rho_{\vec{m}_a}^{(c)}], \quad (4.55)$$

where we are summing over  $\mathcal{N}$  runs of the experiment ( $\Leftrightarrow$  sets of measurement results  $\vec{m}_a = \{m_{j,t}^{(a)}\}$ ). This represents a challenge: As we have seen before, the averaged dynamics evolves towards the featureless stationary state  $\overline{\rho_{t \rightarrow \infty}^{(c)}} \propto \mathbb{1}$ , which reveals no information about the interplay of the Hamiltonian and the measurements:

$$\overline{\langle \mathcal{O} \rangle}(t \rightarrow \infty) \propto \text{tr}[\mathcal{O}\mathbb{1}]. \quad (4.56)$$

To access non-trivial information, we have to consider higher moments of  $\rho^{(c)}$ , e.g. in the form<sup>22</sup>:

$$\overline{\langle \mathcal{O} \rangle \langle \mathcal{O} \rangle} = \overline{\text{tr}[\mathcal{O}\rho^{(c)}]^2} \neq \text{tr}[\mathcal{O}\overline{\rho^{(c)}}]^2. \quad (4.57)$$

An example is shown in Fig. 4.9 and  $\overline{\langle \mathbf{n}_i \rangle \langle \mathbf{n}_j \rangle - \langle \mathbf{n}_i \mathbf{n}_j \rangle}$  or  $\overline{S_{\text{vN}}}$  being further examples. Physically, the ‘pinned’ dynamics ( $\gamma_M/J \gg 1$ ) is characterized by a near-product state with  $\langle \mathbf{n}_i \mathbf{n}_j \rangle \stackrel{|i-j| \gg 1}{\approx} \langle \mathbf{n}_i \rangle \langle \mathbf{n}_j \rangle$  such that connected correlations like  $\langle \mathbf{n}_i \rangle \langle \mathbf{n}_j \rangle - \langle \mathbf{n}_i \mathbf{n}_j \rangle$  are strongly suppressed. Similarly, the deviations from the flat particle number distribution (given by  $\overline{\langle \mathbf{n}_i \rangle} = 1/2$ ) can be characterized by  $(\langle \mathbf{n}_i \rangle - \frac{1}{2})^2$  and should be non-vanishing. A version, which is relevant to many body system, is the observation that the particle number and therefore the parity is well defined in a large subsystem  $A$ . Correspondingly, the *parity variance*  $P_{|A|}$ , defined in (4.58), should be non-vanishing even for  $|A| \gg 1$ . In the presence of a bath (or mixed states in general), observables like correlations

---

<sup>22</sup>Related to the Edwards-Anderson order parameter [20, 32, 155, 157, 235, 236] in the theory of spin glasses.

and the subsystem parity variance are still reasonable quantities. However, the von Neumann entanglement entropy  $S_{\text{vN}}(A)$  is plagued by a (volume law) scaling (as we have already seen in Sec. 4.3)<sup>23</sup>. A related measure of correlations is the mutual information  $I_m(A, B) = S_{\text{vN}}(A) + S_{\text{vN}}(B) - S_{\text{vN}}(AB)$  between subsystems  $A$  and  $B$ , which due to its structure is not plagued by the volume law scaling. An alternative *entanglement* measure for mixed states is the logarithmic entanglement negativity, introduced in Sec. 4.3. In summary, we classify the interplay of unitary evolution, measurements and dephasing based on:

$$\begin{aligned}
\text{subsystem parity variance: } P_{|A|} &= \overline{\langle \prod_{j \in A} (2n_j - 1) \rangle^2} = \overline{\langle \prod_{j \in A} e^{i\pi n_j} \rangle^2}, \\
\text{density-density correlation: } C_{ij} &= \overline{\langle n_i \rangle \langle n_j \rangle - \langle n_i n_j \rangle} \stackrel{\text{pure states}}{=} \overline{|\langle c_i^\dagger c_j \rangle|^2}, \\
\text{entanglement entropy (pure states): } S_{\text{vN}}(A) &= -\text{tr}[\rho_A \cdot \log(\rho_A)] = 2I_m, \\
\text{mutual information: } I_m(A, B) &= S_{\text{vN}}(A) + S_{\text{vN}}(B) - S_{\text{vN}}(AB), \\
\text{log negativity: } \mathcal{E}(A) &= \log(\|\rho^{TA}\|).
\end{aligned} \tag{4.58}$$

## 4.5.2 Limiting Case: Unitary Evolution and Measurements

The first scenario we analyze is the interplay of unitary evolution and (continuous) measurements. To characterize the properties of the (free) fermion evolution, we follow two approaches:

1. Study the **stationary limit** for initially pure states.
2. Study the **dynamics of purification** of an initially mixed state (which afterwards evolves according to (i)).

In the first case, the analysis is massively simplified because an initially Gaussian state, e.g.,  $|0101\dots\rangle$ , will stay Gaussian (see App. A.2 for more details), a feature that will be spoiled in the presence of a bath.

**Stationary approach:** The stationary properties of this fermion model have been studied in, e.g., Refs. [17, 18] (see also Refs. [176–178, 188, 189, 198, 199, 237] for related models), revealing a measurement-induced phase transition. For strong measurements, a shortly correlated, weakly entangled phase ( $M$ ) is found with a transition towards an extended critical phase ( $C$ ) with algebraically scaling correlation functions and a logarithmically scaling entanglement entropy, see Fig. 4.10(b). The  $(1+1)$  dimensionality of the model and the  $U(1)$  symmetry, together with the finding of exponentially vs. algebraically decaying correlations, are hallmarks of a BKT transition (analytically studied in Refs. [19, 20]). This scenario is also supported by a finite size scaling analysis in the vicinity of the critical point [18, 189] (as well as Ref. [20]).

To further illustrate the qualitative change in the behavior, we extract the subsystem parity variance  $P_{|A|}$ , supplementing the study in Ref. [18]. For

<sup>23</sup>In particular the maximally mixed state  $\rho^{(c)} \propto \mathbb{1} \rightarrow \rho_A^{(c)} \propto \mathbb{1}_A$  would result in the largest possible entropy (it is also formally not an entanglement measure for mixed states).

$\gamma_M/J \ll 1$ ,  $P_{|A|}$  decays algebraically (Fig. 4.10(a)). In this regime, we anticipate a critical behavior and therefore make use of the rescaled length  $L \sin(\pi|A|/L)/\pi$  (as it would emerge for a conformal theory [9, 18, 198]). This decay corresponds to strong fluctuations of the particle number parity in subsystem  $A$ . In contrast, for  $\gamma_M/J \sim 1$ ,  $P_{|A|}$  saturates for a large enough subsystem size, indicating a well-defined parity in subsystem  $A$ .

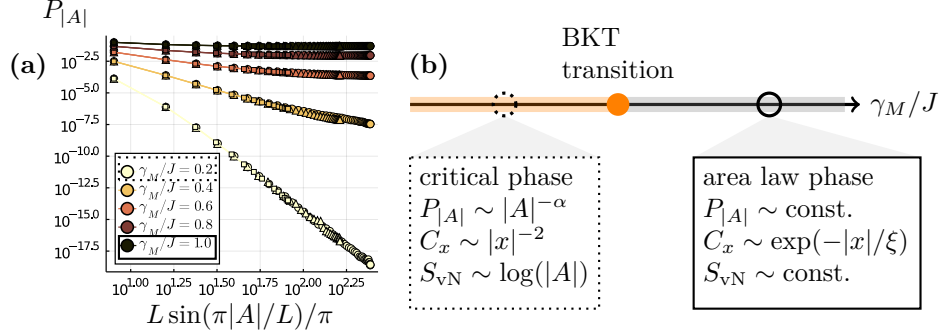


**Figure 4.10:** (a) Subsystem resolved parity variance (log-log) for  $L = 256, 512, 768$  (square, triangle, circle), plotted against the rescaled length in anticipation of a conformal regime for  $\gamma_M/J \ll 1$ . (b) Qualitative phase diagram of the fermionic model subject to weak measurements of the local particle number with two phases: (i) algebraically correlated phase (with  $S_{vN}(A) \sim \log(|A|)$ ) and (ii) short-ranged correlated phase (with  $S_{vN}(A) \sim \text{const.}$ ).

**Dynamical approach:** Starting from a mixed state, the measurement dynamics enforces the evolution towards a pure state (*purification*). The capacity of the model to allow for a strongly entangled state or not also directly influences the purification dynamics. The purification is substantially slower once the stationary state can sustain strong entanglement. As pioneered in Refs. [31, 165], we can distinguish qualitatively different phases by identifying the speed of purification (as a function of  $L$ ). A related probe of these different dynamical regimes was introduced in Ref. [165]: Instead of starting from a fully (or strongly) mixed state, we entangle the state with a single or a few reference ancillas, which do not have any dynamics on their own. Over time, the monitoring dynamics will reduce the entanglement between system and ancilla until reaching a product state. Following this route, we extract a purification time scale that either grows as  $\sim L$  (weak measurements) or depends only weakly on the system size (strong measurements). Our setup consists of coupling a single ancilla qubit ( $B$ ) to the system ( $S$ ), initializing the state as<sup>24</sup>

$$\begin{aligned}
 |\psi_{SB}\rangle &= \frac{1}{\sqrt{2}}|\psi_0\rangle \otimes |0\rangle + \frac{1}{\sqrt{2}}|\psi_1\rangle \otimes |1\rangle, \\
 |\psi_0\rangle &= |1010\dots\rangle, \quad |\psi_1\rangle = |0110\dots\rangle.
 \end{aligned} \tag{4.59}$$

Afterwards, we let the system evolve under measurement-induced dynamics.

<sup>24</sup>Another option would be to start from  $\rho^{(c)} \propto \mathbb{1}$ , but this is technically not feasible for large system sizes.

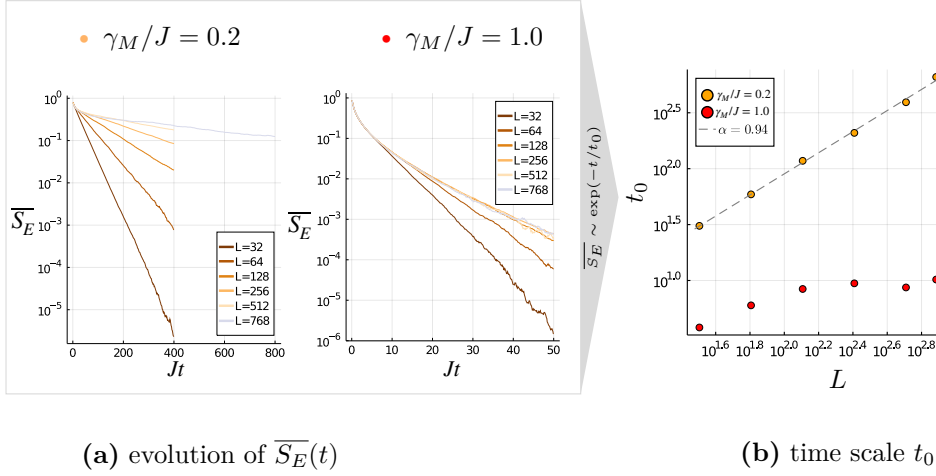


**Figure 4.11:** Dynamical perspective onto the measurement-induced transition: (a) Time evolution of the entanglement  $\overline{S}_E$  between system and an ancilla qubit for: for (i)  $\bullet$   $\gamma_M/J = 0.2$  and (ii)  $\bullet$   $\gamma_M/J = 1.0$  (system sizes  $L = 32, 64, 128, 256, 512, 768$ ). (b) Purification time  $t_0$  as a function of  $L$  (from fit of exponential decay), where the system size dependence depends on the parameter regime. For (i) it grows roughly linearly ( $\alpha$ : best algebraic fit), whereas for (ii) it saturates as a function of  $L$  for  $L \geq 256$ . Numerical details: (i)  $L = 32$ :  $n_{avg} = 10^5$ ;  $L = 64 - 256$ :  $n_{avg} = 4 \times 10^3$ ;  $L = 512$ :  $n_{avg} = 10^3$ ;  $L = 768$ :  $n_{avg} = 250$ . (ii)  $L \leq 256$ ,  $n_{avg} = 4 \times 10^4$ ;  $L = 512, 768$ :  $n_{avg} = 4 \times 10^3$ .

The reduced density matrix of the system is given by  $\rho_{S,t}^{(c)} = \text{tr}_B[|\psi_{SB,t}\rangle\langle\psi_{SB,t}|]$ :

$$\rho_{S,t}^{(c)} = p_0(t)|\psi_{0,t}\rangle\langle\psi_{0,t}| + p_1(t)|\psi_{1,t}\rangle\langle\psi_{1,t}|. \quad (4.60)$$

The purification of the density matrix over time corresponds to growing overlap of the states:  $|\langle\psi_{0,t}|\psi_{1,t}\rangle| \rightarrow 1$ . We quantify this evolution by tracking the entanglement between the ancilla and the system (which initially is maximal):

$$S_E = -\text{tr}[\rho_B \log_2(\rho_B)] = -\text{tr}[\rho_S \log_2(\rho_S)]. \quad (4.61)$$

Averaging this quantity over multiple runs gives rise to  $\overline{S}_E(t)$ , see Fig. 4.11. For long times, the averaged entropy decays exponentially  $\overline{S}_E(t) \sim \exp(-t/t_0)$ , with a system size dependent  $t_0(L)$ . In the weak measurement regime,  $t_0$  grows nearly linearly with the system size  $L$ , as expected for a conformal field theory [238] with a dynamical critical exponent  $z = 1$ . For strong measurements,  $t_0$  flattens as function of  $L$ , indicating an area law phase. Both are shown in Fig. 4.11(b).

**Remark:** Our initial state, (4.59), corresponds to a weakly mixed state (from the perspective of the system). For a strongly mixed initial state and in the parameter regime of the critical phase, an algebraic decay of  $\overline{S}_{vN}$  is expected initially [19, 31, 165, 238], turning into an exponential one for long times. Similarly, an algebraic decay  $\overline{S}_{vN} \sim (t/L)^{-1}$  is observed at a critical point [31], turning into an exponential one once the entanglement becomes small (around one bit).

**Box 19: Purification and mixed states in the quantum trajectory approach**

So far, we have considered the measurement dynamics of initially pure states. In the following, we derive the dynamics of an initially *mixed* state under measurements (see also, e.g., Refs. [22, 239]). A generic density matrix can be written as an ensemble of pure states

$$\rho^{(c)} = \sum_{\alpha} p_{\alpha} |\psi^{(\alpha)}\rangle \langle \psi^{(\alpha)}|. \quad (4.62)$$

In one time step with measurement outcomes  $\{m_j\}$  for each lattice site, it evolves into the state

$$\rho^{(c)} \rightarrow \left( \prod_{i=1}^L M_{m_i}^{(i)} \right) \rho^{(c)} \left( \prod_{j=1}^L M_{m_j}^{(j)\dagger} \right). \quad (4.63)$$

In the limit of  $\delta t \rightarrow 0$ , the evolution operators can be trotterized. In our case, they read (see also Ref. [17]):

$$\rho^{(c)} \rightarrow \mathbf{V} \rho^{(c)} \mathbf{V}^{\dagger} = \sum_{\alpha} p_{\alpha} \mathbf{V} |\psi^{(\alpha)}\rangle \langle \psi^{(\alpha)}| \mathbf{V}^{\dagger}, \quad (4.64)$$

$$\mathbf{V} = \exp \left[ \sum_{j=1}^L \sqrt{\gamma_M} \Delta W_j (\mathbf{n}_j - \langle \langle \mathbf{n}_j \rangle \rangle) - \gamma_M \delta t (\mathbf{n}_j - \langle \langle \mathbf{n}_j \rangle \rangle)^2 \right].$$

Here,  $\langle \langle \mathbf{n}_j \rangle \rangle := \text{tr}(\mathbf{n}_j \rho^{(c)}) = \sum_{\alpha} p_{\alpha} \langle \mathbf{n}_j \rangle_{\alpha}$  is the average of  $\mathbf{n}_j$  over the whole ensemble. Therefore, the combined unitary and measurement evolution reads:

$$\rho_{t+\delta t}^{(c)} \approx e^{-i\mathbf{H}\delta t} \mathbf{V} \rho_t^{(c)} \mathbf{V}^{\dagger} e^{i\mathbf{H}\delta t} = \sum_{\alpha} p_{\alpha}(t + \delta t) |\psi_{t+\delta t}^{(\alpha)}\rangle \langle \psi_{t+\delta t}^{(\alpha)}|. \quad (4.65)$$

This corresponds to an update of the probabilities and the states in the ensemble according to:

$$\begin{aligned} |\psi_{t+\delta t}^{(\alpha)}\rangle &= \frac{e^{-i\mathbf{H}\delta t} \mathbf{V} |\psi_t^{(\alpha)}\rangle}{\sqrt{\langle \psi_t^{(\alpha)} | \mathbf{V}^{\dagger} \mathbf{V} | \psi_t^{(\alpha)} \rangle}}, \\ p_{\alpha}(t + \delta t) &= p_{\alpha}(t) \langle \psi_t^{(\alpha)} | \mathbf{V}^{\dagger} \mathbf{V} | \psi_t^{(\alpha)} \rangle. \end{aligned} \quad (4.66)$$

## 4.6 Solving the conditional Master Equation for small Systems – Including Dephasing

- We analyze the density-density correlation function and the subsystem parity variance for system sizes of  $L = 10$  in the presence of dephasing. Additionally, we consider the log negativity and mutual information for  $L = 8$  (being numerically expensive quantities to extract, even for  $L = 10$ ).

In the absence of a bath, an initially pure state stays pure under the measurement and unitary dynamics. Additionally, an initially mixed state will purify over time. If the pure states are also Gaussian states, this leads to a tremendous simplification and system sizes of  $L \sim \mathcal{O}(10^2 - 10^3)$  are reachable (see, e.g., Refs. [17, 18, 188]). However, the coupling to a dephasing bath renders the reduced description of the system mixed and *non-Gaussian*. Therefore, the numerical solution of  $\rho_t^{(c)}$  is limited to small system sizes, with only limited informative value regarding larger system sizes. Nevertheless, the small scale analysis provides a first guide line to understand the influence of the additional dephasing bath.

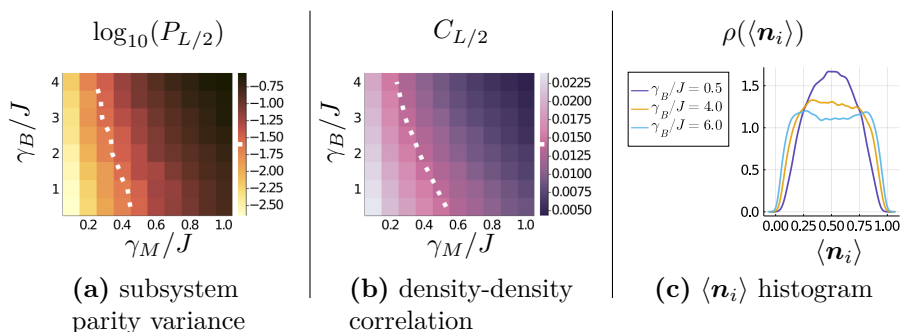


**Figure 4.12:** Overview of a fermionic system subject to unitary evolution, measurements and a bath with  $L = 10$  ( $L/2$  fermions). In (a) and (b) the log of (i) the parity variance for  $|A| = L/2$  and (ii) the density-density correlations at  $l = L/2$  are shown in the  $(\gamma_M/J, \gamma_B/J)$  parameter plane. Both indicate a rough bipartition (dotted lines are a guide to the eye). (c) Probability density  $\rho(\langle \mathbf{n}_i \rangle)$  of the local occupation number  $\langle \mathbf{n}_i \rangle$  for  $\gamma_M/J = 0.3$  and different  $\gamma_B/J$  with a unimodal distribution for small to intermediate  $\gamma_B/J$ , turning into a bimodal distribution for  $\gamma_B/J \gg 1$ .

The correlations, subsystem parity variance and distribution of the local particle numbers  $\rho(\langle \mathbf{n}_i \rangle)$  are plotted in Fig. 4.12. First, for  $\gamma_B = 0$ , the density-density correlations  $C_{L/2}$  are overall larger (less strongly decaying) for weak measurements  $\gamma_M/J \ll 1$ , crossing over to a stronger decay for stronger measurements. Complementarily, the subsystem parity variance is suppressed for  $\gamma_M/J \ll 1$ , in contrast to the strong measurement limit, see Fig. 4.12(a),(b). Similarly, the distribution  $\rho(\langle \mathbf{n}_i \rangle)$  is peaked around  $\langle \mathbf{n}_i \rangle \approx 1/2$  for weak measurements, turning into a bimodal distribution for strong measurements (in accordance with a stronger pinning onto number eigenstates).

From the information theoretic point of view, the mutual information<sup>25</sup>, plotted in Fig. 4.13(c), is largest for weak to moderate measurement rates. In the limit  $\gamma_B = 0$  and pure states, it is proportional to the entanglement entropy  $S_{vN}(A)$  (see again (4.58)). These are small system indicators of the measurement-induced transition studied numerically in Ref. [18] for large system sizes and analytically in Ref. [19].

<sup>25</sup>The mutual information is also an upper bound to correlations between  $A$  and  $B$ , see Ref. [146].

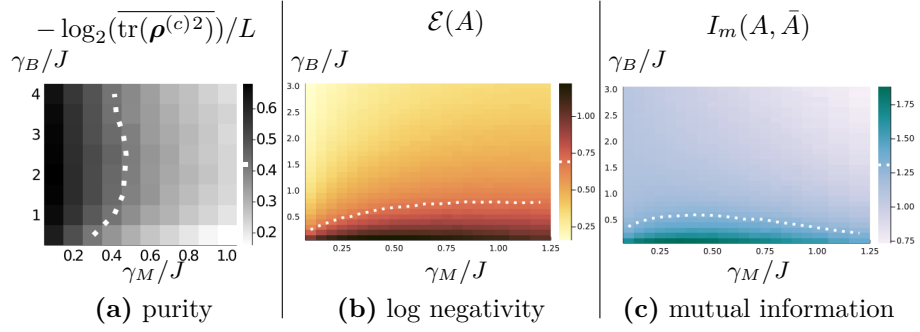


**Figure 4.13:** Overview of measures of global properties of  $\rho^{(c)}$ : (a) log of the averaged purity, (b) log negativity  $\mathcal{E}(A)$ , and (c) mutual information  $I_m(A, \bar{A})$  between two subsystems of size  $L/2$ . The purity indicates a third regime, with strongly mixed states to the left of the dashed line (guide to the eye), in accord with the regime of lowest values of  $\mathcal{E}(A)$ .  $\mathcal{E}(A)$  and  $I_m$  are largest for the regime of weak bath strength and moderate measurement strength.

In the other limiting case ( $\gamma_M = 0, \gamma_B > 0$ ), the state evolves into a strongly mixed state with (exponentially) suppressed purity and small log negativity, see Fig. 4.13(a),(b). Both quantities indicate the approach towards the featureless and unentangled state  $\rho^{(c)} \rightarrow \mathbb{1}$ . In the intermediate range ( $\gamma_M > 0, \gamma_B > 0$ ), the regime of larger subsystem parity  $P_{L/2}$  increases for  $\gamma_B \neq 0$ . Complementarily, the regime of more strongly decaying correlations is extending towards smaller  $\gamma_M$ . The purity instead decreases notably for  $\gamma_B > \gamma_M$  (close to the  $\gamma_B$ -axis), indicating the strong mixedness induced by the bath. In the limit  $\gamma_B \gg \gamma_M$  the situation is changed: the purity becomes larger, suggesting that the interplay of strong dephasing and moderate measurements tend to purify the states. Qualitatively, this corresponds to the suppression of the scrambling dynamics of the unitary evolution due to strong dephasing, which therefore enhances the measurement-induced dynamics. The information gained by the weak measurements about the local particle numbers is only weakly altered by the unitary dynamics, favoring states close to pure product states. Together with the log negativity (and mutual information) being most pronounced for  $\gamma_B/J < 1$ , we can qualitatively identify three regimes:

- (C): significant correlations and entanglement, while the purity is large and the local parity is not well-defined.
- ( $C_D$ ): significant correlations, while the purity and log negativity are small and the local parity is not well-defined.
- (M): more strongly decaying correlations with a well-defined parity and large purity.

To investigate the fate of these regimes for (thermodynamically) large systems, we pair two approaches: (i) the numerical investigation for larger system sizes based on quantum trajectories and (ii) an analytical approach based on effective bosonic version of the model. The second approach is suitable for the thermodynamic limit  $L \rightarrow \infty$  and the corresponding long-wavelength physics.

**Remark:** The purity  $\text{tr}[\rho_S^2]$  is related to the Renyi entanglement entropy  $S_2(S)$  between the bath ancillas and the system ( $S$ ):  $\text{tr}[\rho_S^2] = \exp(-S_2)$ . It is therefore expected for, e.g., bosonic Gaussian CFT's [193] that  $S_2(S)$  scales with the system size whenever  $\gamma_B \neq 0$  (and  $\gamma_M \neq 0$ ), which would disqualify the purity in itself as a measure to distinguish thermodynamically different phases. As an example of the averaged purity for different accessible system sizes  $L$ , see Fig. 4.14. Nevertheless, measures like  $I_m = S_{\text{vN}}(A) + S_{\text{vN}}(B) - S_{\text{vN}}(AB)$  and  $\mathcal{E}$  can be sensitive about the correlations or entanglement between two subsystems even in case of mixed states with possibly different scalings with  $L$  for  $L \rightarrow \infty$  (see, e.g., Refs. [173, 174, 193, 219, 240, 241]).

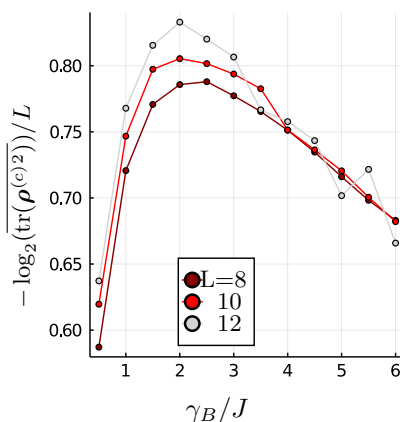


**Figure 4.14:** Log of the averaged purity as a function of  $\gamma_B/J$ , rescaled by the system size  $L$  (for  $\gamma_M/J = 0.5$ ).

## 4.7 Analytical Approach: Observables from Replica Approach

Numerically, the ‘observables’ as given in (4.58), are obtained by evolving and averaging over many quantum trajectories with different measurement outcomes to perform the average  $\overline{(\dots)}$ . This approach is manageable for Gaussian states even up to large system sizes. Nevertheless, we want to make statements in the thermodynamic limit  $L \rightarrow \infty$  about the possibility of different thermodynamic phases. In this limit, a description in terms of an effective model is favorable which only takes into account the long distance degrees of freedom - the bosonic theory. Therefore, we discuss in the following:

- General replica setting, which allows us to work (analytically) with non-random objects.
- Application of this setting to the effective bosonic model to study the long distance limit.

### 4.7.1 Measurements in the bosonic Theory – Model Definition

In the following, we bundle the ingredients to describe the time evolution of the effective bosonic model (which have already been mentioned before):

- **Unitary part:** The unitary part is described by the quadratic Hamiltonian  $\mathbf{H}$  in (4.44) and gives rise to the contribution

$$\mathcal{L}_H[\rho^{(c)}] = -i \left[ \mathbf{H}, \rho^{(c)} \right].$$

- **Measurement part:** The fermionic measurement operator  $\mathbf{n}_i$  (with measurement strength  $\gamma_M$ ) is replaced by two bosonic measurements operators in analogy to the bath case [19]:

$$\text{linear: } \mathbf{L}_x^{(\text{lin})} = -\frac{1}{\pi} \partial_x \phi_x, \quad \text{non-linear: } \mathbf{L}_x^{(\text{nlin})} = m \cos(2\phi_x). \quad (4.67)$$

Each operator comes with the same measurement strength  $\gamma_M$ , giving rise to two contributions in the conditional Master equation:

$$\begin{aligned} \mathcal{L}_M[\rho^{(c)}] = & -\frac{\gamma_M \delta t}{2} \int_x \left[ \mathbf{L}_x^{(\text{lin})}, \left[ \mathbf{L}_x^{(\text{lin})}, \right] \right] + \sqrt{\gamma_M} \int_x \Delta W_x \left\{ \mathbf{L}_x^{(\text{lin})} - \langle \mathbf{L}_x^{(\text{lin})} \rangle, \rho^{(c)} \right\} \\ & - \frac{\gamma_M \delta t}{2} \int_x \left[ \mathbf{L}_x^{(\text{nlin})}, \left[ \mathbf{L}_x^{(\text{nlin})}, \right] \right] + \sqrt{\gamma_M} \int_x \Delta W_x \left\{ \mathbf{L}_x^{(\text{nlin})} - \langle \mathbf{L}_x^{(\text{nlin})} \rangle, \rho^{(c)} \right\}. \end{aligned}$$

- **Dephasing part:** The dephasing bath operators  $\mathbf{L}_i = \mathbf{n}_i$  (with bath strength  $\gamma_B$ ) are replaced by the same two bosonic operators (4.67), each with the same strength  $\gamma_M$ :

$$\mathcal{L}_B[\rho^{(c)}] = -\frac{\gamma_B \delta t}{2} \int_x \left[ \mathbf{L}_x^{(\text{lin})}, \left[ \mathbf{L}_x^{(\text{lin})}, \rho^{(c)} \right] \right] - \frac{\gamma_B \delta t}{2} \int_x \left[ \mathbf{L}_x^{(\text{nlin})}, \left[ \mathbf{L}_x^{(\text{nlin})}, \rho^{(c)} \right] \right].$$

The competition in the fermion model lies in coherent hopping on the one hand and pinning onto number eigenstates  $|\{n_i\}\rangle$  by measuring the particle number on the other hand. In the bosonic model, the competition is rooted in the measurement operators favoring eigenstates of  $\phi_x$ , whereas the  $(\partial_x \theta_x)^2$ -term in the Hamiltonian tends to delocalize the eigenstates in the  $\phi$ -basis. As we will see in the following,  $\mathbf{L}_x^{(\text{lin})}$  does not induce a transition but stabilizes, e.g., algebraic correlations (see Sec. 4.7.2) and therefore describes the long distance properties of the weak measurement phase [19]. This is an advantage compared to the fermionic model: the quadratic fermion part ( $\mathbf{H}$  only) describes the evolution into a volume law state, which is not stable against weak measurements (as we have seen). The transition is driven by  $\mathbf{L}_x^{(\text{nlin})} = m \cos(2\phi_x)$ , which induces a finite, non-vanishing scale in the system at large distances ( $k \rightarrow 0$ ) *once it describes a relevant perturbation*.

**Remark:** In the following, we will often use discrete sums instead of integrals over  $x$ . The reason is the easier readability and connection to the (discrete) fermionic setup. In a final step, the sums should always be replaced by integrals in case of the effective bosonic description.

#### 4.7.2 Interlude: Exact Solution of Connected Correlation Functions in case of linear Measurement Operators

Before we are going to discuss the replica theories and related RG calculation, we consider an exactly solvable case. Once the non-linear measurement and bath operator are absent, the density-density correlations can be calculated exactly (discussed in Refs. [19, 193]) without the need of a replica theory. The important point here is that the exact solvability remains in tact even in the

presence of a bath. Restricting ourselves to linear measurement/bath operators, the density-density correlations read:

$$\begin{aligned} C_y &\approx -\frac{1}{\pi^2} \left\langle \frac{1}{2} \{ \partial_x \phi_x - \langle \partial_x \phi_x \rangle, \partial_x \phi_{x+y} - \langle \partial_x \phi_{x+y} \rangle \} \right\rangle \\ &= -\frac{1}{\pi^2} (\langle \partial_x \phi_x \partial_x \phi_{x+y} \rangle - \langle \partial_x \phi_x \rangle \langle \partial_x \phi_{x+y} \rangle). \end{aligned} \quad (4.68)$$

This correlation function is a special case of the expectation value of operators like  $\mathcal{O}_{AB} := \frac{1}{2} \{ \mathbf{A} - \langle \mathbf{A} \rangle, \mathbf{B} - \langle \mathbf{B} \rangle \}$ , where  $\mathbf{A}$  and  $\mathbf{B}$  are linear operators. The expectation value  $\langle \mathcal{O}_{AB} \rangle$  for  $t \rightarrow \infty$  can be found exactly, because its dynamics is *deterministic* for Gaussian states (all stochastic parts cancel out). To see this, consider the time evolution of any expectation value:

$$d\langle \mathcal{O} \rangle = i\langle [\mathbf{H}, \mathcal{O}] \rangle - \frac{\gamma_M + \gamma_B}{2} dt \sum_i \langle [\mathbf{L}_i, [\mathbf{L}_i, \mathcal{O}]] \rangle + \sqrt{\gamma_M} \sum_i dW_i \langle \{ \mathbf{L}_i - \langle \mathbf{L}_i \rangle, \mathcal{O} \} \rangle.$$

In the special case of  $\mathcal{O} = \mathcal{O}_{AB}$ , the last line vanishes exactly (as we will show below) and we can solve it in the stationary limit  $d\langle \mathcal{O}_{AB} \rangle \stackrel{!}{=} 0$ . The reason is that the last line is the expectation value of three fields *with vanishing means*, evaluated for a Gaussian state. According to Wick's theorem, such expressions vanish. The remaining deterministic equation is of algebraic Riccati type, admitting a stationary solution that can be found exactly (see Ref. [19, 193] for further details) with

$$\text{momentum space: } C_k \sim |k|, \quad \text{real space: } C_y \sim \frac{1}{|y|^2}. \quad (4.69)$$

It describes the aforementioned algebraic correlations in the weak measurement phase and is valid in the absence *and presence* of a dephasing bath (as we show below).

#### Box 20: Details about the exact solution of simple correlation functions

First, we show that the stochastic part is vanishing for Gaussian states:

$$dW_i \langle \{ \mathbf{L}_i - \langle \mathbf{L}_i \rangle, \mathcal{O}_{AB} \} \rangle \stackrel{!}{=} 0.$$

To only ingredient we need is Wick's theorem for  $\langle \mathbf{ABC} \rangle$ . This expectation value vanishes for operators shifted by their mean:  $\tilde{\mathcal{O}} := \mathcal{O} - \langle \mathcal{O} \rangle$ :  $\langle \tilde{\mathbf{L}} \tilde{\mathbf{A}} \tilde{\mathbf{B}} \rangle = 0$ . Since the operator  $\mathcal{O}_{AB}$  by construction only involves the operators  $\tilde{\mathbf{A}}$  and  $\tilde{\mathbf{B}}$ , we get:

$$\langle \{ \mathbf{L}_i - \langle \mathbf{L}_i \rangle, \mathcal{O}_{AB} \} \rangle = \frac{1}{2} \langle \tilde{\mathbf{L}}_i \tilde{\mathbf{A}} \tilde{\mathbf{B}} \rangle + \frac{1}{2} \langle \tilde{\mathbf{L}}_i \tilde{\mathbf{B}} \tilde{\mathbf{A}} \rangle = 0.$$

To find the exact relative correlation function, we will adapt the strategy derivation in Ref. [19] (also Ref. [193]) and start from a lattice version of the bosonic model with conjugate operators  $[\mathbf{Q}_i, \mathbf{P}_j] = i\delta_{ij}$  with

$$\mathbf{Q}_i = \frac{\phi_{i+1} - \phi_{i-1}}{2\pi}, \quad \mathbf{P}_i = \theta_i, \quad (4.70)$$

continued on next page

continued from page before

and a Hamiltonian

$$\mathbf{H} = \sum_{i,j} \mathbf{Q}_i V_{ij} \mathbf{Q}_j + \mathbf{P}_i W_{ij} \mathbf{P}_j, \quad (4.71)$$

$$V = \frac{\nu\pi}{2} \mathbb{1}, \quad W_{ij} = \frac{\nu}{2\pi} (\delta_{ij} - \delta_{i-1,j} - \delta_{i+1,j}). \quad (4.72)$$

Finally, we can calculate the stationary correlations  $C_{ab}^{AB} := \langle \mathcal{O}_{ab}^{AB} \rangle$ :  $d\langle \mathcal{O}_{ab}^{AB} \rangle = 0$ . The correlator involves local operators  $\mathbf{A}, \mathbf{B}$  at lattice sites  $a$  and  $b$  (which are either  $\mathbf{P}_a$  or  $\mathbf{Q}_a$  and  $\mathbf{L}_a \sim \mathbf{Q}_a$ ). Therefore,  $C_{ab}^{AB}$  can be read as a matrix with indices  $a, b$ . The time evolution of such an expectation value depends on three parts: (i) unitary part, (ii) Lindblad part and (iii) Measurement/Ito product part, stemming from the identity:

$$d(\langle \mathbf{A}\mathbf{B} \rangle - \langle \mathbf{A} \rangle \langle \mathbf{B} \rangle) = d\langle \mathbf{A}\mathbf{B} \rangle - (d\langle \mathbf{A} \rangle) \langle \mathbf{B} \rangle - \langle \mathbf{A} \rangle (d\langle \mathbf{B} \rangle) - d\langle \mathbf{A} \rangle d\langle \mathbf{B} \rangle.$$

**Measurement part:** The last contribution (in orange), evaluated for  $C_{ab}^{AB}$ , gives rise to:

$$-\gamma_M \langle \{ \mathbf{L}_i - \langle \mathbf{L}_i \rangle, \mathbf{A}_a - \langle \mathbf{A}_a \rangle \} \rangle \langle \{ \mathbf{L}_i - \langle \mathbf{L}_i \rangle, \mathbf{B}_b - \langle \mathbf{B}_b \rangle \} \rangle = -4\gamma_M C_{ia}^{LA} C_{ib}^{LB},$$

which only depends on  $\gamma_M$ . This non-linear term leads to a unique stationary solution (it is absent for  $\gamma_M = 0$ ).

**Lindblad part:** The Lindblad contribution reads:

$$-\frac{\gamma_M + \gamma_B}{2} dt \sum_i \langle [ \mathbf{Q}_i, [ \mathbf{Q}_i, \mathcal{O}_{ab}^{AB} ] ] \rangle = +(\gamma_M + \gamma_B) \delta_{ab} \delta_{A,P} \delta_{B,P}. \quad (4.73)$$

**Unitary part:** To evaluate the unitary part, we have to keep in mind that the matrices  $V, W$  are symmetric and  $C_{ab}^{AB} = C_{ba}^{BA}$ , which allows us to write

$$\langle [ \mathbf{H}, \mathcal{O}_{ab}^{PP} ] \rangle = +i(VC^{QP})_{ab} + i(C^{PQ}V)_{ab}, \quad (4.74)$$

$$\langle [ \mathbf{H}, \mathcal{O}_{ab}^{QQ} ] \rangle = -i(WC^{PQ})_{ab} - i(C^{QP}W)_{ab}. \quad (4.75)$$

**Stationary solution:** The stationary solutions fulfill  $dC_{ab}^{AB} = 0$ . Considering the two cases  $\mathbf{A} = \mathbf{B} = \mathbf{P}$  and  $\mathbf{A} = \mathbf{B} = \mathbf{Q}$ , we get two coupled matrix equations:

$$0 = -VC^{QP} - C^{QP}V - 4\gamma_M(C^{QP})^2 + (\gamma_M + \gamma_B)\mathbb{1},$$

$$0 = WC^{PQ} + C^{PQ}W - 4\gamma_M(C^{PQ})^2.$$

The first equation gives rise to

$$C^{QP} = \frac{1}{2} \sqrt{\frac{\gamma_M}{\gamma_M + \gamma_B} \mathbb{1} + \frac{1}{4(\gamma_M + \gamma_B)^2} V^2} - \frac{1}{4(\gamma_M + \gamma_B)} V \propto \mathbb{1}. \quad (4.76)$$

continued on next page

continued from page before

Therefore,  $C^{QQ}$  can be found from the second equation:

$$(C^{QQ})^2 = \frac{1}{8\gamma_M(\gamma_M + \gamma_B)} W(\sqrt{4\gamma_M(\gamma_M + \gamma_B)\mathbb{1} + V^2} - V) \propto W. \quad (4.77)$$

**Fourier transforming:** Going to momentum space and assuming translational invariance:  $C^{QQ}(k, k') = \delta(k + k')C^{QQ}(k)$  with  $k \in [-\pi/a, \pi/a]$  (where  $a$  is the lattice spacing), we get:  $C^{QQ}(k \rightarrow 0) = \alpha \cdot |k|$ , where the constant is defined as

$$\alpha := \frac{\nu^2}{4\sqrt{2}\gamma_M(\gamma_M + \gamma_B)} \sqrt{\sqrt{\frac{16\gamma_M(\gamma_M + \gamma_B)}{\nu^2\pi^2} + 1} - 1}. \quad (4.78)$$

### 4.7.3 General Construction of the Replica Theory

Two challenges in indentifying measurement-induced transitions are rooted in observables being (i) non-linear in the conditional density matrix  $\rho^{(c)}$  and (ii) that  $\rho^{(c)}$  are themselves stochastic objects. The point mentioned first also arises in the context of entanglement entropy calculations (for closed systems), which requires an (infinite) hierarchy of copies of the density matrix. To this end, *replicated* density matrices [9, 54, 155–157] can be used, consisting of multiple copies of the same state. The simplest example is the two-replica density matrix  $\rho^{(2R)} = \overline{\rho^{(c)} \otimes \rho^{(c)}}$ , operating on the Hilbert space  $\mathcal{H}^{(2R)} = \mathcal{H} \otimes \mathcal{H}$ . Observables like  $\overline{\langle \mathcal{O} \rangle^2}$  can be expressed in terms of  $\rho^{(2R)}$ :

$$\overline{\langle \mathcal{O} \rangle^2} = \overline{\text{tr}[(\mathcal{O}^{(1)} \cdot \mathcal{O}^{(2)})\rho^{(c)} \otimes \rho^{(c)}]} = \text{tr}[(\mathcal{O}^{(1)} \cdot \mathcal{O}^{(2)}) \underbrace{\overline{\rho^{(c)} \otimes \rho^{(c)}}}_{=: \rho^{(2R)}}]$$

Here, operators like  $\mathcal{O}^{(1)} := \mathcal{O} \otimes \mathbb{1}$  act on the extended Hilbert space  $\mathcal{H}^{(2R)}$ . By construction,  $\rho^{(2R)}$  is non-stochastic and gives access to all expectation values involving two or less  $\rho^{(c)}$ 's. It already encodes information relevant for the phase transition, like the behavior of density-density correlations or the subsystem parity variance. Therefore, we will concentrate on the dynamics of  $\rho^{(2R)}$  in the following. Note that it also encodes the heating to an infinite temperature state (if applicable):

$$\text{tr}[\mathcal{O}^{(j)}\rho^{(2R)}] = \overline{\langle \mathcal{O} \rangle} \rightarrow \langle \mathcal{O} \rangle_\infty. \quad (4.79)$$

#### Box 21: Higher replicas

Formally, we can define a hierarchy of replica density matrices

$$\rho^{(nR)} := \underbrace{\overline{\rho^{(c)} \otimes \rho^{(c)} \otimes \dots}}_{n \text{ times}}, \quad (4.80)$$

continued on next page

continued from page before

consisting of *equal* copies of the conditional states. They act on the  $n$ -replica Hilbert space  $\mathcal{H}^{(nR)} := \bigotimes^n \mathcal{H}$ . Operators only acting on a replica  $\alpha$  are constructed as

$$\mathcal{O}^{(\alpha)} = \mathbb{1} \otimes \dots \otimes \mathbb{1} \otimes \underbrace{\mathcal{O}}_{\text{position } \alpha} \otimes \mathbb{1} \dots \otimes \mathbb{1}. \quad (4.81)$$

As already discussed, observables in the long time limit ( $t \rightarrow \infty$ ) linear in  $\rho^{(c)}$  will be determined by the infinite temperature state. This heating is reflected in all replica density matrices:

$$\text{tr}[\mathcal{O}^{(j)} \rho^{(nR)}] = \overline{\langle \mathcal{O} \rangle} \rightarrow \langle \mathcal{O} \rangle_{\infty}. \quad (4.82)$$

This replica approach lends itself to the following strategy: (i) find the evolution equation  $\partial_t \rho^{(2R)}$  (or  $\partial_t \rho^{(nR)}$ ); (ii) formulate this theory in terms of a field theory (amenable to a renormalization treatment) and (iii) extract the long wavelength behavior.

#### 4.7.4 Executive Summary – Replica Approach in the bosonic Theory

In the following sections, we derive the evolution equation  $\partial_t \rho^{(2R)}$  and its corresponding field theoretic formulation for the bosonic theory. Since there are multiple steps involved, we briefly summarize the main points in the following as a guideline.

The separation of measurement and bath operators into  $\mathbf{L}_x^{(\text{lin})}$  and  $\mathbf{L}_x^{(\text{nl})}$  gives rise to an ordering principle: Firstly, we evaluate the influence of the linear measurement operators onto the dynamics. Secondly, we check under which conditions the non-linear parts are relevant.

**Linear case:** In case of linear measurement operators, the dynamics separates into two (independent) components (‘relative’ and ‘absolute’) and  $\rho^{(2R)}$  can be written as a product state  $\rho^{(2R)} = \rho^{(a)} \otimes \rho^{(r)}$ . The ‘absolute/relative’ basis is defined as:

$$\phi_x^{(a)} := \frac{\phi_x^{(1)} + \phi_x^{(2)}}{\sqrt{2}}, \quad \phi_x^{(r)} := \frac{\phi_x^{(1)} - \phi_x^{(2)}}{\sqrt{2}}, \quad (4.83)$$

where  $\rho^{(a)}$  is heating up (similarly to the Lindblad scenario), but  $\rho^{(r)}$  encodes non-trivial information in its stationary state. To make this transparent, consider  $C_{ij}$  and  $P_{|A|}$ , which only depend on  $\mathbf{n}_i^{(1)} - \mathbf{n}_i^{(2)}$ . This operator combination translates into an operator<sup>26</sup> that only acts on  $\rho^{(r)}$ :

$$\mathbf{n}_i^{(1)} - \mathbf{n}_i^{(2)} \rightsquigarrow -\frac{1}{\pi} \partial_x \left( \phi_x^{(1)} - \phi_x^{(2)} \right) = -\frac{\sqrt{2}}{\pi} \partial_x \phi_x^{(r)}. \quad (4.84)$$

<sup>26</sup>Here, we ignore the non-linear contributions.

**Analogy to system-bath coupling:** The role of the absolute and relative mode can also be interpreted in terms of a system ( $r$ ) and a bath ( $a$ ). Once we include the non-linear terms, the system dynamics gets affected by the bath, though the bath is still heating up. Going along the analogy of a system-bath coupling, we derive the effective dynamics of  $\rho^{(r)}$  by tracing out the absolute mode. We obtain a path integral description (translating operators into fields), which gives access to:

$$\text{tr}[\mathcal{O}^{(r)} \overline{\rho^{(c)} \otimes \rho^{(c)}}] \approx \int \mathcal{D}[\phi_c^{(r)}, \phi_q^{(r)}] \mathcal{O}^{(r)} e^{i \int_X \frac{1}{2} \Phi_X^T G_0^{-1} \Phi_X + i \Delta S_r}, \quad (4.85)$$

with<sup>27</sup>  $\Phi_X^T = (\phi_{c,X}^{(r)}, \phi_{q,X}^{(r)})$ . In case of only linear measurement operators, the inverse propagator  $G_0^{-1}$  of the relative mode reads (using the rescaling  $t \rightarrow \nu t$ ):

$$G_0^{-1} = -\frac{1}{\pi} \begin{pmatrix} i \frac{1}{\pi} 2 \frac{\gamma_M}{\nu} \partial_x^2 & \partial_t^2 - \partial_x^2 \\ \partial_t^2 - \partial_x^2 & i \frac{1}{\pi} 2 \frac{(\gamma_M + \gamma_B)}{\nu} \partial_x^2 \end{pmatrix}. \quad (4.86)$$

It describes a scale invariant theory and is directly related to correlations like  $\langle \phi_x^{(r)} \phi_y^{(r)} \rangle$ , which encode the features of phase ( $C$ ).

**Including non-linearities:** The non-linear measurement operators induce couplings between the relative and absolute mode. These couplings result in sine-Gordon like interaction terms (once the absolute mode is integrated out):

$$\Delta S_r = \int d^2 X [i \lambda_c \cos(4\phi_{c,X}) + i \lambda_q \cos(4\phi_{q,X}) + i \lambda_{cq}^{(c)} \cos(2\phi_{c,X}) \cos(2\phi_{q,X}) + \lambda_{cq}^{(s)} \sin(2\phi_{c,X}) \sin(2\phi_{q,X})]. \quad (4.87)$$

These contributions are formulated in the *Keldysh basis*, incorporating two classes of terms: (i)  $\lambda_c, \lambda_q$  (depending only on  $\phi_c$  or  $\phi_q$ ) and (ii)  $\lambda_{cq}$ 's, describing a coupling between the classical and quantum components. To identify the dominant physics at long distances, we analyze the relevance of the interaction terms at large distances based on a momentum shell RG. We identify three different scenarios:

1. All interaction terms are irrelevant at large scales.
2. Only  $\lambda_q$  becomes relevant, reminiscent of an effective temperature scale.
3.  $\lambda_{cq}$ 's become most relevant.

Though we do not have direct access to the interacting cases, we can qualitatively interpret the relevant interactions as inducing mass scales [205] at the level of the Green's function (the mass terms  $m_{M_r}, m_{M_i}$  and  $m_D$  are real-valued):

$$(C): \quad G^{-1} = G_0^{-1}, \quad (4.88)$$

$$(C_D): \quad G^{-1} = G_0^{-1} + i m_D (\mathbb{1} - \sigma_z), \quad (4.89)$$

$$(M): \quad G^{-1} = G_0^{-1} + m_{M_r} \sigma_x + i m_{M_i} \mathbb{1}. \quad (4.90)$$

<sup>27</sup>The role and meaning of the classical ( $c$ ) and quantum ( $q$ ) component (Keldysh basis) is explained in Sec. 4.7.7.

**Observable consequences:** Indicators like  $C_y$  and  $P_{|A|}$  are determined by  $G^{-1}$ , based on the identification:

$$C_y \approx -\frac{1}{\pi^2} \langle \partial_x \phi_x^{(r)} \partial_x \phi_{x+y}^{(r)} \rangle, \quad (4.91)$$

$$P_{|A|} \approx \langle e^{i\sqrt{2}(\phi_0^{(r)} - \phi_{|A|}^{(r)})} \rangle \approx e^{-((\phi_0^{(r)} - \phi_{|A|}^{(r)})^2)}. \quad (4.92)$$

Therefore,  $C_y$  and  $P_{|A|}$  are sensitive to the presence or absence of the induced mass terms. The corresponding  $\phi$ -correlations and the different scalings of the observables are summarized in Tab. 4.2.

	$\langle \phi_0^{(r)} \phi_y^{(r)} \rangle$	$C_y$	$P_{ A }$
case (C),(C <sub>D</sub> )	$\sim \log( y )$	$\sim  y ^{-2}$	$\sim  A ^{-K}$
case (M)	$\sim \exp(- y /\xi)$	$\sim \exp(- y /\xi)$	const.

**Table 4.2:** Correlations in the different regimes identified in the RG analysis of the bosonic replica model, based on the correlation length  $\xi$  and a propagator-dependent exponent  $K$ .

### 4.7.5 Dynamics of Replicas – Part 1: Replica Master Equation

In the last sections, we have seen that connected correlation functions (of linear operators) can be found exactly as long as we are dealing with *linear* measurement operators. The aforementioned approach does not require the introduction of replicas. Nevertheless, within the replica approach, we recover the same results *and* it allows us to include non-linear measurement operators ( $\cos(2\phi_x)$ ) in the picture.

The strategy is the following:

1. Derive the dynamical equation for the replica density matrices (replica master equation), in particular for  $\rho^{(2R)} = \overline{\rho^{(c)} \otimes \rho^{(c)}}$ .
2. Identify suitable degrees of freedom (absolute and relative) in case of linear measurement operators.
3. Include non-linear terms and identify, if and when these terms become *relevant* at large distances (via a RG analysis). Relevant non-linearities indicate a strongly interacting theory and the generation of an effective mass scale.

---

To derive the replica master equation, we have to average over the measurement outcomes (the noise). For a discrete time step  $\delta t$  this takes the form:

$$\text{discrete:} \quad \rho_{t+\delta t}^{(2R)} = \overline{\rho_{t+\delta t}^{(c)} \otimes \rho_{t+\delta t}^{(c)}}$$

Replacing  $\rho_{t+\delta t}^{(c)}$  with the expression in (4.54), we get the time evolution equation:

$$\begin{aligned} \rho_{t+\delta t}^{(2R)} = & \rho_t^{(2R)} + i\delta t[\rho_t^{(2R)}, \mathbf{H}^{(1)} + \mathbf{H}^{(2)}] - \frac{1}{2}(\gamma_M + \gamma_B)\delta t \sum_i \left( [\mathbf{L}_i^{(1)}, [\mathbf{L}_i^{(1)}, \rho_t^{(2R)}]] \right. \\ & \left. + [\mathbf{L}_i^{(2)}, [\mathbf{L}_i^{(2)}, \rho_t^{(2R)}]] \right) + \underbrace{\gamma_M \delta t \sum_i \overline{\left\{ \tilde{\mathbf{L}}_i^{(2)}, \{\tilde{\mathbf{L}}_i^{(1)}, \rho_t^{(c)} \otimes \rho_t^{(c)} \} \right\}}}_{\text{measurement-induced interaction between replicas}}, \end{aligned} \quad (4.93)$$

with  $\tilde{\mathbf{L}}^{(i)} := \mathbf{L}^{(i)} - \langle \mathbf{L}^{(i)} \rangle$ . Expectation values of operators that only act on a single replica are the same for all replicas:  $\langle \mathbf{L}_i^{(1)} \rangle = \langle \mathbf{L}_i^{(2)} \rangle$  since the replicas are identical. The first and second term in (4.93) correspond to the Hamiltonian and Lindblad operators, acting individually on the replicas (in the enlarged Hilbert space). Since we use the *same* initial state for each conditional evolution, the initial replica state is a product state  $\rho_{t=0}^{(2R)} = \rho_{t=0} \otimes \rho_{t=0}$ . It would remain a product state under the evolution of the first two contributions. Only the last term in (4.93) induces a coupling between the replicas and turns  $\rho_t^{(2R)}$  eventually into a non-product state. Besides cross coupling terms between replicas, the last contribution also includes non-linear contributions in the form of expectation values. Their presence requires even higher order replicas to describe the evolution. Formally, the dynamics of  $\rho^{(2R)}$  is coupled to  $\rho^{(3R)}$  and  $\rho^{(4R)}$  (replicas are coupled hierarchically). To disentangle the last expression, we separate it into three parts:

$$\begin{aligned} \overline{\mathcal{L}_C[\rho_t^{(c)} \otimes \rho_t^{(c)}]} & := \sum_i \overline{\left\{ \tilde{\mathbf{L}}_i^{(2)}, \{\tilde{\mathbf{L}}_i^{(1)}, \rho_t^{(c)} \otimes \rho_t^{(c)} \} \right\}} = \\ & \sum_i \left\{ \mathbf{L}_i^{(1)}, \{\mathbf{L}_i^{(2)}, \rho^{(2R)}\} \right\} - \overline{\langle \mathbf{L}_i \rangle \{ \mathbf{L}_i^{(1)} + \mathbf{L}_i^{(2)}, \rho_t^{(c)} \otimes \rho_t^{(c)} \}} + 4 \overline{\langle \mathbf{L}_i \rangle^2 \rho_t^{(c)} \otimes \rho_t^{(c)}}. \end{aligned} \quad (4.94)$$

The first term describes the cross coupling and the last two terms contain expectation values. Therefore, the last two terms also involve higher-order replicas (since every expectation value requires another copy of the state):

$$\begin{aligned} \overline{\mathcal{L}_C[\rho_t^{(c)} \otimes \rho_t^{(c)}]} & = \overline{\mathcal{L}_C[\rho_t^{(2R)}, \rho_t^{(3R)}, \rho_t^{(4R)}]} = \sum_i \left\{ \mathbf{L}_i^{(1)}, \{\mathbf{L}_i^{(2)}, \rho_t^{(2R)}\} \right\} \\ & - 2 \sum_i \text{tr}_3 \left[ \{ (\mathbf{L}_i^{(1)} + \mathbf{L}_i^{(2)}) \mathbf{L}_i^{(3)}, \rho_t^{(3R)} \} \right] + 4 \sum_i \text{tr}_{3,4} \left[ \mathbf{L}_i^{(3)} \mathbf{L}_i^{(4)} \rho_t^{(4R)} \right], \end{aligned} \quad (4.95)$$

where  $\text{tr}_n[\dots]$  denotes the partial trace over the  $n$ th replica. This gives rise to an infinite hierarchy of coupled master equations, which will not be exactly solvable (except for certain limiting cases, see info box).

#### Box 22: Exact replica solution

A similar construction can be used to find  $d\rho^{(nR)}$  for any higher-order replica, resulting in (4.99). In the limiting case of  $\mathbf{H} = 0$  and measure-

continued on next page

continued from page before

ment and bath operators being equal ( $\mathbf{L}_i = \mathbf{n}_i$ ), we can exactly solve the stationary limit of the  $n$ -replica master equations. The master equations consist of (4.99) and the analogues terms from (4.93). Consider an arbitrary initial state:

$$\rho_0 = \sum_{\alpha, \alpha'} \rho_{\alpha\alpha'} |\{n\}_\alpha\rangle \langle \{n\}_{\alpha'}|. \quad (4.96)$$

Dephasing will suppress the off-diagonal elements of  $\rho_{\alpha\alpha'}$ . Measurements increase our knowledge about the local particle number and force the state into a pure product state

$$\rho_{t \rightarrow \infty}^{(c)} = |\{n\}_\alpha\rangle \langle \{n\}_\alpha| \quad \text{with prob. } p_\alpha = \rho_{\alpha\alpha}. \quad (4.97)$$

The exact solution for all replica density matrices is given by

$$\rho_{t \rightarrow \infty}^{(nR)} = \sum_{\alpha} p_{\alpha} \bigotimes_{i=1}^n |\{n\}_\alpha\rangle \langle \{n\}_\alpha|. \quad (4.98)$$

It commutes with all  $\mathbf{L}_i$ 's and results in  $\mathcal{L}_C = 0$ , giving rise to a stationary state. The normalized stationary replica solutions, (4.98), reflect the reduction onto the diagonal with the weights given by the initial state. The coupling term for replica  $n$  reads:

$$\begin{aligned} \mathcal{L}_C[\rho_t^{(nR)}, \rho_t^{((n+1)R)}, \rho_t^{((n+2)R)}] &= \frac{1}{2} \sum_{i=1}^L \sum_{\alpha, \beta=1, \alpha \neq \beta}^n \left[ \{\mathbf{L}_i^{(\alpha)}, \{\mathbf{L}_i^{(\beta)}, \rho_t^{(nR)}\} \right. \\ &- 2\text{tr}_{n+1} \left[ \{(\mathbf{L}_i^{(\alpha)} + \mathbf{L}_i^{(\beta)})\mathbf{L}_i^{(n+1)}, \rho_t^{((n+1)R)}\} \right] \\ &\left. + 4\text{tr}_{n+1, n+2} \left[ \mathbf{L}_i^{(n+1)} \mathbf{L}_i^{(n+2)} \right] \rho_t^{((n+2)R)} \right]. \end{aligned} \quad (4.99)$$

**Decoupling the hierarchy:** In the following, we seek for an approximation, which decouples the different orders of replicas. At the level of  $\rho^{(2R)}$ , one approach is to decouple the fluctuating expectation values from the replica density matrix:

$$\begin{aligned} \overline{\langle \mathbf{L}_i \rangle \rho^{(c)} \otimes \rho^{(c)}} &\approx \overline{\langle \mathbf{L}_i \rangle} \cdot \rho^{(2R)} = \langle \langle \mathbf{L}_i^{(1)} \rangle \rangle \cdot \rho^{(2R)}, \\ \overline{\langle \mathbf{L}_i \rangle^2 \rho^{(c)} \otimes \rho^{(c)}} &\approx \overline{\langle \mathbf{L}_i \rangle^2} \cdot \rho^{(2R)} = \langle \langle \mathbf{L}_i^{(1)} \mathbf{L}_i^{(2)} \rangle \rangle \cdot \rho^{(2R)}, \end{aligned} \quad (4.100)$$

with  $\langle \langle \mathcal{O} \rangle \rangle := \text{tr}[\mathcal{O} \rho^{(2R)}]$ . To justify this approximation in the bosonic formulation, we first consider  $\gamma_B = 0$  and linear measurement operators. It was shown in Ref. [19] that the exact connected correlation functions, found from the approach outlined in Sec. 4.7.2, are the exact same using this decoupling approximation. Therefore, this approximation might be referred to as ‘exact’ in this context. Adding (linear) bath operators ( $\gamma_B \neq 0$ ), the same correlation functions can still be inferred exactly, as we have seen in Sec. 4.7.2. The same scaling is obtained from the approximate dynamics (see Sec. 4.8 and also

Ref. [193]).

**Normalization:** Since all other contributions in Eq. (4.93) are norm preserving, we approximate  $\mathcal{L}_C$  using (4.94) and the requirement of norm-preservation:

$$\begin{aligned} \overline{\mathcal{L}_C} &\approx \sum_i \left( -4\tilde{C}_i \rho^{(2R)} + \{ \mathbf{L}_i^{(2)} - \langle \langle \mathbf{L}_i^{(2)} \rangle \rangle, \{ \mathbf{L}_i^{(1)} - \langle \langle \mathbf{L}_i^{(1)} \rangle \rangle, \rho^{(2R)} \} \} \right), \\ \tilde{C}_i &:= \langle \langle \mathbf{L}_i^{(1)} \mathbf{L}_i^{(2)} \rangle \rangle - \langle \langle \mathbf{L}_i^{(1)} \rangle \rangle \langle \langle \mathbf{L}_i^{(2)} \rangle \rangle. \end{aligned} \quad (4.101)$$

Using this norm-preserving approximation, we can write down a closed evolution equation for  $\rho^{(2R)}$ . To this end, we introduce the Lindblad superoperators:

$$\mathcal{L}_{\mathcal{O}}[\rho] := -\frac{1}{2} [\mathcal{O}, [\mathcal{O}, \rho]], \quad (4.102)$$

and we regroup terms according to  $\tilde{\mathbf{L}}_i^{(1)} \pm \tilde{\mathbf{L}}_i^{(2)}$ . This regrouping reveals the absolute/relative structure, where we define  $\tilde{\mathbf{L}}_i^{(\alpha)} := \mathbf{L}_i^{(\alpha)} - \langle \langle \mathbf{L}_i^{(\alpha)} \rangle \rangle$ . The full evolution equation reads:

$$\begin{aligned} \rho_{t+\delta t}^{(2R)} &= +i\delta t [\rho_t^{(2R)}, \mathbf{H}^{(1)} + \mathbf{H}^{(2)}] \\ &+ \frac{1}{2} \gamma_B \delta t \sum_i \underbrace{\left( \mathcal{L}_{\tilde{\mathbf{L}}_i^{(1)} + \tilde{\mathbf{L}}_i^{(2)}}[\rho_t^{(2R)}] + \mathcal{L}_{\tilde{\mathbf{L}}_i^{(1)} - \tilde{\mathbf{L}}_i^{(2)}}[\rho_t^{(2R)}] \right)}_{\text{heating Lindblad terms}} \\ &+ \delta t \gamma_M \sum_i \underbrace{\left( \tilde{\mathbf{L}}_i^{(1)} + \tilde{\mathbf{L}}_i^{(2)} \right) \rho_t^{(2R)} \left( \tilde{\mathbf{L}}_i^{(1)} + \tilde{\mathbf{L}}_i^{(2)} \right)}_{\text{(heating) contour coupling}} \\ &- \delta t \gamma_M \underbrace{\left\{ \frac{1}{2} \sum_i \left( \tilde{\mathbf{L}}_i^{(1)} - \tilde{\mathbf{L}}_i^{(2)} \right)^2, \rho_t^{(2R)} \right\}}_{\text{non-Hermitian Hamiltonian}} - 4\gamma_M \delta t \sum_i \tilde{C}_i \rho_t^{(2R)}. \end{aligned} \quad (4.103)$$

Eq. (4.103) is the closed, non-linear evolution equation for  $\rho_t^{(2R)}$ , which we will analyze in the following subsections.

**Stationary limit:** If we are only interested in the stationary limit of the evolution, we can approximate the remaining expectation values  $\langle \langle \mathbf{L}_i^{(\alpha)} \rangle \rangle$  by their stationary ones. The stationary values are only numbers, which will allow us to convert the operator-based master equation (4.103) into a path integral formulation. To evaluate  $\langle \langle \mathcal{O}^{(\alpha)} \rangle \rangle$  for  $t \rightarrow \infty$ , we note that  $\overline{\rho^{(c)}}$  heats up to the infinite temperature state. Therefore, linear expectation values  $\langle \langle \mathcal{O}^{(\alpha)} \rangle \rangle = \overline{\langle \mathcal{O} \rangle}$  can be evaluated with respect to  $\overline{\rho^{(c)}} \sim \mathbb{1}$ . For our bosonic model this amounts to:

$$\langle \langle \partial_x \phi_x^{(\alpha)} \rangle \rangle = \overline{\text{tr} \left( \partial_x \phi_x \rho_t^{(c)} \right)} \xrightarrow{t \rightarrow \infty} 0, \quad \langle \langle \cos(2\phi_x^{(\alpha)}) \rangle \rangle \xrightarrow{t \rightarrow \infty} 0. \quad (4.104)$$

### 4.7.6 Symmetries in the Replica Formulation

So far, we have discussed a general construction of a replica master equation in case of measurements and a coupling to a bath. The qualitative properties at long times and at large scales are determined by the symmetries in the system.

In this replica setup, we have two symmetry contributions: (i) symmetries of the conditional evolution equation (here: each operator preserves the particle number -  $U(1)$  symmetry) and (ii) additional replica exchange symmetries (see, e.g., Refs. [20, 159]). To identify possible symmetry breaking phase transitions, both contributions are important. In the following, we discuss some of the replica exchange symmetries and identify the presence of a bath with an *explicitly* broken replica symmetry (compare also to Refs. [20, 160, 173]).

**Operator perspective:** We start with the 'replica' symmetries at the operator level (4.103) and afterwards consider their incarnation at the path integral level:

1.  $\gamma_B \neq 0$ : We can exchange the replica labels (1)  $\leftrightarrow$  (2) for all operators in (4.103) (we refer to this as the 'global' replica exchange symmetry).
2.  $\gamma_M = 0$ : We can additionally exchange replica labels (1)  $\leftrightarrow$  (2) for operators acting only from the left (or right) onto  $\rho^{(2R)}$ . This additional symmetry is broken by the term  $(\tilde{\mathcal{L}}^{(1)} - \tilde{\mathcal{L}}^{(2)})\rho^{(2R)}(\tilde{\mathcal{L}}^{(1)} - \tilde{\mathcal{L}}^{(2)})$  in (4.103), stemming from the Lindblad superoperator. This term is absent in the absence of a bath.

**State perspective:** Another angle to look at these (replica) symmetries is to study the properties of the state  $\rho^{(2R)}$  itself for  $\gamma_B = 0$  and  $\gamma_B \neq 0$ . In the absence of a bath and starting from a pure state,  $\rho^{(2R)}$  is given by

$$\gamma_B = 0: \quad \rho_t^{(2R)} = \overline{|\psi_t^{(c)}\rangle\langle\psi_t^{(c)}| \otimes |\psi_t^{(c)}\rangle\langle\psi_t^{(c)}|} = \mathcal{N}^{-1} \sum_{\alpha} \overline{|\psi_t^{(\alpha)}\rangle\langle\psi_t^{(\alpha)}| \otimes |\psi_t^{(\alpha)}\rangle\langle\psi_t^{(\alpha)}|},$$

where  $\alpha$  runs over all  $\mathcal{N}$  noise realizations (different measurement outcomes). The 'contraction' lines indicate, which objects we can exchange: (i) the replicas in total or (ii) only the bras (or kets respectively). However, in the presence of a bath ( $\gamma_B \neq 0$ ), even an initially pure state will become (partially) mixed. Therefore, we have

$$\gamma_B \neq 0: \quad \rho_t^{(2R)} = \overline{\rho_t^{(c)} \otimes \rho_t^{(c)}} = \mathcal{N}^{-1} \sum_{\alpha} \overline{\rho_t^{(\alpha)} \otimes \rho_t^{(\alpha)}}, \quad (4.105)$$

where only the 'global' exchange symmetry is still intact.

**Field theory perspective:** The translation into the language of a Keldysh path integral<sup>28</sup> goes as follows: operators  $\phi, \theta$  acting from left or right onto the replica  $j$  are translated into fields  $\phi_+^{(j)}, \theta_+^{(j)}$  (left) and  $\phi_-^{(j)}, \theta_-^{(j)}$  (right) respectively (the subscript  $\pm$  is also referred to as *contours*) [4, 19, 69]. The weight of different field configurations is dictated by an action  $S$ . In the presence of measurements *and* dephasing, the action is invariant under exchanging replica labels on *both* contours simultaneously. In the absence of a dephasing bath, also labels on a *single* contour can be exchanged, providing an additional symmetry:

$$\begin{aligned} \gamma_B \neq 0: \quad & \phi_+^{(1)}, \theta_+^{(1)} \leftrightarrow \phi_+^{(2)}, \theta_+^{(2)} \quad \text{and} \quad \phi_-^{(1)}, \theta_-^{(1)} \leftrightarrow \phi_-^{(2)}, \theta_-^{(2)}, \\ \gamma_B = 0: \quad & \phi_+^{(1)}, \theta_+^{(1)} \leftrightarrow \phi_+^{(2)}, \theta_+^{(2)} \quad \text{or} \quad \phi_-^{(1)}, \theta_-^{(1)} \leftrightarrow \phi_-^{(2)}, \theta_-^{(2)}. \end{aligned} \quad (4.106)$$

<sup>28</sup>Introduce in more detail in Sec. 4.7.7.

It is this explicitly broken symmetry, at the level of the generator of the dynamics, as well as the state, which opens the possibility of new phases (induced by the competition of a bath, measurements, and a Hamiltonian). In the following, we construct the corresponding field theory and identify the role of the presence or absence of this additional symmetry for physics at large distances.

### 4.7.7 Dynamics of Replicas – Part 2: Linear Measurement Operators

We derive the individual master equations for the ‘absolute’ and ‘relative’ mode. From there, we construct the Keldysh path integral description in the stationary limit.

#### Absolute and relative Mode

Looking back at (4.103), we observe a prominent structure: the measurement and bath operators only appear in the combination  $\tilde{\mathbf{L}}^{(1)} \pm \tilde{\mathbf{L}}^{(2)}$ . In case of linear measurement (and bath) operators,  $\mathbf{L}_x \sim \partial_x \phi_x$ , we can make use of this structure by going into the ‘relative’ and ‘absolute’ basis [19]

$$\begin{aligned}\phi_x^{(a)} &:= \frac{\phi_x^{(1)} + \phi_x^{(2)}}{\sqrt{2}}, & \phi_x^{(r)} &:= \frac{\phi_x^{(1)} - \phi_x^{(2)}}{\sqrt{2}}, \\ \theta_x^{(a)} &:= \frac{\theta_x^{(1)} + \theta_x^{(2)}}{\sqrt{2}}, & \theta_x^{(r)} &:= \frac{\theta_x^{(1)} - \theta_x^{(2)}}{\sqrt{2}}.\end{aligned}$$

If we assume that the initial state is a product state in this new basis:  $\rho^{(2R)} = \rho^{(a)} \otimes \rho^{(r)}$ , the time evolved state stays in a product state. However,  $\rho^{(a)}$  and  $\rho^{(r)}$  behave very differently. The difference is already manifest at the level of  $\langle\langle \phi_x^{(a,r)} \rangle\rangle$ : due to  $\langle\langle \phi_x^{(1)} \rangle\rangle = \langle\langle \phi_x^{(2)} \rangle\rangle$ , we have

$$\langle\langle \phi_x^{(a)} \rangle\rangle = \sqrt{2} \langle\langle \phi_x^{(1)} \rangle\rangle, \quad \langle\langle \phi_x^{(r)} \rangle\rangle = 0. \quad (4.107)$$

Since  $\langle\langle \phi_x^{(1)} \rangle\rangle$  displays heating dynamics, the relation above suggests that the absolute part will (and has to) heat up. The individual master equations read

$$\begin{aligned}\partial_t \rho^{(a)} &= -i[\mathbf{H}^{(a)}, \rho^{(a)}] - \frac{\gamma_B}{2\pi^2} \sum_x \left[ \partial_x \phi_x^{(a)}, \left[ \partial_x \phi_x^{(a)}, \rho^{(a)} \right] \right] \\ &+ \frac{2\gamma_M}{\pi^2} \sum_x \partial_x (\phi_x^{(a)} - \langle\langle \phi_x^{(a)} \rangle\rangle) \rho^{(a)} \partial_x (\phi_x^{(a)} - \langle\langle \phi_x^{(a)} \rangle\rangle) \\ &- \frac{2\gamma_M}{\pi^2} \sum_x \left( \langle\langle (\partial_x \phi_x^{(a)})^2 \rangle\rangle - \langle\langle \partial_x \phi_x^{(a)} \rangle\rangle^2 \right) \rho^{(a)},\end{aligned} \quad (4.108)$$

---


$$\begin{aligned}\partial_t \rho^{(r)} &= -i[\mathbf{H}^{(r)}, \rho^{(r)}] - \frac{\gamma_B}{2\pi^2} \sum_x \left[ \partial_x \phi_x^{(r)}, \left[ \partial_x \phi_x^{(r)}, \rho^{(r)} \right] \right] \\ &- \frac{\gamma_M}{\pi^2} \sum_x \left\{ (\partial_x \phi_x^{(r)})^2, \rho^{(r)} \right\} + \frac{2\gamma_M}{\pi^2} \langle\langle (\partial_x \phi_x^{(r)})^2 \rangle\rangle \rho^{(r)} \\ &= -i \left( \mathbf{H}_{\text{eff}} \rho^{(r)} - \rho^{(r)} \mathbf{H}_{\text{eff}}^\dagger \right) + (\text{normalization}).\end{aligned} \quad (4.109)$$

The gray-colored terms are needed to preserve the normalization, though there is no need for both density matrices to be normalized individually<sup>29</sup>. The Hamiltonians  $\mathbf{H}^{(a,r)}$  are the same as in (4.44) but with the operators  $\phi^{(a,r)}, \theta^{(a,r)}$ .

In the following, we analyze the two individual evolutions:

**Absolute part,  $\gamma_B = 0$ :** The absolute part  $\rho^{(a)}$  evolves into an infinite temperature like state [19] with an indefinitely growing number of excitations (at least linear in time) and correlations (assuming that  $\rho^{(a)}$  is Gaussian):

$$\text{number of excitations:} \quad \langle \mathbf{b}_{\sigma,q}^{(a)\dagger} \mathbf{b}_{\sigma,q}^{(a)} \rangle (t \rightarrow \infty) \rightarrow \infty, \quad (4.110)$$

$$\text{correlations:} \quad \langle \phi_q^{(a)} \phi_{-q}^{(a)} \rangle (t \rightarrow \infty) \rightarrow \infty, \quad (4.111)$$

see App. E.3 for further details. This scenario is reminiscent of the heating of  $\rho_S$  in the presence of dephasing (without measurements).

**Relative part,  $\gamma_B = 0$ :** The relative density matrix instead evolves under a non-Hermitian Hamiltonian  $\mathbf{H}_{\text{eff}}$ . Its normalized solution reads:

$$\begin{aligned} \mathbf{H}_{\text{eff}} &:= \mathbf{H}^{(r)} - i \frac{\gamma_M}{\pi^2} \sum_x (\partial_x \phi_x^{(r)})^2, \\ \rho_t^{(r)} &= \frac{e^{-i\mathbf{H}_{\text{eff}}t} \rho_0^{(r)} e^{i\mathbf{H}_{\text{eff}}^\dagger t}}{\text{tr}[e^{-i\mathbf{H}_{\text{eff}}t} \rho_0^{(r)} e^{i\mathbf{H}_{\text{eff}}^\dagger t}]}. \end{aligned} \quad (4.112)$$

The imaginary part of  $\mathbf{H}_{\text{eff}}$  is non-positive and the evolution ‘cools’ the state  $\rho_t^{(r)}$  into a (unique) pure dark state (see Ref. [19]):

$$\rho_t^{(r)} \rightarrow |\psi_D\rangle\langle\psi_D|. \quad (4.113)$$

In contrast to  $\rho^{(a)}$ , the stationary state of  $\rho_t^{(r)}$  depends on the details of the model and contains information about possible phase transitions.

**Role of dephasing:** If there is a residual coupling to an environment, the same decoupling into absolute and relative degrees of freedom still works, though both modes are subject to additional Lindblad evolution. The qualitative heating of the absolute mode will not be affected, but  $\rho^{(r)}$  will approach a mixed state as well. Overall, the different cases are summarized in Tab. 4.3.

	$\rho^{(2R)}$ (fermionic)	$\rho^{(2R)}$ (bosonic)
$\gamma_B = 0$	$\approx$ (non-trivial)	$\approx \rho^{(a)} \otimes  \psi_D\rangle\langle\psi_D $
$\mathbf{H} = 0$	$= \sum_j p_j \otimes_{i=1}^2  \{n\}_j\rangle\langle\{n\}_j $	$= \sum_j p_j \otimes_{i=1}^2  \{\phi_x\}_j\rangle\langle\{\phi_x\}_j $
$\gamma_M = 0$	$\propto \mathbb{1} \otimes \mathbb{1}$	$\propto \mathbb{1} \otimes \mathbb{1}$

**Table 4.3:** Overview: Two-replica density matrix  $\rho_{t \rightarrow \infty}^{(2R)}$  for the different limiting cases and in the fermionic as well as bosonic description with  $\phi_x |\{\phi_x\}_j\rangle = \phi_x |\{\phi_x\}_j\rangle$ .

<sup>29</sup>Therefore, we can also leave the additional terms out, though they will reappear once we calculate expectation values.

**Summary:** The separation of the dynamics into (i) the heating dynamics of the absolute mode and (ii) the ‘cooling’ dynamics of the relative mode is a key feature for the following analysis. The presence of non-linear measurement operators will not qualitatively alter the heating dynamics of the absolute mode. Therefore, we can study the interacting dynamics of the relative mode by integrating out the absolute mode in the spirit of a weak coupling between a system and a bath.

### Box 23: About the normalization

If we leave out the overall normalization of  $\rho^{(2R)}$ , expectation values (e.g., for the absolute mode) have to be expressed as:

$$\frac{\text{tr}[\mathcal{O}^{(a)}\rho^{(a)} \otimes \rho^{(r)}]}{\text{tr}[\rho^{(a)} \otimes \rho^{(r)}]} = \frac{\text{tr}[\mathcal{O}^{(a)}\rho^{(a)}]}{\text{tr}[\rho^{(a)}]}. \quad (4.114)$$

The dynamic evolution of such an expectation value reads

$$\partial_t \langle \langle \mathcal{O}^{(a)} \rangle \rangle = \frac{\text{tr}[\mathcal{O} \partial_t \rho^{(a)}]}{\text{tr}[\rho^{(a)}]} - \frac{\text{tr}[\mathcal{O} \rho^{(a)}]}{\text{tr}[\rho^{(a)}]^2} \text{tr}[\partial_t \rho^{(a)}]. \quad (4.115)$$

In terms of properly normalized expectation values, this takes the form

$$\begin{aligned} \partial_t \langle \langle \mathcal{O}^{(a)} \rangle \rangle &= i \langle \langle [\mathbf{H}^{(a)}, \mathcal{O}^{(a)}] \rangle \rangle - \frac{1}{2} \gamma_B \cdot \underbrace{\langle \langle \mathcal{L}[\mathcal{O}^{(a)}] \rangle \rangle}_{\text{bath contribution}} \\ &\quad + \gamma_M \int_{x'} \langle \langle \partial_{x'} \tilde{\phi}_{x'}^{(a)} \mathcal{O}^{(a)} \partial_{x'} \tilde{\phi}_{x'}^{(a)} \rangle \rangle - \gamma_M \langle \langle \mathcal{O}^{(a)} \rangle \rangle \cdot \int_{x'} \langle \langle (\partial_{x'} \tilde{\phi}_{x'}^{(a)})^2 \rangle \rangle, \end{aligned}$$

with  $\tilde{\phi}_x := \phi_x - \langle \langle \phi_x \rangle \rangle$ . In this scenario (including only linear measurement operators), the evolution of *linear* operators  $\mathcal{O}^{(a)}$  are unaffected by the measurement-induced terms in the second line once  $\rho^{(a)}$  is Gaussian.

### Construction of the Field Theory – Quadratic Part of the Action

Our goal is to analyze the stability of the critical phase, where the interacting terms are irrelevant and the long distance theory is massless. At the replica level, we perform a RG analysis at the level of the path integral formulation. The construction of the path integral is based on the master equation Eq. (4.103) in the stationary limit, making use of stationary expectation values Eq. (4.104). In the following, we briefly sketch the construction of the Keldysh path integral and analyze the significance of the associated terms in the action.

The properties of, e.g.,  $C_y$  and  $P_{|A|}$  are encoded in the correlators

$$\langle \phi_x^{(r)} \phi_y^{(r)} \rangle = \text{tr} \left[ \phi_x^{(r)} \phi_y^{(r)} \rho_t^{(2R)} \right]. \quad (4.116)$$

The path integral can be understood as a generating function for these correlations. To construct it, we make use of the canonical conjugate variables and

their eigenstates:

$$\left[ \underbrace{\Theta_x}_{\partial_x \theta_x / \pi}, \phi_{x'} \right] = -i\delta(x - x'), \quad \langle \phi_x | \Theta_x \rangle = e^{i\Theta_x \phi_x}. \quad (4.117)$$

The eigenstates of each of the two operators provide a basis and completeness relations ( $= \mathbb{1}$ ), which allows us to write<sup>30</sup>

$$\langle \phi_x^{(r)} \phi_y^{(r)} \rangle = \text{tr} \left[ \mathbb{1}_{\Theta, t, +} \phi_x^{(r)} \phi_y^{(r)} \mathbb{1}_{\phi, t, +} \rho_t^{(2R)} \mathbb{1}_{\phi, t, -} \mathbb{1}_{\Theta, t, +} \right]. \quad (4.118)$$

The  $\pm$  index indicates, whether the  $\mathbb{1}$  operators have been inserted to the left (+) or the right (-) of the density matrix. Since we are dealing with Markovian dynamics, the state at time  $t$  only depends on the state at time  $t - \delta t$ :  $\rho_t^{(2R)} = \mathcal{L}[\rho_{t-\delta t}^{(2R)}]$ . Therefore, we can replace  $\rho_t^{(2R)}$  in terms of  $\rho_{t-\delta t}^{(2R)}$  in the above expression and insert another set of identities etc.. Iterating this procedure, we finally get (see App. B for a detailed derivation) the Keldysh path integral [4, 19, 69, 188]:

$$\langle \phi_x \phi_y \rangle \approx \int \mathcal{D}[\theta_{\pm}^{(a,r)}, \phi_{\pm}^{(a,r)}] \phi_{t,+,x} \phi_{t,+,y} e^{iS} \Big|_{\text{boundary conditions}}, \quad (4.119)$$

$$S = S_a^{(0)} + S_r^{(0)} + \Delta S_{r,a},$$

where the boundary conditions include, e.g., the initial conditions. The path integral consists of a ‘sum’ over all field configurations, weighted by the complex factor  $e^{iS}$  (comparable to the partition sum in equilibrium statistical mechanics). Understanding how these weights, determined by the *action*  $S$ , behave on large scales will be the main focus in the next sections. To turn this construction into a *generating function*, we introduce ‘source fields’  $J_{\sigma, X}$ :

$$Z[J] = \int \mathcal{D}[\theta_{\pm}^{(a,r)}, \phi_{\pm}^{(a,r)}] e^{iS + i \int_X \sum_{\sigma=\pm} \sigma J_{\sigma, X} \phi_{\sigma, X}}, \quad (4.120)$$

with  $X = (t, x)$ . Therefore, correlation functions are obtained as, e.g.,

$$-\frac{1}{Z[0]} \frac{\delta}{\delta J_{\sigma, X}} \frac{\delta}{\delta J_{\sigma, Y}} Z[J_{\sigma}] \Big|_{J=0} = \langle \phi_{\sigma}(X) \phi_{\sigma}(Y) \rangle,$$

with  $Z[0] = \text{tr}[\rho_t^{(2R)}]$ . The form of the action  $S$  can be inferred from the master equation. As an example, we consider a generalized Lindblad superoperator of the form

$$\mathcal{L}[\rho_t] = \int dx a L[\phi_x] \rho_t L[\phi_x] + b \{L^2[\phi_x], \rho_t\}. \quad (4.121)$$

Here,  $L[\cdot]$  are functions of the operators  $\phi_x$  and  $a, b$  are real numbers. The corresponding action reads:

$$iS_{\mathcal{L}} = \int dt dx \{ a L[\phi_{x,t}^+] L[\phi_{x,t}^-] + b (L^2[\phi_{x,t}^+] + L^2[\phi_{x,t}^-]) \}. \quad (4.122)$$

The first two contributions in the action  $S$  in (4.119) describe the individual quadratic parts for absolute and relative mode. These stem from the quadratic

<sup>30</sup>The identities are  $\mathbb{1} = \mathbb{1}^{(a)} \otimes \mathbb{1}^{(r)}$ .

Hamiltonian and the linear measurement operators (as in (4.122)). The remaining part,  $\Delta S_{r,a}$ , incorporates all higher order interactions (from the non-linear measurement operators). In the following, we focus on the long time, stationary limit: we assume that the system is space translation invariant as well as time translation invariant. Therefore, we can work with a single set of frequencies ( $\omega$ ) and a single set of momenta ( $k$ ) (instead of two in the more general case). Note that the construction of the path integral becomes tractable because the expectation values in the stationary limit are treated as numbers. In the bosonic case, they are even vanishing.

**Relative mode:** Information about correlations etc. are encoded in the relative dynamics, governed by (4.109) for  $\rho^{(r)}$ . The master equation translates into

$$S_r^{(0)} = \int dt \int dx \sum_{\sigma=\pm} \left[ \sigma \left( \Theta_{\sigma,X}^{(r)} \partial_t \phi_{\sigma,X}^{(r)} - \frac{\nu}{2\pi} (\pi^2 \Theta_{\sigma,X}^{(r)})^2 - \frac{\nu}{2\pi} (\partial_x \phi_{\sigma,X}^{(r)})^2 \right) + i \frac{(\gamma_M + \frac{1}{2}\gamma_B)}{\pi^2} (\partial_x \phi_{\sigma,X}^{(r)})^2 - i \frac{\gamma_B}{\pi^2} (\partial_x \phi_{+,X}^{(r)}) (\partial_x \phi_{-,X}^{(r)}) \right]. \quad (4.123)$$

The correlations like  $C_y$  only depend on  $\phi^{(r)}$ . Therefore, we construct an effective theory for  $\phi^{(r)}$  alone by integrating out the field  $\Theta^{(r)}$ , based on:

$$\int \mathcal{D}[\Theta^{(r)}] e^{i \int_{x,t} \sigma \Theta_{\sigma,X}^{(r)} \partial_t \phi_{\sigma,X}^{(r)} - \sigma \frac{\nu}{2\pi} (\pi \Theta_{\sigma,X}^{(r)})^2} = \mathcal{N} \times e^{+i \frac{\sigma}{2\pi\nu} \int (\partial_t \phi_{\sigma,X}^{(r)})^2}.$$

In the stationary limit, we work in Fourier space (of space and time)<sup>31</sup>, where the action reads ( $Q = (k, \omega)$ ):

$$S_r^{(0)} = \frac{1}{2} \int \frac{d^2 Q}{(2\pi)^2} (\vec{\Phi}_{-Q}^{(r)})^T \underbrace{\begin{pmatrix} A_+^{(r)} & -i\gamma_B \frac{1}{\pi^2} k^2 \\ -i\gamma_B \frac{1}{\pi^2} k^2 & A_-^{(r)} \end{pmatrix}}_{G_{0,r,\text{contour}}^{-1}} \vec{\Phi}_Q^{(r)}, \quad (4.124)$$

$$\vec{\Phi}_Q^{(r)} := \begin{pmatrix} \phi_{+,Q}^{(r)} \\ \phi_{-,Q}^{(r)} \end{pmatrix}, \quad A_\sigma^{(r)} := \sigma \left( \frac{1}{\nu\pi} \omega^2 - \frac{\nu}{\pi} k^2 \right) + \frac{i}{\pi^2} (2\gamma_M + \gamma_B) k^2.$$

As we have mentioned earlier, the presence of a bath is also indicated by an explicit symmetry breaking. At the level of the action in (4.124), this manifests as a finite coupling between the contours (off-diagonal terms). For  $\gamma_B = 0$ , the unbroken replica exchange symmetry reads

$$\phi_+^{(r)} \rightarrow -\phi_+^{(r)} \quad \text{or} \quad \phi_-^{(r)} \rightarrow -\phi_-^{(r)}.$$

**Absolute mode:** Similarly, we obtain the quadratic part of the action for the

<sup>31</sup>Our convention:  $f(x, t) = f(X) = \int_{-\infty}^{\infty} \frac{d\omega}{2\pi} \frac{dk}{2\pi} e^{i(\omega t + kx)} f(k, \omega) = \int \frac{d^2 Q}{(2\pi)^2} e^{i\vec{Q}\vec{X}} f(Q)$ .

absolute mode (in Fourier space):

$$S_a^{(0)} = \frac{1}{2} \int \frac{d^2 Q}{(2\pi)^2} (\vec{\Phi}_{-Q}^{(a)})^T \underbrace{\begin{pmatrix} A_+^{(a)} & -i \frac{(\gamma_B + 2\gamma_M)}{\pi^2} k^2 \\ -i \frac{(\gamma_B + 2\gamma_M)}{\pi^2} k^2 & A_-^{(a)} \end{pmatrix}}_{G_{0,a,\text{contour}}^{-1}} \vec{\Phi}_Q^{(a)}, \quad (4.125)$$

$$A_\sigma^{(a)} = \sigma \left( \frac{1}{\nu\pi} \omega^2 - \frac{\nu}{\pi} k^2 \right) + i \frac{\gamma_B}{\pi^2} k^2.$$

The correlation functions  $\langle \phi_{\sigma,X}^{(a)} \phi_{\sigma',Y}^{(a)} \rangle$  are determined by the Green's function  $G_{0,a,\text{contour}}$ . As we can see from the example in (4.129), the behavior of the correlations is determined by the poles of the Green's function,  $\omega_{\text{Pol}}(k)$ . One feature of the absolute mode are poles of  $G_{0,a,\text{contour}}$  that lie on the real axis (similar to the 'standard' Lindblad scenario) [19]. They herald the absence of a stationary state with finite correlations.

**Changing basis:** Looking back at our initial example:  $\langle \phi_x \phi_y \rangle$ , we anticipate that there is more than one option to translate this expectation value into the field theoretic language (at least for the standard Keldysh scenario<sup>32</sup>). By cyclically shifting the operators  $\phi$  in (4.118) from acting both to the left of  $\rho$  to (i) one from the left and one from the right or (ii) both from the right, we get

$$\langle \phi_x \phi_y \rangle = \langle \phi_{+,x} \phi_{+,y} \rangle = \langle \phi_{-,x} \phi_{+,y} \rangle = \langle \phi_{-,x} \phi_{-,y} \rangle. \quad (4.126)$$

Therefore, the contour description has some redundancies [4, 69]. An alternative basis, making use of this structure, is the *Keldysh basis* ( $c$ : classical,  $q$ : quantum):

$$\phi_c^{(a,r)} = \frac{\phi_+^{(a,r)} + \phi_-^{(a,r)}}{\sqrt{2}}, \quad \phi_q^{(a,r)} = \frac{\phi_+^{(a,r)} - \phi_-^{(a,r)}}{\sqrt{2}}. \quad (4.127)$$

For the replica master equation of the relative mode, the same action reads:

$$S_r^{(0)} = \frac{1}{2} \int \frac{d^2 Q}{(2\pi)^2} (\vec{\Phi}_{-Q}^{(r)})^T \underbrace{\begin{pmatrix} i \frac{1}{\pi^2} 2\gamma_M k^2 & \frac{1}{\pi\nu} \omega^2 - \frac{\nu}{\pi} k^2 \\ \frac{1}{\pi\nu} \omega^2 - \frac{\nu}{\pi} k^2 & \frac{i}{\pi^2} 2(\gamma_M + \gamma_B) k^2 \end{pmatrix}}_{=G_0^{-1}} \vec{\Phi}_Q^{(r)}. \quad (4.128)$$

In this description, the measurement couplings  $\gamma_M$  appear symmetrically in the  $c-c$  sector and  $q-q$  sector. In contrast, the bath couples *only* to the quantum component. To reconcile this with our earlier symmetry consideration: (i) for  $\gamma_B = 0$  we can exchange  $\phi_q^{(r)} \leftrightarrow \phi_c^{(r)}$ , whereas for (ii)  $\gamma_B \neq 0$  we only have the symmetry  $\{\phi_c^{(r)}, \phi_q^{(r)}\} \leftrightarrow \{-\phi_c^{(r)}, -\phi_q^{(r)}\}$ .

**Physical significance:** We have seen before that the dephasing bath leads to a decay of the off-diagonal contributions in the density matrix. In the Keldysh formulation, dephasing only affects the  $\phi_{q,Q} \phi_{q,-Q}$  components in the action. It results in the suppression of fluctuations away from  $\phi_{q,Q} = 0$  (since it qualitatively contributes a factor  $\exp(-\gamma_M q^2 |\phi_{q,Q}|^2)$  in the path integral).

<sup>32</sup>A word of caution: The structure of the relative mode path integral is not of the usual Keldysh structure, therefore not all identities can be transferred to the relative case.

**Box 24: Accessing correlation functions**

To turn the path integral, described by the quadratic action  $S := \frac{1}{2} \int \frac{d^2 Q}{(2\pi)^2} \vec{\Phi}_{-Q}^T G^{-1} \vec{\Phi}_Q$ , into a generating function we add source terms  $J_\sigma$  to  $iS$  according to [4]

$$i \int \frac{d^2 Q}{(2\pi)^2} \sum_{\sigma=\pm} \sigma J_{\sigma,-Q} \phi_{\sigma,Q} = i \int d^2 X \underbrace{\sum_{\sigma=\pm} \sigma J_{\sigma,X} \phi_{\sigma,X}}_{J_{c,X} \phi_{q,X} + J_{q,X} \phi_{c,X}} .$$

Correlators are obtained by taking derivatives with respect to the sources as given in the main text. For simplicity, we consider the case  $\gamma_B = 0$ : to obtain  $Z[J]$ , we integrate out the fields  $\phi_\sigma$ . To this end, we use  $\tilde{\phi}_{\sigma,Q} = \phi_{\sigma,Q} + J_{\sigma,Q} \frac{\pi}{\sigma(\frac{1}{\nu}\omega^2 - \nu k^2) + i\frac{2\gamma_1}{\pi} k^2}$ , which constitutes a Gaussian integral. After performing the Gaussian integral, we get:

$$Z[J] \propto \exp \left( -\frac{i}{2} \int \frac{d^2 Q}{(2\pi)^2} \sum_{\sigma=\pm} J_{\sigma,Q} G_{\sigma\sigma}(Q) J_{\sigma,Q} \right),$$

where in this special case  $G_{\sigma\sigma}$  is a diagonal matrix. Moving back to real space, we can accordingly write

$$Z[J] \propto \exp \left( -\frac{i}{2} \int d^2 X \int d^2 Y \sum_{\sigma} J_{\sigma,X} G_{\sigma\sigma}(X-Y) J_{\sigma,Y} \right),$$

$$G_{\sigma\sigma}(X-Y) = \int \frac{d^2 Q}{(2\pi)^2} \frac{\pi e^{-i\vec{Q}\vec{X}}}{\sigma(\frac{1}{\nu}\omega^2 - \nu k^2) + i\frac{2\gamma_1}{\pi} k^2}.$$

Correlators are therefore obtained as:

$$\langle \phi_{\sigma,X} \phi_{\sigma,Y} \rangle = -\frac{1}{Z[0]} \frac{\delta}{\delta J_{\sigma,X}} \frac{\delta}{\delta J_{\sigma,Y}} Z[J] \Big|_{J=0} = iG_{\sigma\sigma}(X-Y).$$

In the Keldysh basis, we get similarly for  $a, b \in \{c, q\}$ :

$$\langle \phi_{a,X} \phi_{b,X} \rangle = -\frac{1}{Z[0]} \frac{\delta}{\delta J_{\bar{a},X}} \frac{\delta}{\delta J_{\bar{b},Y}} Z[J_c, J_q] \Big|_{J=0} = iG_{ab}(X-Y),$$

where  $\bar{a}$  is the respective other index.

### 4.7.8 Dynamics of Replicas – Part 3: Non-linear Measurement Operators

At the level of  $\rho^{(2R)}$ , we have access to the density-density correlations  $C_y$  and the subsystem parity variance, which take the following form in the bosonic

theory:

$$C_y \approx -\frac{1}{\pi^2} \langle \partial_x \phi_x^{(r)} \partial_x \phi_{x+y}^{(r)} \rangle, \quad (4.129)$$

$$P_{|A|} \approx \left\langle e^{i\sqrt{2}(\phi_0^{(r)} - \phi_{|A|}^{(r)})} \right\rangle \approx e^{-\langle (\phi_0^{(r)} - \phi_{|A|}^{(r)})^2 \rangle}. \quad (4.130)$$

Both expressions depend only on the relative mode, which in hindsight is to be expected: since  $\rho^{(a)}$  heats up, the non-trivial information is encoded in the relative mode. The combination of (i) the separation  $\rho^{(2R)} \approx \rho^{(a)} \otimes \rho^{(r)}$  and (ii) the relevant information begin encoded in  $\rho^{(r)}$  is reminiscent of the scenario of a weak system ( $r$ ) - environment ( $a$ ) coupling. Even in the presence of non-linear measurement operators, we do not expect that these bounded operators qualitatively alter the heating of the absolute mode [19]. Nevertheless, they can qualitatively affect the relative mode due to coupling terms like  $\cos(\sqrt{2}(\phi^{(a)} + \phi^{(r)}))$ . Similar to the system-bath scenario,  $\rho^{(r)}$  is altered by the coupling to the bath, whereas the bath density matrix, here  $\rho^{(a)}$ , is assumed to be stationary [16].

Therefore, the ‘system’ of interest is the relative part of  $\rho^{(2R)}$ . In the spirit of tracing out the bath, we will focus onto  $\rho^{(r)}$ , defined by

$$\rho^{(r)} = \text{tr}_a[\rho^{(2R)}] \quad (4.131)$$

and derive its effective master equation (including interactions). Formally, we are integrating out the absolute mode, which we perform on the path integral level in the stationary limit. Starting point is the full action

$$S[\phi^{(a)}, \phi^{(r)}] = S_r^{(0)} + S_a^{(0)} + \Delta S_{+,-}. \quad (4.132)$$

The corresponding path integral can be rewritten as

$$Z = \int \mathcal{D}[\phi^{(r)}] e^{iS_r^{(0)}} \underbrace{\int \mathcal{D}[\phi^{(a)}] e^{iS_a^{(0)} + i\Delta S_{+,-}}}_{:= \langle e^{i\Delta S_{+,-}} \rangle_a} \stackrel{!}{=} \int \mathcal{D}[\phi^{(r)}] e^{iS[\phi^{(r)}]}. \quad (4.133)$$

We will integrate out  $\phi^{(a)}$  in a perturbative fashion and therefore restrict ourselves to observables depending only on  $\phi^{(r)}$ . The perturbative treatment is based on the formal identity

$$iS[\phi^{(r)}] = iS_r^{(0)} + \log \left( \langle e^{i\Delta S_{+,-}} \rangle_a \right). \quad (4.134)$$

The perturbative input is to expand the second expression, formally assuming that corrections are small. Up to second order, the expansion reads

$$\begin{aligned} \log \left( \langle e^{i\Delta S_{+,-}} \rangle_a \right) &\approx \log \left( 1 + i \langle \Delta S_{+,-} \rangle_a - \frac{1}{2} \langle \Delta S_{+,-}^2 \rangle_a \right) \\ &\approx i \langle \Delta S_{+,-} \rangle_a - \frac{1}{2} \langle \Delta S_{+,-}^2 \rangle_a + \frac{1}{2} \langle \Delta S_{+,-} \rangle_a^2. \end{aligned} \quad (4.135)$$

In summary, the original quadratic action of the relative mode is complemented by a first and second order correction term:

$$S[\phi^{(r)}] = S_r^{(0)} + \underbrace{\langle \Delta S_{+,-} \rangle_a + \frac{i}{2} (\langle \Delta S_{+,-}^2 \rangle_a - \langle \Delta S_{+,-} \rangle_a^2)}_{:= \Delta S_r}. \quad (4.136)$$

This approach is feasible since the diverging correlations of the heated absolute mode result in many vanishing/suppressed contributions. The full calculation is performed in App. H for our model. The result takes the form of sine-Gordon like terms

$$\begin{aligned} \Delta S_r = \int d^2 X & \left[ i\lambda_c \cos(4\phi_{c,X}^{(r)}) + i\lambda_q \cos(4\phi_{q,X}^{(r)}) \right. \\ & \left. + i\lambda_{cq}^{(c)} \cos(2\phi_{c,X}^{(r)}) \cos(2\phi_{q,X}^{(r)}) + \lambda_{cq}^{(s)} \sin(2\phi_{c,X}^{(r)}) \sin(2\phi_{q,X}^{(r)}) \right], \end{aligned} \quad (4.137)$$

where the  $\lambda$ 's are real-valued interaction couplings with dimension  $[\lambda] = [x]^{-2}$ . The action  $S[\phi^{(r)}]$  is the effective description that captures the behavior of, e.g.,  $C_y$  and  $P_{|A|}$ . In the following, we investigate under which conditions interaction terms will become relevant.

**Remark:** The role of the bath non-linearities is also incorporated in (4.137): they do not lead to *different* couplings compared to the measurement scenario, but they modify the initial coupling strengths. The more drastic effect of the bath stems from the modified propagator.

## 4.8 Correlation Functions and RG Analysis

In the last sections, we have constructed the dynamics of the replica density matrices (in particular  $\rho^{(2R)}$ ) and derived the path integral description in the stationary limit. In the following, we study the stability of the quadratic theory of the relative mode towards the interacting contributions (due to  $\mathbf{L}_x^{(\text{nl})}$ ) by successively integrating out short distance modes. Many of the following line of arguments are similar to, e.g., Ref. [242] for the RG analysis of the sine-Gordon model.

In a first step, we define the fixed point theory whose stability we like to probe (in analogy to the KZM discussion in the previous chapter). We rescale  $t \rightarrow \nu t$ , such that space and time have the same dimension  $[x] = [t]$  and the inverse propagator<sup>33</sup>  $G_0^{-1}$  of the relative mode reads:

$$G_0^{-1} = -\frac{1}{\pi} \begin{pmatrix} i\frac{1}{\pi} 2\frac{\gamma_M}{\nu} \partial_x^2 & \partial_t^2 - \partial_x^2 \\ \partial_t^2 - \partial_x^2 & i\frac{1}{\pi} 2\frac{(\gamma_M + \gamma_B)}{\nu} \partial_x^2 \end{pmatrix}. \quad (4.138)$$

The corresponding action describes a Gaussian fixed point theory under the RG under the symmetric rescaling (note that the fields themselves are dimensionless  $[\phi] = 1$ ):

$$\begin{aligned} x & \rightarrow \tilde{x} = x/b, & k & \rightarrow \tilde{k} = kb, \\ t & \rightarrow \tilde{t} = t/b, & \omega & \rightarrow \tilde{\omega} = \omega/b. \end{aligned} \quad (4.139)$$

In line with the scale free nature of the Green's function, the equal-time correlation functions are algebraic and read in Fourier space ( $a, b \in \{c, q\}$ ):

$$\langle \phi_{a,(0,k)}, \phi_{b,(0,-k)} \rangle = \chi_{ab} \frac{\alpha_{ab}}{|k|}, \quad \chi_{ab} = \begin{cases} 1 & a = b \\ -i & a \neq b \end{cases}. \quad (4.140)$$

<sup>33</sup>Related to the action  $S_0^{(r)} = \frac{1}{2} \int \frac{d^2 Q}{(2\pi)^2} \Psi_Q^T G_0^{-1} \Psi_Q$ .

The prefactor  $\alpha_{ab}$  defined in (4.142). This scaling behavior is in line with the earlier result based on the (exact) analysis (see again Eq. (4.69)). The correlation function

$$C_y \sim \langle \partial_x \phi_x \partial_x \phi_{x+y} \rangle \rightarrow C_k \sim k^2 \langle \phi_{(0,k)} \phi_{(0,-k)} \rangle \sim |k| \quad (4.141)$$

reproduces the exact scaling behavior in the absence of a mass scale<sup>34</sup>. The coefficients of the expression above are given by

$$\begin{pmatrix} \alpha_{cc} \\ \alpha_{qq} \\ \alpha_{cq} \end{pmatrix} = \begin{pmatrix} \frac{\gamma_M + \gamma_B}{\nu} \\ \frac{\gamma_M}{\nu} \\ \frac{\pi}{2}(1 - |z|^2) \end{pmatrix} \cdot f(z). \quad (4.142)$$

They depend on the pole of the propagator  $\omega_{\text{Pol}}(k) = \pm z|k|, \pm z^*|k|$  (extracted from (4.138) in Fourier space) and the function  $f(z)$ :

$$z^2 = 1 + i \frac{2}{\pi} \sqrt{\frac{\gamma_M(\gamma_M + \gamma_B)}{\nu^2}}, \quad f(z) = i \frac{1}{|z|^2(z - z^*)}. \quad (4.143)$$

#### 4.8.1 Momentum Shell RG– Part 1: First Order Analysis

To derive the effective theory at long distances, we integrate out (or trace out) the short distance degrees of freedom. To this end, each field is separated into short (<) and long (>) distance modes relative to the momentum cutoff  $\Lambda \sim \frac{1}{a}$ . The separation reads  $\phi_X = \phi_X^> + \phi_X^<$  with:

$$\phi_X^> = \int_{|k| < \Lambda/b} \frac{dk}{2\pi} \int_{-\infty}^{\infty} \frac{d\omega}{2\pi} \phi_Q e^{i\vec{Q}\vec{X}}, \quad \phi_X^< = \int_{|k| > \Lambda/b} \frac{dk}{2\pi} \int_{-\infty}^{\infty} \frac{d\omega}{2\pi} \phi_Q e^{i\vec{Q}\vec{X}}.$$

As a reminder: The three conceptual steps of the RG are

1. **Integrate out the short distance modes**, here the modes with  $|k| \in [\Lambda/b, \Lambda]$ , in the spirit of a partial trace  $\rho_{>}^{(r)} = \text{tr}_{<}[\rho^{(r)}]$ .
2. **Rescale the length scales** to regain the same resolution (which makes the coarse-grained theory comparable to the initial one).
3. **Renormalize the fields** such that, e.g., the leading kinetic term stays invariant.

In summary, the action is transformed as  $S[\phi, \{g_i\}] \rightarrow S[\phi^{(b)}, \{g_i^{(b)}\}]$  with renormalized couplings  $\{g_i^{(b)}\}$ . For  $b \rightarrow 0$ , we can derive *flow equations* for the couplings.

In practice and similar to the separation of the relative and absolute mode, we split the action into three contributions:

$$S[\phi^{(r)}] = S_r^{(0)}[\phi_{<}^{(r)}] + S_r^{(0)}[\phi_{>}^{(r)}] + \Delta S^{(r)}[\phi_{<}^{(r)}, \phi_{>}^{(r)}] := S_0^> + S_0^< + \Delta S. \quad (4.144)$$

<sup>34</sup>Here, we assume that operator expectation values  $\langle \phi_x \phi_y \rangle$  correspond to the leading contribution of field versions:  $\langle \phi_{c,(0,x)} \phi_{c,(0,y)} \rangle$  or  $\langle \phi_{q,(0,x)} \phi_{q,(0,y)} \rangle$ . Therefore, we left out the index intentionally.

The last term describes the coupling between the different fields, which we treat perturbatively. We use the same scheme as before in (4.134) and (4.136), such that the action reads<sup>35</sup>

$$S[\phi_{>}] \approx S_0^> + \langle \Delta S \rangle_{<} + \frac{i}{2} (\langle \Delta S^2 \rangle_{<} - \langle \Delta S \rangle_{<}^2). \quad (4.145)$$

The expectation values  $\langle \phi_a^<(X) \phi_b^<(X) \rangle_{<}$  are obtained by integrating over  $|k| \in [\Lambda/b, \Lambda]$ :

$$\begin{aligned} \langle \phi_{a,X}^< \phi_{b,X}^< \rangle_{<} &:= \int_{\Lambda/b < |k| < \Lambda} \frac{dk}{2\pi} \langle \phi_{a,(t,-k)} \phi_{b,(t,k)} \rangle |_{t=0} \\ &= 2 \int_{\Lambda/b}^{\Lambda} \frac{dk}{2\pi} \frac{\alpha_{ab}}{k} = \chi_{ab} \frac{\alpha_{ab}}{\pi} \log(b). \end{aligned} \quad (4.146)$$

The factor of 2 originates from the two  $k$ -regimes around  $-\Lambda/b$  and  $\Lambda/b$ . At first order, we have to evaluate  $\langle \Delta S \rangle_{<}$ . It gives rise to four additional terms in the action according to the four terms in (4.137). In the following, we demonstrate the RG procedure for a single term in  $\langle \Delta S \rangle_{<}$ .

**Integrate out:** We consider the  $\lambda_c$  term in (4.137):

$$\lambda_c \int d^2 X \langle \cos(4(\phi_{c,X}^> + \phi_{c,X}^<)) \rangle_{<} = \lambda_c \int d^2 X \cos(4\phi_{c,X}^>) e^{-8\langle (\phi_{c,X}^<)^2 \rangle_{<}}. \quad (4.147)$$

The correlator appearing in the expression is evaluated according to (4.146).

**Rescale:** To regain the same momentum resolution, the next step in the RG is the rescaling step. Since we are expanding around the space time symmetric action, we rescale space and time symmetrically according to (4.139). This gives rise to an overall contribution

$$\underbrace{\lambda_c b^{2 - \frac{8}{\pi} \alpha_{cc}}}_{=:\lambda_c(b)} \int d^2 X \cos(4\phi_{c,X}^>). \quad (4.148)$$

Rewriting the factor  $b = e^s$  with  $s \ll 1$ , we finally get the flow equation

$$\partial_s \lambda_c \approx \left( 2 - \frac{8}{\pi} \alpha_{cc} \right) \lambda_c. \quad (4.149)$$

**Renormalize:** The kinetic part of the action is unchanged at this order, therefore no further rescaling of the field is performed.

As anticipated, the flow of  $\lambda_c$  is a threshold phenomenon: only once  $\alpha_{cc}$  is small enough,  $\lambda_c$  will grow. Repeating similar steps for all interaction terms

<sup>35</sup>  $\langle \mathcal{O} \rangle_{<} := \int \mathcal{D}[\phi^<] \mathcal{O} e^{iS_0^<}$ .

(couplings:  $\lambda_c, \lambda_q, \lambda_{cq}^{(c)}, \lambda_{cq}^{(s)}$ ) gives rise to the set of first order flow equations:

$$\begin{aligned}\partial_s \lambda_c &\approx \left(2 - \frac{8}{\pi} \alpha_{cc}\right) \lambda_c, & \partial_s \lambda_{cq}^{(c)} &\approx \left(2 - \frac{2}{\pi} (\alpha_{cc} + \alpha_{qq})\right) \lambda_{cq}^{(c)} - \frac{4}{\pi} \alpha_{cq} \lambda_{cq}^{(s)}, \\ \partial_s \lambda_q &\approx \left(2 - \frac{8}{\pi} \alpha_{qq}\right) \lambda_q, & \partial_s \lambda_{cq}^{(s)} &\approx \left(2 - \frac{2}{\pi} (\alpha_{cc} + \alpha_{cq})\right) \lambda_{cq}^{(s)} + \frac{4}{\pi} \alpha_{cq} \lambda_{cq}^{(c)}.\end{aligned}$$

Making use of the ‘intra contour’ couplings  $\lambda_{\pm} = (\lambda_{cq}^{(c)} \pm i \lambda_{cq}^{(s)})/2$ , we can rewrite:

$$\begin{aligned}\partial_s \lambda_+ &\approx \left(2 - \frac{2}{\pi} (\alpha_{cc} + \alpha_{qq}) + i \frac{4}{\pi} \alpha_{cq}\right) \lambda_+, \\ \partial_s \lambda_- &\approx \left(2 - \frac{2}{\pi} (\alpha_{cc} + \alpha_{qq}) - i \frac{4}{\pi} \alpha_{cq}\right) \lambda_-. \end{aligned} \tag{4.150}$$

Therefore, all flow equations have a similar structure to the first order BKT flow equations [70, 205, 242]. The important features of these flow equations are:

- In the absence of a bath ( $\gamma_B = 0$ ), the intact additional symmetry:  $\phi_c \leftrightarrow \phi_q$  enforces  $\alpha_{cc} = \alpha_{qq}$  and therefore  $\lambda_c(s) = \lambda_q(s)$ . Consequently, the  $\lambda_{cq}$ ’s are always more relevant or become relevant earlier compared to  $\lambda_c, \lambda_q$ . This leads to a reduction of complexity, since the interactions  $\lambda_c, \lambda_q$  can be neglected.
- In the presence of a bath, the coefficients  $\alpha_{cc}$  and  $\alpha_{qq}$  deviate from each other (see (4.142)). Once  $\gamma_B \geq 2\gamma_M$ ,  $\lambda_q$  can become more relevant than the  $\lambda_{cq}$ ’s. This opens the possibility of a new phase, only realizable for the interplay of measurements and dephasing.
- In the limiting case  $\gamma_B = 0$  and  $\gamma_M/\nu \rightarrow 0$ , the couplings  $\lambda_{cq}$  become marginal, in accord with the limit of free fermions at half filling [70]. This is reasonable since the model reduces to the unitary fermionic hopping model in this limit.

Once any of the interactions becomes relevant, their RG flow is unbounded and does not reach another fixed point. Nevertheless, we can interpret the cosine interaction terms as generating an effective mass scale. Once, e.g.<sup>36</sup>,  $|\lambda_q/m^2| \gg 1$ , the term  $\lambda_q \cos(4\phi_{q,X})$  in the action confines  $\phi_{q,X}$  to one of the extrema, say  $\phi_{q,X} = 0$ . Approximating the term to second order<sup>37</sup> results in an effective mass term

$$\text{strong coupling limit:} \quad \lambda_q \cos(4\phi_{q,X}) \xrightarrow{\sim} -8\lambda_q \phi_{q,X}^2 + \text{const..}$$

Therefore, we roughly identify a phase diagram with three different phases shown in Fig. 4.15(c) and summarized in Tab. 4.4.

The novel ingredient is phase ( $C_D$ ) with the mass term  $m_D$ : similar to pure dephasing, it only affects the  $qq$ -sector of the action. In contrast to dephasing, it has no momentum dependence and is reminiscent of a finite temperature

<sup>36</sup> $m$  is the prefactor stemming from the regularization in the bosonization procedure.

<sup>37</sup>There are also other excitations like solitons, connecting different minima, but we will not cover them here (see Appendix E in Ref. [205]).

phase	relevant coupling	interaction	eff. quad. theory
(C)	no coupling relevant	-	$G_0^{-1}$
(M)	$\lambda'_{cq}s$ are relevant	$\cos(2\phi_c)\cos(2\phi_q)$	$G_0^{-1} + m_{M_r}\sigma_x + im_{M_i}\mathbb{1}$
(C <sub>D</sub> )	$\lambda_q$ becomes relevant	$\cos(4\phi_q)$	$G_0^{-1} + im_D(\mathbb{1} - \sigma_z)$

**Table 4.4:** Overview of the different qualitative phases from first order perturbation theory.

term  $\sim T\phi_{q,X}^2$  (in the limit, where the temperature is the dominant scale in the model). In both cases, the term leads to a suppression of the fluctuations between  $\phi_+$  and  $\phi_-$ . This affects the non-diagonal terms in the density matrix in the  $\phi$ -basis. A major difference to a single replica equilibrium scenario is the existence of a finite entry in the  $cc$ -sector (which is ruled out in the common Keldysh theory, reflecting causality [4, 69]). This entry induces a pole structure of the form:

$$\lim_{k \rightarrow 0} \omega_{\text{Pol}}(k) \sim \begin{cases} \text{const.}, \\ \pm|k| \end{cases} \Rightarrow C_y \sim |y|^{-2}. \quad (4.151)$$

Therefore, the leading behavior of the correlation functions stays the same compared to phase (C) (in the absence of  $m_D$ ). Switching from the effective bosonic description to the fermionic description, we interpret this dephasing scenario as confining  $\rho^{(2R)}$  onto its diagonal elements (in the occupation number basis). However, the interplay with the scrambling and measurement dynamics supports diffusional dynamics onto the diagonal, giving rise to a scaling behavior. We will consider this limit from the *fermionic* perspective in more detail in Sec. 4.10.

**Remark:** The phase boundary obtained at first order has to be considered with care. As an example: for  $\gamma_B = 0$ , the Gaussian fixed point is always unstable towards the non-linear perturbation (see Fig. 4.15(c)). We have to include at least the second order corrections to get a more trustworthy prediction of the phases. The technical reason is that only at second order, the quadratic parts (derivative terms) of the theory are renormalized as well.

### 4.8.2 Momentum Shell RG– Part 2: Second Order Analysis

At second order in perturbation theory, the derivative terms in the quadratic part of the theory are renormalized (and generated) as well. Therefore, we make use of a more flexible parametrization:

$$G_0^{-1} = \begin{pmatrix} i(\eta_{qq}^2 k^2 - \epsilon_{qq}^2 \omega^2) & \epsilon_{cq}^2 \omega^2 - \eta_{cq}^2 k^2 \\ \epsilon_{cq}^2 \omega^2 - \eta_{cq}^2 k^2 & i(\eta_{cc}^2 k^2 - \epsilon_{cc}^2 \omega^2) \end{pmatrix}. \quad (4.152)$$

All derivative couplings  $\epsilon_{ab}$  and  $\eta_{ab}$  will be renormalized, fed by the flow of the interaction couplings  $\lambda$ . Formally, this leads to a set of approximate flow equations for the six derivative couplings and four interaction couplings (neglecting less relevant contributions generated at second order). We give the explicit

expressions and full derivation in App. I and discuss the implications in the following. The tentative phase diagram<sup>38</sup>, extracted by tracking the most strongly growing couplings, is shown in Fig. 4.15 with exemplary  $s$ -resolved flows.

**Gaussian fixed point:** First of all, there is a stable, extended phase ( $C$ ), described by a Gaussian fixed point in the RG. Here, all interaction terms are irrelevant at large scales, indicating the stability of the Gaussian fixed point.

**Phase ( $M$ ):** For  $\gamma_B = 0$ , the transition towards an interaction dominated regime ( $M$ ) takes place at a finite value of  $\gamma_M/\nu$ . In this regime, the couplings  $\lambda_{cq}$ 's are most dominant, but all  $\lambda$ 's are growing. For finite  $\gamma_B/\nu < 1.5$ , the transition point is shifted towards smaller  $\gamma_M/\nu$  as expected (though beyond  $\gamma_M/\nu, \gamma_B/\nu \sim 1$  the analysis becomes questionable)<sup>39</sup>. This behavior supports the idea that strong dephasing *enhances* the measurement-induced pinning onto number eigenstates (by suppressing the scrambling dynamics). The corresponding interaction terms can be interpreted as generating an effective mass scale  $m_M$ :  $G^{-1} = G_0^{-1} + m_{M_r}\sigma_x + im_{M_i}\mathbb{1}$ , inducing a finite length scale and exponentially decaying correlations with

$$\lim_{k \rightarrow 0} \omega_{\text{Pol}}(k) = \text{const.} \quad .$$

**Phase ( $C_D$ ):** The left half of the phase diagram, on top of phase ( $C$ ), is dominated by phase ( $C_D$ ). It is characterized by either  $\lambda_c$  or  $\lambda_q$  being most relevant (with the other couplings remaining small). Therefore, in contrast to phase ( $M$ ), only a *single* interaction term is growing in magnitude, generating a mass term of the form  $i(1 \pm \sigma_z)m_D$ . As already mentioned before, the evolution of  $\rho^{(r)}$  is not of Lindblad type (e.g. there is a finite entry in the  $cc$ -sector) and the clear physical distinction between  $\phi_c$  and  $\phi_q$  is not given. Accordingly, we interpret the growth of either  $\lambda_c$  or  $\lambda_q$  as belonging to the same physical scenario.

**Summary:** The overall scenario is qualitatively in line with the findings of the quantum trajectory simulations for small systems. However, the precise form and position of the phase boundary are varying (compared to a complementary numerical analysis of larger systems in Sec. 4.9). To recapitulate, the derivation of these second order flow equations is based on two major approximations: (i) Integrating out the absolute mode perturbatively and (ii) treating the interactions in  $S^{(r)}$  perturbatively. The second approximation is controlled for  $|\lambda/m^2| \ll 1$ , a condition that depends on the initial couplings provided by the approximation in (i). Due to the perturbative treatment of the absolute-relative coupling, the initial couplings  $\lambda$  are also perturbative in  $\gamma_M/\nu, \gamma_B/\nu$ . This restricts the predictive power of the perturbative RG to  $\gamma_M/\nu, \gamma_B/\nu \ll 1$ .

**Remark (1):** An additional feature of the RG flow equations is the possibility that the complex poles (encode in  $z$ ) of the propagator also flow (on contrast to the case with  $\gamma_B = 0$  [19]). In the regions with larger  $\gamma_B/\nu$ , this additional flow results in a breakdown of the RG flow due to the poles wandering onto the real axis (such that the correlator is not well defined anymore). Real poles also emerge in the presence of pure dephasing, where they indicate the divergence of

<sup>38</sup>With the initial conditions given in (1.5).

<sup>39</sup>In this regime, all interaction couplings are growing, therefore we also interpret the spot around  $\gamma_M/\nu \approx 0.55$  as part of the this regime.

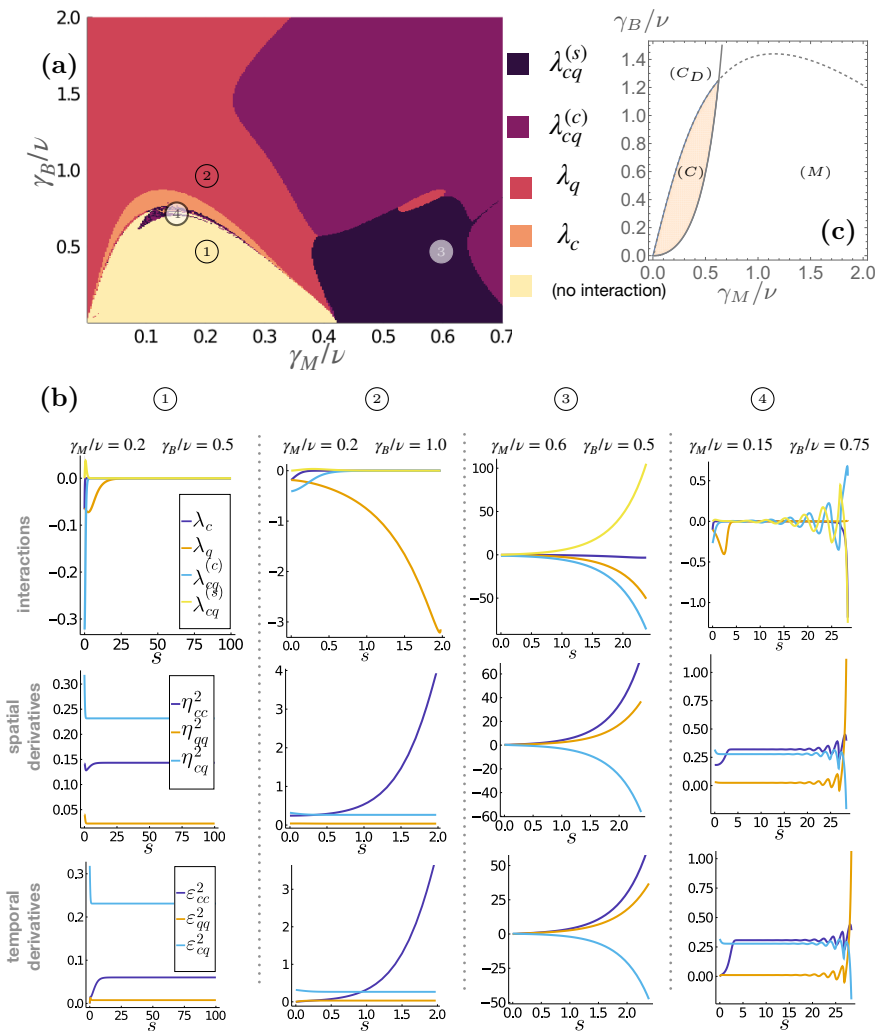


**Figure 4.15:** (a) Phase diagram from solving the second order RG flow equations up to  $s = s_f$ , Eq. (I.34), indicating, whether some coupling (brighter colors) or no coupling (light orange) becomes relevant (see App. I.8 for more details). (b) Examples of the resolved flows with case (1): no interaction becomes relevant, corresponding to (C); case (2): only  $\lambda_q$  grows significantly, indicating (C<sub>D</sub>) (the flow breaks down at some  $s < s_f$ , where real poles in the propagator emerge); case (3): multiple couplings are growing in magnitude, corresponding to (M); case (4): blurred, oscillatory regime on top of (C). If the flow breaks down early, the most relevant coupling is estimated from the largest (absolute) change  $|\dot{\lambda}(s)|$ . (c) First order phase diagram: the orange region corresponds to no relevant interaction, in (C<sub>D</sub>) only  $\lambda_q$  is relevant and in (M) only  $\lambda_{cq}$ 's are relevant. In the upper right corner, multiple interactions are relevant.

$\phi$  fluctuations (as discussed in, e.g., Ref. [243]). They herald a strongly mixed, infinite temperature state. Comparing this scenario to the RG flow, it is not a priori clear whether the emergence of real poles corresponds to (i) a physical meaningful (heating) behavior or (ii) is an indicator that higher order terms are needed in the RG to compensate this effect (a formidable task though).

**Remark (2):** The blurred region above phase (C) can be associated with another numerical instability. During the flow in this region, the interaction couplings become very small at some scale, in line with asymptotically vanishing values. However, for sufficiently long integration times, the near-vanishing couplings start to grow again and result in an oscillatory behavior (Fig. 4.15(b)-4).

#### Box 25: Symmetric case

In the limiting case  $\gamma_B = 0$ , the  $\pm$ -contours decouple<sup>a</sup>. At the quadratic level, this is the effect of the additional symmetry (see again (4.106)). Including interactions, it is not a priori obvious that no contour couplings are generated or become relevant (like  $\cos(2\sqrt{2}\phi_{+,X})\cos(2\sqrt{2}\phi_{-,X})$  related to  $\cos(4\phi_{c,X}), \cos(4\phi_{q,X})$ ). Nevertheless, the first order equations already indicate that these interactions are always less relevant than  $\cos(2\sqrt{2}\phi_{\pm,X})$ , which preserve the decoupling. This in turn supports the evolution into a (pure) dark state and the flow equations can be massively simplified (less couplings; reduction to a single contour; no flow of the poles) and we only need to track the flow of the interaction  $\lambda_+$  and the derivative couplings  $\epsilon_+$  and  $\eta_+$ . We can also interpret this as reducing the problem to a Feynman path integral for the state

$$|\psi^{(r)}(t)\rangle = e^{-i\mathbf{H}_{\text{eff}}t}|\psi_0^{(r)}\rangle,$$

turning the necessity of two Keldysh contours obsolete. By introducing the effective derivative coupling<sup>b</sup>  $K_+ := \frac{i\epsilon_+\eta_+}{\alpha_+}$ , they reduce to two equations of BKT type:

$$\partial_s \lambda_+ = \left(2 - \frac{2}{\pi} \frac{1}{K_+}\right) \lambda_+, \quad \partial_s K_+^2 = 64\lambda_+^2 A_2, \quad (4.153)$$

see App. I.6 for more details. In contrast to the equilibrium case, the couplings are complex [19]. Therefore, the interaction coupling will become less relevant at second order (for  $\gamma_M/\nu \ll 1$ ), stabilizing the Gaussian fixed point. This is comparable to a sine-Gordon model with *imaginary* couplings [244] (see also Ref. [19] for an extended discussion).

<sup>a</sup>Up to a possible regularization, as also present in the Keldysh scenario [69] due to initial conditions and the closing of the contours at final time  $t_f$ .

<sup>b</sup>With  $\alpha_\sigma := \text{sgn}(\text{Im}(\eta_\sigma/\epsilon_\sigma))$ .

In the following, we pair this long distance, analytical perspective with a numerical investigation based on quantum trajectories. As a physical reminder: we can think of the dynamics under consideration as coupling each lattice site at each time step to *two* ancillary qubits. One of them is measured and we keep

track of the record (measurement-induced dynamics) and the other one is left entangled with the system and has to be traced out (bath dynamics).

## 4.9 Fermionic numerical Investigation: Ensemble of Quantum Trajectories

In the presence of measurements and unitary evolution, an initially pure state  $\rho^{(c)}$  stays pure. Furthermore, unitary hopping as well as measuring the local particle number leave a Gaussian state Gaussian. Therefore, the states can be described efficiently, e.g., in terms of a  $L \times N$  matrix  $U$  and the correlation matrix  $D = UU^\dagger$  (see App. A.2)[17, 18, 176, 178, 188, 198, 199]. For those states, correlation functions and, e.g., the entanglement entropy can be efficiently calculated from the correlation matrix [17]. In the presence of an additional bath, each  $\rho^{(c)}$  will inevitably involve into a mixed state. Nonetheless, for suitable initial conditions, they can be written as an *ensemble* of Gaussian states:

$$\rho_t^{(c)} = \sum_{\alpha} p_{\alpha}(t) |\psi_t^{(\alpha)}\rangle \langle \psi_t^{(\alpha)}|, \quad \sum_{\alpha} p_{\alpha}(t) = 1.$$

Here, the members  $|\psi_t^{(\alpha)}\rangle$  are not necessarily mutually orthogonal. In the following, we derive the approximate evolution of such a state and discuss the advantages and disadvantages of this approach. One advantage of this representation is that a sum of Gaussian states still gives access to quantities like

$$\left( \text{tr} \left[ \mathcal{O} \rho^{(c)} \right] \right)^2 = \left( \sum_{\alpha} p_{\alpha} \langle \mathcal{O} \rangle_{\alpha} \right)^2, \quad \langle \mathcal{O} \rangle_{\alpha} := \langle \psi^{(\alpha)} | \mathcal{O} | \psi^{(\alpha)} \rangle,$$

where  $\langle \mathcal{O} \rangle_{\alpha}$  can be calculated from the correlation matrices  $D_{\alpha}$  of the individual Gaussian states. However, there are two drawbacks: (i) the overall state is not Gaussian anymore, which means that, e.g., the purity or entanglement measures like the entanglement negativity are numerically more expensive to evaluate<sup>40</sup>; (ii) depending on the initial condition,  $\rho^{(c)}$  might involve a huge number of states<sup>41</sup>. From a practical perspective, we have to limit the size of the ensemble to some finite value, which in turn implies that strongly mixed states cannot be (reliably) represented in this approach.

**Technical derivation:** To derive the time evolution of the ensemble, we follow the approach introduced in Refs. [23, 239]. In Sec. 4.5.2, we have already derived the evolution of (mixed) states  $\rho^{(c)}$  under measurement dynamics. In contrast, the evolution due to a dephasing bath corresponds to the *sum* over the different measurement trajectories  $\rho^{(c)}$  (corresponding to our ignorance about the outcomes):

$$\overline{\rho^{(c)}} = \sum_{\beta} p_{\beta} \cdot \rho_{\beta}^{(c)}. \quad (4.154)$$

<sup>40</sup>To extract the purity, the overlaps  $\langle \psi_t^{(\beta)} | \psi_t^{(\alpha)} \rangle$  between all members need to be calculated.

<sup>41</sup>As an example: if the initial state is the maximally mixed state, we can choose the different members  $|\psi_{t=0}^{(\alpha)}\rangle = |\{n\}_{\alpha}\rangle$  to be the occupation number, forming a basis of the Hilbert space, which has a dimension exponentially large in  $L$ .

This sum runs over all possible sets of measurements outcomes  $\{m_1, m_2, \dots\}$ , labelled by  $\beta$ . However, the full set of possible ‘measurement paths’ will grow exponentially<sup>42</sup>. Therefore, we restrain the sum to a finite number of trajectories<sup>43</sup>  $n_{\text{ens}}$ . Starting from an initially pure state, the individual measurement trajectories  $|\psi_t^{(\alpha)}\rangle$  stay pure and the density matrix  $\overline{\rho_{t+\delta t}^{(c)}}$ , summed over the measurement outcomes, is approximated as:

$$\overline{\rho_{t+\delta t}^{(c)}} \approx \frac{1}{n_{\text{ens}}} \sum_{\alpha=1}^{n_{\text{ens}}} \mathbf{U}_{\alpha} |\psi_t^{(\alpha)}\rangle \langle \psi_t^{(\alpha)}| \mathbf{U}_{\alpha}^{\dagger}, \quad (4.155)$$

$$\mathbf{U}_{\alpha} = \exp \left[ \sum_j \sqrt{\gamma_B} \Delta W_j^{(\alpha)} (\mathbf{n}_j - \langle \mathbf{n}_j \rangle_{\alpha}) - \gamma_B \delta t (\mathbf{n}_j - \langle \mathbf{n}_j \rangle_{\alpha})^2 \right].$$

Each  $\mathbf{U}_{\alpha}$  describes an independent measurement process with  $\overline{\Delta W_j^{(\alpha)} \Delta W_{j'}^{(\alpha')}} = \delta_{\alpha, \alpha'} \delta_{j, j'} \delta t$ . It is important to note that there can be many different measurement protocols that give rise to the *same* dephasing Lindblad dynamics.

**Technical summary:** The infinitesimal evolution of the ensemble of pure states under unitary evolution, measurements and a dephasing bath is given by the direct combination of the individual processes (see also again Eq. (4.64)):

$$\text{measurement : } |\psi\rangle\langle\psi| \rightarrow \mathbf{V}|\psi\rangle\langle\psi|\mathbf{V}^{\dagger},$$

$$\rho_{t+\delta t}^{(c)} \approx \mathbf{V}\rho_t^{(c)}\mathbf{V}^{\dagger},$$

$$\text{bath : } \rho_{t+\delta t}^{(c)} \approx \rho_t^{(c)} - \frac{\gamma_B}{2} \delta t \sum_i [\mathbf{n}_i, [\mathbf{n}_i, \rho]],$$

$$\approx \sum_{\alpha=1}^{n_{\text{ens}}} \mathbf{U}_{\alpha} |\psi^{(\alpha)}\rangle \langle \psi^{(\alpha)}| \mathbf{U}_{\alpha}^{\dagger},$$

$$\text{combination : } \rho^{(c)} \approx \sum_{\alpha=1}^{n_{\text{ens}}} \mathbf{U}_{\alpha} \mathbf{V} |\psi^{(\alpha)}\rangle \langle \psi^{(\alpha)}| \mathbf{V} \mathbf{U}_{\alpha}^{\dagger},$$

$$\approx \sum_{\alpha=1}^{n_{\text{ens}}} p_{\alpha} |\psi_{\alpha}\rangle \langle \psi_{\alpha}|,$$

where  $\mathbf{V}$  describes the read out measurement and the  $\mathbf{U}_{\alpha}$ ’s describe measurements, where the outcome is unknown to us. In summary, the

continued on next page

<sup>42</sup>For a single lattice site it would be  $2^{N_T}$  with  $N_T$  the number of time steps. For a lattice of site  $L$  it is already  $(2^L)^{N_T}$ .

<sup>43</sup>The required number of trajectories depends on observables we like to study. Therefore, whether a reduction of computational complexity is achieved in this approach depends on the observables, see, e.g., Ref. [245].

continued from page before

weights and states in the ensemble get updated according to:

$$\begin{aligned}
 \rho_{t+\delta t}^{(c)} &= \sum_{\alpha} p_{\alpha}(t + \delta t) |\psi_{t+\delta t}^{(\alpha)}\rangle \langle \psi_{t+\delta t}^{(\alpha)}|, \\
 |\psi_{t+\delta t}^{(\alpha)}\rangle &= \frac{e^{-i\mathbf{H}\delta t} \mathbf{V} \mathbf{U}_{\alpha} |\psi_t^{(\alpha)}\rangle}{\sqrt{\langle \psi_t^{(\alpha)} | \mathbf{U}_{\alpha}^{\dagger} \mathbf{V}^2 \mathbf{U}_{\alpha} | \psi_t^{(\alpha)} \rangle}}, \\
 p_{\alpha}(t + \delta t) &= p_{\alpha}(t) \langle \psi_t^{(\alpha)} | \mathbf{U}_{\alpha}^{\dagger} \mathbf{V}^2 \mathbf{U}_{\alpha} | \psi_t^{(\alpha)} \rangle.
 \end{aligned}
 \tag{4.156}$$

The interplay of unitary evolution, measurements and dephasing in terms of the ensemble description is sketched in Fig. 4.16. Measurements tend to purify the ensemble onto a single member, which itself will wander around in the Hilbert space due to the unitary part. Dephasing instead leads to an ensemble of diverse states. Dephasing instead leads to an ensemble of diverse states.

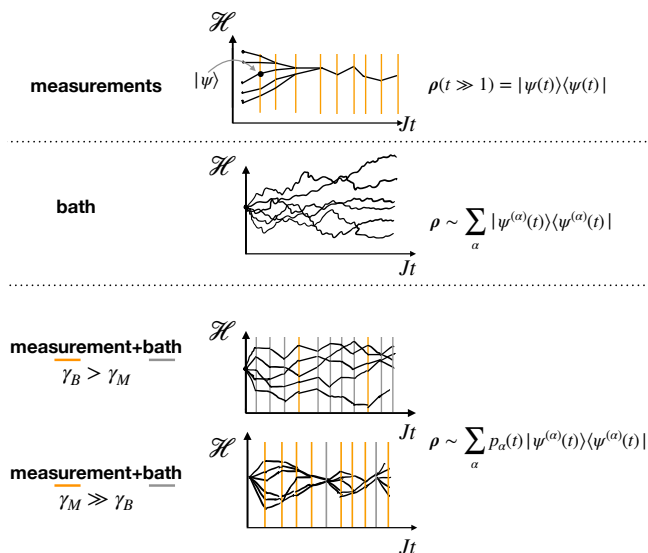


**Figure 4.16:** Sketch of different scenarios in the ensemble approach, where points correspond to states in the Hilbert space  $\mathcal{H}$  (vertical axis): (i) In the presence of measurements (orange lines), even an initially mixed state will purify; (ii) under dephasing (gray lines) the state becomes more mixed and the ensemble consists of many different states; (iii) measurements and dephasing compete and will either keep the states in the ensemble close by (strong measurements) or will lead to a broadening (strong dephasing).

**Remark:** The operators  $\mathbf{V}$  describe a specific, here particle number sensitive, interaction between the system  $\rho^{(c)}$  and the ancillary qubits. Therefore, the form of  $\mathbf{V}$  is fixed by the choice of interactions. The operators  $\mathbf{U}_{\alpha}$  instead describe independent measurement processes for the different ensemble members. The requirement for  $\mathbf{U}_{\alpha}$  is that *summing* over the different measurement

outcomes results in the dephasing bath dynamics. Therefore, a dephasing bath based on Lindblad operators  $L_i = \mathbf{n}_i$  does *not* fix the operators  $U_\alpha$  uniquely. There can be different *unravellings* that give rise to the same dephasing bath dynamics. An alternative measurement process that gives rise to dephasing are measurements where the measurement outcomes are random and state independent. They give rise to a random unitary evolution in the form of:

$$U_\alpha^{(I)} = \exp \left[ i \sum_j \sqrt{\gamma_B} \Delta W_j^{(\alpha)} \mathbf{n}_j \right]. \quad (4.157)$$

Here,  $\overline{\Delta W_j} = 0$  and  $\overline{\Delta W_j \Delta W_{j'}} = \delta_{j,j'} \delta t$ . We make use of this unravelling for the dephasing bath dynamics to avoid an artificial bias towards the measurement-induced phase. In Sec. 4.10.2, we will discuss this alternative measurement scenario in more detail.

### 4.9.1 Quantum Trajectory Picture in the Presence of a Bath

To compare the predictions of the effective bosonic theory with the fermionic model, we use the ensemble of quantum trajectories for system sizes  $L = 128 - 256$  and  $n_{\text{ens}} = 500$  if not stated differently (see also App. A.3). In the ensemble approach, two factors determine the numerical complexity. Firstly, all  $n_{\text{ens}}$  states in the ensemble have to be updated *simultaneously* for each time step. This is necessary since the evolution depends on  $\langle\langle \mathbf{n}_i \rangle\rangle$ , which in turn depends on all ensemble members. Secondly, the simulations have to be repeated  $n_{\text{avg}}$  times to perform a stochastic average of observables. Therefore, the numerical complexity is increased compared to the ‘standard’ quantum trajectory approach used, e.g., to simulate the Lindblad equation<sup>44</sup>. In the following, we focus on *qualitative* features in the different parameter regimes. However, we cannot make definite statements about sharp phase transitions due to the limited system sizes. Accessible quantities are the density-density correlations  $C_l$ , the subsystem parity variance  $P_{|A|}$ , and the distribution of  $\langle \mathbf{n}_i \rangle$ . We identify two different regimes: (i)  $C_l \sim |l|^{-2}$  and  $P_{|A|} \sim |A|^{-K}$  (phase (C), (C<sub>D</sub>)) and (ii) a regime with more strongly decaying correlations and a flattening  $P_{|A|}$  (phase (M)). The numerical method is not well-suited to describe, e.g., the purity, which would require  $n_{\text{ens}} \sim \dim[\mathcal{H}]$  in the worst case. Therefore, we do not attempt to separate phase (C) and (C<sub>D</sub>) in this approach. In the following, we consider the two related scenarios of (i) measurements and a dephasing bath and (ii) imperfect measurements.

**Measurement and bath:** To get a first orientation in the  $(\gamma_M/J, \gamma_B/J)$ -phase diagram, we plot the subsystem parity variance  $P_{|A|}$  for  $|A| = L/2$  in Fig. 4.17(a) on a logarithmic scale. Qualitatively, a bipartition of the phase diagram can be identified with a regime of strongly suppressed subsystem parity variance. However, different phases have to be classified according to the *scaling* of  $P_{|A|}$  with the subsystem size. To complement this analysis, we plot the density-density correlations  $C_l$  as a function of the rescaled length  $L \sin(\pi l/L)/\pi$  (in expectation of a conformal behavior). At  $\gamma_M/J = 0.3$  and  $\gamma_B/J = 0.5$  ( $L \leq 256$ ), the density-density correlations are still approximately decaying as

<sup>44</sup>The numerical cost is at least as high as using  $n_{\text{ens}} \times n_{\text{avg}}$  pure state quantum trajectories.

$C_l \sim |l|^{-2}$ . In contrast, increasing the bath strength to  $\gamma_B/J \gg 1$  indicates a more rapid decay ( $\sim |l|^{-5/2}$  shown as a reference) for  $L = 192$ . Due to the limited system size, we cannot make a definite statement about the long distance behavior of the decay. At these intermediate system sizes, the behavior could indicate (i) an algebraic behavior or (ii) correspond to a transient towards an exponential decay. A qualitative change is supported by the  $\langle \mathbf{n}_i \rangle$  distributions: they change from being unimodal with  $\langle \mathbf{n}_i \rangle \approx 0.5$  in phase (C) towards a (more) bimodal distribution for  $\gamma_B/J \gg 1$  (in line with a more pronounced pinning scenario).

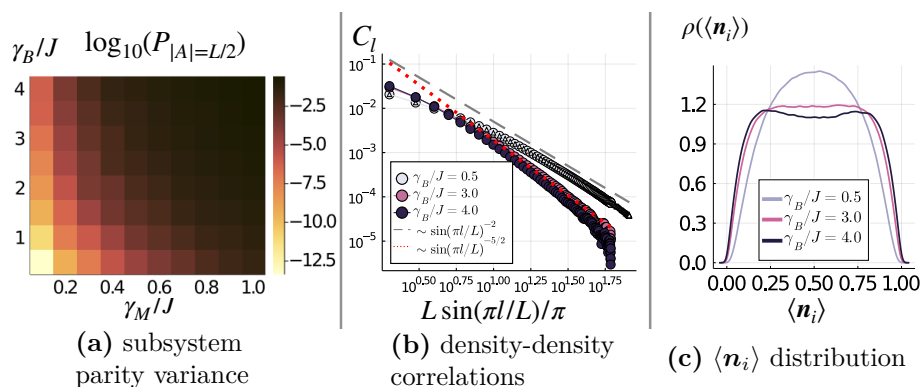


**Figure 4.17:** Quantum trajectory results for measurements and a dephasing bath: (a) half-system parity variance ( $|A| = L/2$ ) for  $L = 128$ ; (b) density-density correlations  $C_l$  (log-log) for different  $\gamma_B/J$  and fixed  $\gamma_M/J = 0.3$  for system sizes  $L = 192$  (and additionally  $L = 256$  (triangles) for  $\gamma_B/J = 0.5$ ). (c) Distribution  $\rho(\langle \mathbf{n}_i \rangle)$  of the local particle number for  $L = 192$ , turning from unimodal ( $\gamma_B/J = 0.5$ ) towards a more bimodal distribution ( $\gamma_B/J = 4.0$ ).

## 4.9.2 Quantum Trajectory Picture in the Presence of imperfect Measurements

As we have mentioned before, the interplay of measurements of the local particle number and dephasing ( $\gamma_M/\nu$  vs.  $\gamma_B/\nu$ ) are directly related to imperfect measurements. In the second case, we only have partial access to the measurement outcomes ( $\gamma$  vs. measurement probability of the ancillas  $\eta$ ). In Fig. 4.18, the numerical results for small and large system sizes are summarized. For  $\gamma/J \sim 1$  and  $\eta \approx 1$ , we observe the measurement-dominated phase. The conditional states are close to number eigenstates with a subsystem parity variance  $P_{|A|}$ , which flattens for large subsystem sizes  $|A| \rightarrow L/2$  (see Fig. 4.18(a')) with  $L = 128, 192$ ). Once  $\eta$  is reduced, a decay of  $P_{|A|}$  becomes notable on larger subsystem sizes, most pronounced for  $\eta = 0.2$  in Fig. 4.18(a'). Complementary, the density-density correlation decays rapidly for  $\eta = 1$ , but approaches  $C_l \sim |l|^{-2}$  for smaller  $\eta$ . This qualitative behavior is again reflected in the  $\langle \mathbf{n}_i \rangle$  distributions, which evolves from a bimodal distribution at  $\eta = 1$  into a distribution with a single peak around  $\langle \mathbf{n}_i \rangle \approx 0.5$  for  $\eta = 0.2$ . To translate this back into the language of  $(\gamma_M, \gamma_B)$ : In the limit  $\eta \rightarrow 0$ , we are approximately

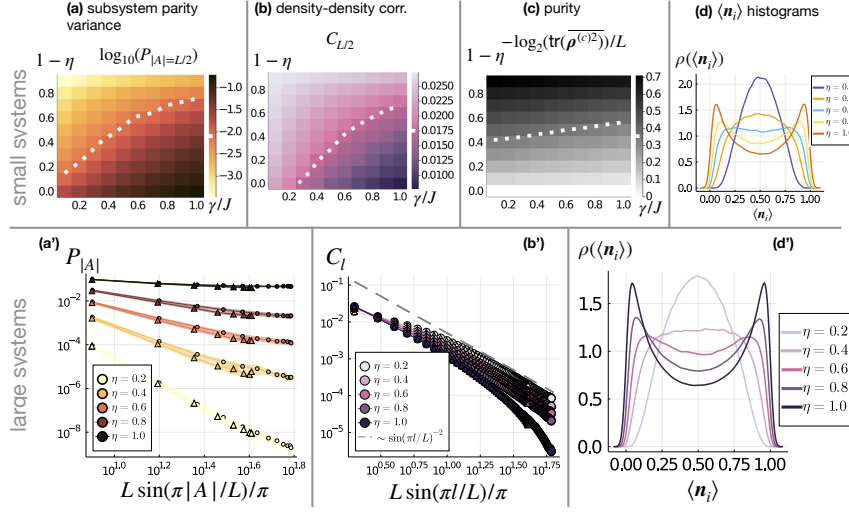


**Figure 4.18:** Overview of the imperfect measurement scenario, described by  $(\gamma, \eta)$ . (top) Solving the master equation for small systems ( $L = 10$ ); (bottom) quantum trajectory approach for  $L = 128, 192$ . (a) Half-system parity variance for  $L = 10$  and (a') subsystem resolved parity variance for  $L = 128, 192$  (triangles, circles) for  $\gamma/J = 1.0$ . (b) Overview of density-density correlations for  $|A| = L/2$  and (b') subsystem resolved for fixed  $\gamma/J = 1.0$  and  $L = 128, 192$  (triangles, circles). (c) Averaged purity of  $\rho^{(c)}$ . (d), (d') Distribution  $\rho(\langle n_i \rangle)$  of the expected local particle number for  $\gamma/J = 1.0$  ( $L = 10$  and  $L = 192$ ).

working at a fixed  $\gamma_B \approx \gamma$ , but reducing  $\gamma_M \rightarrow 0$ . Therefore, by reducing  $\eta$ , we are entering the phase (C) or ( $C_D$ ).

## 4.10 Outlook: Effective (fermionic) Descriptions

In the last sections, we used three different approaches to study the interplay of unitary evolution, measurements and dephasing: (i) numerically exact solution for small systems (fermionic), (ii) long wavelength effective replica theory (bosonic) and (iii) quantum trajectory simulations (fermionic). From these approaches, we extracted indicators for three different regimes (C), ( $C_D$ ) and (M). In the following subsections, we zoom in onto phase ( $C_D$ ), which is absent in the absence of dephasing. We focus onto the limit  $\gamma_B/J \gg 1$ , where we can treat the fermion dynamics perturbatively. We argue that (i) an effective description of the dynamics in the dephasing-free subspace can be found, and (ii) depending on the observables, a reduction to a simplified Gaussian model is plausible.

### 4.10.1 Dynamics in the dephasing-free Subspace

The novel aspect of the fermionic measurement dynamics *in the presence of a bath* is the predicted regime ( $C_D$ ) (featuring algebraic correlations, while  $\rho^{(c)}$

is strongly mixed/dephased). The guiding idea is that the strong ( $\gamma_B/J \gg 1$ ) dephasing Lindblad dynamics suppresses the off-diagonal contributions in the density matrix  $\rho^{(c)}$  (in the occupation number basis). Therefore, the remaining dynamics can be effectively described as taking place on the diagonal (the dephasing-free subspace). We make this point more precise by performing a perturbative analysis<sup>45</sup>, starting from the evolution operator for the conditional density matrix:

$$\partial_t \rho^{(c)} = \underbrace{\mathcal{L}_H[\rho^{(c)}]}_{\text{unitary}} + \underbrace{\mathcal{L}'_M[\rho^{(c)}]}_{\text{stochastic}} + \underbrace{\eta \mathcal{L}_B[\rho^{(c)}]}_{\text{Lindblad}}, \quad \eta := \frac{\gamma_M + \gamma_B}{J}. \quad (4.158)$$

Here,  $\mathcal{L}'_M[\rho^{(c)}]$  describes the *stochastic*, non-linear part of the evolution and  $\mathcal{L}_B[\rho^{(c)}]$  collects all Lindblad-type contributions. In the following, we consider the limit  $\eta \gg 1$ , corresponding to strong dephasing. The non-trivial dynamics is therefore confined to the dephasing-free subspace, here the diagonal elements of the density matrix. Therefore, we split  $\rho^{(c)}$  into a diagonal part  $\rho_{\parallel}^{(c)}$  and an off-diagonal part  $\rho_{\perp}^{(c)}$ . With the perturbative ansatz of the form  $\rho^{(c)} = \rho_0^{(c)} + \eta^{-1} \rho_1^{(c)} + \eta^{-2} \rho_2^{(c)} + \dots$ , we can find the perturbative dynamics on this subspace [182]. As a second order effect, the Hamiltonian part induces an effective diffusion on the diagonal of order  $\eta^{-1}$  (see App. G):

$$\partial_t \rho_{\parallel}^{(c)} \stackrel{\eta \gg 1}{\approx} \frac{\gamma_M}{J} \sum_l dW_l \{ \mathbf{n}_l - \langle \mathbf{n}_l \rangle, \rho_{\parallel}^{(c)} \} + 2\eta^{-1} \left( \mathcal{L}_1[\rho_{\parallel}^{(c)}] + \mathcal{L}_2[\rho_{\parallel}^{(c)}] \right). \quad (4.159)$$

The dynamics is composed of two parts: (i) a measurement-induced stochastic part and (ii) two Lindblad operators describing incoherent hopping:

$$\mathcal{L}_j[\rho] := \sum_l \mathbf{L}_l^{(j)} \rho (\mathbf{L}_l^{(j)})^\dagger - \frac{1}{2} \{ (\mathbf{L}_l^{(j)})^\dagger \mathbf{L}_l^{(j)}, \rho \} \quad \begin{cases} \mathbf{L}_l^{(1)} := \mathbf{c}_{l+1}^\dagger \mathbf{c}_l, \\ \mathbf{L}_l^{(2)} := \mathbf{c}_l^\dagger \mathbf{c}_{l+1}. \end{cases}$$

These Lindblad parts are a quantum analog of a simple symmetric exclusion process (SSEP) [181]. They lead to an (undirected) diffusion of, e.g., the occupation number as we have seen before:

$$\text{only Lindblad evolution:} \quad \partial_t \mathbf{n}_m = 2\eta^{-1} \underbrace{(\mathbf{n}_{m-1} - 2\mathbf{n}_m + \mathbf{n}_{m+1})}_{=: \Delta_x \mathbf{n}_m}. \quad (4.160)$$

Including the measurement-induced dynamics, the expectation values evolve as

$$\partial_t \langle \mathbf{n}_m \rangle = \frac{2\gamma_M}{J} \sum_l dW_l (\langle \mathbf{n}_m \mathbf{n}_l \rangle - \langle \mathbf{n}_m \rangle \langle \mathbf{n}_l \rangle) + 2\eta^{-1} \Delta_x \langle \mathbf{n}_m \rangle, \quad (4.161)$$

being part of a hierarchy of equations. The diffusion due to the Lindblad operators, controlled by  $\eta^{-1}$ , is strongly suppressed if either  $\gamma_B/J \gg 1$  and/or  $\gamma_M/J \gg 1$ . For  $\gamma_B \neq 0$ , this opens the possibility to suppress  $\eta^{-1}$  *without* requiring  $\gamma_M/J \gg 1$ . Therefore, a competition of the terms in (4.159) becomes possible. For very weak measurements  $\gamma_M/J \ll \eta^{-1}$ , the dynamics is dominated by the diffusion, being randomly stirred by the stochastic term. For

<sup>45</sup>See also Ref. [164] in the measurement context and Refs. [180–182, 221–223] in the Lindblad/random unitary context.

strong measurements, the stochastic term tends to pin the states to number eigenstates. An open question is whether the above model can indeed describe a phase transition.

**Summary:** In the perturbative regime  $\eta \gg 1$ , we get diffusional dynamics competing with the pinning dynamics of the measurements. For  $\gamma_M/J \ll \eta^{-1}$ , we still expect the diffusional dynamics to be relevant up to

$$\frac{\gamma_B^*}{J} \gamma_M/J \ll 1 \left( \frac{\gamma_M}{J} \right)^{-1}. \quad (4.162)$$

For  $\gamma_B \gg \gamma_B^*$ , regime ( $M$ ) is expected. Such a behavior of  $\gamma_B^*$  is qualitatively in line with the numerical findings, see again Fig. 4.17(a).

### 4.10.2 Random Unitary Evolution as a Proxy for a Bath

A numerical challenge in the presence of a dephasing bath is the loss of the Gaussian nature of the density matrix  $\rho^{(c)}$ . For this reason, we made use of an ensemble of Gaussian states to approximate  $\rho^{(c)}$ . In the ensemble approach, the bath dynamics is described by summing up a set of trajectories (unravelling), corresponding to an unknown set of measurement outcomes. The unravelling is not unique and we used a *random unitary unravelling*, which we will discuss in more detail in the following. The guiding question for this section is: (1) To what extent does a single member of the ensemble entails properties of the full ensemble? Related to that: (2) Is there an approximation or a substitute for the bath dynamics in terms of a Gaussian evolution? The answer to both questions is a tentative yes, but with a restriction onto a class of observables that only depend on  $\mathbf{n}_i$ .

**Random unitary evolution:** The *random unitary unravelling* is based on an alternative measurement protocol, which bears the same resemblance of the dephasing bath dynamics. Starting point is again the coupling of a single fermionic lattice site to an ancilla qubit as in Sec. 4.2. The ancilla is prepared in the initial state  $|a\rangle = |0\rangle$ , but is measured in the  $x$ -basis [21]. The corresponding operators describing the state evolution are (see again Ref. [21]):

$$\mathbf{M}_+^{(j)} = \frac{1}{\sqrt{2}} [(\mathbb{1} - \mathbf{n}_j) + e^{-i\theta} \mathbf{n}_j], \quad \mathbf{M}_-^{(j)} = \frac{1}{\sqrt{2}} [(\mathbb{1} - \mathbf{n}_j) + e^{i\theta} \mathbf{n}_j]. \quad (4.163)$$

Both operators  $\mathbf{M}_\alpha^{(j)}$  have the property  $\mathbf{M}_\alpha^\dagger \mathbf{M}_\alpha = \frac{1}{2} \mathbb{1}$ . Since the measurement probability is given by  $p_\alpha = \text{tr}[\rho^{(c)} \mathbf{M}_\alpha^\dagger \mathbf{M}_\alpha]$ , both measurement outcomes are equally likely:  $p_0 = p_1 = \frac{1}{2}$ . In contrast to the measurements discussed before, the probabilities are *independent* of the state  $\rho^{(c)}$ . Therefore, we also refer to this as a non-informative measurement. The evolution equation for  $\theta = \sqrt{\gamma_I \delta t}$  follows as:

$$\begin{aligned} |\psi^{(c)'}\rangle - |\psi^{(c)}\rangle &\approx \mp i \sqrt{\gamma_I} \Delta Z_j \mathbf{n}_j |\psi^{(c)}\rangle - \frac{1}{2} \gamma_I \delta t \mathbf{n}_j |\psi^{(c)}\rangle, \\ \Delta Z_j &= \pm \sqrt{\delta t} \quad (\text{with equal probabilities}). \end{aligned} \quad (4.164)$$

Notably, the evolution does not depend on expectation values. Therefore, we can interpret the evolution as stemming from a *random unitary operator* for a

time step  $\delta t$

$$U_j^{(I)} = \exp(i\sqrt{\gamma_I}\Delta Z_j \mathbf{n}_j). \quad (4.165)$$

Comparing this expression with the non-linear measurement operator in (4.64), we can think of the noise in (4.165) as being imaginary. Therefore we use the superscript  $I$ , see App. F for more details. So far, we have used  $U^{(I)}$  as an unravelling of the dephasing bath. In the following, we first analyze the properties of individual trajectories that evolve under  $U^{(I)}$  and  $\exp(-i\mathbf{H}\delta t)$ . Afterwards, we consider the interplay with measurements.

**Properties of the random unitary evolution:** The describe the dephasing Lindblad dynamics with the help of  $U^{(I)}$ , we have to *sum* over the individual trajectories to obtain  $\rho_S$ . However, also individual trajectories display partly similar behavior as the mixed state, as we will consider in the following. Individual trajectories evolve according to:

$$d\rho^{(c)} = -i[\mathbf{H}, \rho^{(c)}]dt - \frac{\gamma_I}{2} \sum_{i=1}^L [\mathbf{n}_i, [\mathbf{n}_i, \rho^{(c)}]]dt + i\sqrt{\gamma_I} \sum_{i=1}^L dZ_i(t) [\mathbf{n}_i, \rho^{(c)}]. \quad (4.166)$$

Notable feature of this evolution in case of pure states are:

- The stationary entanglement entropy follows a volume law:  $\overline{S_{\text{vN}}}(L/2) \sim L$ . The entanglement grows as  $\sim \sqrt{t}$ , analyzed in Ref. [17] (see also Ref. [246]). See also Fig. 4.19(a).
- Density-density correlations  $C_l$  become flat and are of the order of  $\mathcal{O}(L^{-1})$ . For an initial Néel state,  $C_l$  reaches values comparable to an infinite temperature state, see Fig. 4.19(b),(c).
- In the limit  $\gamma_I/J \gg 1$ , the model is equivalent to models studied in, e.g., Refs. [182, 186]. Leading properties are determined by the non-random equilibrium state. However, the coherent evolution gives rise to subleading corrections as was shown in Ref. [182]. The states  $\rho_{t \rightarrow \infty}^{(c)}$  still have structure: since the random unitary evolution is Gaussian, the information about the state is encoded in  $D_{ij}$ . Since the evolution is unitary as well, the quantities  $\text{tr}[D^m]$  with  $m \in \mathbb{N}$  are constant under the evolution (see also the info box below). The stationary properties are determined by these invariant quantities.

In summary, the evolution due to additional random unitary evolution features similarities with the infinite temperature state, but with subleading corrections (see also Ref. [183]).

**Individual ensemble members:** In the context of measurements and dephasing, we can roughly interpret the individual trajectories resulting from  $U^{(I)}$  as single members of the ensemble<sup>46</sup>. In the following, we analyze to what extent we can use quantum trajectories *without* averaging over non-informative

<sup>46</sup>Technically, this is *not* correct in the presence of measurements and a bath: the evolution of each ensemble member depends on the collective expectation value  $\langle \mathbf{n}_l \rangle = \sum_{\alpha} p_{\alpha} \text{tr}[\mathbf{n}_l \rho^{(\alpha)}]$ , which requires the knowledge of all ensemble members at each point in time.

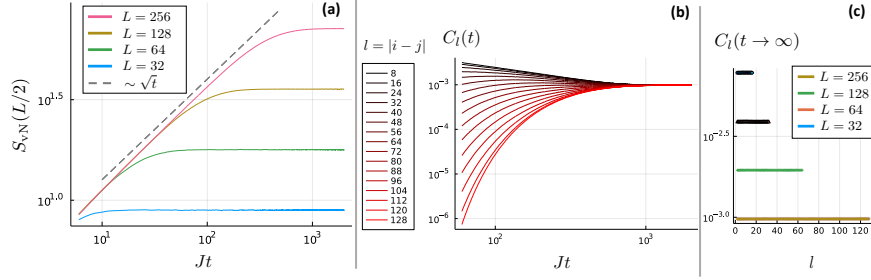


**Figure 4.19:** Evolution due to hopping Hamiltonian with additional random unitary evolution: **(a)** Entanglement entropy  $S_{vN}(L/2)$  growth over time. **(b)** Time evolution of the density-density correlations for different distances  $l$  and  $L = 256$ . **(c)** Stationary density-density correlations for system sizes  $L = 32 - 256$  ( $\gamma_I/J = 0.5$  with  $n_{avg} = 400$ ).

measurement outcomes to approximate the measurement+dephasing dynamics. Without averaging, the states evolve under (i) unitary evolution from the Hamiltonian, (ii) random unitary evolution due to the non-informative measurements and (iii) non-unitary, non-linear evolution due to measurements:

$$\begin{aligned}
 d\rho^{(c)} = & -i[\mathbf{H}, \rho^{(c)}]dt - \frac{\gamma_I + \gamma_M}{2} \sum_{i=1}^L [\mathbf{n}_i, [\mathbf{n}_i, \rho^{(c)}]]dt \\
 & + i\sqrt{\gamma_I} \sum_{i=1}^L dZ_i(t) [\mathbf{n}_i - \langle \mathbf{n}_i \rangle, \rho^{(c)}] \\
 & + \sqrt{\gamma_M} \sum_{i=1}^L dW_i(t) \{ \mathbf{n}_i - \langle \mathbf{n}_i \rangle, \rho^{(c)} \}.
 \end{aligned} \tag{4.167}$$

**Qualitative picture:** The interplay of the two processes is shown in Fig. 4.9 for the example of a single fermion on two lattice sites. For  $\gamma_M = 0$ , the dynamics due to the random unitary evolution is strongly fluctuating without a preferred direction (Fig. 4.9(b)). However, once weak measurements are present  $\gamma_M/J \ll 1$ , the additional random unitary evolution will *enhance* localization, see Fig. 4.9(c).

In hindsight, this bears a resemblance with the interplay of the dephasing bath with measurements. In the limit  $\gamma_B/J \gg 1$ , dephasing enhances phase ( $M$ ). In the following, we address the question to what extent the resemblance is quantitative. We argue that in the limit  $\gamma_B/J \gg 1$  and  $\gamma_I/J \gg 1$ , the dynamics *on the diagonal* of  $\rho^{(c)}$  is approximately the same for (i) measurements and dephasing and (ii) measurements and random unitary evolution. Therefore, observables that only depend on the operators  $\mathbf{n}_i$  are comparable in both cases.

#### Box 26: Random unitary evolution

The measurement scenario we have discussed in the previous chapters is based on *non-linear* stochastic Schrödinger equations. In case of the

continued on next page

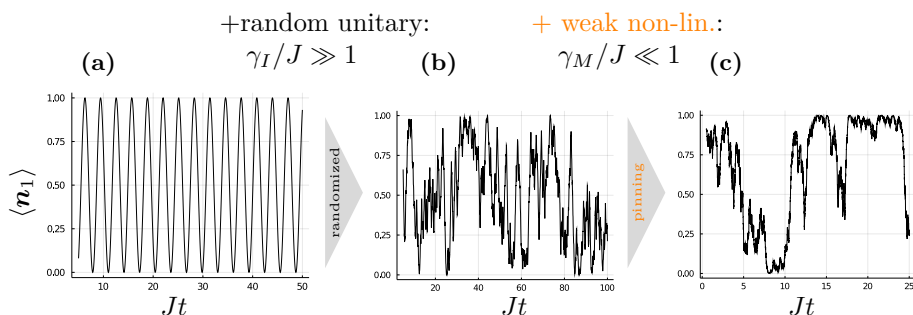


**Figure 4.20:** Interplay of unitary evolution and different measurements. (a) Unitary evolution; (b) Adding non-informative measurements ( $\gamma_M/J = 0$ ,  $\gamma_I/J = 10$ ) accompanied by a random unitary evolution. (c) Adding weak informative measurements ( $\gamma_M/J > 0$ ) will lead to a pinning scenario (here:  $\gamma_M/J = 0.2$ ,  $\gamma_I/J = 12$ ).

continued from page before

random unitary evolution, the dynamics, (4.166), is linear and preserves Gaussian states. See also Ref. [182] for a directly related model. The dynamics of the correlation matrix takes the form

$$dD_t = -i[h, D_t] + i\gamma_I [D_t, dZ_t], \quad (4.168)$$

where  $dZ_t = \text{diag}(dZ_{1,t}, \dots, dZ_{N,t})$ . The evolution of  $D_t$  is described by unitary operators  $U_t$  (here in discrete time):

$$D_{t+\delta t} \approx e^{-ih\delta t} e^{i\gamma_I \Delta Z} D_t e^{-i\gamma_I \Delta Z} e^{ih\delta t} = U_t D_t U_t^\dagger. \quad (4.169)$$

The unitary evolution implies that  $\text{tr}[D_t] = \text{const.}$ , as well as  $\text{tr}[D_t^m] = \text{const.}$  [182]. Therefore, partial information about the initial state is preserved during the evolution. Parallel to the discussion before, we can access the properties of correlation functions by studying replicas. The two replica evolution equation reads (compare also to [183, 186]):

$$\partial_t \rho_t^{(2R)} = -i[\mathbf{H}^{(1)} + \mathbf{H}^{(2)}, \rho_t^{(2R)}] + \frac{\gamma_I}{2} \sum_i \mathcal{L}_{\mathbf{n}_i^{(1)} + \mathbf{n}_i^{(2)}}[\rho_t^{(2R)}]. \quad (4.170)$$

In contrast to the previous case, this is a Lindblad-type equation and does not involve a coupling to higher replicas. It is reminiscent of the dephasing fermion model with an additional internal degree of freedom. An in depth analysis for a closely related model can be found in Ref. [186].

### 4.10.3 Effective Dynamics due to additional random unitary Evolution

An important difference between (i) the evolution in the presence of dephasing and measurements and (ii) random unitary evolution and measurements is the

purity of the state. In the first case, the evolved states are mixed, whereas in the second case the states are (or can be) pure. However, observables that are *not* sensitive to these global features might be comparable in both cases. This is reminiscent of a thermalizing closed quantum system, where we evaluate *local* observables either with respect to the (globally) pure state or the thermal Gibbs state.

Along this line of thought, we argue that observables like  $C_x$  and  $P_{|A|}$  are comparable within both approaches and the limit  $\gamma_B/J = \gamma_I/J \gg 1$ . Both observables only depend on the diagonal entries of  $\rho^{(c)}$  as well as  $\rho^{(2R)}$ . In the limit  $\gamma_B/J \gg 1$ , the resulting effective dynamics of the diagonal of  $\rho^{(c)}$  takes the form in (4.159). Along the same lines, we can derive the effective dynamics on the diagonal for random unitary evolution and measurements for  $\gamma_I/J \gg 1$ . Using the same perturbative approach, the evolution *on the diagonal* is the same as the one of a dephasing bath<sup>47</sup>. The technical reason is that the additional stochastic term in (4.167) does *not* act onto the diagonal elements. Furthermore, it does not produce a second order contribution (in contrast to the Hamiltonian) in the perturbation theory. Therefore, the dynamics on the diagonal takes the form (compare again to (4.159)):

$$\partial_t \rho_{\parallel}^{(c)} \approx \frac{\gamma_M}{J} \sum_l dW_l \{ \mathbf{n}_l - \langle \mathbf{n}_l \rangle, \rho_{\parallel}^{(c)} \} + \frac{2J}{\gamma_I + \gamma_M} \left( \mathcal{L}_1[\rho_{\parallel}^{(c)}] + \mathcal{L}_2[\rho_{\parallel}^{(c)}] \right). \quad (4.171)$$

This suggests that in the limit  $\gamma_I/J \gg 1$ , the dynamics *relevant for operators depending on  $\mathbf{n}_j$* , is approximately the same compared to the dephasing scenario in (4.159) once  $\gamma_I/J = \gamma_B/J \gg 1$ .

**Remark:** Using a different approach to calculate the perturbative dynamics is based on using the interaction picture (discussed in App. G). The result, (G.18), deviates in that it still contains a stochastic, *coherent* contribution.

**Numerical investigation:** In Fig. 4.21, the density-density correlations, entanglement entropy and the distribution of  $\langle \mathbf{n}_i \rangle$  are shown in case of the proxy model (random unitary evolution with measurements). The correlations and the  $\langle \mathbf{n}_i \rangle$  distributions show the same behavior we have seen for the first model (compare to Fig. 4.17). For  $\gamma_I/J \gg 1$  and  $L = 512$ , the algebraic scaling in  $C_l$  is only a transient phenomenon, turning into stronger decay. This behavior could not be resolved in the ensemble approach due to the limitation to  $L \leq 256$ . Since we are dealing with pure, Gaussian states we also have direct access to the entanglement entropy  $S_{vN}(L/2)$ . For  $\gamma_I/J \gg 1$ , it deviates from the log-law, in accord with the more strongly decaying correlations.

**Bosonic description:** The aforementioned analysis was focusing on the realm of phase ( $C_D$ ). Adding random unitary evolution to the QSD dynamics does not spoil an effective description in terms of bosons. Therefore, we study the role of random unitary evolutions (instead of a bath) in the  $(\gamma_M, \gamma_I)$ -phase diagram.

---

<sup>47</sup>The dynamics can be approximated along two lines: (i) using the same perturbative approach as before or (ii) going into the ‘interaction’ picture, adapting the approach in Ref. [180] for a directly related model. The second approach is discussed in App. G.

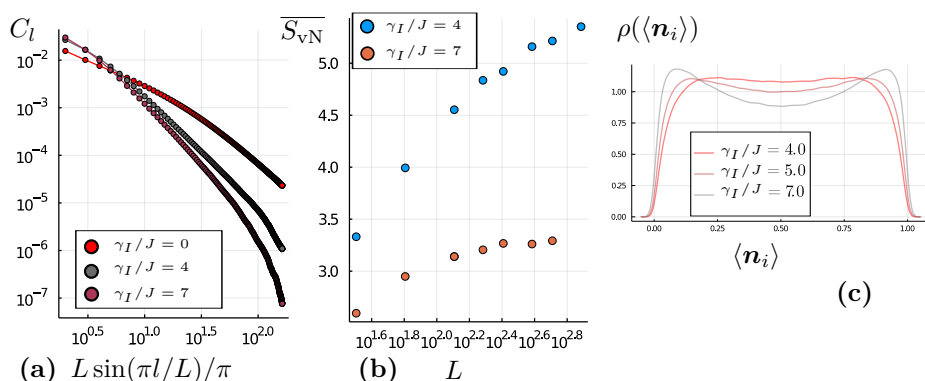


**Figure 4.21:** (a) Density-density correlations  $C_l$  for  $\gamma_I/J = 0, 4, 7$  and  $\gamma_M/J = 0.2$  (log-log scale for  $L = 512$ ). (b) Entanglement entropy  $\overline{S_{vN}}(L/2)$  for  $\gamma_I/J = 4, 7$  and  $\gamma_M/J = 0.2$ , indicating a deviation from the log law (semi-log scale). (c) Distribution of  $\langle n_i \rangle$  for  $\gamma_I/J = 4, 5, 7$  and  $\gamma_M/J = 0.2$  (indicating a trend towards a bimodal distribution for increasing  $\gamma_I/J$ ;  $L = 128$ ).

In contrast to dephasing, the random unitary evolution does *not* enter the inverse propagator  $G_0^{-1}$  of the relative mode. However, it does affect the initial couplings  $\lambda_{\pm}/m^2 \rightarrow \frac{1}{2}(\frac{\gamma_M}{\nu} - \frac{\gamma_I}{\nu})$  and therefore modifies the phase diagram (see App. I.7 for further details<sup>48</sup>).

Including the random unitary evolution to the measurement dynamics leads to the same RG equations (4.153). However, the initial couplings depend on  $\gamma_I$  as well and the phase diagram is shown in Fig. 4.22. In contrast to the bath scenario, the regime (C) (or rather: the combination of (C) and (C<sub>D</sub>) in the bath case) is compact, although we expect a  $\sim 1/\gamma_M$  behavior without a transition at finite  $\gamma_B/J$ . The phase diagram depends on the initial coupling strengths, which we have calculated perturbatively for  $\gamma_M/\nu, \gamma_I/\nu \ll 1$ . Therefore, we do not expect the analysis to hold beyond  $\gamma_M/\nu, \gamma_I/\nu \ll 1$ .

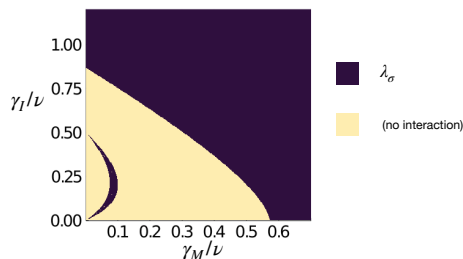


**Figure 4.22:** Phase diagram (2nd order RG) for a bosonic model with measurements ( $\gamma_M/\nu$ ) and random unitary evolution ( $\gamma_I/\nu$ ). A darker color indicates the growth of couplings under the RG and a lighter color indicates a shrinking of the couplings. The darker island for  $\gamma_M/\nu \leq 0.1$  corresponds to a regime of slowly growing couplings (which finally diverge).

**Remark:** The modified initial couplings depend on  $(\gamma_M - \gamma_I)/\nu$ , which can become small in the blue island region

<sup>48</sup>Note that for  $\gamma_M/J - \gamma_I/J \ll 1$  also the second-order contributions should be included eventually.

in Fig. 4.22. Here, the second order corrections are larger than the first order corrections.

## 4.11 Summary, Limitations and Outlook

In this chapter, we have discussed four different approaches to measurement-induced dynamics in the presence of dephasing, each having its advantages and shortcomings. Before discussing each individually, we outline the implications of the results. One challenging question in the area of measurement-induced transitions is how to extract ‘observables’ like  $\langle \mathcal{O} \rangle^2$  experimentally. Formally, this would require multiple copies of the same state or differently put: multiple experiments with the same measurement outcomes. To circumvent this issue, one can ask if  $\langle \mathcal{O} \rangle$  can be approximated by using  $n$  trajectories with only partly agreeing measurement outcomes  $\vec{m}$ . Using such a subset of trajectories to approximate  $\langle \mathcal{O} \rangle$  is related to using the ‘effective’ conditional state  $\rho_{\vec{m}}^{(c)}$ :

$$\langle \mathcal{O} \rangle \approx \frac{1}{n} \sum_{i=1}^n \langle \psi_{\vec{m}}^{(i)} | \mathcal{O} | \psi_{\vec{m}}^{(i)} \rangle \approx \text{tr} \left[ \mathcal{O} \rho_{\vec{m}}^{(c)} \right] \quad \text{with} \quad \rho_{\vec{m}}^{(c)} \approx \frac{1}{n} \sum_{i=1}^n |\psi_{\vec{m}}^{(i)}\rangle \langle \psi_{\vec{m}}^{(i)}|. \quad (4.172)$$

However, since only a fraction of the measurement outcomes are equivalent, the conditional state corresponds to an *imperfect* measurement with  $\eta < 1$  (or  $\gamma_B \neq 0$ ). If we treat  $\rho_{\vec{m}}^{(c)}$  as a proxy for a perfect measurement scenario ( $\eta = 1$ ), we can be misguided since  $\langle \mathcal{O} \rangle_{\eta>0} \neq \langle \mathcal{O} \rangle_{\eta=0}$ . Even taking  $\eta < 1$  into account can still hinder us from analyzing the ideal measurement-induced transition, since the phase described by  $\eta \ll 1$  can be different from the phase at  $\eta \sim 1$ . Nevertheless, this is another variant of the issue we raised at the beginning of the chapter: How to experimentally detect the transitions? A possibility is the aforementioned *post-selection*, which becomes intractable for large systems/long time evolutions. An alternative approach are *pre-selections* as recently investigated [169] or the use of only a few ancilla systems for tracking the purification dynamics (as we have discussed for  $\gamma_B = 0$ ) [33, 165].

In the following, we briefly collect some of the more technical issues and open questions from the different fermionic and bosonic approaches used in this chapter.

**Fermionic approaches:** The first fermionic approach (numerical solution of the conditional master equation) is limited to small system sizes, but gives access to correlations as well as entanglement measures. The complementary quantum trajectory approach for large systems already involves further approximations (e.g. the restriction of the number of ensemble members) and only grants efficient access to quantities like  $C_{ij}$  and  $P_{|A|}$  and is not well controlled. In the last approach, we considered a perturbative treatment in the limit  $\gamma_B/J \gg 1$  of strong dephasing. We compared the perturbative dynamics with the dynamics due to random unitary evolutions *replacing* the bath dynamics. In the limit  $\gamma_B/J \gg 1$ , both approaches give rise to the same dynamics *on the diagonal* of  $\rho^{(c)}$ . This in turn justifies the usage of a *finite* ensemble of quantum trajectories. As long as we focus onto observables which are functions of  $\mathbf{n}_j$ :  $f(\{\mathbf{n}_j\})$ , also individual pure states in the ensemble behave similar to  $\rho^{(c)}$ . The perturbative treatment also reveals a competition between ‘localizing’ measurements and diffusion on the diagonal. Nevertheless, it is an open question if this perturbative

model can capture the transition from phase  $(C_D)$  to  $(M)$ .

**Bosonic approach:** We described the long distance physics for  $L \rightarrow \infty$  in terms of an *effective* bosonic model, which is amenable to a momentum shell RG [19, 188]. It is an effective description with the same universal properties as the fermionic model. In this description, also fermionic interactions like [70]

$$\begin{aligned} \mathbf{n}_{\pm,x} \mathbf{n}_{\pm,x} &\rightarrow (\partial_x \phi_x \mp \partial_x \theta_x)^2, \\ \mathbf{n}_{+,x} \mathbf{n}_{-,x} &\rightarrow (\partial_x \phi_x)^2 - (\partial_x \theta_x)^2, \end{aligned}$$

can be incorporated and only modify the quadratic sector of the bosonic model. Nonetheless, this approach also has shortcomings. In the presence of heating, the description will eventually break down for long times (see Refs. [218, 243]) and will not be able to describe the heating of the fermionic system anymore. This is plausible since the bosonic model is based on the bosonization of the Dirac model. The Dirac model in turn can be seen as an effective description of the fermionic lattice model close to  $\pm k_F$ , but with an infinite set of non-physical states added. This becomes problematic once these modes get excited, as the heating dynamics will eventually do. In the absence of a bath, this can affect the heating absolute mode, which nevertheless will not change the overall physical picture. However, in the presence of a bath and in the regime  $(C_D)$ , the effect onto the relative mode might not be ignored anymore.

**Role of purity:** Physically, we distinguished three different phases:  $(C)$ ,  $(C_D)$  and  $(M)$ . We associated phase  $(C_D)$  with a strong suppression of the off-diagonal elements in  $\rho^{(2R)}$  (in accord with the emergence of a term  $\sim T_{\text{eff}} \phi_q^{(r)2}$  in the bosonic replica action). As we have already noted in passing, for monitored bosonic CFT's, the purity was extracted in Ref. [193]. In case of imperfect measurements ( $\eta < 1$ ), the purity is exponentially suppressed in the system size. Since we expect phase  $(C)$  to be described effectively by a CFT, it seems doubtful to use the purity as a measure to distinguish this phase from  $(C_D)$  in the thermodynamic limit. From the symmetry point of view, it was argued in other models that the explicit breaking of replica exchange symmetries due to bulk decoherence (can) lead to (i) a volume law scaling in  $\overline{S_{vN}}$  [20] and/or (ii) even the maximally mixed state [173]. This would be in line with an extensive scaling of the Renyi entropy  $\overline{S^{(2)}}$  and an exponentially suppressed purity in the whole phase diagram. However, this does not automatically imply the washing out of measurement-induced phases in the presence of a bath (as, e.g., in Ref. [175]). In the presence of additional physical symmetries, as is the case for the fermionic model at hand or the  $\mathbb{Z}_2$  symmetric models studied in Refs. [20, 172], different phases can stay intact. To characterize the phases from an information theoretical point of view and to circumvent the above mentioned issue, the entanglement negativity could be a valuable tool [173, 174, 193, 219, 240, 241]. However, it can be a challenging task to extract it from a (bosonic) field theory (but was achieved for, e.g., boundary driven models by mapping to a statistical physics model [173]). In this light, it is an open question how to relate the new emergent mass/'temperature' scale in the relative mode and phase  $(C_D)$  to observable consequences and/or information theoretical measures.

**Quality of phase transitions:** From the analysis above, the RG gives evidence

for the stability of phase (C) in a finite parameter region. Less clear instead (from the RG perspective) are the properties and transitions between the other phases, which we expect to be partly rooted in the insufficiency of the bosonic model (see discussion before). Due to the numerical challenges for strongly mixed and non-Gaussian states, we cannot make a sharp prediction about these transitions (or crossovers) in the thermodynamic limit based on simulations. However, some limitations might be overcome with alternative methods like, e.g., matrix product states [216, 218, 247, 248]. Nevertheless, strong dephasing can also lead to a simplification by reducing the quantum dynamics onto dynamics on the diagonal of the density matrix (as outlined in the last section). It is an interesting but open question if a transition between ( $C_D$ ) and ( $M$ ) can be effectively described in this setup and whether a ‘classical’ phase transition is emerging.

**Dynamical perspective:** In the absence of a bath, the dynamical purification can be used to identify possible phase transitions [31, 165] (see Sec. 4.5.2). We expect that a similar strategy should be possible in the presence of a bath: the mutual information  $I_m$  (or similar quantities) between one or a few ancillas, initially entangled with the system, can be tracked. For an example, see Fig. 4.23. For long times, system and ancilla ‘decorrelate’ with an exponential decay of  $\overline{I_m}(t)$ . Adapting the findings for  $\gamma_B = 0$ , we hypothesize that the corresponding decay time scale in  $\overline{I_m}(t)$  should have a  $L$ -dependent scaling for phase (C).

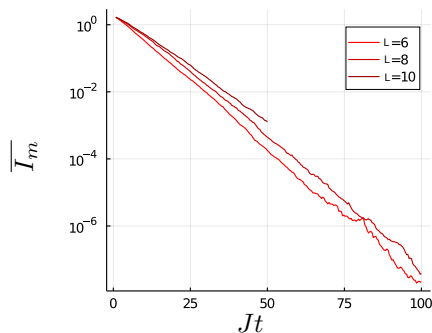


**Figure 4.23:** Mutual information  $\overline{I_m}(S, B)$  between an ancilla qubit ( $B$ ) and an imperfectly ( $\eta = 0.9$ ) monitored fermion system ( $S$ ) of size  $L$  and  $L/2$  fermions for  $\gamma/J = 0.2$ .

**Relation to other methods:** The measurement-induced transitions are based on the properties of the individual quantum trajectories. In earlier works, the statistical properties of quantum (jump) trajectories have been studied in [249–251] based on the probability  $P_t(K) = \text{tr}[\rho^{(K)}(t)]$  to find  $K$  events/quantum jumps induced by the dynamics at time  $t$ . This question can be mapped onto a generalized quantum master equation. The leading properties of the dynamics are described by the largest eigenvalue of this master equation. This approach is still based on a single ‘replica’, therefore it is not clear whether this strategy can be adapted to measurement-induced transitions where the transition is masked at the level of *linear* averages.



## 5 | Conclusion

In the last chapters, we have investigated (dynamic) settings in quantum systems ranging from ground state settings for static Hamiltonians  $\mathbf{H}$ , to time-dependent Hamiltonians  $\mathbf{H}(t)$  and environmental dephasing and measurements. In all these scenarios, as well as their interplay, a collective behavior like phase transitions and universality can emerge. The models we have discussed are directly or indirectly related to elementary spin models with Hamiltonian  $\mathbf{H}$ , measured operators  $\mathbf{M}_l$  (with projection operators  $\mathbf{P}_{l,\pm}$ ) and Lindblad operators  $\mathbf{L}_l$ :

$$\text{Hamiltonian: } \mathbf{H} = -g \sum_l \sigma_l^z - J_x \sum_l \sigma_l^x \sigma_{l+1}^x - J_y \sum_l \sigma_l^y \sigma_{l+1}^y, \quad (5.1)$$

$$\text{measurements: } \mathbf{M}_l = \sigma_l^z, \quad \mathbf{P}_{l,\pm} = \frac{1}{2} (\mathbb{1} \pm \sigma_l^z), \quad (5.2)$$

$$\text{dephasing: } \mathbf{L}_l = \frac{1}{2} (\mathbb{1} - \sigma_l^z). \quad (5.3)$$

Phase transitions and universality are closely related to the symmetries of the (competing) terms. In the ground state and driven scenario, the competition is rooted in the non-commuting transversal field term ( $g$ ) and the XY terms ( $J_x \neq J_y$ ) with a shared  $\mathbb{Z}_2$  symmetry. In case of measurements, the competition is similar, but the model features a  $U(1)$  symmetry<sup>1</sup> ( $J_x = J_y, g = 0$ ).

In case of a slow drive, we have shown that the universal breaking of adiabaticity (and connected observable behavior) can result from equilibrium relevant *and* irrelevant couplings at the level of the model (5.1). Drives along or across a phase boundary can reveal different scaling, but universal, exponents associated with the different driven couplings. This analysis complements the RG analysis in Ref. [41]. However, the quadratic setting hints at two challenges. Firstly, there are indications that long drives are needed to make the scaling from equilibrium *irrelevant* couplings observable. Secondly, the associated scalings become observable only for drives that run nearly parallel to the phase boundary. Therefore, it seems that an experimental realization requires good control of the parameters involved and long coherence times. However, these are in parts model-dependent properties. So far, we confined the model-based analysis to quadratic (fermion) models. The RG analysis instead also applies for interacting theories. Therefore, a further step to substantiate the possibilities

---

<sup>1</sup>However, for the measurement scenario, the  $U(1)$  symmetry is not necessarily required for the phenomenology [20, 176] (since it is the symmetry *at the replica level* that is relevant).

and limitations of the generalized KZM should be the investigation of interacting models. Complementarily, the investigation of the generalized KZM in quantum simulations of the transverse XY or similar models would be interesting. An alternative implementation for drives of irrelevant couplings could be based on Ising Hamiltonians ( $J_y = 0$ ) with additional controllable terms like  $g_2(t) \sum_i \sigma_i^z \sigma_{i+1}^z$ . The coupling  $g_2$  is as well irrelevant at equilibrium [2].

Making use of unitary evolution *and* measurements, an *extended* critical phase can be stabilized in (free) fermion models [18]. We have shown that this phase is also stable against weak dephasing. On the one hand, dephasing can emerge due to the coupling to, e.g., a bosonic (e.g., phonon) bath or in the context of optical lattices [51]. On the other hand, it describes *imperfect* measurements where a fraction of the measurement outcomes are not known to the observer. Therefore, the stability against weak dephasing also implies the robustness against some imperfections in the measurements. For strong dephasing and weak measurements, we found indicators for a new phase, still displaying scale invariant behavior for the dynamics on the diagonal of  $\rho^{(c)}$ . In contrast, we *hypothesize* that measures like the entanglement negativity are suppressed in this phase. However, the numerical as well as analytical methods we chose are challenged by the strongly mixed properties and the non-Gaussian ones in the presence of strong dephasing. Therefore, the properties of this new phase and the quality of the phase transition (or crossover) are still not fully settled.

In the above setting, the measurement and bath operators commute (similar to the case discussed in Ref. [32]). However, depending on, e.g., the NISQ devices under consideration, other sources of decoherence might become important, which do not necessarily commute with either the Hamiltonian nor the measurement operators. This in turn can enrich the competitions and possible phases. Finally, one challenge in the realm of measurement-induced transitions is the *detection* in experiments. Approaches to make active use of the measurement outcomes in the form of outcome-dependent feedback is an interesting (and open) investigation [169, 171, 252].

**Acknowledgements:** First of all, I would like to thank Sebastian for the chance to work in his group and dive into diverse topics in the realm of non-equilibrium physics. I am glad that we often had the chance for extended and helpful discussions. Here, Sebastian always provided the bigger picture (not my personal strength to be honest). Furthermore, he supported my decision and plans to go into a teaching direction. I am very grateful for that.

Staying some years at the institute also gave me the chance to teach many different tutorials, where I discovered my enthusiasm for teaching. Therefore, the time during the doctorate was not only a scientific experience, but also clarified for me what I would like to do afterwards.

Furthermore, I like to thank Steven for the collaboration on the Kibble-Zurek project and for the countless and fruitful discussions we had regarding its details (over a cup of tea). Another thanks goes to Nico, Bernhard, Ori and all other members of our office and the group during the time - in particular for moral support. Similarly, I like to thank my parents and my brother for constant support and interest in what (and how) I am doing.

There are two persons, who I like to mention explicitly: Michael and Clara. The collaboration with Michael taught me a lot about (non-equilibrium) physics and how to think more physically about the problems at hand. Michael always had an open ear for my (detail) questions. Furthermore, and maybe even more importantly, he could always calm be down when I was running into another problem that seemed to be unsolvable. Many thanks for the support and also helpful comments during the last stages of the doctorate. Here, I also like to thank Petra for prove reading the thesis. Finally, I like to thank Clara. I am not (always) a simple person, in particular in regard to physics/work. Clara always kept a clear head and structured mine. Without her there would presumably be no thesis (yet).



# A | Gaussian States

Even though the (typical) time evolution of a quantum mechanical state is linear, a complexity arises due to the exponentially large (in the number of particles) Hilbert space, which can make it difficult to access large system sizes. One class of states, which withstands this problem, are ‘Gaussian’ states, where a parametrization in terms of a polynomial number of parameters is possible. In the following, we will summarize some of the important properties of Gaussian states, used in the main text. A very readable reference, which will use throughout is Ref. [63].

*The discussions in Secs. A.1-A.3 are partly adapted and extended from the publications [42, 147].*

Similarly as a Gaussian distribution, fermionic Gaussian states are fully characterized by the second moments of the basic operators, the creation and annihilation operators  $\mathbf{c}_i^\dagger, \mathbf{c}_i$ :  $\langle \mathbf{c}_i^\dagger \mathbf{c}_j \rangle, \langle \mathbf{c}_i^\dagger \mathbf{c}_j^\dagger \rangle, \langle \mathbf{c}_i \mathbf{c}_j \rangle$ . Higher moments are entirely determined by these expectation values (Wicks’ theorem).

**Field theory:** One form we encounter in Sec. 2.2.2 are Gaussian *field theories*. Here, the action is quadratic in terms of Grassmann fields:

$$S = \vec{\psi}^T M \vec{\psi}, \quad (\text{A.1})$$

with some matrix  $M$ . In this case, the calculation of expectation values is reduced to calculating Gaussian integrals (see, e.g., Ref. [52]).

**Operator perspective:** At the operator level, a fermionic Gaussian state is defined as [63]:

$$\rho = \frac{1}{Z} \exp(-\vec{c}^\dagger h \vec{c}), \quad Z = \text{tr} \left[ \exp(-\vec{c}^\dagger h \vec{c}) \right], \quad (\text{A.2})$$

$$\vec{c}^T = (\mathbf{c}_1, \dots, \mathbf{c}_l, \mathbf{c}_1^\dagger, \dots, \mathbf{c}_l^\dagger), \quad (\text{A.3})$$

for some given hermitian matrix  $h$ . We can interpret  $\rho$  as the thermal state of the effective Hamiltonian  $\beta \mathbf{H} = \frac{1}{2} \vec{c}^\dagger h \vec{c}$ . Its properties are encoded in the correlation matrix  $G$ :

$$G_{c,mn} = \begin{pmatrix} \langle \mathbf{c}_m \mathbf{c}_n^\dagger \rangle & \langle \mathbf{c}_m \mathbf{c}_n \rangle \\ \langle \mathbf{c}_m^\dagger \mathbf{c}_n^\dagger \rangle & \langle \mathbf{c}_m^\dagger \mathbf{c}_n \rangle \end{pmatrix}. \quad (\text{A.4})$$

To relate  $G_{c,mn}$  with the matrix  $h$ , we can first use a Bogoliubov/fermionic

transformation  $U$  to diagonalize the Hamiltonian:

$$\tilde{\mathbf{c}}^\dagger h \tilde{\mathbf{c}} = \sum_l \epsilon_l \left( \chi_l^\dagger \chi_l - \chi_l \chi_l^\dagger \right), \quad \tilde{D} = U^\dagger h U. \quad (\text{A.5})$$

In terms of the  $\chi$  fermions, the correlation matrix is given by

$$G_{\chi, mn} = \begin{pmatrix} \langle \chi_m^\dagger \chi_n^\dagger \rangle & \langle \chi_m^\dagger \chi_n \rangle \\ \langle \chi_m \chi_n^\dagger \rangle & \langle \chi_m \chi_n \rangle \end{pmatrix} = \begin{pmatrix} \delta_{mn}(1 - \langle \chi_m^\dagger \chi_m \rangle) & 0 \\ 0 & \delta_{mn} \langle \chi_m^\dagger \chi_m \rangle \end{pmatrix}. \quad (\text{A.6})$$

Therefore, all information is encoded in the occupations  $\langle \chi_m^\dagger \chi_m \rangle$ . They are related to the energies of the Hamiltonian according to [63]:

$$\langle \chi_m^\dagger \chi_m \rangle = \frac{1}{1 + e^{2\epsilon_m}}. \quad (\text{A.7})$$

To obtain the correlation matrix  $G_{c, mn}$  of the original fermions, the same transformation  $U$  can be used:  $G_c = U G_\chi U^\dagger$ .

• **Purity:** The density matrix is pure in the limit  $\epsilon_m \rightarrow \pm\infty$ . In terms of the correlation matrix, this translates into [63]:

$$\text{purity condition:} \quad G^2 = G. \quad (\text{A.8})$$

In case of particle number conservation (relevant for our measurement discussion) and  $\langle \mathbf{c}_i \mathbf{c}_j \rangle \equiv 0$ , all information is encoded in

$$D_{ij} := \langle \mathbf{c}_i^\dagger \mathbf{c}_j \rangle. \quad (\text{A.9})$$

Here,  $D_{ij}$  is the correlation matrix used in the main text. The purity condition is similarly given by  $D^2 = D$ .

• **Wick's theorem:** The aforementioned Wick's theorem allows us to express arbitrary expectation values with respect to the 2-operator correlation functions.

**Field theory:** In case of the expectation values of  $2N$  fields [52]:

$$\langle \psi_{m_1} \psi_{m_2} \dots \psi_{m_N} \bar{\psi}_{l_N} \dots \bar{\psi}_{l_1} \rangle = \sum_P \text{sgn}(P) M_{m_1 l_{P1}}^{-1} \dots M_{m_N l_{PN}}^{-1}$$

the result is given by the sum (all possible permutations  $P$ ) over the product of pairings  $\langle \psi_m \bar{\psi}_l \rangle = M_{ml}^{-1}$  (see Ref. [52] for more details).

**Operator perspective:** Given a set of creation and annihilation operators, a similar result holds. For example, the expectation value of four operators gives rise to all terms where two operators are paired up (taking into account possible signs in case of fermions) [17, 253]. In case of number conservation, this example reads:

$$\langle \mathbf{c}_i^\dagger \mathbf{c}_j \mathbf{c}_k^\dagger \mathbf{c}_l \rangle = \langle \mathbf{c}_i^\dagger \mathbf{c}_j \rangle \langle \mathbf{c}_k^\dagger \mathbf{c}_l \rangle + \langle \mathbf{c}_i^\dagger \mathbf{c}_l \rangle \langle \mathbf{c}_j \mathbf{c}_k^\dagger \rangle. \quad (\text{A.10})$$

In case of bosons, a similar strategy can be applied (though additional possible signs are absent). However, some care has to be taken once the expectation

values like  $\langle \mathbf{b} \rangle \neq 0$  in the bosonic case.

• **Time evolution with quadratic Hamiltonians:** The important feature of Gaussian states is that they stay Gaussian during the time evolution with a (time-dependent) *quadratic* Hamiltonian:  $\mathbf{U}(t) = \mathbf{T} \exp\left(-i \int^t \mathbf{H}(t') dt'\right)$  (where  $\mathbf{T}$  denotes the time ordering operator) (see also Ref. [63]). The time evolved state takes the form  $\mathbf{U} \rho \mathbf{U}^\dagger$ , though it is enough to consider the one product of exponentials of the form  $e^{\mathbf{X}} e^{\mathbf{Y}} = e^{\mathbf{Z}}$ , with  $e^{\mathbf{X}} = \mathbf{U}$ ,  $e^{\mathbf{Y}} = \rho$ . Both  $\mathbf{X}, \mathbf{Y}$  are quadratic in the creation and annihilation operators. According to the Baker-Campbell-Hausdorff formula, the operator  $\mathbf{Z}$  is built from commutators of  $\mathbf{X}, \mathbf{Y}$ , which in turn can always be reduced to the form  $[\mathbf{AB}, \mathbf{CD}]$  with  $\mathbf{A}, \mathbf{B}, \mathbf{C}, \mathbf{D} \in \{\mathbf{c}_i, \mathbf{c}_j^\dagger\}$ . Due to the canonical (anti-)commutation relations, any such commutator remains quadratic in the creation/annihilation operators:

$$[\mathbf{X}, \mathbf{Y}] \rightarrow [\mathbf{AB}, \mathbf{CD}] = ((\text{at most}) \text{quadratic in } \mathbf{c}, \mathbf{c}^\dagger). \quad (\text{A.11})$$

Therefore, any further commutator also fulfills:

$$[\mathbf{EF}, [\mathbf{AB}, \mathbf{CD}]] = ((\text{at most}) \text{quadratic in } \mathbf{c}, \mathbf{c}^\dagger). \quad (\text{A.12})$$

Together with the Baker-Campbell-Hausdorff formula, this guarantees that  $\mathbf{Z}$  in  $e^{\mathbf{X}} e^{\mathbf{Y}} = e^{\mathbf{Z}}$  is a quadratic operator as well: a Gaussian state stays Gaussian.

**Entanglement entropy (for the transverse XY model):** Since the ground state for the transverse XY model is a Gaussian state, all information is contained in the covariance or correlation matrix. In terms of the quasi-particles in momentum space, the correlation matrix takes a simple form, which can afterwards be transformed into the one for the original fermions:

$$G_{\chi, k} = \begin{pmatrix} 1 & 0 \\ 0 & 0 \end{pmatrix}, \quad G_{c, k} = U_k G_{\chi, k} U_k^\dagger = \begin{pmatrix} |u_k|^2 & u_k v_k^* \\ u_k^* v_k & |v_k|^2 \end{pmatrix}. \quad (\text{A.13})$$

In real space, the correlations are obtained as (see, e.g., Ref. [12, 176]):

$$G_{c, mn} = \begin{pmatrix} \langle \mathbf{c}_m \mathbf{c}_n^\dagger \rangle & \langle \mathbf{c}_m \mathbf{c}_n \rangle \\ \langle \mathbf{c}_m^\dagger \mathbf{c}_n^\dagger \rangle & \langle \mathbf{c}_m^\dagger \mathbf{c}_n \rangle \end{pmatrix} \begin{cases} \langle \mathbf{c}_m \mathbf{c}_n^\dagger \rangle = \frac{1}{L} \sum_k \langle \mathbf{c}_k \mathbf{c}_k^\dagger \rangle e^{ika(m-n)}, \\ \langle \mathbf{c}_m \mathbf{c}_n \rangle = \frac{e^{i\pi/2}}{L} \sum_k \langle \mathbf{c}_k \mathbf{c}_{-k} \rangle e^{ika(m-n)}. \end{cases}$$

Knowledge of the correlation functions in real space is sufficient to further determine, e.g., the entanglement between two subsystems. Following Ref. [63], for Gaussian states the information about a subsystem  $A$  for an observer limited to that subsystem is given by the correlation matrix *restricted to*  $A$ . In case of  $G$  or  $D$  we write  $G|_A$  or  $D|_A$  respectively. Therefore, the reduced density matrix  $\rho_A$  is itself a Gaussian state. The entanglement entropy in turn only depends on the eigenvalues of  $\rho_A$ , which we can obtain from the known correlation matrix. In terms of the ‘diagonalized’ form of  $\rho_A$  (with occupations  $\langle \chi_l^\dagger \chi_l \rangle$ ), the entropy is given by [8, 63]):

$$S_{\text{vN}}(A) = - \sum_{l \in A} \left( \langle \chi_l^\dagger \chi_l \rangle \ln \left( \langle \chi_l^\dagger \chi_l \rangle \right) + (1 - \langle \chi_l^\dagger \chi_l \rangle) \ln \left( 1 - \langle \chi_l^\dagger \chi_l \rangle \right) \right). \quad (\text{A.14})$$

Practically, this means that we can calculate  $S_{\text{vN}}(A)$  by diagonalizing the correlation matrix  $G|_A$  and inserting the eigenvalues (= occupations) in (A.14).

## A.1 Jordan-Wigner Transformation

The Jordan-Wigner transformation [254] (see also Refs. [2, 11, 55–57, 60, 141, 142, 255–258]) describes spin- $\frac{1}{2}$  operators in terms of non-local strings of fermion operators. The spin operators are  $\sigma_l^x, \sigma_l^y, \sigma_l^z$  at lattice site  $l$ . They fulfill the commutation relations  $[\sigma_l^\alpha, \sigma_m^\beta] = 2i\epsilon_{\alpha\beta\gamma}\sigma_l^\gamma\delta_{lm}$ . Equivalently, we can use the operators  $\sigma_l^\pm, \sigma_l^z$  with

$$\left. \begin{aligned} \sigma_l^+ &= \frac{1}{2}(\sigma_l^x + i\sigma_l^y), \\ \sigma_l^- &= \frac{1}{2}(\sigma_l^x - i\sigma_l^y), \end{aligned} \right\} [\sigma_l^\pm, \sigma_m^z] = \mp 2\sigma_l^\pm\delta_{lm}. \quad (\text{A.15})$$

The fermionic operators instead are defined by

$$\{\mathbf{c}_l, \mathbf{c}_m^\dagger\} = \delta_{lm}, \quad \{\mathbf{c}_l, \mathbf{c}_m\} = \{\mathbf{c}_l^\dagger, \mathbf{c}_m^\dagger\} = 0. \quad (\text{A.16})$$

Locally, spins and fermions behave similarly though spin operators at different lattice sites commute whereas fermion operators anti-commute. To reinstall commutation relations, a string  $\prod_{m<n}(1-2\mathbf{c}_m^\dagger\mathbf{c}_m)$  is added. It takes the number parity to the left of the fermion into account, such that the spin operators are expressed as

$$\left. \begin{aligned} \sigma_n^z &= 1 - 2\mathbf{c}_n^\dagger\mathbf{c}_n, \\ \sigma_n^x &= (\mathbf{c}_n^\dagger + \mathbf{c}_n) \prod_{m<n}(1 - 2\mathbf{c}_m^\dagger\mathbf{c}_m), \\ \sigma_n^y &= i(\mathbf{c}_n^\dagger - \mathbf{c}_n) \prod_{m<n}(1 - 2\mathbf{c}_m^\dagger\mathbf{c}_m), \end{aligned} \right\} \begin{aligned} \sigma_n^+ &= \mathbf{c}_n \prod_{m<n}(1 - 2\mathbf{c}_m^\dagger\mathbf{c}_m), \\ \sigma_n^- &= \mathbf{c}_n^\dagger \prod_{m<n}(1 - 2\mathbf{c}_m^\dagger\mathbf{c}_m). \end{aligned} \quad (\text{A.17})$$

Alternatively, we can express fermions in terms of spins:

$$\mathbf{c}_l^\dagger = \sigma_l^- \prod_{m<l} \sigma_m^z, \quad \mathbf{c}_l = \sigma_l^+ \prod_{m<l} \sigma_m^z. \quad (\text{A.18})$$

The relevant scenarios for our discussion are interaction between nearest-neighbor (or second-nearest-neighbor) spins. The typical terms take the following form in the fermionic representation:

real space	mom. space
$\mathbf{c}_j^\dagger\mathbf{c}_{j+1} + \mathbf{c}_{j+1}^\dagger\mathbf{c}_j = \frac{1}{2} [\sigma_j^x\sigma_{j+1}^x + \sigma_j^y\sigma_{j+1}^y]$	$\rightarrow 2\cos(ka)\mathbf{c}_k^\dagger\mathbf{c}_k,$
$\mathbf{c}_j^\dagger\mathbf{c}_{j+1}^\dagger + \mathbf{c}_{j+1}\mathbf{c}_j = \frac{1}{2} [\sigma_j^x\sigma_{j+1}^x - \sigma_j^y\sigma_{j+1}^y]$	$\rightarrow \sin(ka) (\mathbf{c}_{-k}^\dagger\mathbf{c}_k^\dagger + \mathbf{c}_k\mathbf{c}_{-k}),$
$\mathbf{c}_j^\dagger\mathbf{c}_{j+2} + \text{h.c.} = \frac{1}{2} [\sigma_j^x\sigma_{j+2}^x + \sigma_j^y\sigma_{j+2}^y] \sigma_{j+1}^z$	$\rightarrow 2\cos(2ka)\mathbf{c}_k^\dagger\mathbf{c}_k$
$\mathbf{c}_j^\dagger\mathbf{c}_{j+2}^\dagger + \text{h.c.} = \frac{1}{2} [\sigma_j^x\sigma_{j+2}^x - \sigma_j^y\sigma_{j+2}^y] \sigma_{j+1}^z$	$\rightarrow \sin(2ka) (\mathbf{c}_{-k}^\dagger\mathbf{c}_k^\dagger + \mathbf{c}_k\mathbf{c}_{-k}).$

(A.19)

## A.2 Gaussian States in Measurement Scenarios

### Time evolution in the presence of measurements:

In the following, we briefly list the kind of states we are dealing with depending on the scenario:

- An initial Gaussian state stays Gaussian under the unitary evolution due to a quadratic Hamiltonian. Furthermore, if we add additional measurements, the evolved state is still Gaussian. For the model discussed in Sec. 4.4, we first sort the dynamic contributions according to trivial operators and non-trivial ones with  $\mathbf{n}_j^2 = \mathbf{n}_j$ . The time evolution operator reads

$$\mathbf{U}_{j,t}^{(R)} \approx (\text{factor}) \cdot \exp\left(\left[\Delta W_j \sqrt{\delta t} - \delta t(1 - 2\langle \mathbf{n}_j \rangle)\right] \mathbf{n}_j\right), \quad (\text{A.20})$$

where the prefactor only changes the overall norm of the state (not relevant for single trajectories). In summary, this operator also preserves the Gaussian character (up to a normalization).

- If we are dealing with a dephasing bath instead, the Gaussian property is lost, though we can still efficiently simulate  $D_{ij} = \langle \mathbf{c}_i^\dagger \mathbf{c}_j \rangle$ .
- Combining measurements and a dephasing bath also leads to a loss of this last property - the evolution is non-Gaussian and the hierarchy of correlation functions does not decouple.

**Gaussian state scenario:** In case of a Gaussian evolution, we only need to keep track of the correlation matrix  $D$ , though it is advantageous to keep track of  $|\psi\rangle$  directly, as pioneered in Ref. [17]. The state evolves as:

$$|\psi_{t+\delta t}\rangle \approx \mathbf{U}_{j,t}^{(R)} e^{-i\mathbf{H}\delta t} |\psi_t\rangle, \quad (\text{A.21})$$

and the state can be parametrized in terms of  $N$  fermions at all times (due to particle number conservation). This means that at each point in time there is a set of fermions created by  $\{\chi_{j,t}^\dagger\}_{j=1}^N$  with  $\{\chi_j, \chi_l^\dagger\} = \delta_{j,l}$ , or differently put: the single particles states  $\chi_j^\dagger|0\rangle$  are orthonormal to each other. A parametrization is given in terms of the  $L \times N$  matrix  $U_t$ :

$$|\psi_t\rangle = \prod_{i=1}^N \left( \sum_{j=1}^L U_{ji,t} \mathbf{c}_j^\dagger \right) |0\rangle = \prod_{i=1}^N \chi_i^\dagger |0\rangle. \quad (\text{A.22})$$

The requirement for  $\langle 0 | \chi_l \chi_j^\dagger | 0 \rangle = \delta_{lj}$  translates into  $U_t^\dagger U_t = \mathbb{1}$ . The time evolution in terms of the matrix  $U_t$  can be approximately written as [17]

$$\begin{aligned} \text{time evolution: } \tilde{U}_{t+\delta} &= M e^{-i\mathbf{H}\delta t} U_t, \\ \text{matrices: } h_{ij} &= J \delta_{|i-j|,1}, \quad M_{ij} = \delta_{ij} e^{\Delta W_j \sqrt{\delta t} - \delta t(1-2\langle \mathbf{n}_j \rangle)}, \end{aligned} \quad (\text{A.23})$$

though the state, parametrized by  $\tilde{U}_{t+\delta t}$ , is not yet normalized. At time  $t + \delta t$  we still have  $N$  orthogonal modes, which requires that the columns of  $U_{t+\delta t}$  have to be orthonormal to each other. Therefore, we perform a Gram-Schmidt decomposition and only keep the orthonormal contributions in  $\tilde{U}_{t+\delta t}$ . In this context, this amounts to a  $QR$ -decomposition:  $Q$  is a  $L \times L$  unitary matrix and  $R$  an  $L \times N$  upper triangular matrix:

$$\tilde{U}_{t+\delta t} = QR = Q_1 R_1. \quad (\text{A.24})$$

The second equality is an equal rewriting with the  $L \times N$  matrix  $Q_1$  with orthonormal columns and the upper triangular  $N \times N$  matrix  $R_1$ . This matrix product corresponds to the decomposition of the columns ('vectors') in  $\tilde{U}_{t+\delta t}$  into the sum of orthonormal states (encoded in  $Q_1$ ) with the weights in the sum given by the entries in  $R_1$ . Therefore,  $Q_1$  is the desired matrix with the property  $Q_1^\dagger Q_1 = \mathbb{1}$  and we choose  $U_{t+\delta t} = Q_1$  (see also Ref. [17]). The correlation matrix is the matrix product:

$$U_{t+\delta t} U_{t+\delta t}^\dagger = D_{t+\delta t}. \quad (\text{A.25})$$

**Comparison: conditional master equation (non-Gaussian states)** To solve the conditional master equations, we restrict ourselves to the fixed particle number Hilbert space  $\mathcal{H}$  with  $N = L/2$  fermions and  $\dim[\mathcal{H}] = \binom{L}{L/2}$ . All operators are therefore  $\dim[\mathcal{H}] \times \dim[\mathcal{H}]$  matrices and we trotterize and re-exponentiate the time evolution (valid up to order  $\delta t$ ):

$$\left. \begin{aligned} U_H &= \exp(-i\mathbf{H}\delta t), \\ \mathbf{O}_{ij} &:= \left( \sum_{l=1}^L n_l^{(i)} n_l^{(j)} \right) |\{n\}_i\rangle\langle\{n\}_j|, \\ \mathbf{D} &= \exp\left(\left(\mathbf{O} - \frac{L}{2}\mathbb{1}\right) \gamma_B \delta t\right), \\ \mathbf{V}_{ij} &= \delta_{ij} \exp\left(\left(\left[\Delta W_j \sqrt{\delta t} - \delta t(1 - 2\langle n_j \rangle)\right]\right)\right), \end{aligned} \right\} \rho_{t+\delta t}^{(c)} \approx \mathbf{D} \cdot \left( \mathbf{V} U_H \rho_t^{(c)} U_H^\dagger \mathbf{V}^\dagger \right). \quad (\text{A.26})$$

Here,  $n_l^{(i)}$  is the number of particles at site  $l$  in state  $|\{n\}_i\rangle$ . The dephasing of off-diagonal matrix elements is given by the element-wise  $(\cdot)$  multiplication with the dephasing matrix  $\mathbf{D}$ .

**Observables from Gaussian states:** Given the description of the Gaussian states in terms of the matrix  $U$  and  $D = UU^\dagger$  [17, 18, 176], we can directly access the density-density correlations  $C_{ij}$ , as well as the subsystem parity variance  $P_{|A|}$ :

$$C_{ij} = \overline{\langle \mathbf{n}_i \rangle \langle \mathbf{n}_j \rangle} - \overline{\langle \mathbf{n}_i \mathbf{n}_j \rangle} = \overline{|\langle \mathbf{c}_i^\dagger \mathbf{c}_j \rangle|^2}, \quad (\text{A.27})$$

$$P_{|A|} = \det(2 \cdot D|_A - \mathbb{1}|_A)^2. \quad (\text{A.28})$$

Here,  $D|_A$  is the subset of the matrix  $D$  with indices in region  $A$  and the overline indicates the average over different measurement trajectories. For the expression  $C_{ij}$ , we used Wick's theorem:

$$\langle \mathbf{c}_j^\dagger \mathbf{c}_j \mathbf{c}_k^\dagger \mathbf{c}_k \rangle = \langle \mathbf{n}_j \rangle \langle \mathbf{n}_k \rangle - \langle \mathbf{c}_j^\dagger \mathbf{c}_k \rangle \langle \mathbf{c}_k^\dagger \mathbf{c}_j \rangle - \langle \mathbf{c}_j^\dagger \mathbf{c}_k \rangle \delta_{j,k}. \quad (\text{A.29})$$

**Observables from sums of Gaussian states:** Once  $\rho^{(c)}$  is described by a convex sum of (Gaussian) states, the density-density correlations are given by

$$C_{ij} = \overline{\langle \mathbf{n}_i \rangle} \cdot \overline{\langle \mathbf{n}_j \rangle} - \overline{\langle \mathbf{n}_i \mathbf{n}_j \rangle}, \quad \langle \langle \mathbf{O} \rangle \rangle := \text{tr}[\mathbf{O} \rho^{(c)}] = \sum_{\alpha=1}^{n_{\text{ens}}} p_\alpha \langle \mathbf{O} \rangle_\alpha. \quad (\text{A.30})$$

In the following, we derive the relationship of  $C_{i \neq j}$  with the correlation function of the individual Gaussian ensemble members:

$$D^{(\alpha)} = U^{(\alpha)}U^{(\alpha)\dagger}, \quad D_{ij}^{(\alpha)} = \langle \psi^{(\alpha)} | \mathbf{c}_i^\dagger \mathbf{c}_j | \psi^{(\alpha)} \rangle = \langle \mathbf{c}_i^\dagger \mathbf{c}_j \rangle_\alpha.$$

The first part in the correlator can be written as

$$\overline{\langle \langle \mathbf{n}_i \rangle \rangle \cdot \langle \langle \mathbf{n}_j \rangle \rangle} = \overline{\sum_{\alpha, \alpha'} p_\alpha p_{\alpha'} D_{ii}^{(\alpha)} D_{jj}^{(\alpha')}}, \quad (\text{A.31})$$

where  $D_{ij}^{(\alpha)}$  corresponds to the correlation function of the individual ensemble members. The remaining part of the correlator:

$$\overline{\langle \langle \mathbf{n}_i \mathbf{n}_j \rangle \rangle} = \overline{\langle \langle \mathbf{c}_i^\dagger \mathbf{c}_i \mathbf{c}_j^\dagger \mathbf{c}_j \rangle \rangle} = \overline{\sum_{\alpha} p_\alpha \langle \mathbf{c}_i^\dagger \mathbf{c}_i \mathbf{c}_j^\dagger \mathbf{c}_j \rangle_\alpha} \quad (\text{A.32})$$

can be simplified (using Wicks theorem as in (A.29)):

$$\overline{\langle \langle \mathbf{n}_i \mathbf{n}_j \rangle \rangle} = \overline{\sum_{\alpha} p_\alpha \left( D_{ii}^{(\alpha)} D_{jj}^{(\alpha)} - |D_{ij}^{(\alpha)}|^2 + D_{ii}^{(\alpha)} \delta_{ij} \right)}. \quad (\text{A.33})$$

In summary, the density-density correlation function is given by

$$C_{ij} = \overline{\sum_{\alpha, \alpha'} p_\alpha p_{\alpha'} D_{ii}^{(\alpha)} D_{jj}^{(\alpha')}} - \overline{\sum_{\alpha} p_\alpha \left( D_{ii}^{(\alpha)} D_{jj}^{(\alpha)} - |D_{ij}^{(\alpha)}|^2 + D_{ii}^{(\alpha)} \delta_{ij} \right)}, \quad (\text{A.34})$$

only requiring the knowledge of the probabilities  $p_\alpha$  and the corresponding correlation matrices  $D^{(\alpha)}$ .

**Remark:** In the limit of  $\gamma_B/J \sim \mathcal{O}(1)$  or  $\gamma_M/J \sim \mathcal{O}(1)$ , fluctuations between the different ensemble members become large. For a finite number of trajectories, this can even result in negative values for  $C_{ij}$  (see, e.g., Fig. 4.17(b) for the visible effect of those fluctuations at  $\gamma_B/J = 4$ ). We assume that a larger ensemble size could mitigate this issue, which nevertheless is not a practical option.

---

**Limiting the ensemble size:** For any practical purposes, we have to limit the ensemble size to some finite number  $n_{\text{ens}}$  of states, each coming with a weight  $p_\alpha$ . During the time evolution, these weights are updated, eventually resulting in some weights becoming vanishingly small, ‘depleting’ the ensemble. To counteract this effect, we use a recycling procedure, introduced in Ref. [239] (for this context). Initially, we set some threshold  $p_{\text{thres}}$  ( $p_{\text{thres}} = 10^{-4}$  for  $n_{\text{ens}} = 500$  if not stated differently):

1. Identify the states with  $p_\alpha < p_{\text{thres}}$ .
2. Identify the *most likely* state with  $p_\beta = p_{\text{max}}$  and replace  $|\psi^{(\alpha)}\rangle$  by a copy of  $|\psi^{(\beta)}\rangle$ .
3. Change the weights of the original state  $|\psi^{(\beta)}\rangle$  and its copy to half its value:  $p_\alpha, p_{\text{max}} \rightarrow p_\alpha = p_\beta = p_{\text{max}}/2$ .

4. Normalize the full set of probabilities.

The idea is that by ‘recycling’ the most likely state, the ensemble is essentially unchanged without reducing the ensemble size:

$$p_\alpha |\psi^{(\alpha)}\rangle\langle\psi^{(\alpha)}| + p_\beta |\psi^{(\beta)}\rangle\langle\psi^{(\beta)}| \approx \frac{p_\beta}{2} |\psi^{(\beta)}\rangle\langle\psi^{(\beta)}| + \frac{p_\beta}{2} |\psi^{(\beta)}\rangle\langle\psi^{(\beta)}|.$$

### A.3 Numerical Parameters

The numerical simulations of the fermion systems are based on the parameters:  $L$  (system size),  $J\delta t$  (time step),  $JT$  (running time),  $n_{\text{avg}}$  (number of independent runs) and  $n_{\text{ens}}$  (ensemble size, if applicable). The initial state is chosen to be  $\rho_{t=0}^{(c)} = |\psi\rangle\langle\psi|$  with  $|\psi\rangle = |0101\dots\rangle$ .

	$L$	$J\delta t$	$JT$	$n_{\text{avg}}$
Fig. 4.12	10	0.01	40	400
Fig. 4.18(top)	10	0.02	20-80	400
Fig. 4.13	8	0.01	40	400

**Table A.1:** Numerical parameters used for the simulation of the full conditional density matrix where longer times corresponds to  $\gamma_M/J = 0.1, 0.2$ .

	$L$	$J\delta t$	$JT$	$n_{\text{ens}}$	$n_{\text{avg}}$
Fig. 4.17(a) (top)	128	0.05	200	500	50
Fig. 4.17(b),(c) (top)	192	0.05	200-300	500	400
	256	0.05	200	500	200
Fig. 4.18(bottom)	128, 192	0.05	200	500	50
Fig. 4.10(a)	256-512	0.05	300	-	400
	768	0.05	300	-	200

**Table A.2:** Numerical parameters for the ensemble simulations with the initial condition given in the text, where only for Fig. 4.17(a) top an ensemble of random number eigenstates has been used.

**Technical remark:** For this work, the following programs/languages have been used:

- Wolfram Mathematica (in particular in the context of the AIA approximation)
- Programming language Julia with different packages (in particular for the trajectory simulations and for solving the RG equations)

# B | Keldysh Field Theory for a (bosonic) Master Equation

In the following we will derive the path integral representation of a master equation for real bosonic operators (see also, e.g., Ref. [4]). Irrespective of the kinds of operators which are used, the strategy is always the same: use eigenstates of the basic operators (e.g. coherent states for annihilation operators) and insert identity operators, constructed from these eigenstates at proper places. For the real bosonic operators which we consider here, we make use of canonical commutation relations and the eigenstates of  $\phi_x$  and  $\Theta_x = \frac{\partial_x \theta_x}{\pi}$ :

$$[\Theta_x, \phi_{x'}] = -i\delta(x - x') \quad \begin{cases} \phi_x |\phi_x\rangle = \phi_x |\phi_x\rangle, \\ \Theta_x |\Theta_x\rangle = \Theta_x |\Theta_x\rangle, \\ \langle \phi_x | \Theta_x \rangle = e^{i\Theta_x \phi_x}. \end{cases} \quad (\text{B.1})$$

Starting point is the (time discrete) quantum master equation for hermitian Lindblad operators  $\mathbf{L} = \mathbf{L}^\dagger$  and a density matrix  $\rho_N$  at time step  $N$  (for simplicity we just consider a single one, the generalization is straightforward):

$$\rho_N = \rho_{N-1} + \delta t \left( -i[\mathbf{H}, \rho_{N-1}] + \mathbf{L}\rho_{N-1}\mathbf{L} - \frac{1}{2}(\mathbf{L}^2\rho_{N-1} + \rho_{N-1}\mathbf{L}^2) \right). \quad (\text{B.2})$$

We are finally interested in calculating expectation values  $\langle \mathcal{O} \rangle = \text{tr}[\mathcal{O}\rho_N]$ . To do so, we start by going into a new basis using completeness relations for  $\phi$  and  $\Theta$ . With the index  $\pm$  we indicate whether the identities have been inserted to the right (+) or to the left (-) of  $\rho$ :

$$\begin{aligned} \rho_N &= \mathbb{1}_{\Theta_{N,+}} \mathbb{1}_{\phi_{N,+}} \rho_N \mathbb{1}_{\phi_{N,-}} \mathbb{1}_{\Theta_{N,-}} \\ &= \int d\Theta_{N,+} d\Theta_{N,-} d\phi_{N,+} d\phi_{N,-} e^{-i\Theta_{N,+}\phi_{N,+}} e^{+i\Theta_{N,-}\phi_{N,-}} \langle \phi_{N,+} | \rho_N | \phi_{N,-} \rangle | \Theta_{N,+} \rangle \langle \Theta_{N,-} |. \end{aligned}$$

We can iterate this procedure by expressing  $\rho_N$  in terms of  $\rho_{N-1}$  using the rhs of (B.2). Afterwards, we insert an additional set of identities (this time with index  $N-1$ ). All resulting terms are of the form ( $\mathbf{A}, \mathbf{B}$  some arbitrary operators

depending on  $\Theta, \phi$ ):

$$\begin{aligned} \langle \phi_{N,+} | \mathbf{A} \rho_{N-1} \mathbf{B} | \phi_{N,-} \rangle &= \langle \phi_{N,+} | \mathbb{1}_{\Theta_{N-1,+}} \mathbf{A} \mathbb{1}_{\phi_{N-1,+}} \rho_{N-1} \mathbb{1}_{\phi_{N-1,-}} \mathbf{B} \mathbb{1}_{\Theta_{N-1,-}} | \phi_{N,-} \rangle \\ &= e^{i\Theta_{N-1,+}(\phi_{N,+} - \phi_{N-1,+})} e^{-i\Theta_{N-1,-}(\phi_{N,-} - \phi_{N-1,-})} \times \\ &A(\phi_{N-1,+}, \Theta_{N-1,+}) B(\phi_{N-1,-}, \Theta_{N-1,-}) \langle \phi_{N-1,+} | \rho_{N-1} | \phi_{N-1,-} \rangle. \end{aligned}$$

Using this expression together with (B.2), we get

$$\begin{aligned} \rho_N &= \int d(\dots) e^{i\Theta_{N-1,+}(\phi_{N,+} - \phi_{N-1,+})} e^{-i\Theta_{N-1,-}(\phi_{N,-} - \phi_{N-1,-})} \\ &\quad \times \left( 1 + \delta t \left[ -iH(\Theta_{N-1,+}, \phi_{N-1,+}) + iH(\Theta_{N-1,-}, \phi_{N-1,-}) + 2L(\phi_{N-1,+})L(\phi_{N-1,-}) \right. \right. \\ &\quad \left. \left. - \frac{1}{2}(L^2(\phi_{N-1,+}) + L^2(\phi_{N-1,-})) \right] \right) \\ &\quad \times \langle \phi_{N-1,+} | \rho_{N-1} | \phi_{N-1,-} \rangle e^{-i\Theta_{N,+}\phi_{N,+}} e^{+i\Theta_{N,-}\phi_{N,-}} | \Theta_{N,+} \rangle \langle \Theta_{N,-} |, \end{aligned}$$

where  $d(\dots)$  contains all the integration elements from  $\mathbb{1}_N, \mathbb{1}_{N-1}$  insertions. Repeating this construction, we can compactly write down a path integral representation of the density matrix (valid in the limit  $\delta t \rightarrow 0$ ):

$$\begin{aligned} \rho_N &\approx \int \mathcal{D}[\phi_{\pm}, \Theta_{\pm}] e^{iS} \underbrace{\langle \phi_{0,+} | \rho_0 | \phi_{0,-} \rangle}_{\text{initial condition}} e^{-i\Theta_{N,+}\phi_{N,+}} e^{+i\Theta_{N,-}\phi_{N,-}} | \Theta_{N,+} \rangle \langle \Theta_{N,-} | \\ S &:= \sum_{j=1}^N \delta t \sum_{\sigma=\pm} \left( +\sigma (\Theta_{j-1,\sigma} \Delta_t \phi_{j,\sigma} - H_{j-1,\sigma}) + \frac{i}{2} L_{j-1,\sigma}^2 \right) - 2iL_{j-1,+}L_{j-1,-}. \end{aligned}$$

Here,  $H_{j-1,\sigma}$  corresponds to the Hamiltonian where the operators have been replaced with the fields at time step  $j-1$  and contour index  $\sigma$ .

# C | AIA vs. exact Results, Fitting and adiabatic non- perturbative Contributions

This discussion is adapted from the publication [42].

For the minimal (spin) model with  $z = 3$ , we can directly compare the exact result (Landau-Zener) for  $\hat{t}_i = -\infty$  and  $\hat{t}_f = +\infty$  with the AIA approximation, which in this case is based on  $p_k = |\langle -(\hat{t}_k^*) | +(-\hat{t}_k^*) \rangle_k|^2$ . The adiabaticity breaking time  $\hat{t}_k^*$  is extracted from the same expression, (3.68), discussed before with  $\hat{\mu}_k = 0$ . As anticipated, the agreement is quite good, also for the generalized drive scenario with two drive scales. The Landau-Zener result indicates that the (asymptotic) contribution to the excitation density is non-analytic. This is also the case for higher order drives in the limit  $\hat{t}_{k,f} \rightarrow +\infty$  and a slow drive  $\hat{v}_k \rightarrow 0$ .

The leading contribution stems from complex zeros of the energy difference  $\mathcal{E}(\hat{t}_k^{c,l}, k)$  ( $n$  zeros for an order  $n$  drive) in the complex time plane:

$$\mathcal{E}(\hat{t}_k^{c,l}, k) = 0, \quad (\hat{t}_k^{c,l})^n = \left( \frac{-\hat{\mu}_k \pm i}{\hat{v}_k} \right).$$

The excitation density at momentum  $k$  is given by a sum of the non-analytic

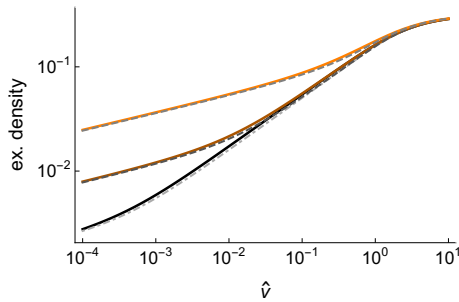


**Figure C.1:** Excitation density (log-log) for the minimal model ( $z = 3$ ): AIA approximation (full lines) vs. the exact results (dashed lines) for  $\phi - \pi/2 = 10^{-2}, 10^{-5}, 10^{-8}$  (from top to bottom).

contributions [85, 86]:

Dykhne-Davis-Pechukas (DDP) approximation :

$$p_k \approx \left| \sum_{l=1}^n \sigma_l \exp \left( i \mathcal{D}(\hat{t}_k^c, l) \right) \right|^2, \quad \mathcal{D}(\hat{t}_k) := 2 \int_0^{\hat{t}_k} \mathcal{E}(\tau') d\tau', \quad (\text{C.1})$$

$$\sigma_l = 4i \lim_{\hat{t}_k \rightarrow \hat{t}_c^l} (\hat{t}_k - \hat{t}_c^l) \gamma(\hat{t}_k) = \pm 1.$$

From  $\mathcal{D}(\hat{t}_k)$ , we can extract the leading scaling. By rescaling time  $\hat{v}_k \hat{t}^n = y^n$ , we get

$$\mathcal{D}(\hat{t}_c) = \hat{v}_k^{-\frac{1}{n}} 2 \int_0^{y(\hat{t}_c)} \mathcal{E}(y) dy =: \hat{v}_k^{-\frac{1}{n}} \mathcal{I}(\hat{\mu}_k). \quad (\text{C.2})$$

The integral  $\mathcal{I}(\hat{\mu}_k)$  only depends on  $\hat{\mu}_k$ . If the integral is a constant (as a function of  $k$ ) to good approximation, the behavior of  $\hat{v}_k$  determines the scaling of  $n_E$ . It takes the role of an adiabaticity parameter (see also Ref. [140] for the quadratic case): once  $\hat{v}_k \gtrsim 1$  the excitation is of order  $\mathcal{O}(1)$  in agreement with adiabaticity breaking. This approximation reproduces the exact Landau-Zener-Majorana-Stückelberg [46–48] for  $n = 1$ . In this case, only one pole contributes and we get

$$p_k(\hat{t}_{k,f} \rightarrow \infty) \approx \exp(-2\text{Im}\mathcal{D}(\hat{t}_k^c)) = \exp(-\pi \hat{v}_k^{-1}). \quad (\text{C.3})$$

**Fitting approach:** In the main text, we used the fitting function

$$n_{\text{fit}}(\hat{v}) = A \left( \left( 1 + \left( \frac{\hat{v}}{\hat{v}^*} \right)^{\frac{\alpha_{\perp} - \alpha_{\parallel}}{p}} \right) \hat{v}^{\frac{\alpha_{\parallel}}{p}} \right)^p \quad (\text{C.4})$$

to extract (i) the scaling exponents from  $\alpha_{\perp}$  and  $\alpha_{\parallel}$  and (ii) the crossover velocity  $\hat{v}^*$ . In Fig. C.2, examples of  $n_E(\hat{v}; \phi)$  and the fits for the transverse XY model are shown (compare also to Fig. 3.8 again). The fits are in good agreement with the AI data. Note that we keep the parameter  $p$  as a free parameter as well. Its values are shown in Fig. C.2(b).

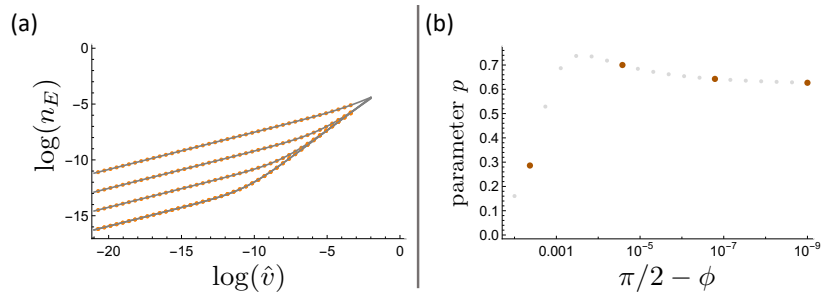


**Figure C.2:** Transverse XY model: **(a)** AI approximation for  $n_E(\hat{v}; \phi)$  for different angles (orange dots) and the numerical fits  $f(\hat{v})$  (gray lines). **(b)** Extracted parameter  $p$  for different angles. The red marked dots correspond to the  $\phi$  values used in (a) (from left to right in (b) corresponds to top to bottom in (a)). The values of  $\phi$  correspond to the ones used in the main text Fig. 3.8.



# D | Bosonization

## General Construction & Linear Dispersion

We discuss the idea of bosonization and follow Ref. [202] due to its technical clarity (though we leave out some fine details), but also keep notational connection to Ref. [205]. We use a Hamiltonian with a linear dispersion although the bosonization identities do not rely on the linear nature of the dispersion. Note that in our notation the length of the system is  $La$  ( $L$ : number of lattice sites,  $a$ : lattice distance). There is an infinite, but discrete, set of momenta  $k = \frac{2\pi}{La} \cdot m$  with  $m \in \mathbb{Z}$ .

As we have already mentioned in the main text (see (4.8)), we consider the full field operator for  $\eta$ -fermions in real space (where  $\eta$  can, e.g., correspond to a replica index or contour index etc.):

$$\psi_{\eta,x} \approx e^{-ik_F x} \frac{1}{\sqrt{La}} \sum_{k=-\infty}^{\infty} e^{ikx} c_{-, \eta, k} + e^{+ik_F x} \frac{1}{\sqrt{La}} \sum_{k=-\infty}^{\infty} e^{-ikx} c_{+, \eta, k}. \quad (\text{D.1})$$

The ground state |GS) is given by the state with all  $k < 0$  ( $\sigma, \eta$ )-fermion states filled. The basic particle-hole excitations on top of this state are given by

$$\left. \begin{aligned} \mathbf{b}_{\sigma, \eta, q > 0}^\dagger &= i \left( \frac{2\pi}{La|q|} \right)^{1/2} \sum_{k=-\infty}^{\infty} c_{\sigma, \eta, k+q}^\dagger c_{\sigma, \eta, k}, \\ \mathbf{b}_{\sigma, \eta, q} &= -i \left( \frac{2\pi}{La|q|} \right)^{1/2} \sum_{k=-\infty}^{\infty} c_{\sigma, \eta, k-q}^\dagger c_{\sigma, \eta, k}, \end{aligned} \right\} [\mathbf{b}_{\sigma, \eta, q}, \mathbf{b}_{\sigma', \eta', q'}^\dagger] = \delta_{qq'} \delta_{\sigma\sigma'} \delta_{\eta\eta'}. \quad (\text{D.2})$$

The structural relation between the fermionic Hilbert/Fock space and the bosonic creation/annihilation operators is summarized in Fig. D.1. One key ingredient is that for a fixed number of ( $\sigma, \eta$ )-fermions, collected in  $\vec{N}$  (relative to the ground state), each state  $|\psi_{\vec{N}}\rangle \in \mathcal{H}_{\vec{N}}$  can be reached by applying a proper function of bosonic creation operators:  $|\psi_{\vec{N}}\rangle = f(\mathbf{b}^\dagger)|\vec{N}\rangle_0$  [202] onto the bosonic vacuum state  $|\vec{N}\rangle_0$  ( $\mathbf{b}_{\sigma, \eta, q}|\vec{N}\rangle_0 = 0$ ). To transfer between different fermion numbers, the Klein factor is introduced as

$$U_{\sigma, \eta}^\dagger |\psi_{\vec{N}}\rangle = f(\mathbf{b}^\dagger) \mathbf{c}_{q_{\min}, \sigma, \eta}^\dagger |\vec{N}_0\rangle,$$

where  $\mathbf{c}_{q_{\min}, \sigma, \eta}^\dagger$  creates a ( $\sigma, \eta$ )-fermion in the lowest unoccupied mode.

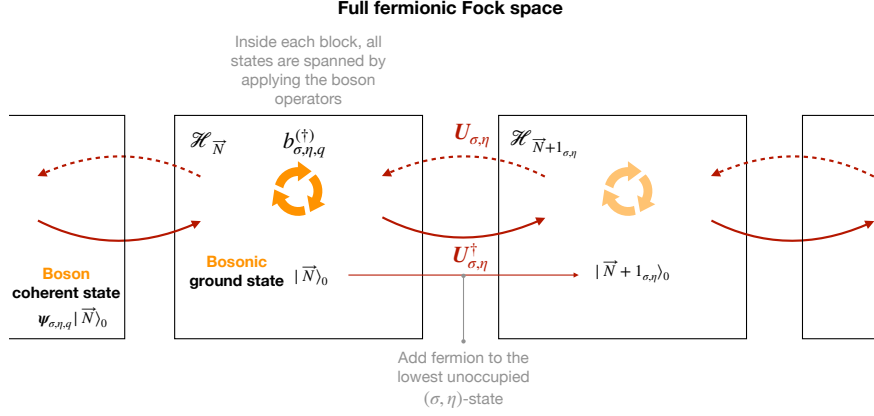


**Figure D.1:** Schematic relations between the fermionic operators  $\psi_{\sigma, \eta, q}$  in Fock space  $\mathcal{F}$  and the bosonic ones (which span the entire Hilbert space for a fixed fermion number  $\vec{N}$  (including different species of fermions, labelled by  $\sigma, \eta$ )). Notation partly adapted from Ref. [202, 205].

**Actual construction:** Similarly to the heuristic discussion, we like to define a field operator  $\phi_{\sigma, \eta, x}$  by looking at the fermionic density:

$$\rho_{\sigma, \eta, x} \stackrel{!}{=} \underbrace{\rho_{0, \sigma, \eta}}_{\text{mean density}} - \underbrace{\frac{1}{\pi} \partial_x \phi_{\sigma, \eta, x}}_{\text{fluctuations}}. \quad (\text{D.3})$$

Due to the infinite amount of occupied states, a meaningful density is the normal-ordered<sup>1</sup> one, denoted by<sup>2</sup>  ${}^* \dots {}^*$ :

$$\begin{aligned} \rho_{\sigma, \eta, x} &= {}^* \psi_{\sigma, \eta, x}^\dagger \psi_{\sigma, \eta, x} {}^* = \frac{1}{La} \sum_q e^{-i\sigma qx} \sum_{k=-\infty}^{\infty} {}^* c_{\sigma, \eta, k-q}^\dagger c_{\sigma, \eta, k} {}^* \\ &= \underbrace{\frac{i}{La} \sum_{q>0} \sqrt{\frac{La|q|}{2\pi}} \left( e^{-i\sigma qx} \mathbf{b}_{\sigma, \eta, q} - e^{+i\eta qx} \mathbf{b}_{\sigma, \eta, q}^\dagger \right)}_{=:-\frac{1}{\pi} \partial_x \phi_{\sigma, \eta, x}} + \frac{1}{La} \underbrace{\sum_{k=-\infty}^{\infty} {}^* c_{\sigma, \eta, k}^\dagger c_{\sigma, \eta, k} {}^*}_{=: \mathbf{N}_{\sigma, \eta}}. \end{aligned} \quad (\text{D.4})$$

(D.5)

The operators  $\phi_{\sigma, \eta, x}$  are defined as:

$$\phi_{\sigma, \eta, x} = + \lim_{A \rightarrow 0} \frac{\sigma \pi}{La} \sum_{q>0} \sqrt{\frac{La|q|}{2\pi}} e^{-Aq/2} \frac{1}{q} \left( e^{-i\sigma qx} \mathbf{b}_{\sigma, \eta, q} + e^{+i\sigma qx} \mathbf{b}_{\sigma, \eta, q}^\dagger \right), \quad (\text{D.6})$$

which are regularized by  $A$ , an effective inverse momentum scale (e.g.  $\Lambda^{-1}$ ) [202]. For a model, where modes had to be artificially added, the allowed values of  $q$  in  $\mathbf{b}_{\sigma, \eta, q}^\dagger$  have to be restricted. Otherwise non-physical modes would play a role. This is achieved by the exponential factor, limiting the range  $q \lesssim 1/A$

<sup>1</sup>With respect to the fermionic vacuum state |GS).

<sup>2</sup>Meaning:  ${}^* \psi_{\sigma, \eta, x}^\dagger \psi_{\sigma, \eta, x} {}^* = \psi_{\sigma, \eta, x}^\dagger \psi_{\sigma, \eta, x} - \langle \text{GS} | \psi_{\sigma, \eta, x}^\dagger \psi_{\sigma, \eta, x} | \text{GS} \rangle$ .

(though formally the limit  $A \rightarrow 0$  has to be taken). These fields have the property<sup>3</sup> (for  $A \rightarrow 0$ )

$$[\phi_{\sigma,\eta,x}, \partial_{x'} \phi_{\sigma',\eta',x'}] = \delta_{\sigma\sigma'} \delta_{\eta\eta'} \frac{1}{2} \pi i \sigma \left( \sum_{m \in \mathbb{Z}} \delta(x - x' - mL a) - \frac{1}{L a} \right) \quad (\text{D.7})$$

$$\xrightarrow{L \rightarrow \infty} \delta_{\sigma\sigma'} \delta_{\eta\eta'} \frac{1}{2} \pi i \sigma \delta(x - x'). \quad (\text{D.8})$$

As we have already argued heuristically, the fermionic operators should be an exponential function of bosonic operators:  $\psi \sim \exp(B(\mathbf{b}, \mathbf{b}^\dagger))$ . By checking the commutators with  $\mathbf{b}, \mathbf{b}^\dagger$

$$\begin{aligned} [\mathbf{b}_{\sigma,\eta,q}^\dagger, \psi_{\sigma,\eta,x}] &= -i \sqrt{\frac{2\pi}{L a |q|}} e^{-i\sigma q x} \psi_{\sigma,\eta,x}, \\ [\mathbf{b}_{\sigma,\eta,q}, \psi_{\sigma,\eta,x}] &= \left( -i \sqrt{\frac{2\pi}{L a |q|}} e^{-i\sigma q x} \right)^* \psi_{\sigma,\eta,x}, \end{aligned} \quad (\text{D.9})$$

we can find the expression for  $\psi_{\sigma,\eta,x}$ . First, we probe these commutators onto the bosonic ground states  $|\vec{N}\rangle_0$ . We see that  $\psi_{\sigma,\eta,q} |\vec{N}\rangle_0$  is an eigenstate of  $\mathbf{b}$  [202]:

$$\mathbf{b}_{\sigma,\eta,q} (\psi_{\sigma,\eta,q} |\vec{N}\rangle_0) = i \sqrt{\frac{2\pi}{L a |q|}} e^{i\sigma q x} (\psi_{\sigma,\eta,q} |\vec{N}\rangle_0). \quad (\text{D.10})$$

Therefore, it is a *coherent state* (see again info box in Sec. 2.1.2). In terms of  $\mathbf{b}^\dagger$ , it takes the (anticipated) form

$$\psi_{\sigma,\eta,q} |\vec{N}\rangle_0 = U_{\sigma,\eta} \lambda_{\sigma,\eta} \exp \left[ \sum_{q>0} i \sqrt{\frac{2\pi}{L a |q|}} e^{i\sigma q x} \mathbf{b}_{\sigma,\eta,q}^\dagger \right] |\vec{N}\rangle_0. \quad (\text{D.11})$$

Here,  $U_{\sigma,\eta}$  decreases the fermion number by one and  $\lambda_{\sigma,\eta}$  is some phase factor (operator) (which we determine later). This fits to a refined ansatz of the form  $\psi \sim \exp(i\varphi^\dagger(\mathbf{b}^\dagger)) \exp(i\varphi'(\mathbf{b}))$ , since the last factor only contributes a factor of 1 once acting onto  $|\vec{N}\rangle_0$ . To find the general form of  $\psi_{\sigma,\eta,x}$  we use this ansatz and the identity

$$[\mathbf{A}, e^{\mathbf{B}}] = \mathbf{C} e^{\mathbf{B}}, \quad \mathbf{C} := [\mathbf{A}, \mathbf{B}] \quad \text{valid for } [\mathbf{A}, \mathbf{C}] = [\mathbf{B}, \mathbf{C}] = 0, \quad (\text{D.12})$$

and find from Eq. (D.9):

$$\varphi_{\sigma,\eta,x}^\dagger = \sum_q \sqrt{\frac{2\pi}{L a |q|}} e^{+i\sigma q x} \mathbf{b}_{\sigma,\eta,q}^\dagger, \quad \varphi'_{\sigma,\eta,x} = \varphi_{\sigma,\eta,x} \quad (\text{D.13})$$

(compare to Eq. (D.6)). Therefore, we get<sup>4</sup>

$$\psi_{\sigma,\eta,x} = U_{\sigma,\eta} \lambda_{\sigma,\eta} e^{+i\varphi_{\sigma,\eta,x}} e^{+i\varphi_{\sigma,\eta,x}^\dagger} = \left( \frac{L a}{2\pi A} \right)^{1/2} U_{\sigma,\eta} \lambda_{\sigma,\eta} e^{i\sigma 2\phi_{\sigma,\eta,x}}. \quad (\text{D.14})$$

<sup>3</sup>By using the bosonic commutation relations and the Poisson formula.

<sup>4</sup>Note that we are using a slightly different convention compared to Ref. [202]. In particular, we have:  $2\sigma\phi_{\sigma,\eta,x} = (\varphi_{\sigma,\eta,x} + \varphi_{\sigma,\eta,x}^\dagger)$ .

In the second equality, we have used the Baker-Campbell-Hausdorff<sup>5</sup> relation to identify  $\phi_{\sigma,\eta,x}$ . Finally, we need to identify the operator  $\lambda_{\sigma,\eta}$  and therefore the missing (exact) prefactor, where we only need to consider  $|\vec{N}\rangle_0$  and [202]

$${}_0\langle\vec{N}|\mathbf{U}_{\sigma,\eta}^\dagger\mathbf{c}_{\sigma,\eta,k}|\vec{N}\rangle_0 = \begin{cases} 1 & k = \frac{2\pi}{La}N_{\sigma,\eta}, \\ 0 & \text{otherwise.} \end{cases} \quad (\text{D.15})$$

Here,  $N_{\sigma,\eta}$  is the number of  $(\sigma,\eta)$ -fermions in the state  $|\vec{N}\rangle_0$ . Therefore, the combination  $\mathbf{U}_{\sigma,\eta}^\dagger\psi_{\sigma,\eta,x}$  leaves the fermion number unchanged, and the overlap reads

$${}_0\langle\vec{N}|\mathbf{U}_{\sigma,\eta}^\dagger\psi_{\sigma,\eta,x}|\vec{N}\rangle_0 = \lambda_{\sigma,\eta} = \frac{1}{\sqrt{La}}e^{-i\sigma\frac{2\pi}{La}N_{\sigma,\eta}x}. \quad (\text{D.16})$$

Updating the number  $\lambda_{\sigma,\eta}$  to an operator, the fermion operator is exactly identical to

$$\psi_{\sigma,\eta,x} = \frac{1}{\sqrt{2\pi A}}\mathbf{U}_{\sigma,\eta}e^{-i\sigma\frac{2\pi}{La}N_{\sigma,\eta}x}e^{i\sigma 2\phi_{\sigma,\eta,x}}. \quad (\text{D.17})$$

Based on these operators and the commutation relation (D.8) (in the  $L \rightarrow \infty$  limit), we can construct the operators  $\phi_{\eta,x}$  and  $\theta_{\eta,x}$ , which fulfill  $[\phi_{\eta,x}, \partial_x\theta_{\eta',x'}] = \delta_{\eta\eta'}i\pi\delta(x-x')$  [205]:

$$\phi_{\eta,x} := (\phi_{+,\eta,x} + \phi_{-,\eta,x}), \quad \theta_{\eta,x} := (\phi_{+,\eta,x} - \phi_{-,\eta,x}). \quad (\text{D.18})$$

Using these, the fermion operators takes the form

$$\psi_{\sigma,\eta,x} = \frac{1}{\sqrt{2\pi A}}\mathbf{U}_{\sigma,\eta}e^{-i\sigma\frac{2\pi}{La}N_{\sigma,\eta}x}e^{-i\sigma\phi_{\eta,x}+i\theta_{\eta,x}}. \quad (\text{D.19})$$

### Bosonized Hamiltonian: Linear Dispersion

As we have already argued, the bosonic modes are particle-hole excitations. For a linear model

$$\mathbf{H} = \sum_{\sigma,\eta} \sum_{k=-\infty}^{\infty} v_F k^* \mathbf{c}_{\sigma,\eta,k}^\dagger \mathbf{c}_{\sigma,\eta,k^*}, \quad (\text{D.20})$$

with energy eigenstate  $|\epsilon\rangle$  we have:

$$[\mathbf{H}, \mathbf{b}_{\sigma,\eta,q}^\dagger] = v_F q \mathbf{b}_{\sigma,\eta,q}^\dagger \quad \Rightarrow \quad \mathbf{H} \mathbf{b}_{\sigma,\eta,q}^\dagger |\epsilon\rangle = (\epsilon + v_F q) \mathbf{b}_{\sigma,\eta,q}^\dagger |\epsilon\rangle, \quad (\text{D.21})$$

meaning that by acting with  $\mathbf{b}^\dagger$ 's, we can create (arbitrary) energy eigenstates (actually all of them). From this we can already anticipate the form of the Hamiltonian in bosonic terms:

$$\mathbf{H} = \sum_{\sigma,\eta} \sum_{q>0} v_F q \mathbf{b}_{\sigma,\eta,q}^\dagger \mathbf{b}_{\sigma,\eta,q} + (\text{ground state contribution}). \quad (\text{D.22})$$

<sup>5</sup>We need to evaluate the commutator  $[\phi_{\sigma,\eta,x}, \phi_{\sigma,\eta,x'}] = \dots = \frac{1}{4} \sum_{m=-\infty}^{\infty} \frac{1}{m} e^{-m(\frac{2\pi A}{La} - i\sigma\frac{2\pi}{La}(x-x'))} = -\frac{1}{4} \ln\left(1 - e^{-\frac{2\pi}{La}(A+i\sigma(x-x'))}\right)$ , which for  $L \rightarrow \infty$  reproduces the above result (see Ref. [202] for more details).

The second contribution can be determined by looking at the bosonic vacuum states  $|\vec{N}\rangle_0$  containing no excitations [202]. Since the Hamiltonian does not change the number of  $(\sigma, \eta)$ -fermions, the states  $|\vec{N}\rangle_0$  are indeed eigenstates with an energy (where the  $k$ 's are multiples of  $\frac{2\pi}{La}$ ):

$${}_0\langle\vec{N}|\mathbf{H}|\vec{N}\rangle_0 = \frac{2\pi}{La}v_F \sum_{\sigma,\eta} \frac{1}{2}N_{\sigma,\eta}(N_{\sigma,\eta} + 1). \quad (\text{D.23})$$

Therefore, in terms of bosonic creation and annihilation operators we have

$$\mathbf{H} = \sum_{\sigma,\eta} \left[ v_F \sum_{q>0} q \mathbf{b}_{\sigma,\eta,q}^\dagger \mathbf{b}_{\sigma,\eta,q} + \frac{2\pi}{La} \frac{v_F}{2} \mathbf{N}_{\sigma,\eta} (\mathbf{N}_{\sigma,\eta} + 1) \right]. \quad (\text{D.24})$$

The first term is just equivalent to

$$\int dx \frac{v_F}{\pi} {}^* (\partial_x \phi_{\sigma,\eta,x})^2 {}^* = \int dx \frac{v_F}{2\pi} {}^* [(\partial_x \phi_{\eta,x})^2 + (\partial_x \theta_{\eta,x})^2] {}^*, \quad (\text{D.25})$$

which gives rise to the familiar bosonized form of the (Dirac) Hamiltonian (the normal ordering for bosons refers to  $|\vec{N}\rangle_0$ ).

**Remark (full density):** The full density operator is expressed as

$$\begin{aligned} \psi_{\eta,x}^\dagger \psi_{\eta,x} &= \psi_{+,\eta,x}^\dagger \psi_{+,\eta,x} + \psi_{-,\eta,x}^\dagger \psi_{-,\eta,x} + \left( e^{2ik_F x} \psi_{-,\eta,x}^\dagger \psi_{+,\eta,x} + \text{h.c.} \right) \\ &= -\frac{1}{\pi} \partial_x \phi_{\eta,x} + \frac{1}{2\pi A} \left( \mathbf{U}_{+,\eta}^\dagger \mathbf{U}_{-,\eta} e^{2ik_F x} e^{-i\frac{2\pi}{La}(\mathbf{N}_{+,\eta} + \mathbf{N}_{-,\eta})} e^{2i\phi_{\eta,x}} + \text{h.c.} \right), \end{aligned}$$

where we already see that the second term, corresponding to a conversion of  $(+ \leftrightarrow -)$  fermions, cannot be entirely expressed in terms of bosonic operators. Furthermore, since  $\mathbf{U}_+^\dagger \mathbf{U}_- \neq \mathbf{U}_-^\dagger \mathbf{U}_+$ , the term cannot simply be identified as a  $\cos(2\phi_{\eta,x} + \dots)$ . Nevertheless, in many cases it might be acceptable to make such an identification (see, e.g., Ref. [206] for a discussion).



# E | Heating Dynamics

## E.1 Lindblad Dynamics from weak System-Bath Coupling

The derivation, leading to the Lindblad equation, in the main text is based on a simplified model. A more ‘physical’ approach is presented here, even though it parallels much of the original discussion (following Refs. [16, 50]). The overall model is  $\mathbf{H} = \mathbf{H}_S + \mathbf{H}_B + \mathbf{H}_{\text{int}}$  and we work in the interaction picture

$$\tilde{\mathbf{H}}_{\text{int}} = \sum_l \tilde{\mathbf{S}}_l \otimes \tilde{\mathbf{B}}_l, \quad (\text{E.1})$$

with  $\tilde{\mathbf{S}}_l$  and  $\tilde{\mathbf{B}}_l$  hermitian operators on  $\mathcal{H}_S$  and  $\mathcal{H}_B$ . The time evolution of the system-bath density matrix  $\tilde{\rho}$  is given by the exact von Neumann equation:

$$\partial_t \tilde{\rho} = -i [\tilde{\mathbf{H}}_{\text{int}}, \tilde{\rho}(t)] = -i [\tilde{\mathbf{H}}_{\text{int}}, \tilde{\rho}(0)] - \int_0^t ds [\tilde{\mathbf{H}}_{\text{int}}(t), [\tilde{\mathbf{H}}_{\text{int}}(s), \tilde{\rho}(s)]]. \quad (\text{E.2})$$

We initially assume that  $\rho \approx \rho_S \otimes \rho_B$  and  $[\rho_B, \mathbf{H}_B] = 0$ . Furthermore, we assume that

$$\text{Born approx.: } \tilde{\rho}(t) \approx \tilde{\rho}_S(t) \otimes \tilde{\rho}_B. \quad (\text{E.3})$$

Loosely speaking, this approximation incorporates that the time scale of the bath  $t_B$  is smaller than our resolution time scale. The dynamics of the reduced density matrix  $\tilde{\rho}_S$  is given by  $\langle (\mathcal{O}_B)_B := \text{tr}[\mathcal{O}_B \tilde{\rho}_B] \rangle$ :

$$\begin{aligned} \partial_t \tilde{\rho}_S(t) &\approx -i \underbrace{\sum_k \langle \tilde{\mathbf{B}}_k(t) \rangle_B [\tilde{\mathbf{S}}_k, \tilde{\rho}_S(t)]}_{\text{will be neglected}} - \text{tr}_B \left[ \int_0^t ds [\tilde{\mathbf{H}}_{\text{int}}(t), [\tilde{\mathbf{H}}_{\text{int}}(s), \tilde{\rho}_S(s) \otimes \tilde{\rho}_B]] \right] \\ &\approx - \int_0^t \sum_{k,l} \langle \tilde{\mathbf{B}}_k(0) \tilde{\mathbf{B}}_l(t-s) \rangle_B (\tilde{\mathbf{S}}_k(t) \tilde{\mathbf{S}}_l(s) \tilde{\rho}_S(s) - \tilde{\mathbf{S}}_l(s) \tilde{\rho}_S(s) \tilde{\mathbf{S}}_k(t)) + \text{h.c.} \end{aligned} \quad (\text{E.4})$$

The expression is non-local in time, the right hand side depends on  $\tilde{\rho}_S(s)$ . However, the contributions of the bath depend on  $(t-s)$  and we assume that

they decay on a time scale  $t_B$  faster than the time scales relevant for the system ( $S$ ). Therefore, we approximate  $\tilde{\rho}_S(s) \rightarrow \tilde{\rho}_S(t)$  and, for the same reason, extend the integration to infinity [16]:

$$\text{Born-Markov approx.: } \partial_t \tilde{\rho}_S(t) \approx -\text{tr}_B \left[ \int_0^\infty ds [\tilde{\mathbf{H}}_{\text{int}}(t), [\tilde{\mathbf{H}}_{\text{int}}(t-s), \tilde{\rho}_S(t) \otimes \tilde{\rho}_B]] \right].$$

This amounts to replacing  $\tilde{\rho}_S(s) \rightarrow \tilde{\rho}_S(t)$  and  $\tilde{\mathbf{S}}_l(s) \rightarrow \tilde{\mathbf{S}}_l(t-s)$  in (E.4). To further evaluate the expression, we assume that the  $\mathbf{H}_S$  has discrete and non-degenerate eigenvalues. The idea is that we are interested in time scales (compared to the inverse gap of  $\mathbf{H}_S$ ) and will neglect terms that oscillate fast compared to this time scale. To this end, we use the eigenstates  $\{|\epsilon_\alpha\rangle\}$  as a basis, such that the time dependence of the remaining operators becomes:

$$\begin{aligned} \mathbf{H}_S &= \sum_\alpha \epsilon_\alpha |\epsilon_\alpha\rangle\langle\epsilon_\alpha|, \\ \mathbf{S}_l &= \sum_{\alpha,\beta} \langle\epsilon_\alpha|\mathbf{S}_l|\epsilon_\beta\rangle |\epsilon_\alpha\rangle\langle\epsilon_\beta| \\ &= \sum_\omega \underbrace{\sum_{\epsilon_\beta - \epsilon_\alpha = \omega} \langle\epsilon_\alpha|\mathbf{S}_l|\epsilon_\beta\rangle |\epsilon_\alpha\rangle\langle\epsilon_\beta|}_{=:\mathbf{S}_l(\omega)}, \\ \tilde{\mathbf{S}}_l(t) &= \sum_\omega e^{-i\omega t} \mathbf{S}_l(\omega) = \sum_\omega e^{+i\omega t} \mathbf{S}_l^\dagger(\omega). \end{aligned}$$

If we use the expressions for  $\tilde{\mathbf{S}}_l(t), \tilde{\mathbf{S}}_k(t-s)$  in the updated version of (E.4), the time dependence appears in terms of  $e^{i(\omega' - \omega)t} e^{i\omega s}$  for the combination of operators  $\mathbf{S}_k(\omega)$  and  $\mathbf{S}_l^\dagger(\omega')$  [16, 50]. Assuming that we are only interested in time scales much larger than the largest scale set by  $\mathbf{H}_S$  ( $\sim 1/\min_{\omega \neq \omega'} |\omega - \omega'|$ ), oscillatory terms in time can be ignored [50]

$$\text{Rotating-wave/secular approx.: } \sum_{\omega,\omega'} e^{i(\omega - \omega')t} f(\omega, \omega') \approx \sum_\omega f(\omega, \omega).$$

This finally leaves us with the Lindblad master equation [50]:

$$\begin{aligned} \partial_t \tilde{\rho}_S(t) &\approx \sum_{k,l,\omega} \underbrace{\int_0^\infty ds e^{i\omega s} \langle \tilde{\mathbf{B}}_k(s) \tilde{\mathbf{B}}_l(0) \rangle_B}_{=:\frac{1}{2}\gamma_{kl}(\omega) + ih_{kl}(\omega)} \left[ \mathbf{S}_l(\omega) \tilde{\rho}_S(t) \mathbf{S}_k^\dagger(\omega) - \mathbf{S}_k^\dagger(\omega) \mathbf{S}_l(\omega) \tilde{\rho}_S(t) \right] + \text{h.c.} \\ &=: -i[\tilde{\mathbf{H}}_{\text{LS}}, \tilde{\rho}_S(t)] + \sum_{k,l,\omega} \gamma_{kl}(\omega) \left[ \mathbf{S}_l(\omega) \tilde{\rho}_S(t) \mathbf{S}_k^\dagger(\omega) - \frac{1}{2} \{ \mathbf{S}_k^\dagger(\omega) \mathbf{S}_l(\omega), \tilde{\rho}_S(t) \} \right], \end{aligned}$$

where the first term is an effective Hamiltonian (based on the hermitian matrix  $h_{kl}$ ) and  $\gamma_{kl}$  is a positive matrix [50]. In a last step, we can diagonalize the matrix  $\gamma$ , define new Lindblad operators  $\mathbf{L}_k(\omega)$  (as in the main text) and go

back to the Schrödinger picture:

### Lindblad master equation

$$\partial_t \rho_S(t) \approx -i[\mathbf{H}_S + \mathbf{H}_{LS}, \rho_S(t)] + \sum_{k,\omega} \left[ \mathbf{L}_k(\omega) \rho_S(t) \mathbf{L}_k^\dagger(\omega) - \frac{1}{2} \{ \mathbf{L}_k^\dagger(\omega) \mathbf{L}_k(\omega), \rho_S(t) \} \right]. \quad (\text{E.5})$$

## E.2 Heating under Lindblad Dynamics

Following the analysis in Ref. [243], we consider the heating dynamics due to density operators  $\mathbf{L} = -\frac{1}{\pi} \partial_x \phi_x$  with  $\phi_x = \phi_{+,x} + \phi_{-,x}$ . We show that  $\phi_x^2$  and  $\theta_x^2$  are growing (linearly) in time:

$$\begin{aligned} \frac{1}{La} \int dx \phi_{\sigma,x}^2(t) &= \frac{1}{La} \sum_{q>0} \frac{\pi}{q} e^{-Aq} \mathbf{n}_{\sigma,q}(t) \sim \gamma t, \\ \frac{1}{La} \int dx \phi_{+,x} \phi_{-,x} &= -\frac{1}{La} \sum_{q>0} \frac{\pi}{2q} e^{-Aq} \left( \mathbf{b}_{+,q} \mathbf{b}_{-,q} + \mathbf{b}_{+,q}^\dagger \mathbf{b}_{-,q}^\dagger \right) \\ &\sim (\text{oscillating}). \end{aligned} \quad (\text{E.6})$$

Therefore, we first consider the individual densities  $\mathbf{n}_{\sigma,q}$  of the  $\pm$  bosons in momentum space and show that they increase linearly in time (making use of the Heisenberg picture):

$$\partial_t \mathbf{n}_{\sigma,q} = +i[\mathbf{H}, \mathbf{n}_{\sigma,q}] + \gamma_B \mathcal{L}_{-\frac{1}{\pi} \partial_x \phi_x}^* [\mathbf{n}_{\sigma,q}] = +\gamma_B \frac{q}{2\pi} \quad (\text{E.7})$$

(where the same heating would result if we had  $\mathbf{L} \sim \partial_x \phi_{\sigma,q}$  individually). Similarly, we can calculate the evolution of the off-diagonal contribution  $\mathbf{m}_q = \mathbf{b}_{+,q}^\dagger \mathbf{b}_{-,q}^\dagger$ :

$$\partial_t \mathbf{m}_q = 2i\nu q \mathbf{m}_q + \gamma \frac{q}{\pi} \Rightarrow \mathbf{m}_q(t) = -i \frac{\gamma}{2\nu\pi} (e^{+2i\nu q t} - 1) + e^{+i\nu q t} \mathbf{m}_q(0). \quad (\text{E.8})$$

These contributions are bounded, therefore it is the linearly increasing occupation number which drives the dynamics of quantities like  $\phi_x^2$ .

## E.3 Heating of the absolute Mode

In the following, we discuss the non-linear evolution equations for the absolute mode (in the case of linear measurement operators), see again (4.108). The aim is to show that  $\langle \phi_x^2 \rangle \rightarrow \infty$  for long times, being compatible with a state that indefinitely heats up. Note that we mostly do not explicitly write the contribution of the normalization but rather indicate, which term will be cancelled by it.

### Expectation values of single fields:

The expectation values of linear operators are only affected by the dynamics

due to the Hamiltonian:

$$\begin{aligned}
 \partial_t \langle \mathbf{b}_{\sigma,q} \rangle &= -i \frac{\nu}{2\pi} q^2 \langle \mathbf{b}_{\sigma,q} \rangle, \\
 \partial_t \langle \phi_q \rangle &= -i\nu q \langle \theta_q \rangle, \\
 \partial_t \langle \theta_q \rangle &= -i\nu q \langle \phi_q \rangle, \\
 \partial_t \langle \phi_{\sigma,q} \rangle &= -i\nu q \langle \phi_{\sigma,q} \rangle.
 \end{aligned} \tag{E.9}$$

Due to the normalization factor in the evolution equation of  $\rho^{(a)}$ , all measurement-induced contributions cancel out for linear fields.

### Expectation values of quadratic fields:

To derive the overall evolution equations, we start with the contribution from the Hamiltonian:

$$\begin{aligned}
 [\mathbf{H}, \phi_x^2] &= -i\nu \{ \partial_x \theta_x, \phi_x \} \\
 [\mathbf{H}, \theta_x^2] &= -i\nu \{ \theta_x, \partial_x \phi_x \} \\
 [\mathbf{H}, \{ \theta_x, \partial_x \phi_x \}] &= -i2\nu [ +\theta_x \partial_x^2 \theta_x + (\partial_x \phi_x)^2 ], \\
 [\mathbf{H}, \{ \phi_x, \partial_x \theta_x \}] &= -i2\nu [ +\phi_x \partial_x^2 \phi_x + (\partial_x \theta_x)^2 ].
 \end{aligned} \tag{E.10}$$

In a first step, we switch to the creation/annihilation operator perspective and use translational invariance (so we assume that the initial state is translationally invariant). The commutators with the Hamiltonian give rise to

$$\begin{aligned}
 [\mathbf{H}, \mathbf{b}_{\sigma,q}^\dagger \mathbf{b}_{\sigma',q'}] &= 0, \\
 [\mathbf{H}, \mathbf{b}_{\sigma,q}^\dagger \mathbf{b}_{\sigma',q'}^\dagger] &= 2\nu q \mathbf{b}_{\sigma,q}^\dagger \mathbf{b}_{\sigma',q'}^\dagger, \\
 [\mathbf{H}, \mathbf{b}_{\sigma,q} \mathbf{b}_{\sigma',q'}] &= -2\nu q \mathbf{b}_{\sigma,q} \mathbf{b}_{\sigma',q'}.
 \end{aligned} \tag{E.11}$$

Considering some arbitrary operator  $\mathcal{O}$ , the measurement-induced term in (4.108) acts as ( $\tilde{\mathcal{O}} := \mathcal{O} - \langle \mathcal{O} \rangle$ )

$$\begin{aligned}
 \gamma_M \int_{x'} \langle \partial_{x'} \tilde{\phi}_{x'} \mathcal{O} \partial_{x'} \tilde{\phi}_{x'} \rangle &= - \left\langle \sum_{q' > 0} \frac{\pi \gamma_M q'}{2} \left( - \sum_{\gamma} \tilde{\mathbf{b}}_{\gamma,q'} \mathcal{O} \mathbf{b}_{\gamma,q'}^\dagger - \sum_{\gamma} \tilde{\mathbf{b}}_{\gamma,q'}^\dagger \mathcal{O} \tilde{\mathbf{b}}_{\gamma,q'} \right. \right. \\
 &\quad \left. \left. + \tilde{\mathbf{b}}_{+,q'} \mathcal{O} \tilde{\mathbf{b}}_{-,q'} + \tilde{\mathbf{b}}_{-,q'} \mathcal{O} \tilde{\mathbf{b}}_{+,q'} \right. \right. \\
 &\quad \left. \left. + \tilde{\mathbf{b}}_{+,q'}^\dagger \mathcal{O} \tilde{\mathbf{b}}_{-,q'}^\dagger + \tilde{\mathbf{b}}_{-,q'}^\dagger \mathcal{O} \tilde{\mathbf{b}}_{+,q'}^\dagger \right) \right\rangle.
 \end{aligned} \tag{E.12}$$

Starting from  $\mathcal{O} = \tilde{\mathbf{b}}_{\sigma,q}^\dagger \tilde{\mathbf{b}}_{\sigma,q}$ , the first line in (E.12) gives rise to

$$\begin{aligned}
 \frac{\pi \gamma_M q}{2} \left( \langle \tilde{\mathbf{b}}_{\sigma,q} \tilde{\mathbf{b}}_{\sigma,q}^\dagger \rangle^2 + \langle \tilde{\mathbf{b}}_{\bar{\sigma},q} \tilde{\mathbf{b}}_{\sigma,q} \rangle \langle \tilde{\mathbf{b}}_{\sigma,q}^\dagger \tilde{\mathbf{b}}_{\bar{\sigma},q}^\dagger \rangle + \sum_{\gamma} \sum_p \langle \tilde{\mathbf{b}}_{\gamma,p} \tilde{\mathbf{b}}_{\gamma,p}^\dagger \rangle \langle \tilde{\mathbf{b}}_{\sigma,q}^\dagger \tilde{\mathbf{b}}_{\sigma,q} \rangle \right. \\
 \left. + \langle \tilde{\mathbf{b}}_{\sigma,q}^\dagger \tilde{\mathbf{b}}_{\sigma,q} \rangle^2 + \langle \tilde{\mathbf{b}}_{\bar{\sigma},q} \tilde{\mathbf{b}}_{\sigma,q} \rangle \langle \tilde{\mathbf{b}}_{\sigma,q}^\dagger \tilde{\mathbf{b}}_{\bar{\sigma},q}^\dagger \rangle + \sum_{\gamma} \sum_p \langle \tilde{\mathbf{b}}_{\gamma,p}^\dagger \tilde{\mathbf{b}}_{\gamma,p} \rangle \langle \tilde{\mathbf{b}}_{\sigma,q}^\dagger \tilde{\mathbf{b}}_{\sigma,q} \rangle \right).
 \end{aligned} \tag{E.13}$$

The second and third line give rise to

$$\begin{aligned}
& -\frac{\pi\gamma_M q}{2} \left( \langle \tilde{\mathbf{b}}_{+,q} \tilde{\mathbf{b}}_{-,q} \rangle \left( \langle \tilde{\mathbf{b}}_{\sigma,q}^\dagger \tilde{\mathbf{b}}_{\sigma,q} \rangle + \langle \tilde{\mathbf{b}}_{\sigma,q} \tilde{\mathbf{b}}_{\sigma,q}^\dagger \rangle \right) + 2 \sum_p \langle \tilde{\mathbf{b}}_{-,p} \tilde{\mathbf{b}}_{+,p} \rangle \langle \tilde{\mathbf{b}}_{\sigma,q}^\dagger \tilde{\mathbf{b}}_{\sigma,q} \rangle \right. \\
& \left. + \langle \tilde{\mathbf{b}}_{-,q} \tilde{\mathbf{b}}_{+,q} \rangle \left( \langle \tilde{\mathbf{b}}_{\sigma,q}^\dagger \tilde{\mathbf{b}}_{\sigma,q} \rangle + \langle \tilde{\mathbf{b}}_{\sigma,q} \tilde{\mathbf{b}}_{\sigma,q}^\dagger \rangle \right) + 2 \sum_p \langle \tilde{\mathbf{b}}_{+,p} \tilde{\mathbf{b}}_{-,p} \rangle \langle \tilde{\mathbf{b}}_{\sigma,q}^\dagger \tilde{\mathbf{b}}_{\sigma,q} \rangle \right). \tag{E.14}
\end{aligned}$$

Combining these terms, we get a time-evolution

$$\begin{aligned}
\partial_t \langle \tilde{\mathbf{b}}_{\sigma,q}^\dagger \tilde{\mathbf{b}}_{\sigma,q} \rangle &= \frac{\gamma_M q}{2\pi} \left( \langle \tilde{\mathbf{b}}_{\sigma,q} \tilde{\mathbf{b}}_{\sigma,q}^\dagger \rangle^2 + \langle \tilde{\mathbf{b}}_{\sigma,q}^\dagger \tilde{\mathbf{b}}_{\sigma,q} \rangle^2 + 2 \langle \tilde{\mathbf{b}}_{+,q} \tilde{\mathbf{b}}_{-,q} \rangle \langle \tilde{\mathbf{b}}_{+,q}^\dagger \tilde{\mathbf{b}}_{-,q}^\dagger \rangle \right. \\
& \quad \left. - (\langle \tilde{\mathbf{b}}_{+,q} \tilde{\mathbf{b}}_{-,q} \rangle + \langle \tilde{\mathbf{b}}_{+,q}^\dagger \tilde{\mathbf{b}}_{-,q}^\dagger \rangle) (\langle \tilde{\mathbf{b}}_{\sigma,q} \tilde{\mathbf{b}}_{\sigma,q}^\dagger \rangle + \langle \tilde{\mathbf{b}}_{\sigma,q}^\dagger \tilde{\mathbf{b}}_{\sigma,q} \rangle) \right) \\
& \quad + \sum_{p>0} \frac{\gamma_{MP}}{2\pi} \left( \sum_\gamma \langle \tilde{\mathbf{b}}_{\gamma,p}^\dagger \tilde{\mathbf{b}}_{\gamma,p} + \tilde{\mathbf{b}}_{\gamma,p} \tilde{\mathbf{b}}_{\gamma,p}^\dagger \rangle - 2 \langle \tilde{\mathbf{b}}_{+,p} \tilde{\mathbf{b}}_{-,p} + \tilde{\mathbf{b}}_{+,p} \tilde{\mathbf{b}}_{-,p} \rangle \right) \langle \tilde{\mathbf{b}}_{\sigma,q}^\dagger \tilde{\mathbf{b}}_{\sigma,q} \rangle \\
& = \frac{\gamma_M q}{2\pi} (1 + |B_{\sigma,q}|^2 + |C_{\sigma,q}|^2) + \underbrace{\left( \sum_{p>0} \frac{\gamma_{MP}}{2\pi} \langle \mathbf{A}_p^\dagger \mathbf{A}_p + \mathbf{A}_p \mathbf{A}_p^\dagger \rangle \right)}_{\geq 0} \langle \tilde{\mathbf{b}}_{\sigma,q}^\dagger \tilde{\mathbf{b}}_{\sigma,q} \rangle.
\end{aligned}$$

The gray marked term should be canceled by the normalization factor and we have defined

$$\begin{aligned}
B_{\sigma,q} &:= \langle \tilde{\mathbf{b}}_{\sigma,q} \tilde{\mathbf{b}}_{\sigma,q}^\dagger \rangle - \langle \tilde{\mathbf{b}}_{+,q} \tilde{\mathbf{b}}_{-,q} \rangle, \\
C_{\sigma,q} &:= \langle \tilde{\mathbf{b}}_{\sigma,q} \tilde{\mathbf{b}}_{\sigma,q}^\dagger \rangle - \langle \tilde{\mathbf{b}}_{+,q} \tilde{\mathbf{b}}_{-,q} \rangle, \\
\mathbf{A}_q &:= \tilde{\mathbf{b}}_{+,q}^\dagger - \tilde{\mathbf{b}}_{-,q}. \tag{E.15}
\end{aligned}$$

The equation implies that the occupation number of the bosonic modes grows at least linearly in time (similar to the Lindblad case, we have discussed in the main text). A similar analysis applies for, e.g.,  $\mathcal{O} = \langle \tilde{\mathbf{b}}_{+,q} \tilde{\mathbf{b}}_{-,q} \rangle$ :

$$\begin{aligned}
\partial_t \langle \tilde{\mathbf{b}}_{+,q} \tilde{\mathbf{b}}_{-,q} \rangle &= \left( -i2\nu q + \underbrace{\left( \sum_{p>0} \frac{\gamma_{MP}}{2\pi} (1 + \delta_{q,p}) \langle \mathbf{A}_p^\dagger \mathbf{A}_p + \mathbf{A}_p \mathbf{A}_p^\dagger \rangle \right)}_{\geq 0} \right) \cdot \langle \tilde{\mathbf{b}}_{+,q} \tilde{\mathbf{b}}_{-,q} \rangle + \frac{2\gamma_M q}{2\pi} |\langle \tilde{\mathbf{b}}_{+,q} \tilde{\mathbf{b}}_{-,q} \rangle|^2 \\
& \quad - \underbrace{\frac{\gamma_M q}{2\pi} \left( \langle \tilde{\mathbf{b}}_{+,q} \tilde{\mathbf{b}}_{+,q} \rangle \langle \tilde{\mathbf{b}}_{-,q} \tilde{\mathbf{b}}_{-,q}^\dagger \rangle + \langle \tilde{\mathbf{b}}_{+,q} \tilde{\mathbf{b}}_{+,q}^\dagger \rangle \langle \tilde{\mathbf{b}}_{-,q}^\dagger \tilde{\mathbf{b}}_{-,q} \rangle \right)}_{\leq 0}.
\end{aligned}$$

However, this expression is not very telling. Therefore, we switch to the description in terms of the conjugate variables in Fourier space again.

### Conjugate variables in Fourier space:

In the following, we work with the conjugate variables in momentum space:  $[\phi_q, \theta_{-q}] = \frac{\pi}{q}$ . The Hamiltonian takes the form (where we for now work with the convention as in Ref. [205]):

$$\mathbf{H} = \frac{\nu}{2\pi} \int_q q^2 (\theta_q \theta_{-q} + \phi_q \phi_{-q}). \tag{E.16}$$

The overall time evolution of the expectation value  $\langle \mathcal{O} \rangle$  takes the form:

$$\partial_t \langle \mathcal{O} \rangle = i[\mathbf{H}, \mathcal{O}] + \frac{2\gamma_M}{\pi^2} \int_p p^2 \langle \tilde{\phi}_p \mathcal{O} \tilde{\phi}_{-p} \rangle + (\text{normalization contribution}). \quad (\text{E.17})$$

For the correlation function  $\mathcal{O} = \phi_q \phi_{-q}$ , we find:

$$\begin{aligned} \partial_t \langle \phi_q \phi_{-q} \rangle = &+ i \frac{\nu q}{2} (\langle \{ \phi_q, \theta_{-q} \} \rangle - \langle \{ \phi_{-q}, \theta_q \} \rangle) \\ &+ \frac{2\gamma_M}{\pi^2} \left( 2q^2 \langle \tilde{\phi}_{-q} \tilde{\phi}_q \rangle^2 + \int_p p^2 \langle \tilde{\phi}_{-p} \tilde{\phi}_p \rangle \cdot \langle \phi_{-q} \phi_q \rangle \right). \end{aligned} \quad (\text{E.18})$$

Terms marked gray are cancelled out by the normalization factor in the evolution equation. The dynamics of the anti-commutators takes the form:

$$\begin{aligned} \partial_t \langle \{ \phi_q, \theta_{-q} \} \rangle = &+ i 2\nu q (\langle \phi_q \phi_{-q} \rangle - \langle \theta_q \theta_{-q} \rangle) + \frac{2\gamma_M}{\pi^2} 2q^2 \langle \tilde{\phi}_q \tilde{\phi}_{-q} \rangle \langle \{ \tilde{\phi}_q, \tilde{\theta}_{-q} \} \rangle \\ &+ \frac{2\gamma_M}{\pi^2} \int_p p^2 \langle \tilde{\phi}_p \tilde{\phi}_{-p} \rangle \cdot \langle \{ \phi_q, \theta_{-q} \} \rangle, \\ \partial_t \langle \{ \phi_{-q}, \theta_q \} \rangle = &(\partial_t \langle \{ \phi_q, \theta_{-q} \} \rangle)^*. \end{aligned}$$

Therefore, the dynamics of their difference is only determined by the measurement-induced part (with a positive prefactor). Finally, for  $\mathcal{O} = \theta_q \theta_{-q}$ , we get:

$$\begin{aligned} \partial_t \langle \theta_q \theta_{-q} \rangle = &+ i \frac{\nu q}{2} (\langle \{ \theta_q, \phi_{-q} \} \rangle - \langle \{ \phi_q, \theta_{-q} \} \rangle) \\ &+ \frac{2\gamma_M}{\pi^2} \left( q^2 (|\langle \tilde{\phi}_{-q} \tilde{\theta}_q \rangle|^2 + |\langle \tilde{\phi}_q \tilde{\theta}_{-q} \rangle|^2) + \int_p p^2 \langle \tilde{\phi}_p \tilde{\phi}_{-p} \rangle \cdot \langle \theta_q \theta_{-q} \rangle \right) \end{aligned}$$

The time evolution equations for  $\partial_t \langle |\phi_q|^2 \pm |\theta_q|^2 \rangle$  can be evaluated directly. In the case with a relative minus sign, we have:

$$\begin{aligned} \partial_t \langle |\phi_q|^2 - |\theta_q|^2 \rangle = &+ i\nu q (\langle \{ \phi_q, \theta_{-q} \} \rangle - \langle \{ \phi_{-q}, \theta_q \} \rangle), \\ \partial_t \langle \{ \phi_q, \theta_{-q} \} - \{ \phi_{-q}, \theta_q \} \rangle = &+ 4i\nu q \langle |\phi_q|^2 - |\theta_q|^2 \rangle, \end{aligned} \quad (\text{E.19})$$

which gives rise to a bounded contribution. For the other case, we have:

$$\partial_t \langle |\theta_q|^2 + |\phi_q|^2 \rangle \geq 0, \quad (\text{E.20})$$

which leads to an (unbounded) growth. Since the difference between  $\langle |\theta_q|^2 \rangle$  and  $\langle |\phi_q|^2 \rangle$  is bounded, we get  $\langle \phi_q \phi_{-q} \rangle \rightarrow \infty$  (similarly to  $\langle \tilde{\mathbf{b}}_{\sigma,q}^\dagger \tilde{\mathbf{b}}_{\sigma,q} \rangle$ ).

# F | Different Measurement Protocols

Regarding indirect measurements of the system by coupling to an ancilla, we can distinguish three different cases [21]. One case was discussed in Sec. 4.4. As a reminder, the interaction between system and ancilla is supposed to be weak,  $\theta \ll 1$ .

1. The choice of the initial state of the ancilla  $|a\rangle = |0\rangle$  will lead to a measurement probability  $p_0 \approx 1$  for the outcome  $\sigma = 0$  after the interaction. Therefore, for most measurements, the dynamics will be deterministic. Only rarely, the result 1 will be measured, which will result in a sizable change of the state: a *quantum jump* (briefly discussed below).
2. Picking  $|a\rangle = |0\rangle$  but measuring in the  $x$ -basis gives rise to a very different result: using the same logic, here  $p_0 = p_1 = 1/2$  (as we have shown in the main text).
3. Similarly, changing the initial state to  $|a\rangle = 1/\sqrt{2} \cdot (|0\rangle - i|1\rangle)$  and measuring in the standard basis will give rise to  $p_0 \approx p_1 \approx 1/2$ . Therefore, the outcome is nearly unpredictable on the one hand. On the other hand, the state  $\rho^{(e)}$  will only be slightly changed after each interaction and the corresponding dynamics is referred to as *quantum state diffusion*.

Nevertheless, the last two scenarios are drastically different. The first one gives rise to an effectively stochastic unitary evolution, whereas the second one gives rise to non-linear, non-unitary evolution. The interplay of these two has been discussed in Sec. 4.10.2. Both cases can be cast into a general form of quantum state diffusion, discussed below.

---

**Quantum jumps:** Looking back at (4.34), we anticipate that the form of  $M_i^{(a)}$  will depend on the initial state of the ancilla. In the limit  $\theta \ll 1$ , we can write the state after the interaction up to second order as (see again Ref. [21]):

$$\mathcal{U}(\theta)|\psi\rangle \otimes |\sigma\rangle = |\psi\rangle \otimes |\sigma\rangle - i\theta((\mathbb{1} - \mathbf{n}_j)|\psi\rangle \otimes |\sigma\rangle + \mathbf{n}_j|\psi\rangle \otimes |\sigma'\rangle) - \frac{\theta^2}{2}|\psi\rangle \otimes |\sigma\rangle. \quad (\text{F.1})$$

For  $|a\rangle = |1\rangle$ , we get (the overall phases are uninteresting as they will not give

rise to any observable consequence):

$$\mathbf{M}_0^{(0)} = e^{-i\frac{\theta}{2}} [(\mathbb{1} - \mathbf{n}_j) + \cos(\theta)\mathbf{n}_j] \approx e^{-i\frac{\theta}{2}} \left[ \mathbb{1} - \frac{\theta^2}{2}\mathbf{n}_j \right], \quad (\text{F.2})$$

$$\mathbf{M}_1^{(0)} = -ie^{-i\frac{\theta}{2}} \sin(\theta)\mathbf{n}_j \approx -ie^{-i\frac{\theta}{2}}\theta\mathbf{n}_j \quad (\text{F.3})$$

(the case we have already encountered before). Here,  $\mathbf{M}_0$  is close to the identity operator, whereas  $\mathbf{M}_1$  is a projector, massively altering the state. The corresponding probabilities to measure outcome (0) or (1) are given by:

$$p_0 = (1 - \gamma\delta t\langle\mathbf{n}_j\rangle), \quad p_1 = \gamma\delta t\langle\mathbf{n}_j\rangle. \quad (\text{F.4})$$

Therefore, we measure outcome 0 in most cases. Only rarely, the outcome (1) is measured<sup>1</sup>, which leads to the *projection* onto the space with one particle at site  $j$ .

---

**General form of quantum state diffusion:** All the different measurement scenarios we have discussed here lead to the same *averaged* Lindblad dynamics (here for  $\mathbf{L} = \mathbf{L}^\dagger$ ), which generally would take the form (considering only a single Lindblad operator for simplicity):

$$\partial_t \overline{\rho_t^{(c)}} = -i[\mathbf{H}, \overline{\rho_t^{(c)}}] - \frac{\gamma}{2} [\mathbf{L}, [\mathbf{L}, \overline{\rho_t^{(c)}}]]. \quad (\text{F.5})$$

Each of these cases is an instant of an *unravelling* of the same master equation. The second and third case can be seen as special cases of a form of QSD [196] (in discrete time):

$$|\Psi'\rangle = \left( 1 - i\mathbf{H}\delta t - \frac{1}{2}\tilde{\mathbf{L}}^2\delta t + \Delta W_t\tilde{\mathbf{L}} \right) |\Psi\rangle, \quad \tilde{\mathbf{L}} := \mathbf{L} - \langle\Psi|\mathbf{L}|\Psi\rangle. \quad (\text{F.6})$$

The conditional Master equation evolves as:

$$\begin{aligned} \rho_{t+\delta t}^{(c)} &= \rho_t^{(c)} - i\delta t[\mathbf{H}, \rho_t^{(c)}] - \frac{1}{2}\delta t\{\tilde{\mathbf{L}}^2, \rho_t^{(c)}\} + \Delta W_t\Delta W_t^* \left( \tilde{\mathbf{L}}\rho_t^{(c)}\tilde{\mathbf{L}} \right) \\ &+ \Delta W_t \left( \tilde{\mathbf{L}}\rho_t^{(c)} \right) + \Delta W_t^* \left( \rho_t^{(c)}\tilde{\mathbf{L}} \right), \end{aligned}$$

which requires  $\overline{\Delta W_t\Delta W_t^*} = \delta_{t,t'}\delta t$  and  $\overline{\Delta W_t} = \overline{\Delta W_t^*} = 0$  to recover the quantum master equation for  $\rho_{t+\delta t}^{(c)}$  in (F.5). The noise term  $\Delta W$  can be complex and the measurements and random unitary evolution correspond to its real or imaginary valued version:

$$\begin{aligned} \Delta W_t &= \cos(\theta)\chi_t + i\sin(\theta)\eta_t, \\ \overline{\Delta W_t\Delta W_t^*} &\stackrel{!}{=} \delta_{t,t'}\delta t: \quad \overline{\chi_t\chi_{t'}} = \cos(\theta)^2\delta_{t,t'}\delta t \quad \overline{\eta_t\eta_{t'}} = \sin(\theta)^2\delta_{t,t'}\delta t. \end{aligned}$$

The ‘trotterized’ form of the time-evolution in (F.6) reads:

$$\begin{aligned} \mathbf{U} &= \exp \left( \Delta W_t\tilde{\mathbf{L}} - \alpha(\theta)\tilde{\mathbf{L}}^2\delta t \right) \exp(-i\mathbf{H}\delta t) \\ &= \left( 1 - i\mathbf{H}\delta t - \alpha(\theta)\tilde{\mathbf{L}}^2\delta t + \frac{1}{2}\Delta W_t^2\tilde{\mathbf{L}}^2 + \Delta W_t\tilde{\mathbf{L}} \right) + \mathcal{O}(\delta t^{1.5}), \end{aligned}$$

---

<sup>1</sup>This is also related to the ‘thermodynamics of quantum jump trajectories’, where these rare events are analyzed [249]. In Ref. [176], the post-selected trajectories have been considered, where no rare event takes place (‘no-click limit’).

where  $\alpha(\theta)$  depends on the form of the noise:

$$\text{complex noise: } \alpha(\theta) = \cos^2(\theta) \quad \begin{cases} \text{real noise:} & \alpha = 1, \\ \text{imaginary noise:} & \alpha = 0. \end{cases}$$



# G | Perturbative Dynamics of the Diagonal of the Density Matrix

In the following, we work out the dynamics of  $\rho^{(c)}$  in the limiting case  $\gamma_B/J \gg 1$ . The guiding idea is that in this limit, the non-trivial dynamics will be reduced to those matrix elements that are left invariant under the dephasing (all other terms are strongly suppressed), see also, e.g., Ref. [221] for an example. For dephasing, these are the diagonal elements of the form  $|\{n\}\rangle\langle\{n\}|$ . As an example, consider the case of measurements and a bath in the absence of any unitary evolution. We decompose  $\rho^{(c)}$  in its diagonal and non-diagonal part  $\rho^{(c)} = \rho_{\parallel}^{(c)} + \rho_{\perp}^{(c)}$  and obtain:

$$\begin{aligned}\partial_t \rho_{\parallel}^{(c)} &= \sum_i dW_i \{ \mathbf{n}_i - \text{tr}[\mathbf{n}_i \rho_{\parallel}^{(c)}], \rho_{\parallel}^{(c)} \}, \\ \partial_t \rho_{\perp}^{(c)} &= \mathcal{L}_B[\rho_{\perp}^{(c)}] + \sum_i dW_i \{ \mathbf{n}_i - \text{tr}[\mathbf{n}_i \rho_{\parallel}^{(c)}], \rho_{\perp}^{(c)} \}.\end{aligned}\tag{G.1}$$

Therefore, the dynamics of the diagonal  $\rho_{\parallel}^{(c)}$  decouples from the off-diagonal terms. Including a Hamiltonian, we are confronted with a stochastic master equation (see again Sec. 4.10.1):

$$\partial_t \rho^{(c)} = \mathcal{L}_H[\rho^{(c)}] + \mathcal{L}_M[\rho^{(c)}] + \eta \mathcal{L}_B[\rho^{(c)}],\tag{G.2}$$

$$\mathcal{L}_M[\rho^{(c)}] := \sum dW_i \{ \mathbf{n}_i - \langle \mathbf{n}_i \rangle, \rho^{(c)} \}.\tag{G.3}$$

In the following, we assume  $\eta = (\gamma_M + \gamma_B)/J \gg 1$ . Adapting the discussion in Ref. [180], we make an ansatz  $\rho^{(c)} = \rho_0^{(c)} + \eta^{-1} \rho_1^{(c)} + \eta^{-2} \rho_2^{(c)} + \dots$  with  $\rho_0^{(c)}$  being a diagonal matrix. The evolution equations in orders of  $\eta^{-1}$  are:

$$\text{order 0:} \quad \mathcal{L}_B[\rho_0^{(c)}] = 0,\tag{G.4}$$

$$\text{order 1:} \quad \partial_t \rho_0^{(c)} = \mathcal{L}_H[\rho_0^{(c)}] + \mathcal{L}_M[\rho_0^{(c)}] + \mathcal{L}_B[\rho_1^{(c)}],\tag{G.5}$$

$$\text{order 2:} \quad \partial_t \rho_1^{(c)} = \mathcal{L}_H[\rho_1^{(c)}] + \mathcal{L}_M^{(\eta)}[\rho^{(c)}] + \mathcal{L}_B[\rho_2^{(c)}],\tag{G.6}$$

⋮

Note that the presence of the expectation values requires some care: as an example, the term  $\mathcal{L}_M^{(\eta)}[\rho^{(c)}]$  describes first order contribution. We want to

work out the dynamics on the space left invariant under  $\mathcal{L}_B$  or differently put: the dynamics on the diagonal (in the occupation-number basis). Therefore, we use a projection operator  $\mathbf{\Pi}$ , projecting onto the diagonal. At first order, we get:

$$\partial_t \rho_0^{(c)} = \mathbf{\Pi} \left( \mathcal{L}_H[\rho_0^{(c)}] + \mathcal{L}_M[\rho_0^{(c)}] \right), \quad (\text{G.7})$$

where we used that  $\mathbf{\Pi} \rho \in \text{Ker} \mathcal{L}_B$ , such that  $\mathbf{\Pi} \mathcal{L}_B[\rho_1^{(c)}] = 0$ . Projecting onto the complement with  $(\mathbb{1} - \mathbf{\Pi})$  at first order gives rise to:

$$0 = \left( \mathcal{L}_H[\rho_0^{(c)}] + \mathcal{L}_M[\rho_0^{(c)}] \right)^\perp + \mathcal{L}_B^\perp[\rho_1^{(c)}] = \mathcal{L}_H^\perp[\rho_0^{(c)}] + \mathcal{L}_B^\perp[\rho_1^{(c)}]. \quad (\text{G.8})$$

Projecting with  $\mathbf{\Pi}$  at second order gives rise to:

$$\partial_t \rho_{1,\parallel}^{(c)} = \mathbf{\Pi} \mathcal{L}_H[\rho_1^{(c)}] + \mathbf{\Pi} \mathcal{L}_M^{(\eta)}[\rho^{(c)}]. \quad (\text{G.9})$$

Now we investigate the structure of  $\rho_1^{(c)} = \rho_{1,\parallel}^{(c)} + \rho_{1,\perp}^{(c)}$ . To this end, we assume  $\mathbf{\Pi} \mathcal{L}_H \mathbf{\Pi} = 0^1$ . Therefore, we can make the following identification:

$$(\mathbb{1} - \mathbf{\Pi}) \mathcal{L}_B[\rho_{1,\perp}^{(c)} + \rho_{1,\parallel}^{(c)}] = \mathcal{L}_B[\rho_{1,\perp}^{(c)}] = \mathcal{L}_B^\perp[\rho_{1,\perp}^{(c)}].$$

Together with (G.8) it gives rise to

$$\begin{aligned} (\text{G.8}) \quad \mathbf{\Pi} \mathcal{L}_H \mathbf{\Pi} \stackrel{\perp=0}{\Leftrightarrow} & \mathcal{L}_B^\perp[\rho_{1,\perp}^{(c)}] = -\mathcal{L}_H \mathbf{\Pi} \rho_0^{(c)}, \\ \mathcal{L}_B \text{ invertible on } \perp \text{ Ker } \mathcal{L}_B \stackrel{\Leftrightarrow}{\Leftrightarrow} & \rho_{1,\perp}^{(c)} = -(\mathcal{L}_B^\perp)^{-1} \mathcal{L}_H \mathbf{\Pi} \rho_0^{(c)}. \end{aligned}$$

This works the same way without measurements. Finally, we conclude

$$\partial_t \rho_0^{(c)} = \mathcal{L}_M[\rho_0^{(c)}] \quad (\text{G.10})$$

$$\begin{aligned} \partial_t \rho_{1,\parallel}^{(c)} &= +\mathbf{\Pi} \mathcal{L}_H[\rho_{1,\perp}^{(c)}] + \mathbf{\Pi} \mathcal{L}_M^{(\eta)}[\rho^{(c)}] \\ &= -\mathbf{\Pi} \mathcal{L}_H (\mathcal{L}_B^\perp)^{-1} \mathcal{L}_H \mathbf{\Pi}[\rho_0^{(c)}] + \underbrace{\mathbf{\Pi} \mathcal{L}_M^{(\eta)}[\rho^{(c)}]}_{=\mathcal{L}_M^{(\eta)}[\rho_{\parallel}^{(c)}]}. \end{aligned} \quad (\text{G.11})$$

Therefore, we get an effective evolution equation for the diagonal components of the density matrix

$$\partial_t \rho_{\parallel}^{(c)} \approx \underbrace{\mathcal{L}_M[\rho_0^{(c)}]}_{\approx \mathcal{L}_M[\rho_{\parallel}^{(c)}]} + \eta^{-1} \mathcal{L}_M^{(\eta)}[\rho_{\parallel}^{(c)}] - \eta^{-1} \mathbf{\Pi} \mathcal{L}_H (\mathcal{L}_B^\perp)^{-1} \mathcal{L}_H \mathbf{\Pi}[\rho_{\parallel}^{(c)}], \quad (\text{G.12})$$

(see also again Ref. [180] (appendix D) for a discussion of how to deal with  $(\mathcal{L}_B^\perp)^{-1}$ .) The essential difference to the case of no measurements is that  $\rho_{\parallel}^{(c)}$  still has dynamics at order  $\mathcal{O}(\gamma_M/J)$ . Furthermore, the measurement operator is non-linear, such that the different orders cannot be so easily split. Can these terms compete? In our case

$$\mathcal{L}_M \sim \mathcal{O}\left(\frac{\gamma_M}{J}\right), \quad \eta = \frac{\gamma_M + \gamma_B}{J}, \quad (\text{G.13})$$

<sup>1</sup>As it is clearly the case for the fermionic hopping Hamiltonian.

therefore the analysis is first of all controlled for large  $\gamma_B/J \gg 1$ . During the analysis we did not specify the strength of the measurement-part, therefore it might be small as well. In the absence of a bath, such a treatment would require  $\gamma_M/J \gg 1$ . In turn, this treatment would not be suitable to effectively describe the phase transition.

**Technical details:** To evaluate  $\Pi \mathcal{L}_H (\mathcal{L}_B^\perp)^{-1} \mathcal{L}_H \Pi [\rho_\parallel^{(c)}]$ , we only need a few insights:

- $\mathcal{L}_H \Pi [\rho_\parallel^{(c)}]$  can only produce terms of the form:

$$\rho_{i,\pm} := \mathbf{c}_i^\dagger \mathbf{c}_{i\pm 1} |\{n\}\rangle \langle \{n\}| - |\{n\}\rangle \langle \{n\}| \mathbf{c}_i^\dagger \mathbf{c}_{i\pm 1}.$$

For these cases, the inverse bath operator acts as:

$$(\mathcal{L}_B^\perp)^{-1} [\rho_{i,\pm}] = -\frac{J}{\gamma_B} \rho_{i,\pm},$$

meaning that they are eigenstates with eigenvalue  $-\frac{J}{\gamma_B}$ .

- Building on that, we can write:

$$\Pi \mathcal{L}_H (\mathcal{L}_B^\perp)^{-1} \mathcal{L}_H \Pi [\rho_\parallel^{(c)}] = -\frac{J}{\gamma_B} (-i)^2 \Pi \left[ \mathbf{H}, \left[ \mathbf{H}, \rho_\parallel^{(c)} \right] \right]. \quad (\text{G.14})$$

This expression gives rise to the simple symmetric exclusion-like dynamics discussed in the main text.

- In Sec. 4.10.3, we have discussed the situation where we replaced the bath with random unitary evolution:

$$-\frac{\gamma_B}{2J} \sum_l [\mathbf{n}_l, [\mathbf{n}_l, \rho]] \rightarrow -\frac{\gamma_I}{2J} \sum_l [\mathbf{n}_l, [\mathbf{n}_l, \rho]] + i\sqrt{\frac{\gamma_I}{J}} \sum_l dZ_{l,t} [\mathbf{n}_l, \rho]. \quad (\text{G.15})$$

Here, the ‘imaginary’ noise terms *only* affect the off-diagonal part of the density matrix. Since we are only interested in observables based on  $\mathbf{n}_j$ , we can use a version of  $\mathbf{U}_t^{(I)\dagger}$  to go into an interaction picture [180] (eventually ‘undoing’ the simple part of the time evolution<sup>2</sup>):

$$\tilde{\rho}_t^{(c)} = \mathbf{U}_t^{(I)\dagger} \rho_t^{(c)} \mathbf{U}_t^{(I)}, \quad \text{tr} \left[ f(\{\mathbf{n}_j\}) \rho_t^{(c)} \right] = \text{tr} \left[ f(\{\mathbf{n}_j\}) \tilde{\rho}_t^{(c)} \right]. \quad (\text{G.16})$$

This transformation, in the limit  $\gamma_I/J \gg 1$ , only affects the Hamiltonian non-trivially, as they do not commute. The transformed Hamiltonian becomes stochastic. To go to the interaction picture, we use the unitary operator

$$\mathbf{U}_t = \exp \left( -i \sum_j \sqrt{\frac{\gamma_I + \gamma_M}{J}} Z_{j,t} \mathbf{n}_j \right),$$

<sup>2</sup>Evolution in the interaction picture:  $i\hbar \frac{d}{dt} (\mathbf{U}(t) |\psi(t)\rangle) = i\hbar \left( \frac{d}{dt} \mathbf{U}(t) \right) \mathbf{U}^\dagger |\psi_I(t)\rangle + \mathbf{U}(t) \mathbf{H} \mathbf{U}^\dagger(t) |\psi_I(t)\rangle$ .

which will *not* compensate the stochastic term, but will instead compensate the Lindblad terms. Its version for an infinitesimal time step reads:

$$\mathbf{U}_{t+dt} = \exp\left(-i \sum_j \sqrt{\frac{\gamma_I + \gamma_M}{J}} dZ_{j,t} \mathbf{n}_j\right) \mathbf{U}_t.$$

In the interaction picture, we get two updated contributions:

$$\begin{aligned} \text{noise prefactor: } \sqrt{\frac{\gamma_I}{J}} &\rightarrow -\sqrt{\frac{\tilde{\gamma}}{J}} = -\left(\sqrt{\frac{\gamma_M + \gamma_I}{J}} - \sqrt{\frac{\gamma_I}{J}}\right), \\ \text{Hamiltonian: } \mathbf{H} &\rightarrow \mathbf{U}_t (\mathbf{H} dt) \mathbf{U}_t^\dagger = \sum_j \mathbf{c}_j^\dagger \mathbf{c}_{j+1} d\tilde{Z}_{j,t} + \mathbf{c}_{j+1}^\dagger \mathbf{c}_j d\tilde{Z}_{j,t}^*. \end{aligned}$$

The noise terms are given by

$$d\tilde{Z}_{j,t} := \exp\left(-i \underbrace{\sqrt{\frac{\gamma_I + \gamma_M}{J}}}_{=: \tilde{\eta}} (Z_{j,t} - Z_{j+1,t})\right) dt.$$

Based on the analysis in Ref. [180], we can write

$$d\tilde{Z}_{j,t} d\tilde{Z}_{j,t}^* \stackrel{\tilde{\eta} \rightarrow \infty}{=} \frac{2}{\tilde{\eta}} dt, \quad (\text{G.17})$$

such that the  $d\tilde{Z}_{j,t}$  are themselves complex Gaussian noise processes again. The transformed Hamiltonian describes an ‘ordinary’ stochastic Hamiltonian and the overall time evolution reads

$$\begin{aligned} \partial_t \tilde{\rho}^{(c)} &\approx \frac{\gamma_M}{J} \sum_l dW_l \{ \mathbf{n}_l - \langle \mathbf{n}_l \rangle, \tilde{\rho}_t^{(c)} \} + 2\tilde{\eta}^{-1} \left( \mathcal{L}_1[\tilde{\rho}_t^{(c)}] + \mathcal{L}_2[\tilde{\rho}_t^{(c)}] \right) \\ &- i \sqrt{\frac{\tilde{\gamma}}{J}} \sum_l dZ_{l,t} \left[ \mathbf{n}_l, \tilde{\rho}_t^{(c)} \right] + \sum_l \left( d\tilde{Z}_{l,t}^* \left[ \mathbf{c}_{l+1}^\dagger \mathbf{c}_l, \tilde{\rho}_t^{(c)} \right] + \text{h.c.} \right). \end{aligned} \quad (\text{G.18})$$

In contrast to (4.159), the evolution still describes the full density matrix (in the limit  $\gamma_I/J \gg 1$  and in the interaction picture). The expression is similar to (4.159), however the last two terms in (G.18) are absent in (4.159). Nevertheless, by close inspection we see that (G.18) all but the last term evolve diagonal terms into diagonal terms (and off-diagonal terms into off-diagonal ones). The last term originates from the stochastic Hamiltonian. If we can ignore the last term, the dynamics *on the diagonal* is perturbatively the same as the one for a bath given that  $\gamma_I/J = \gamma_B/J \gg 1$ .

# H | Integrating out the absolute Mode

This discussion is adapted and extended from the publication [147].

In the following, we discuss details about the procedure of integrating out the absolute mode to obtain an effective theory for the relative mode. The interaction terms between the relative and absolute mode are given by (dimensions:  $[m] = [x]^{-1} = [t]^{-1}$ ;  $X := (t, x)$ ):

$$\begin{aligned}
i\Delta S_{+,-} = m^2 \int dt dx & \left\{ \frac{2(\gamma_B + 2\gamma_M)}{\nu} \cos(\sqrt{2}\phi_{+,X}^{(a)}) \cos(\sqrt{2}\phi_{+,X}^{(r)}) \cos(\sqrt{2}\phi_{-,X}^{(a)}) \cos(\sqrt{2}\phi_{-,X}^{(r)}) \right. \\
& + 2\frac{\gamma_B}{\nu} \sin(\sqrt{2}\phi_{+,X}^{(a)}) \sin(\sqrt{2}\phi_{+,X}^{(r)}) \sin(\sqrt{2}\phi_{-,X}^{(a)}) \sin(\sqrt{2}\phi_{-,X}^{(r)}) \\
& - \frac{1}{2} \frac{(\gamma_B + \gamma_M)}{\nu} \left[ \cos(2\sqrt{2}\phi_{+,X}^{(a)}) \cos(2\sqrt{2}\phi_{+,X}^{(r)}) + \cos(2\sqrt{2}\phi_{-,X}^{(a)}) \cos(2\sqrt{2}\phi_{-,X}^{(r)}) \right] \\
& \left. + \sum_{\sigma=\pm} \frac{1}{2} \frac{\gamma_M}{\nu} \left[ \cos(2\sqrt{2}\phi_{\sigma,X}^{(a)}) + \cos(2\sqrt{2}\phi_{\sigma,X}^{(r)}) \right] \right\},
\end{aligned}$$

where the stationary expectation values have already been left out. The correlations for the absolute mode are simple under the **assumptions** of a  $\rho^{(a)}$  being a (i) Gaussian state with vanishing correlations between different lattice sites and that (ii) contour correlations are negligible:

$$\begin{aligned}
\text{(ia)} \quad & \left\langle e^{i\phi_{\sigma,X}^{(a)}} \right\rangle_a = e^{-\frac{1}{2} \langle (\phi_{\sigma,X}^{(a)})^2 \rangle_a} \rightarrow 0, \\
\text{(ib)} \quad & \left\langle e^{i(\phi_{\sigma,X}^{(a)} \pm \phi_{\sigma,Y}^{(a)})} \right\rangle_a = e^{-\frac{1}{2} \langle (\phi_{\sigma,X}^{(a)} \pm \phi_{\sigma,Y}^{(a)})^2 \rangle_a} \rightarrow \begin{cases} m^{-2} \delta(X - Y) & \text{for } + \\ 0 & \text{for } -, \end{cases} \\
\text{(ii)} \quad & \exp \left( - \left\langle \left( \phi_{+,X}^{(a)} \pm \phi_{-,Y}^{(a)} \right)^2 \right\rangle_a \right) \rightarrow 0. \tag{H.1}
\end{aligned}$$

Here, the usage of  $m^{-2}$  stems from the relationship of  $m$  with the effective cut-off scale in the Dirac model (A). Under these assumptions, we can evaluate

$\langle \Delta S_{+,-} \rangle_a$  in a straightforward manner and the correction  $\Delta S_r$  reads:

$$\begin{aligned} \Delta S_r = m^2 \int dt dx & \left\{ -\frac{i}{2} \frac{\gamma_M}{\nu} \sum_{\sigma=\pm} \cos(2\sqrt{2}\phi_{\sigma,X}^{(r)}) + \frac{i}{2} \frac{\gamma_M(\gamma_B + \gamma_M)}{\nu^2} \frac{1}{8} \sum_{\sigma=\pm} \cos(2\sqrt{2}\phi_{\sigma,X}^{(r)}) \right. \\ & - \frac{i}{24} \left[ \left( \frac{(2\gamma_M + \gamma_B)^2}{\nu^2} - \frac{(\gamma_B)^2}{\nu^2} \right) \sum_{\sigma=\pm} \cos(2\sqrt{2}\phi_{\sigma,X}^{(r)}) \right. \\ & \left. \left. + \left( \frac{(2\gamma_M + \gamma_B)^2}{\nu^2} + \frac{(\gamma_B)^2}{\nu^2} \right) \cos(2\sqrt{2}\phi_{+,X}^{(r)}) \cos(2\sqrt{2}\phi_{-,X}^{(r)}) \right] \right\}. \end{aligned} \quad (\text{H.2})$$

We parametrize the interaction terms as follows (in the contours description) ( $d^2 X = dxdt$ ):

**Contour description**

$$\begin{aligned} \Delta S_r =: & \int d^2 X \left[ i \underbrace{\left( \frac{\lambda_{cq}^{(c)} + i\lambda_{cq}^{(s)}}{2} \right)}_{=: \lambda_+} \cos(2\sqrt{2}\phi_{+,X}^{(r)}) + i \underbrace{\left( \frac{\lambda_{cq}^{(c)} - i\lambda_{cq}^{(s)}}{2} \right)}_{=: \lambda_-} \cos(2\sqrt{2}\phi_{-,X}^{(r)}) \right. \\ & + i \underbrace{(\lambda_c + \lambda_q)}_{=: \lambda_{+-}^{(c)}} \cos(2\sqrt{2}\phi_{+,X}^{(r)}) \cos(2\sqrt{2}\phi_{-,X}^{(r)}) \\ & \left. + i \underbrace{(\lambda_q - \lambda_c)}_{=: \lambda_{+-}^{(s)}} \sin(2\sqrt{2}\phi_{+,X}^{(r)}) \sin(2\sqrt{2}\phi_{-,X}^{(r)}) \right]. \end{aligned} \quad (\text{H.3})$$

The same interaction can also be formulated in the Keldysh coordinates:

**Keldysh description**

$$\begin{aligned} \Delta S_r =: & \int d^2 X \left[ i\lambda_c \cos(4\phi_{c,X}^{(r)}) + i\lambda_q \cos(4\phi_{q,X}^{(r)}) \right. \\ & \left. + i\lambda_{cq}^{(c)} \cos(2\phi_{c,X}^{(r)}) \cos(2\phi_{q,X}^{(r)}) + \lambda_{cq}^{(s)} \sin(2\phi_{c,X}^{(r)}) \sin(2\phi_{q,X}^{(r)}) \right]. \end{aligned} \quad (\text{H.4})$$

Note that we have already included couplings, which are absent initially but will be generated under the RG (and higher order terms like  $\cos(4\sqrt{2}\phi_{\sigma,X}^{(r)})$  have been ignored). In the RG discussion, also a mixed representation can be useful:

**Mixed description**

$$\begin{aligned} \Delta S_r = & \int d^2 X \left[ i\lambda_c \cos(4\phi_{c,X}^{(r)}) + i\lambda_q \cos(4\phi_{q,X}^{(r)}) \right. \\ & \left. + i\lambda_+ \cos(2\sqrt{2}\phi_{+,X}^{(r)}) + \lambda_- \cos(2\sqrt{2}\phi_{-,X}^{(r)}) \right]. \end{aligned} \quad (\text{H.5})$$

# I | Details about the Derivation of the Flow Equations

The main results of this chapter have been published in the publication [147]. The following discussion is in large parts adapted and partly extended from the publication [147].

Continuing the discussion in Sec. 4.8.1, we derive the renormalization of the action  $S[\phi^{(r)}] = S_r^{(0)} + \Delta S_r$  of the relative mode, using the momentum shell RG and integrating out short distances modes ( $<$ ) with momenta in the range  $|k| \in [A/b, A]$ . In first and second order, the correction terms read (omitting the index ( $r$ )):

$$S[\phi_{>}] \approx S_0^> + \underbrace{\langle \Delta S \rangle_{<}}_{\text{1st order}} + \underbrace{\frac{i}{2} (\langle \Delta S^2 \rangle_{<} - \langle \Delta S \rangle_{<}^2)}_{\text{second order}}. \quad (\text{I.1})$$

Depending on the interaction term, it will be more helpful to work either in the contour description (H.3) of the interaction terms or in the Keldysh description (H.4). As an example, the terms  $\cos(2\sqrt{2}\phi_{\pm, X})$  are more convenient to deal with in the contour version since they correspond to a coupling term between  $\phi_c$  and  $\phi_q$  in the Keldysh version.

**Remark:** In the following, we will use the notation  $\phi_X \rightarrow \phi(X)$  to enhance the readability.

**Conventions and general properties:**

- **Fourier-transform:**  $f(x, t) = f(X) = \int_{-\infty}^{\infty} \frac{d\omega}{2\pi} \frac{dk}{2\pi} e^{i(\omega t + kx)} f(k, \omega) = \int \frac{d^2 Q}{(2\pi)^2} e^{i\vec{Q}\vec{X}} f(Q)$ .  
Using  $\vec{X} = (t, x)^T$  and  $\vec{Q} = (\omega, k)$ .

- **Parametrization of the quadratic sector:** At second order, the derivative couplings of the action will also be renormalized. Therefore, we use a flexible representation of the form:

$$S_0 = \frac{1}{2} \int \frac{d\omega}{2\pi} \int \frac{dk}{2\pi} (\phi_c(-Q) \phi_q(-Q)) \begin{pmatrix} i(\eta_{qq}^2 k^2 - \epsilon_{qq}^2 \omega^2) & \epsilon_{cq}^2 \omega^2 - \eta_{cq}^2 k^2 \\ \epsilon_{cq}^2 \omega^2 - \eta_{cq}^2 k^2 & i(\eta_{cc}^2 k^2 - \epsilon_{cc}^2 \omega^2) \end{pmatrix} \begin{pmatrix} \phi_c(Q) \\ \phi_q(Q) \end{pmatrix}. \quad (\text{I.2})$$

The corresponding correlators are therefore given by (with  $\chi_{ab}$  as in the main text (4.140)):

$$\begin{aligned} \langle \phi_a(0, k) \phi_b(0, -k) \rangle &=: \chi_{ab} \int \frac{d\omega}{2\pi} \frac{\eta_{ab}^2 k^2 - \epsilon_{ab}^2 \omega^2}{\Delta\epsilon(\omega - z|k|)(\omega + z|k|)(\omega - z^*|k|)(\omega + z^*|k|)} \\ &= \frac{\chi_{ab}}{2} \left[ \frac{\eta_{ab}^2}{\sqrt{\Delta\eta}} - \frac{\epsilon_{ab}^2}{\sqrt{\Delta\epsilon}} \right] \frac{i}{\sqrt{\Delta\epsilon}(z - z^*)}. \end{aligned} \quad (\text{I.3})$$

It depends on the poles of the propagator, which are given by

$$\begin{aligned} z^2 &= \pm \sqrt{\frac{(\epsilon_{cq}^2 \eta_{cq}^2 + \frac{1}{2}(\epsilon_{qq}^2 \eta_{cc}^2 + \epsilon_{cc}^2 \eta_{qq}^2))^2 - \Delta\eta \Delta\epsilon}{\Delta\epsilon^2} + \frac{\epsilon_{cq}^2 \eta_{cq}^2 + \frac{1}{2}(\epsilon_{qq}^2 \eta_{cc}^2 + \epsilon_{cc}^2 \eta_{qq}^2)}{\Delta\epsilon}}, \\ \Delta\epsilon &:= \epsilon_{cc}^2 \epsilon_{qq}^2 + \epsilon_{cq}^4, \quad \Delta\eta := \eta_{cc}^2 \eta_{qq}^2 + \eta_{cq}^4. \end{aligned}$$

• **Properties of the action:** The microscopic action in the contour basis is invariant under exchanging  $\phi_+$  and  $\phi_-$  and complex conjugating all the couplings:

$$\phi_+ \rightarrow \phi_-, \quad \phi_- \rightarrow \phi_+, \quad \{g_i\} \rightarrow \{g_i^*\}. \quad (\text{I.4})$$

As an example, consider the terms  $i \int_X \lambda_+ \cos(2\sqrt{2}\phi_{+,X})$  and  $i \int_X \lambda_- \cos(2\sqrt{2}\phi_{-,X})$  in the action, (H.3). They are converted into each other under (I.4) for  $\lambda_+ = \lambda_-^*$ . This symmetry will be preserved during the RG steps and therefore restrains certain contributions from the RG to be real valued.

• **Initial conditions:** The initial ( $s = 0$ ) derivative and interaction couplings (from integrating out the absolute mode to second order) in the contour basis are given by:

$$\begin{aligned} \eta_{cc}^2(0) &= \frac{2}{\pi^2} \frac{(\gamma_M + \gamma_B)}{\nu}, \quad \eta_{qq}^2(0) = \frac{2}{\pi^2} \frac{\gamma_M}{\nu}, \quad \eta_{cq}^2(0) = \frac{1}{\pi}, \\ \epsilon_{cc}^2(0) &= \epsilon_{qq}^2(0) = 0, \quad \epsilon_{cq}^2(0) = \frac{1}{\pi}, \\ \lambda_c(0)/m^2 &= \lambda_q(0)/m^2 = -\frac{1}{16} \left( \frac{(2\gamma_M + \gamma_B)^2}{\nu^2} + \frac{\gamma_B^2}{\nu^2} \right), \\ \lambda_{cq}^{(e)}(0)/m^2 &= -\frac{\gamma_M}{\nu} + \frac{1}{8} \frac{\gamma_M(\gamma_M + \gamma_B)}{\nu^2} - \frac{1}{4} \left( \frac{(2\gamma_M + \gamma_B)^2}{\nu^2} - \frac{\gamma_B^2}{\nu^2} \right). \end{aligned} \quad (\text{I.5})$$

Note that in this basis all couplings are real, a property that is preserved during the flow.

## I.1 $\langle \Delta S \rangle_{<} - 1\text{st Order Renormalization}$

Integrating out the fast modes in  $\langle \Delta S \rangle_{<}$  leads to the following set of terms:

interactions  $\lambda_c, \lambda_q$ :

$$\begin{aligned} \langle \cos(4(\phi_c^>(X) + \phi_c^<(X))) \rangle_{<} &= \cos(4\phi_c^>(X)) e^{-8\langle (\phi_c^<(X))^2 \rangle_{<}}, \\ \langle \cos(4(\phi_q^>(X) + \phi_q^<(X))) \rangle_{<} &= \cos(4\phi_q^>(X)) e^{-8\langle (\phi_q^<(X))^2 \rangle_{<}}, \end{aligned} \quad (\text{I.6})$$

interactions  $\lambda_{cq}^{(c)}$ :

$$\begin{aligned} &\langle \cos(2(\phi_c^>(X) + \phi_c^<(X))) \cos(2(\phi_q^>(X) + \phi_q^<(X))) \rangle_{<} = \\ &\frac{1}{2} \cos(2(\phi_c^>(X) + \phi_q^>(X))) e^{-2\langle (\phi_c^<(X) + \phi_q^<(X))^2 \rangle_{<}} + \frac{1}{2} \cos(2(\phi_c^>(X) - \phi_q^>(X))) e^{-2\langle (\phi_c^<(X) - \phi_q^<(X))^2 \rangle_{<}} \\ &= \frac{1}{2} [\cos(2\phi_c^>(X)) \cos(2\phi_q^>(X)) - \sin(2\phi_c^>(X)) \sin(2\phi_q^>(X))] e^{-2\langle (\phi_c^<(X) + \phi_q^<(X))^2 \rangle_{<}} \\ &+ \frac{1}{2} [\cos(2\phi_c^>(X)) \cos(2\phi_q^>(X)) + \sin(2\phi_c^>(X)) \sin(2\phi_q^>(X))] e^{-2\langle (\phi_c^<(X) - \phi_q^<(X))^2 \rangle_{<}}, \end{aligned} \quad (\text{I.7})$$

interactions  $\lambda_{cq}^{(q)}$ :

$$\begin{aligned} &\langle \sin(2(\phi_c^>(X) + \phi_c^<(X))) \sin(2(\phi_q^>(X) + \phi_q^<(X))) \rangle_{<} = \\ &-\frac{1}{2} \cos(2(\phi_c^>(X) + \phi_q^>(X))) e^{-2\langle (\phi_c^<(X) + \phi_q^<(X))^2 \rangle_{<}} + \frac{1}{2} \cos(2(\phi_c^>(X) - \phi_q^>(X))) e^{-2\langle (\phi_c^<(X) - \phi_q^<(X))^2 \rangle_{<}} \\ &= \frac{1}{2} \cos(2\phi_c^>(X)) \cos(2\phi_q^>(X)) \left[ -e^{-2\langle (\phi_c^<(X) + \phi_q^<(X))^2 \rangle_{<}} + e^{-2\langle (\phi_c^<(X) - \phi_q^<(X))^2 \rangle_{<}} \right] \\ &+ \frac{1}{2} \sin(2\phi_c^>(X)) \sin(2\phi_q^>(X)) \left[ e^{-2\langle (\phi_c^<(X) + \phi_q^<(X))^2 \rangle_{<}} + e^{-2\langle (\phi_c^<(X) - \phi_q^<(X))^2 \rangle_{<}} \right]. \end{aligned} \quad (\text{I.8})$$

By performing the symmetric rescaling, the flow equations in Sec. 4.8.1 are obtained.

## I.2 2nd Order Renormalization

In the second order RG, many different terms are renormalized and newly created as well, including the derivative couplings and interaction couplings. To deal with the range of terms, we first of all check, which terms are renormalized from which combinations of interaction terms. We label these combinations by the product  $\lambda_i \cdot \lambda_j$ , which emerge in, e.g.,  $\langle \Delta S^2 \rangle_{<}$ :

$$\begin{aligned} \frac{i}{2} (\langle \Delta S^2 \rangle_{<} - \langle \Delta S \rangle_{<}^2) &= \sum_{a,b \in \mathcal{C}} \Delta S_{ab}, \\ \mathcal{C}_K &:= \{c, q, cq^{(c)}, cq^{(s)}\} \text{ or } \mathcal{C}_C := \{+, -, +^{-(c)}, +^{-(s)}\}. \end{aligned}$$

The sets  $\mathcal{C}_K$  and  $\mathcal{C}_C$  specify the set of indices, depending on the description (Keldysh vs. contour). Firstly, the derivative and couplings terms subject to renormalization are given in Tab. I.1. Secondly, we also indicate terms, which we

	2nd order	correction to	neglected
derivative corr.	$\lambda_q^2$	$(\nabla\phi_q)^2$	$\cos(8\phi_q)$
	$\lambda_c^2$	$(\nabla\phi_c)^2$	$\cos(8\phi_c)$
	$\lambda_+^2$	$(\nabla\phi_q)^2, (\nabla\phi_c)^2, (\nabla\phi_c)(\nabla\phi_q)$	$\cos(4\sqrt{2}\phi_+)$
	$\lambda_-^2$	$(\nabla\phi_q)^2, (\nabla\phi_c)^2, (\nabla\phi_c)(\nabla\phi_q)$	$\cos(4\sqrt{2}\phi_-)$
potential corr.	$\lambda_+\lambda_{+-}^{(c)}, \lambda_+\lambda_{+-}^{(s)}$	$\cos(2\sqrt{2}\phi_-)$	$\cos(2\sqrt{2}(2\phi_+ \pm \phi_-))$
	$\lambda_-\lambda_{+-}^{(c)}, \lambda_-\lambda_{+-}^{(s)}$	$\cos(2\sqrt{2}\phi_+)$	$\cos(2\sqrt{2}(2\phi_- \pm \phi_+))$
	$\lambda_+\lambda_-$	$\cos(4\phi_c), \cos(4\phi_q)$	
	$\lambda_c\lambda_q$		$\cos(4\sqrt{2}\phi_\pm)$

**Table I.1:** *Derivative and interaction terms present in the different contributions  $\Delta S_{ab}$ 's from the second order RG, which will either give an (additive) correction or are ignored due to stronger suppression at first order compared to the interaction terms already included in  $\langle\Delta S\rangle_<$ .*

will neglect in the following, because they are more strongly suppressed already at first order. In particular, this refers to terms like  $\cos(8\phi_q)$ , which are much stronger suppressed in first order than  $\cos(4\phi_q)$ .

**Remark:** The list is not exhaustive, there are also interaction terms like  $(\partial_x\phi_\alpha)^2 \cos(\gamma\phi_\beta)$ , which we will neglect as well. In the following, we consider one example in detail and afterwards investigate the different contributions, organized by  $\lambda_i \cdot \lambda_j$ .

#### Example with details:

We start with the terms of order  $\lambda_q^2$ :

$$\Delta S_{qq} = -\frac{i}{4}\lambda_q^2 \int d^2X d^2Y \left[ (e^{-16\langle\phi_q^<(X)\phi_q^<(Y)\rangle} - 1)e^{-16\langle(\phi_q^<)^2\rangle} \cos(4(\phi_q^>(X) + \phi_q^>(Y))) \right. \\ \left. + (e^{+16\langle\phi_q^<(X)\phi_q^<(Y)\rangle} - 1)e^{-16\langle(\phi_q^<)^2\rangle} \cos(4(\phi_q^>(X) - \phi_q^>(Y))) \right].$$

At first, these terms seem hard to handle due to the coordinates  $X$  and  $Y$  being arbitrary. Nevertheless, the correlations at different  $X$  and  $Y = X + \delta X$  with  $(\delta X := (\delta t, \delta x))$  are decaying and therefore we can expand in  $\delta X$  (see, e.g., Ref. [242]). Secondly, for small  $\delta X$ ,  $\cos(4(\phi_q^>(X) + \phi_q^>(Y))) \rightarrow \cos(8\phi_q^>(X))$ , which is less relevant and will be ignored. The relevant term is  $(\nabla^T := (\partial_t, \partial_x))$ :

$$\cos(4(\phi_q^>(X) - \phi_q^>(X + \delta X))) \approx 1 - 8(\delta X \nabla \phi_q^>(X))^2. \quad (I.9)$$

In the next step, we have to evaluate the two exponential factors in  $\Delta S_{qq}$ . The first one is already linear in the small parameter  $s$ :

$$(e^{\pm 16\langle\phi_q^<(X)\phi_q^<(X+\delta X)\rangle} - 1) \approx \underbrace{(\pm 16\langle\phi_q^<(X)\phi_q^<(X + \delta X)\rangle)}_{\sim \mathcal{O}(s)} + \mathcal{O}(s^2). \quad (I.10)$$

For the flow equations we only need to consider expressions of order  $\mathcal{O}(s)$  and

can neglect the second term in (I.10). The second exponential

$$e^{-16\langle(\phi_q^<)^2\rangle} = 1 + \mathcal{O}(s)$$

gives no additional correction. Thirdly, we have to consider the rescaling step: a factor of  $b^2 = e^{2s}$  is added, which also does not change the expression to first order in  $s$ .

At last, we have to evaluate the remaining integrals over  $\delta X$ . Generalizing to arbitrary field combinations, the two possible expressions (with a leading linear scaling in  $s$ ) are given by:

potential corrections:

$$\mathcal{A}_{ab} = \int d^2(\delta X) \langle \phi_a(X) \phi_b(X + \delta X) \rangle \approx \underbrace{\chi_{ab} \frac{i}{\sqrt{\Delta\epsilon}(z^* - z)} \left( \frac{\eta_{ab}^2}{\sqrt{\Delta\eta}} - \frac{\epsilon_{ab}^2}{\sqrt{\Delta\epsilon}} \right)}_{=: A_{ab}} (A_1 \cdot s), \quad (\text{I.11})$$

derivative corrections:

$$\mathcal{B}_{ab}^{(t,x)} = \int d^2(\delta X) \left( \frac{\delta t^2}{\delta x^2} \right) \langle \phi_a(X) \phi_b(X + \delta X) \rangle \approx \chi_{ab} \left( \begin{array}{c} \eta_{ab}^2 \\ \Delta\eta \\ -\frac{\epsilon_{ab}^2}{\Delta\epsilon} \end{array} \right) (A_2 \cdot s). \quad (\text{I.12})$$

The dimensionless, real numbers  $A_1, A_2$  contain the parameter independent contribution of the integrals. Both couplings have to be real, which can be inferred from (i) the symmetry mentioned above (I.4) and (ii) from the limiting case  $\gamma_B = 0$ , resulting in the flow equations derived in Ref. [19]. We derive the overall scaling of these expressions in App. I.3.

In summary, the contribution  $\Delta S_{qq}$  gives rise to additive corrections to the derivative couplings  $\epsilon_{qq}^2$  and  $\eta_{qq}^2$ :

$$\begin{aligned} \Delta S_{qq} &\approx +2i\lambda_q^2 \int d^2 X \int d^2(\delta X) \left[ (e^{+16\langle\phi_q^<(X)\phi_q^<(X+\delta X)\rangle} - 1) (\delta X \nabla \phi_q(X))^2 \right] \\ &\approx 32i\lambda_q^2 \int d^2 X \left( \mathcal{B}_{qq}^{(t)} (\partial_t \phi_q(X))^2 + \mathcal{B}_{qq}^{(x)} (\partial_x \phi_q(X))^2 \right), \end{aligned} \quad (\text{I.13})$$

which, using (I.12), is linear in  $s$ .

### Corrections of the derivative terms at second order

As given in Tab. I.1, the derivative corrections emerge from the terms  $\Delta S_{aa}$ . The corresponding corrections are given below, making use of (I.12) and are derived using the mixed representation (H.5).

$$\begin{aligned}
 \lambda_q^2 : \quad \Delta S_{qq} &= +2i\lambda_q^2 \int d^2 X \int d^2(\delta X) \left[ (e^{+16\langle\phi_q^<(X)\phi_q^<(X+\delta X)\rangle} - 1)(\delta X \nabla \phi_q(X))^2 \right] \\
 &\approx 32i\lambda_q^2 \int d^2 X \left( \mathcal{B}_{qq}^{(t)} (\partial_t \phi_q(X))^2 + \mathcal{B}_{qq}^{(x)} (\partial_x \phi_q(X))^2 \right), \\
 \hline
 \lambda_c^2 : \quad \Delta S_{cc} &= +2i\lambda_c^2 \int d^2 X \int d^2(\delta X) \left[ (e^{+16\langle\phi_c^<(X)\phi_c^<(X+\delta X)\rangle} - 1)(\delta X \nabla \phi_c(X))^2 \right] \\
 &\approx 32i\lambda_c^2 \int d^2 X \left( \mathcal{B}_{cc}^{(t)} (\partial_t \phi_c(X))^2 + \mathcal{B}_{cc}^{(x)} (\partial_x \phi_c(X))^2 \right), \\
 \hline
 \lambda_+^2 : \quad \Delta S_{++} &= +i\lambda_+^2 \int d^2 X \int d^2(\delta X) \left[ (e^{+8\langle\phi_+^<(X)\phi_+^<(X+\delta X)\rangle} - 1)(\delta X \nabla \phi_+(X))^2 \right] \\
 &\approx i8\lambda_+^2 \int d^2 X \left( \mathcal{B}_{++}^{(t)} [(\partial_t \phi_c(X))^2 + (\partial_t \phi_q(X))^2 + 2(\partial_t \phi_c(X))(\partial_t \phi_q(X))] \right. \\
 &\quad \left. + \mathcal{B}_{++}^{(x)} [(\partial_x \phi_c(X))^2 + (\partial_x \phi_q(X))^2 + 2(\partial_x \phi_c(X))(\partial_x \phi_q(X))] \right), \\
 \hline
 \lambda_-^2 : \quad \Delta S_{--} &= +i\lambda_-^2 \int d^2 X \int d^2(\delta X) \left[ (e^{+8\langle\phi_-^<(X)\phi_-^<(X+\delta X)\rangle} - 1)(\delta X \nabla \phi_-(X))^2 \right] \\
 &\approx i8\lambda_-^2 \int d^2 X \left( \mathcal{B}_{--}^{(t)} [(\partial_t \phi_c)^2 + (\partial_t \phi_q)^2 - 2(\partial_t \phi_c(X))(\partial_t \phi_q(X))] \right. \\
 &\quad \left. + \mathcal{B}_{--}^{(x)} [(\partial_x \phi_c(X))^2 + (\partial_x \phi_q(X))^2 - 2(\partial_x \phi_c(X))(\partial_x \phi_q(X))] \right).
 \end{aligned}$$

Since the derivative couplings only get corrected at second order in  $\lambda$ 's, we can directly read off the corresponding flow equations, based on the definition of the quadratic part of the action, (I.2) with  $a \in \{q, c\}$  and  $\bar{a}$  the respective opposite:

$$\begin{aligned}
 \partial_s \eta_{aa}^2 &\approx \left[ -64\lambda_a^2 \frac{\epsilon_{\bar{a}\bar{a}}^2}{\Delta\epsilon} - 4 \left[ (\lambda_{cq}^{(c)})^2 - (\lambda_{cq}^{(s)})^2 \right] \left( \frac{\epsilon_{\bar{a}\bar{a}}^2 + \epsilon_{aa}^2}{\Delta\epsilon} \right) - 16\lambda_{cq}^{(c)} \lambda_{cq}^{(s)} \frac{\epsilon_{cq}^2}{\Delta\epsilon} \right] A_2, \\
 \partial_s \epsilon_{aa}^2 &\approx \left[ -64\lambda_a^2 \frac{\eta_{\bar{a}\bar{a}}^2}{\Delta\eta} - 4 \left[ (\lambda_{cq}^{(c)})^2 - (\lambda_{cq}^{(s)})^2 \right] \left( \frac{\eta_{\bar{a}\bar{a}}^2 + \eta_{aa}^2}{\Delta\eta} \right) - 16\lambda_{cq}^{(c)} \lambda_{cq}^{(s)} \frac{\eta_{cq}^2}{\Delta\eta} \right] A_2, \\
 \partial_s \eta_{cq}^2 &\approx \left[ -8\lambda_{cq}^{(c)} \lambda_{cq}^{(s)} \left( \frac{\epsilon_{cc}^2 + \epsilon_{qq}^2}{\Delta\epsilon} \right) + 8 \left[ (\lambda_{cq}^{(c)})^2 - (\lambda_{cq}^{(s)})^2 \right] \frac{\epsilon_{cq}^2}{\Delta\epsilon} \right] A_2, \\
 \partial_s \epsilon_{cq}^2 &\approx \left[ -8\lambda_{cq}^{(c)} \lambda_{cq}^{(s)} \left( \frac{\eta_{cc}^2 + \eta_{qq}^2}{\Delta\eta} \right) + 8 \left[ (\lambda_{cq}^{(c)})^2 - (\lambda_{cq}^{(s)})^2 \right] \frac{\eta_{cq}^2}{\Delta\eta} \right] A_2.
 \end{aligned}$$

### Corrections of the potential terms at second order

In contrast to the equilibrium BKT analysis, the potential terms are also renormalized at second order, see again Tab. I.1. Using (I.11), the corrections (including rescaling) to the action read:

$$\Delta S_{+,+-} \approx -2i\lambda_+ b^2 \int d^2 X \left[ \lambda_{+-}^{(c)} \mathcal{A}_{++} - \lambda_{+-}^{(s)} \mathcal{A}_{+-} \right] \cos(2\sqrt{2}\phi_-(X)),$$

$$\Delta S_{-,-} \approx -2i\lambda_- b^2 \int d^2 X \left[ \lambda_{+-}^{(c)} \mathcal{A}_{--} - \lambda_{+-}^{(s)} \mathcal{A}_{+-} \right] \cos(2\sqrt{2}\phi_+(X)),$$

-----  
**Combined (Keldysh basis)**

$$\begin{aligned} \Delta S_{\pm,+-} = & \int d^2 X b^2 \left[ -4 \left[ i\lambda_c \lambda_{cq}^{(c)} \mathcal{A}_{cc} + i\lambda_q \lambda_{cq}^{(c)} \mathcal{A}_{qq} - (\lambda_c + \lambda_q) \lambda_{cq}^{(s)} \mathcal{A}_{cq} \right] \cos(2\phi_c) \cos(2\phi_q) \right. \\ & \left. - 4 \left[ \lambda_c \lambda_{cq}^{(s)} \mathcal{A}_{cc} - \lambda_q \lambda_{cq}^{(s)} \mathcal{A}_{qq} + i(\lambda_c + \lambda_q) \lambda_{cq}^{(c)} \mathcal{A}_{cq} \right] \sin(2\phi_c) \sin(2\phi_q) \right], \end{aligned}$$

$$\Delta S_{+,-} \approx -i4\lambda_+ \lambda_- b^2 \int d^2 X \left[ -(\mathcal{A}_{cc} - \mathcal{A}_{qq}) \cos(4\phi_c(X)) + (\mathcal{A}_{cc} - \mathcal{A}_{qq}) \cos(4\phi_q) \right].$$

The additional factor of 2 results from the fact that the terms are a cross product between different  $\lambda_i$ 's and therefore appear twice in the overall correction.

Collecting the first and second order corrections to the potential cosine terms, the flow equations for  $\lambda_i$ 's are obtained by using the first order approximations (I.11) ( $4\pi A_1 =: \bar{A}_1$ ):

$$\partial_s \lambda_c = \left( 2 + \frac{4}{\pi} A_{cc} \right) \lambda_c + \frac{1}{4\pi} \left( (\lambda_{cq}^{(c)})^2 + (\lambda_{cq}^{(s)})^2 \right) (A_{cc} - A_{qq}) \bar{A}_1, \quad (\text{I.14})$$

$$\partial_s \lambda_q = \left( 2 + \frac{4}{\pi} A_{qq} \right) \lambda_q - \frac{1}{4\pi} \left( (\lambda_{cq}^{(c)})^2 + (\lambda_{cq}^{(s)})^2 \right) (A_{cc} - A_{qq}) \bar{A}_1, \quad (\text{I.15})$$

$$\begin{aligned} \partial_s \lambda_{cq}^{(c)} = & \left( 2 + \frac{1}{\pi} \left( (1 - \lambda_c \bar{A}_1) A_{cc} + (1 - \lambda_q \bar{A}_1) A_{qq} \right) \right) \lambda_{cq}^{(c)} \\ & + i \frac{1}{\pi} \left( (2 - (\lambda_c + \lambda_q) \bar{A}_1) A_{cq} \right) \lambda_{cq}^{(s)}, \end{aligned} \quad (\text{I.16})$$

$$\begin{aligned} \partial_s \lambda_{cq}^{(s)} = & \left( 2 + \frac{1}{\pi} \left( (1 + \lambda_c \bar{A}_1) A_{cc} + (1 + \lambda_q \bar{A}_1) A_{qq} \right) \right) \lambda_{cq}^{(s)} \\ & - i \frac{1}{\pi} \left( (2 + (\lambda_c + \lambda_q) \bar{A}_1) A_{cq} \right) \lambda_{cq}^{(c)}. \end{aligned} \quad (\text{I.17})$$

### I.3 Scaling of the Integral Expressions

In the remaining part, we analyze the integral expressions  $\mathcal{A}_{ab}$  ((I.11)) and  $\mathcal{B}_{ab}$  ((I.12)) in more detail and extract the aforementioned scaling behavior. Both expressions depend on the propagator  $\langle \phi_a(0) \phi_b(X) \rangle$ , which in Fourier space takes the qualitative form:

$$\langle \phi_a(-Q) \phi_b(Q) \rangle < \sim \frac{\epsilon_{ab} \omega^2 - \eta_{ab} k^2}{(\omega^2 - z^2 k^2)(\omega^2 - (z^*)^2 k^2)}. \quad (\text{I.18})$$

The scaling of the expressions of  $\mathcal{A}_{ab}$  and  $\mathcal{B}_{ab}$  in turn depends on the poles of the propagator,  $\omega = \pm z|k|, \pm z^*|k|$ . Since we are analyzing the stability of the scale invariant theory, where space and time are treated on equal footing, it is reasonable to 'symmetrize' the above expression in a way which makes  $\omega$  and  $k$

(nearly) exchangeable. To this end, we perform the rescaling:

$$\begin{aligned}\omega^2 &= |z|\tilde{\omega}^2, & t^2 &= |z|^{-1}\tilde{t}^2, \\ k^2 &= |z|^{-1}\tilde{k}^2, & x^2 &= |z|\tilde{x}^2.\end{aligned}\tag{I.19}$$

In turn, the denominator of the above expression (I.18) is symmetric under  $\tilde{x} \leftrightarrow \tilde{t}, \tilde{k} \leftrightarrow \tilde{\omega}$ .

### Scaling of $\mathcal{A}_{ab}$ :

To derive the scaling behavior of  $\mathcal{A}_{ab}$ , we introduce two ‘symmetric’ expressions, based on the above rescaling<sup>1</sup>:

$$\begin{aligned}\mathcal{A}_1^{(\omega)}(\alpha) &= \int d^2\tilde{X} \int \frac{d^2\tilde{Q}}{(2\pi)^2} \frac{\tilde{\omega}^2 e^{-i\tilde{Q}\tilde{X}}}{(\alpha\tilde{\omega}^2 - \alpha^{-1}\tilde{k}^2)(\alpha^{-1}\tilde{\omega}^2 - \alpha\tilde{k}^2)}, \\ \mathcal{A}_1^{(k)}(\alpha) &= \int d^2\tilde{X} \int \frac{d^2\tilde{Q}}{(2\pi)^2} \frac{\tilde{k}^2 e^{-i\tilde{Q}\tilde{X}}}{(\alpha\tilde{\omega}^2 - \alpha^{-1}\tilde{k}^2)(\alpha^{-1}\tilde{\omega}^2 - \alpha\tilde{k}^2)},\end{aligned}\tag{I.20}$$

with  $\alpha := \sqrt{\frac{z^*}{z}}$ . We assume that both expressions are equal, meaning that the transformation  $\tilde{x} \leftrightarrow \tilde{t}, \tilde{k} \leftrightarrow \tilde{\omega}$  leaves the expressions invariant. This in turn implies that we assume that there exists a regularization scheme, which is consistent with this requirement. In this framework,  $\mathcal{A}_{ab}$  can be written as

$$\mathcal{A}_{ab} = \int d^2X \langle \phi_a(0)\phi_b(X) \rangle_{<} = \chi_{ab} \left( \frac{\eta_{ab}^2}{\Delta\epsilon|z|^3} - \frac{\epsilon_{ab}^2}{\Delta\epsilon|z|} \right) \mathcal{A}_1(\alpha),\tag{I.21}$$

$$\Delta\epsilon = \epsilon_{cc}^2\epsilon_{qq}^2 + \epsilon_{cq}^4, \quad \Delta\eta = \eta_{cc}^2\eta_{qq}^2 + \eta_{cq}^4,\tag{I.22}$$

where  $\mathcal{A}_1(\alpha)$  still depends on  $\alpha$  and therefore on the derivative couplings. To extract the remaining scaling, we identify

$$(\alpha - \alpha^{-1})\mathcal{A}_1 = \int \frac{d^2\tilde{X}d^2\tilde{Q}}{(2\pi)^2} \frac{1}{\tilde{\omega}^2 - \tilde{k}^2} e^{-i\tilde{Q}\tilde{X}} =: A_1(s) \approx A_1 \cdot s,\tag{I.23}$$

with  $\alpha^{-1}\tilde{\omega}^2 = \tilde{\omega}^2, \alpha\tilde{k}^2 = \tilde{k}^2$ . The remaining integral does not depend on the derivative couplings and gives rise to an  $s$  dependent constant  $A_1(s) \approx A_1 \cdot s$ . Therefore, we get the relation  $\mathcal{A}_1(\alpha) = \frac{|z|}{z^* - z} A_1$ .

### Scaling of $\mathcal{B}_{ab}^{(t,x)}$ :

The scaling of  $\mathcal{B}_{ab}^{(t,x)}$  is a bit more tedious to extract, though simplifications arise in the limit  $\gamma_B = 0$ , which we take as a starting point. We use two approaches: (i) a direct approach (not generalizable) and (ii) an indirect approach, which, though being less informative, allows us together with (i) to infer the scaling for  $\gamma_B \neq 0$ . For  $\gamma_B = 0$ , the different Keldysh contours are essentially decoupled

<sup>1</sup>We left the integration domains unspecified intentionally, as they can depend on the exact regularization scheme to be used.

(see App. I.6 for more details) and the correlator for the +-contour reads:

$$\langle \phi_+(0)\phi_+(X) \rangle = \int \frac{d^2Q}{(2\pi)^2} \frac{-e^{-i\vec{Q}\vec{X}}(\epsilon_+^2\omega^2 - \eta_+^2k^2)}{(\epsilon_+^2\omega^2 - \eta_+^2k^2)(\epsilon_-^2\omega^2 - \eta_-^2k^2)} \quad (\text{I.24})$$

$$= \int \frac{d^2Q}{(2\pi)^2} \frac{-e^{-i\vec{Q}\vec{X}}((z^*)^{-1}\omega^2 - z^*k^2)}{\epsilon_+\eta_+(z^{-1}\omega^2 - zk^2)((z^*)^{-1}\omega^2 - z^*k^2)}, \quad (\text{I.25})$$

$$z^2 := \frac{\eta_+^2}{\epsilon_+^2}, \quad (z^*)^2 = \frac{\eta_-^2}{\epsilon_-^2}. \quad (\text{I.26})$$

Notice that the numerator and one term in the denominator cancel each other, but we keep this structure for now as it will reappear later. Using the same rescaling as before:

$$\langle \phi_+(0)\phi_+(X) \rangle = - \int \frac{d^2\tilde{Q}}{(2\pi)^2} \frac{e^{-i\tilde{Q}\vec{X}}(\alpha^{-1}\tilde{\omega}^2 - \alpha\tilde{k}^2)}{\epsilon_+\eta_+(\alpha\tilde{\omega}^2 - \alpha^{-1}\tilde{k}^2)(\alpha^{-1}\tilde{\omega}^2 - \alpha\tilde{k}^2)}. \quad (\text{I.27})$$

The integrals  $\mathcal{B}_{ab}^{(t,x)}$  for  $a = b = +$  are given by (making use of translational invariance):

$$\begin{pmatrix} \mathcal{B}_{++}^{(t)} \\ \mathcal{B}_{++}^{(x)} \end{pmatrix} = \int d^2(\delta X) \begin{pmatrix} (\delta t)^2 \\ (\delta x)^2 \end{pmatrix} \langle \phi_+(0)\phi_+(\delta X) \rangle. \quad (\text{I.28})$$

**Approach (i):** the expression can be directly evaluated, simplifying the numerator and denominator (and using a rescaling  $\alpha\tilde{\omega}^2 = \tilde{\omega}^2$  etc.):

$$\begin{aligned} \mathcal{B}_{++}^{(t)} &= - \frac{1}{|z|} \int d^2\tilde{X}\tilde{t}^2 \int \frac{d^2\tilde{Q}}{(2\pi)^2} \frac{e^{-i\tilde{Q}\vec{X}}}{\epsilon_+\eta_+(\alpha\tilde{\omega}^2 - \alpha^{-1}\tilde{k}^2)} \\ &= - \underbrace{\frac{\alpha}{|z|}}_{=\frac{1}{\eta_+^2}} \underbrace{\frac{1}{\epsilon_+\eta_+} \int d^2\tilde{X}\tilde{t}^2 \int \frac{d^2\tilde{Q}}{(2\pi)^2} \frac{\pi e^{-i\tilde{Q}\vec{X}}}{(\tilde{\omega}^2 - \tilde{k}^2)}}_{=:A_2(s)\approx A_2\cdot s} = -\frac{1}{\eta_+^2} A_2(s). \end{aligned} \quad (\text{I.29})$$

$A_2(s)$  is another integral, which does not depend on the propagator details, but will depend on the exact regularization procedure. For  $\gamma_B \neq 0$ , the situation is more difficult because the terms in the numerator and denominator do not cancel each other out.

**Approach (ii):** We split the expression for  $\langle \phi_+(0)\phi_+(X) \rangle$  into two parts, not relying on the cancelations between numerator and denominator:

$$\begin{aligned} \langle \phi_+(0)\phi_+(X) \rangle &= - \underbrace{\int \frac{d^2\tilde{Q}}{(2\pi)^2} \frac{e^{-i\tilde{Q}\vec{X}}\alpha^{-1}\tilde{\omega}^2}{\epsilon_+\eta_+(\alpha\tilde{\omega}^2 - \alpha^{-1}\tilde{k}^2)(\alpha^{-1}\tilde{\omega}^2 - \alpha\tilde{k}^2)}}_{:= -\frac{\alpha^{-1}}{\epsilon_+\eta_+} G^{(\omega)}} \\ &\quad + \underbrace{\int \frac{d^2\tilde{Q}}{(2\pi)^2} \frac{e^{-i\tilde{Q}\vec{X}}\alpha\tilde{k}^2}{\epsilon_+\eta_+(\alpha\tilde{\omega}^2 - \alpha^{-1}\tilde{k}^2)(\alpha^{-1}\tilde{\omega}^2 - \alpha\tilde{k}^2)}}_{:= \frac{\alpha}{\epsilon_+\eta_+} G^{(k)}}, \end{aligned}$$

where we have defined:

$$\mathcal{G}^{(y \in \{k, \omega\})} := \int \frac{d^2 \tilde{Q}}{(2\pi)^2} \frac{e^{-i\tilde{Q}\tilde{X}} \tilde{y}^2}{(\alpha\tilde{\omega}^2 - \alpha^{-1}\tilde{k}^2)(\alpha^{-1}\tilde{\omega}^2 - \alpha\tilde{k}^2)}.$$

The integral expressions (I.28) for  $\mathcal{B}_{++}^{(t,x)}$  therefore reduce to

$$\begin{pmatrix} \mathcal{B}_{++}^{(t)} \\ \mathcal{B}_{++}^{(x)} \end{pmatrix} = \int d^2(\delta\tilde{X}) \begin{pmatrix} |z|^{-1}(\delta\tilde{t})^2 \\ |z|(\delta\tilde{x})^2 \end{pmatrix} \left[ -\frac{\alpha^{-1}}{\epsilon_+\eta_+} G^{(\omega)} + \frac{\alpha}{\epsilon_+\eta_+} G^{(k)} \right]. \quad (\text{I.30})$$

To finalize the evaluation, we have to treat the remaining integrals of, e.g., the form  $\int d^2\tilde{X}\tilde{x}^2 G^{(k)}$ . Since we are working under the assumption of a scheme that treats space and time on equal footing, we identify expressions, which result from exchanging  $\tilde{\omega} \leftrightarrow \tilde{k}$  (as we have done before):

$$\underbrace{\int d^2\tilde{X}\tilde{x}^2 G^{(k)}}_{:=A_x^{(k)}} = \underbrace{\int d^2\tilde{X}\tilde{t}^2 G^{(\omega)}}_{:=A_t^{(\omega)}}, \quad \underbrace{\int d^2\tilde{X}\tilde{t}^2 G^{(k)}}_{:=A_t^{(k)}} = \underbrace{\int d^2\tilde{X}\tilde{x}^2 G^{(\omega)}}_{:=A_x^{(\omega)}}.$$

Expressing  $\mathcal{B}_{++}^{(t,x)}$  in terms of the expressions  $C_{\parallel}, C_{\perp}$ , we get:

$$\begin{aligned} \mathcal{B}_{++}^{(t)} &= \frac{1}{|z|} \left[ -\frac{\alpha^{-1}}{\epsilon_+\eta_+} C_{\parallel} + \frac{\alpha}{\epsilon_+\eta_+} C_{\perp} \right] = \left[ -\frac{1}{\epsilon_+\eta_+} \frac{1}{z^*} C_{\parallel} + \frac{1}{\eta_+^2} C_{\perp} \right], \\ \mathcal{B}_{++}^{(x)} &= \left[ -\frac{1}{\epsilon_+^2} C_{\perp} + z^* \frac{1}{\epsilon_+\eta_+} C_{\parallel} \right]. \end{aligned} \quad (\text{I.31})$$

Comparing this approach to the first approach, we get the conditions:

$$\begin{aligned} \mathcal{B}_{++}^{(t)} &= -\frac{1}{\eta_+^2} A_2(s) \stackrel{!}{=} \left[ -\frac{1}{\epsilon_+\eta_+} \frac{1}{z^*} C_{\parallel} + \frac{1}{\eta_+^2} C_{\perp} \right], \\ \mathcal{B}_{++}^{(x)} &= \frac{1}{\epsilon_+^2} A_2(s) \stackrel{!}{=} \left[ -\frac{1}{\epsilon_+^2} C_{\perp} + z^* \frac{1}{\epsilon_+\eta_+} C_{\parallel} \right]. \end{aligned} \quad (\text{I.32})$$

For  $\gamma_B = 0$ , the  $\pm$  couplings are related by complex conjugation<sup>2</sup>. Therefore, the equations simplify to

$$\left[ -\underbrace{\frac{\epsilon_-\eta_+}{\epsilon_+\eta_-}}_{=:\beta} C_{\parallel} + C_{\perp} \right] = -A_2, \quad \left[ -\underbrace{\frac{\epsilon_+\eta_-}{\epsilon_-\eta_+}}_{\beta^*} C_{\parallel} + C_{\perp} \right] = -A_2.$$

For our case (measurement dynamics),  $\beta$  is a complex quantity and the solution requires  $C_{\parallel} \equiv 0$  (this is different from the equilibrium/statistical mechanics case). Therefore, we have the relationship  $C_{\perp} = -A_2(s) \approx -A_2 \cdot s$ , where both quantities do not depend on other parameters anymore. Furthermore, this relation, as well as  $C_{\parallel} = 0$ , hold true for complex  $z$  (independent of  $\gamma_B = 0$  or  $\gamma_B \neq 0$ ). In turn, we can evaluate (I.12) using the same approach and obtain (in the Keldysh basis):

$$\mathcal{B}_{ab}^{(t,x)} \approx \chi_{ab} \begin{pmatrix} \frac{\eta_{ab}^2}{\Delta\eta} C_{\perp} \\ -\frac{\epsilon_{ab}}{\Delta\epsilon} C_{\perp} \end{pmatrix} = -\chi_{ab} \begin{pmatrix} \frac{\eta_{ab}^2}{\Delta\eta} \\ -\frac{\epsilon_{ab}}{\Delta\epsilon} \end{pmatrix} (A_2 \cdot s). \quad (\text{I.33})$$

The sign of  $A_2$  can again be inferred from the case  $\gamma_B = 0$  and the comparison to the analysis in Ref. [19].

<sup>2</sup> $\epsilon_+^* = \epsilon_-$ ,  $\eta_+^* = \eta_-$  and  $z = \eta_+/\epsilon_+$ .

## I.4 2nd Order Renormalization: Full Set of Flow Equations

$$\begin{aligned}
\partial_s \eta_{cc}^2 &= \left[ -64\lambda_q^2 \frac{\epsilon_{qq}^2}{\Delta\epsilon} - 4 \left( \frac{\epsilon_{cc}^2 + \epsilon_{qq}^2}{\Delta\epsilon} \right) \left( (\lambda_{cq}^{(c)})^2 - (\lambda_{cq}^{(s)})^2 \right) - 16\lambda_{cq}^{(c)} \lambda_{cq}^{(s)} \frac{\epsilon_{cq}^2}{\Delta\epsilon} \right] A_2, \\
\partial_s \eta_{qq}^2 &= \left[ -64\lambda_c^2 \frac{\epsilon_{cc}^2}{\Delta\epsilon} - 4 \left( \frac{\epsilon_{cc}^2 + \epsilon_{qq}^2}{\Delta\epsilon} \right) \left( (\lambda_{cq}^{(c)})^2 - (\lambda_{cq}^{(s)})^2 \right) - 16\lambda_{cq}^{(c)} \lambda_{cq}^{(s)} \frac{\epsilon_{cq}^2}{\Delta\epsilon} \right] A_2, \\
\partial_s \eta_{cq}^2 &= \left[ -8\lambda_{cq}^{(c)} \lambda_{cq}^{(s)} \left( \frac{\epsilon_{cc}^2 + \epsilon_{qq}^2}{\Delta\epsilon} \right) + 8 \left( (\lambda_{cq}^{(c)})^2 - (\lambda_{cq}^{(s)})^2 \right) \frac{\epsilon_{cq}^2}{\Delta\epsilon} \right] A_2, \\
\partial_s \epsilon_{cc}^2 &= \left[ -64\lambda_q^2 \frac{\eta_{qq}^2}{\Delta\epsilon z_1^2 z_2^2} - 4 \left( \frac{\eta_{cc}^2 + \eta_{qq}^2}{\Delta\epsilon z_1^2 z_2^2} \right) \left( (\lambda_{cq}^{(c)})^2 - (\lambda_{cq}^{(s)})^2 \right) - 16\lambda_{cq}^{(c)} \lambda_{cq}^{(s)} \frac{\eta_{cq}^2}{\Delta\epsilon z_1^2 z_2^2} \right] A_2, \\
\partial_s \epsilon_{qq}^2 &= \left[ -64\lambda_c^2 \frac{\eta_{cc}^2}{\Delta\epsilon z_1^2 z_2^2} - 4 \left( \frac{\eta_{cc}^2 + \eta_{qq}^2}{\Delta\epsilon z_1^2 z_2^2} \right) \left( (\lambda_{cq}^{(c)})^2 - (\lambda_{cq}^{(s)})^2 \right) - 16\lambda_{cq}^{(c)} \lambda_{cq}^{(s)} \frac{\eta_{cq}^2}{\Delta\epsilon z_1^2 z_2^2} \right] A_2, \\
\partial_s \epsilon_{cq}^2 &= \left[ -8\lambda_{cq}^{(c)} \lambda_{cq}^{(s)} \left( \frac{\eta_{cc}^2 + \eta_{qq}^2}{\Delta\epsilon z_1^2 z_2^2} \right) + 8 \left( (\lambda_{cq}^{(c)})^2 - (\lambda_{cq}^{(s)})^2 \right) \frac{\eta_{cq}^2}{\Delta\epsilon z_1^2 z_2^2} \right] A_2 \\
\partial_s \lambda_c &= \left( 2 + \frac{4}{\pi} \frac{i}{\Delta\epsilon(z_1 + z_2)} \left( \frac{\eta_{cc}^2}{z_1 z_2} + \epsilon_{cc}^2 \right) \right) \lambda_c \\
&\quad + \frac{1}{4\pi} \left( (\lambda_{cq}^{(c)})^2 + (\lambda_{cq}^{(s)})^2 \right) \frac{i}{\Delta\epsilon(z_1 + z_2)} \left( \frac{\eta_{cc}^2 - \eta_{qq}^2}{z_1 z_2} + (\epsilon_{cc}^2 - \epsilon_{qq}^2) \right) A_1, \\
\partial_s \lambda_q &= \left( 2 + \frac{4}{\pi} \frac{i}{\Delta\epsilon(z_1 + z_2)} \left( \frac{\eta_{qq}^2}{z_1 z_2} + \epsilon_{qq}^2 \right) \right) \lambda_q \\
&\quad - \frac{1}{4\pi} \left( (\lambda_{cq}^{(c)})^2 + (\lambda_{cq}^{(s)})^2 \right) \frac{i}{\Delta\epsilon(z_1 + z_2)} \left( \frac{\eta_{cc}^2 - \eta_{qq}^2}{z_1 z_2} + (\epsilon_{cc}^2 - \epsilon_{qq}^2) \right) A_1, \\
\partial_s \lambda_{cq}^{(c)} &= \left( 2 + \frac{1}{\pi} \frac{i}{\Delta\epsilon(z_1 + z_2)} \left( (1 - \lambda_c A_1) \left( \frac{\eta_{cc}^2}{z_1 z_2} + \epsilon_{cc}^2 \right) + (1 - \lambda_q A_1) \left( \frac{\eta_{qq}^2}{z_1 z_2} + \epsilon_{qq}^2 \right) \right) \right) \lambda_{cq}^{(c)} \\
&\quad + \frac{1}{\pi} \frac{i}{\Delta\epsilon(z_1 + z_2)} (2 - (\lambda_c + \lambda_q) A_1) \left( \frac{\eta_{cq}^2}{z_1 z_2} + \epsilon_{cq}^2 \right) \lambda_{cq}^{(s)}, \\
\partial_s \lambda_{cq}^{(s)} &= \left( 2 + \frac{1}{\pi} \frac{i}{\Delta\epsilon(z_1 + z_2)} \left( (1 + \lambda_c A_1) \left( \frac{\eta_{cc}^2}{z_1 z_2} + \epsilon_{cc}^2 \right) + (1 + \lambda_q A_1) \left( \frac{\eta_{qq}^2}{z_1 z_2} + \epsilon_{qq}^2 \right) \right) \right) \lambda_{cq}^{(s)} \\
&\quad - \frac{1}{\pi} \frac{i}{\Delta\epsilon(z_1 + z_2)} (2 + (\lambda_c + \lambda_q) A_1) \left( \frac{\eta_{cq}^2}{z_1 z_2} + \epsilon_{cq}^2 \right) \lambda_{cq}^{(c)}.
\end{aligned} \tag{I.34}$$

The  $z$ 's encode the poles of the propagator and are given by:

$$\begin{aligned}
z_{\pm}^2 &= \pm \sqrt{\frac{(\epsilon_{cq}^2 \eta_{cq}^2 + \frac{1}{2}(\epsilon_{qq}^2 \eta_{cc}^2 + \epsilon_{cc}^2 \eta_{qq}^2))^2 - \Delta\eta\Delta\epsilon}{\Delta\epsilon^2}} + \frac{\epsilon_{cq}^2 \eta_{cq}^2 + \frac{1}{2}(\epsilon_{qq}^2 \eta_{cc}^2 + \epsilon_{cc}^2 \eta_{qq}^2)}{\Delta\epsilon}, \\
\Delta\epsilon &= \epsilon_{cc}^2 \epsilon_{qq}^2 + \epsilon_{cq}^4, \\
\Delta\eta &= \eta_{cc}^2 \eta_{qq}^2 + \eta_{cq}^4.
\end{aligned} \tag{I.35}$$

Here,  $z_1$  and  $z_2$  are the roots of  $z_{\pm}^2$ , corresponding to poles in the upper half plane with a finite imaginary part (we assume that there are no real poles). In

the simplest case, we have  $z_2 = -z_1^*$ . The initial couplings are given in (I.5). The constants  $A_1, A_2$  are chosen as:

- $A_2 \cdot m^4 = -1/16$  (compensating some prefactors in (I.34)),
- $A_1 \cdot m^2 = -1/10$ .

## I.5 First Order Flow Equations from treating Space and Time on equal Footing

Using the same RG procedure, we should also recover the same flow equations at first order (up to a constant) (see again Sec. 4.8.1). As an example, we consider the renormalization of  $\cos(4\phi_q(X))$ :

$$\left. \begin{array}{l} \text{micro.:} \quad \lambda_q \int d^2 X \cos(4\phi_q(X)) \\ \text{renorm.:} \quad b^2 e^{-8\langle(\phi_q)^2\rangle} \lambda_q \int d^2 X \cos(4\phi_q(X)) \end{array} \right\} \partial_s \lambda_q \approx (2 - 8s^{-1} \underbrace{\langle\phi_q^2\rangle}_{\mathcal{O}(s)}) \lambda_q.$$

Using the same ‘symmetrizing’ approach (I.19), the correlation function at equal times is given by:

$$\begin{aligned} \langle\phi_a\phi_b\rangle &= \chi_{ab} \left( \frac{\eta_{ab}^2}{\Delta\epsilon|z|^3} - \frac{\epsilon_{ab}^2}{\Delta\epsilon|z|} \right) \mathcal{A}_0, \\ \mathcal{A}_0 &:= \int \frac{d^2\tilde{Q}}{(2\pi)^2} \frac{\tilde{k}^2}{(\alpha\tilde{\omega}^2 - \alpha^{-1}k^2)(\alpha^{-1}\tilde{\omega}^2 - \alpha\tilde{k}^2)}, \quad (\alpha - \alpha^{-1})\mathcal{A}_0 = iA_0(s), \end{aligned} \quad (\text{I.36})$$

where  $A_0(s) \approx A_0 \cdot s$  and  $A_0$  is a real number. The corresponding flow equation is given by

$$\partial_s \lambda_q \approx \left( 2 + 8 \frac{i}{z - z^*} \left( \frac{\eta_{qq}^2}{|z|^2} - \frac{\epsilon_{qq}^2}{\Delta\epsilon} \right) A_0 \right) \lambda_q, \quad (\text{I.37})$$

where the original case of a sharp cutoff is recovered for  $A_0 = -|A_0|$  (see again Sec. 4.8.1) with the initial conditions given in (I.5).

## I.6 Limiting Case: Flow Equations for $\gamma_B = 0$

For  $\gamma_B = 0$ , the additional symmetry  $\phi_c \leftrightarrow \phi_q$  locks the  $cc$  and  $qq$  couplings together:  $\eta_{cc} = \eta_{qq}$ ,  $\epsilon_{cc} = \epsilon_{qq}$ . Furthermore,  $\lambda_c, \lambda_q$  are always less relevant than  $\lambda_{\pm}$  and can therefore be ignored from the start. This leads to a contour decoupling, also in the case of interactions, and it is sufficient to consider the couplings for the  $+$ -contour. The inverse Green’s function is given by:

$$\begin{aligned} G_{0,\pm}^{-1} &= i \begin{pmatrix} (\eta_{cc}^2 + i\eta_{cq}^2)k^2 - (\epsilon_{cc}^2 + i\epsilon_{cq}^2)\omega^2 & 0 \\ 0 & (\eta_{cc}^2 - i\eta_{cq}^2)k^2 - (\epsilon_{cc}^2 - i\epsilon_{cq}^2)\omega^2 \end{pmatrix} \\ &:= i \begin{pmatrix} \eta_+^2 k^2 - \epsilon_+^2 \omega^2 & 0 \\ 0 & \eta_-^2 k^2 - \epsilon_-^2 \omega^2 \end{pmatrix}. \end{aligned}$$

**Correlations:** The inverse Green's function gives rise to the correlation function in Fourier space

$$\langle \phi_\sigma(Q) \phi_\sigma(-Q) \rangle = (\eta_\sigma^2 k^2 - \epsilon_\sigma^2 \omega^2)^{-1},$$

where the contour couplings are related by  $(\eta_+^2)^* = (\eta_-^2)$ ,  $(\epsilon_+^2)^* = \epsilon_-^2$ . In the time domain, we get

$$\int_{-\infty}^{\infty} \frac{d\omega}{2\pi} \frac{\pi e^{-i\omega t}}{\epsilon_\sigma^2 \omega^2 - \eta_\sigma^2 k^2} = \frac{\pi}{2} i \alpha_\sigma \frac{e^{i|k||t|} \alpha_\sigma \epsilon_\sigma / \eta_\sigma}{\eta_\sigma \epsilon_\sigma |k|}, \quad \alpha_\sigma := \text{sgn} \left( \text{Im} \left( \frac{\eta_\sigma}{\epsilon_\sigma} \right) \right). \quad (\text{I.38})$$

Initially,  $\epsilon_\sigma^2 = \sigma/\pi$  and  $\eta_\sigma^2 = \sigma - i \frac{2\gamma_M}{\pi^2 \nu}$  (as a sanity check: we always have an exponential decay in time). The equal time correlator reads:

$$\langle \phi_\sigma(X=0) \phi_\sigma(X=0) \rangle = -\alpha_\sigma \frac{\pi}{2} \int_{\Lambda \geq |k| \geq \Lambda/\xi} \frac{dk}{(2\pi)} \frac{1}{\eta_\sigma \epsilon_\sigma |k|} = -\frac{\alpha_\sigma}{2\epsilon_\sigma \eta_\sigma} \log(\xi). \quad (\text{I.39})$$

**Renormalization:** Integrating out the  $k$  modes in  $[\Lambda/e^s, \Lambda]$ , the flow equations for the derivative couplings are:

$$\left. \begin{aligned} \partial_s \eta_{cc}^2 &= -16 \left[ \lambda_+^2 \frac{1}{\epsilon_+^2} + \lambda_-^2 \frac{1}{\epsilon_-^2} \right] A_2, \\ \partial_s \eta_{cq}^2 &= 16 \left[ \lambda_+^2 \frac{1}{\epsilon_+^2} - \lambda_-^2 \frac{1}{\epsilon_-^2} \right] A_2, \end{aligned} \right\} \partial_s \eta_+^2 = -32 \lambda_+^2 \frac{1}{\epsilon_+^2} A_2. \quad (\text{I.40})$$

By symmetry,  $\epsilon_+^2$  evolves as:

$$\partial_s \epsilon_+^2 = -32 \lambda_+^2 \frac{1}{\eta_+^2} A_2. \quad (\text{I.41})$$

Defining  $\Delta\eta := \eta_+^2 \eta_-^2$  and  $\Delta\epsilon := \epsilon_+^2 \epsilon_-^2$ , the interaction coupling  $\lambda_+ = (\lambda_{cq}^{(c)} + i\lambda_{cq}^{(s)})/2$  evolves as:

$$\partial_s \lambda_+ = \left( 2 - \frac{2}{\pi} i \frac{\alpha_z}{\sqrt{\Delta\epsilon}(z-z^*)} \left[ \frac{\eta_{cc}^2 - i\eta_{cq}^2}{\sqrt{\Delta\eta}} - \frac{\epsilon_{cc}^2 - i\epsilon_{cq}^2}{\sqrt{\Delta\epsilon}} \right] \right) \lambda_+ = \left( 2 + \frac{2}{\pi} \frac{i\alpha_+}{\eta_+ \epsilon_+} \right) \lambda_+. \quad (\text{I.42})$$

Combining  $\eta_+$  and  $\epsilon_+$  into  $K_+ := \frac{i\epsilon_+ \eta_+}{\alpha_+}$ , we obtain the flow equations given in the main text (4.153) with the initial condition  $K_+(0) = \frac{1}{\pi} \sqrt{1 - i \frac{2\gamma_M}{\pi\nu}}$  (with  $\alpha_+ = -1$ ).

**Note 1:** To recover the flow equations in Ref. [19],  $A_2$  has to be *negative*. However, there is a difference: In our case, we analyze the flow of  $\partial_s K_+^2$  (also compatible with the standard BKT flow equations), in contrast to  $\partial_s K_+$ .

**Note 2:** In the case  $\gamma_B > 0$ , we have observed that the poles of the propagator can wander onto the real axis. For  $\gamma_B = 0$  instead, the poles  $\omega_{\pm}^2 = z^2 k^2$  with

$$z^2 = \frac{\eta_{cc}^2 + i\eta_{cq}^2}{\epsilon_{cc}^2 + i\epsilon_{cq}^2} = \frac{\eta_{\pm}^2}{\epsilon_{\pm}^2}, \quad (\text{I.43})$$

do not flow:

$$\partial_s z^2 = \partial_s \left( \frac{\eta_{\pm}^2}{\epsilon_{\pm}^2} \right) = 0. \quad (\text{I.44})$$

## I.7 Effective Action for the relative Mode in the Presence of random unitary Evolution

In Sec. 4.10.3, we introduced an additional random unitary evolution (with ‘imaginary noise’) of strength  $\gamma_I$ . This dynamic contribution translates into additional contributions to the action:

$$\begin{aligned} i(\Delta S^{(I)} + \Delta S^{(M)}) = & \\ & - \frac{1}{2} m^2 \int_X \left[ \left( \frac{\gamma_I - \gamma_M}{J} \right) \cos(2\sqrt{2}\phi_{\sigma,X}^{(r)}) \right. \\ & + \left. \left( \frac{\gamma_I - \gamma_M}{\nu} \right) \cos(2\sqrt{2}\phi_{\sigma,X}^{(a)}) + \left( \frac{\gamma_I + \gamma_M}{\nu} \right) \cos(2\sqrt{2}\phi_{\sigma,X}^{(a)}) \cos(2\sqrt{2}\phi_{\sigma,X}^{(r)}) \right] \\ & + 4m^2 \int_X \left( \frac{\gamma_I + \gamma_M}{\nu} \right) \cos(\sqrt{2}\phi_{+,X}^{(a)}) \cos(\sqrt{2}\phi_{-,X}^{(a)}) \cos(\sqrt{2}\phi_{+,X}^{(r)}) \cos(\sqrt{2}\phi_{-,X}^{(r)}). \end{aligned}$$

In the absence of a bath, the decoupling of the  $\pm$  contours for the relative mode is still intact and it is sufficient to consider the renormalization of the terms  $\cos(2\sqrt{2}\phi_{\sigma})$ . Starting point are the first and second order contributions from the coupling of the absolute and relative mode:

$$\langle \Delta S \rangle_{(a)} = \frac{i}{2} \left( \frac{\gamma_I - \gamma_M}{\nu} \right) \sum_{\sigma=\pm} \int d^2 X \cos(2\sqrt{2}\phi_{\sigma,X}^{(r)}), \quad (\text{I.45})$$

$$\frac{i}{2} \left( \langle \Delta S \rangle_{(a)} - \langle \Delta S \rangle_{(a)}^2 \right) \approx -i \left( \left( \frac{\gamma_I}{\nu} \right)^2 + \frac{\gamma_I \gamma_M}{\nu^2} \right) \sum_{\sigma=\pm} \int d^2 X \cos(2\sqrt{2}\phi_{\sigma,X}^{(r)}). \quad (\text{I.46})$$

## I.8 Details about Solving the Flow Equations

A general feature of the BKT type flow equations like (I.34) is that they can result in indefinitely growing couplings beyond the Gaussian phase (there is no interacting fixed point in this perturbative RG). Therefore, the flow has to be terminated once the interaction couplings become large:  $|\lambda/m^2| \gg 1$ . In this regime, the perturbative treatment is not valid anymore. For (I.34), another difficulty is the flow of the poles  $\omega_{\text{Pol}}(s) = z(s)|k|$ . On the one hand,  $z(s)$  can become real at some finite  $s_f \sim \mathcal{O}(1)$ . On the other hand, two poles can coalesce

$z_1 \rightarrow z_2$ , which also renders the flow equations invalide. Otherwise, we terminate the flow at  $s_{\max} = 100$  and identify the most strongly growing coupling, which we take as an indicator for the underlying strong coupling phase, shown in Fig. 4.15(a). The overall scheme reads:

- **Termination condition:** Terminate flow once  $|\lambda/m^2| > 10^2$  and/or the imaginary parts of any pole gets smaller than  $|\text{Im}[z_{1,2}]| < 10^{-10}$ . If none of the above applies, terminate flow at  $s_{\max}$ .
- **Identification:** Check if any interaction fulfills  $|\lambda/m^2| > 10^{-2}$ . In this case, identify the dominant coupling with  $\max_{\{\lambda\}} |\partial_s \lambda|$ , which is plotted in Fig. 4.15(a).
- **Numerical solver:** We use the ‘DifferentialEquations.jl’-package in Julia with the algorithm ‘AutoTsit5(Rosenbrock23())’ with ‘reftol=1e-7, abstol=1e-7’ up to  $s_{\max} = 100$ .

We checked that for different constant  $A_1$  and  $A_2$  a qualitatively similar phase diagram is obtained ( $A_1 = -0.5, \pm 0.1$ ,  $A_2 = -1/2, -1/5, -1/10$  with  $s_{\max} = 50$  and ‘reftol=1e-6, abstol=1e-6’). For larger  $|A_2|$  the region ( $C$ ) shrinks. Using different solvers, the detailed structure in region ( $M$ ) changes, where nevertheless multiple couplings are strongly growing.



# Bibliography

- <sup>1</sup>A. J. Leggett, S. Chakravarty, A. T. Dorsey, M. P. A. Fisher, A. Garg, and W. Zwerger, “Dynamics of the dissipative two-state system”, *Rev. Mod. Phys.* **59**, 1 (1987) DOI: 10.1103/RevModPhys.59.1.
- <sup>2</sup>S. Sachdev, *Quantum Phase Transitions*, 2nd ed. (Cambridge University Press, Cambridge, 2011), DOI: 10.1017/CB09780511973765.
- <sup>3</sup>U. C. Täuber, *Critical Dynamics: A Field Theory Approach to Equilibrium and Non-Equilibrium Scaling Behavior* (Cambridge University Press, Cambridge, 2014), DOI: 10.1017/CB09781139046213.
- <sup>4</sup>L. M. Sieberer, M. Buchhold, and S. Diehl, “Keldysh field theory for driven open quantum systems”, *Rep. Prog. Phys.* **79**, 096001 (2016) DOI: 10.1088/0034-4885/79/9/096001.
- <sup>5</sup>M. A. Nielsen and I. L. Chuang, *Quantum Computation and Quantum Information*, 10th Anniversary Edition (Cambridge University Press, Cambridge, 2010), DOI: 10.1017/CB09780511976667.
- <sup>6</sup>B. Skinner, J. Ruhman, and A. Nahum, “Measurement-Induced Phase Transitions in the Dynamics of Entanglement”, *Phys. Rev. X* **9**, 031009 (2019) DOI: 10.1103/PhysRevX.9.031009.
- <sup>7</sup>M. P. A. Fisher, V. Khemani, A. Nahum, and S. Vijay, “Random quantum circuits”, 2022, DOI: 10.48550/ARXIV.2207.14280, arXiv:2207.14280 [quant-ph], pre-published.
- <sup>8</sup>G. Vidal, J. I. Latorre, E. Rico, and A. Kitaev, “Entanglement in Quantum Critical Phenomena”, *Phys. Rev. Lett.* **90**, 227902 (2003) DOI: 10.1103/PhysRevLett.90.227902.
- <sup>9</sup>P. Calabrese and J. Cardy, “Entanglement entropy and quantum field theory”, *J. Stat. Mech.*, P06002 (2004) DOI: 10.1088/1742-5468/2004/06/P06002.
- <sup>10</sup>J. Dziarmaga, “Dynamics of a quantum phase transition and relaxation to a steady state”, *Adv. Phys.* **59**, 1063–1189 (2010) DOI: 10.1080/00018732.2010.514702.
- <sup>11</sup>J. Dziarmaga, “Dynamics of a Quantum Phase Transition: Exact Solution of the Quantum Ising Model”, *Phys. Rev. Lett.* **95**, 245701 (2005) DOI: 10.1103/PhysRevLett.95.245701.

- <sup>12</sup>L. Cincio, J. Dziarmaga, M. M. Rams, and W. H. Zurek, “Entropy of entanglement and correlations induced by a quench: Dynamics of a quantum phase transition in the quantum Ising model”, *Phys. Rev. A* **75**, 052321 (2007) DOI: 10.1103/PhysRevA.75.052321.
- <sup>13</sup>T. W. B. Kibble, “Topology of cosmic domains and strings”, *J. Phys. A: Math. Gen.* **9**, 1387 (1976) DOI: 10.1088/0305-4470/9/8/029.
- <sup>14</sup>W. H. Zurek, “Cosmological experiments in superfluid helium?”, *Nature* **317**, 505–508 (1985) DOI: 10.1038/317505a0.
- <sup>15</sup>W. H. Zurek, “Cosmological experiments in condensed matter systems”, *Phys. Rep.* **276**, 177–221 (1996) DOI: 10.1016/S0370-1573(96)00009-9.
- <sup>16</sup>H.-P. Breuer and F. Petruccione, *The Theory of Open Quantum Systems* (Oxford University Press, Oxford, 2007), DOI: 10.1093/acprof:oso/9780199213900.003.03.
- <sup>17</sup>X. Cao, A. Tilloy, and A. De Luca, “Entanglement in a free fermion chain under continuous monitoring”, *SciPost Phys.* **7**, 024 (2019) DOI: 10.21468/scipostphys.7.2.024.
- <sup>18</sup>O. Alberton, M. Buchhold, and S. Diehl, “Entanglement Transition in a Monitored Free-Fermion Chain: From Extended Criticality to Area Law”, *Phys. Rev. Lett.* **126**, 170602 (2021) DOI: 10.1103/PhysRevLett.126.170602.
- <sup>19</sup>M. Buchhold, Y. Minoguchi, A. Altland, and S. Diehl, “Effective Theory for the Measurement-Induced Phase Transition of Dirac Fermions”, *Phys. Rev. X* **11**, 041004 (2021) DOI: 10.1103/physrevx.11.041004.
- <sup>20</sup>Y. Bao, S. Choi, and E. Altman, “Symmetry enriched phases of quantum circuits”, *Ann. Phys. (N. Y.)* **435**, 168618 (2021) DOI: 10.1016/j.aop.2021.168618.
- <sup>21</sup>T. A. Brun, “A simple model of quantum trajectories”, *Am. J. Phys.* **70**, 719 (2002) DOI: 10.1119/1.1475328.
- <sup>22</sup>K. Jacobs and D. A. Steck, “A straightforward introduction to continuous quantum measurement”, *Contemp. Phys.* **47**, 279 (2006) DOI: 10.1080/00107510601101934.
- <sup>23</sup>K. Jacobs, *Quantum Measurement Theory and its Applications* (Cambridge University Press, Cambridge, 2014), DOI: 10.1017/CB09781139179027.
- <sup>24</sup>J. Preskill, “Quantum Computing in the NISQ era and beyond”, *Quantum* **2**, 79 (2018) DOI: 10.22331/q-2018-08-06-79.
- <sup>25</sup>N. P. de Leon, K. M. Itoh, D. Kim, K. K. Mehta, T. E. Northup, H. Paik, B. S. Palmer, N. Samarth, S. Sangtawesin, and D. W. Steuerman, “Materials challenges and opportunities for quantum computing hardware”, *Science* **372**, eabb2823 (2021) DOI: 10.1126/science.abb2823.
- <sup>26</sup>A. J. Daley, I. Bloch, C. Kokail, S. Flannigan, N. Pearson, M. Troyer, and P. Zoller, “Practical quantum advantage in quantum simulation”, *Nature* **607**, 667–676 (2022) DOI: 10.1038/s41586-022-04940-6.
- <sup>27</sup>G. Massimo Palma, K.-A. Suominen, and A. K. Ekert, “Quantum Computers and Dissipation”, *Proc. Roy. Soc. A* **452**, 567–584 (1996) DOI: 10.1098/rspa.1996.0029.

- 
- <sup>28</sup>J. Roffe, “Quantum error correction: an introductory guide”, *Contemp. Phys.* **60**, 226–245 (2019) DOI: 10.1080/00107514.2019.1667078.
- <sup>29</sup>P. W. Shor, “Scheme for reducing decoherence in quantum computer memory”, *Phys. Rev. A* **52**, R2493(R) (1995) DOI: 10.1103/PhysRevA.52.R2493.
- <sup>30</sup>S. Choi, Y. Bao, X.-L. Qi, and E. Altman, “Quantum Error Correction in Scrambling Dynamics and Measurement-Induced Phase Transition”, *Phys. Rev. Lett.* **125**, 030505 (2020) DOI: 10.1103/PhysRevLett.125.030505.
- <sup>31</sup>M. J. Gullans and D. A. Huse, “Dynamical Purification Phase Transition Induced by Quantum Measurements”, *Phys. Rev. X* **10**, 041020 (2020) DOI: 10.1103/PhysRevX.10.041020.
- <sup>32</sup>Y. Li and M. P. A. Fisher, “Robust decoding in monitored dynamics of open quantum systems with  $Z_2$  symmetry”, 2021, DOI: 10.48550/ARXIV.2108.04274, arXiv:2108.04274 [quant-ph], pre-published.
- <sup>33</sup>C. Noel, P. Niroula, D. Zhu, A. Risinger, L. Egan, D. Biswas, M. Cetina, A. V. Gorshkov, M. J. Gullans, D. A. Huse, and C. Monroe, “Measurement-induced quantum phases realized in a trapped-ion quantum computer”, *Nat. Phys.* **18**, 760–764 (2022) DOI: 10.1038/s41567-022-01619-7.
- <sup>34</sup>J. M. Koh, S.-N. Sun, M. Motta, and A. J. Minnich, “Experimental realization of a measurement-induced entanglement phase transition on a superconducting quantum processor”, 2022, DOI: 10.48550/ARXIV.2203.04338, arXiv:2203.04338 [quant-ph], pre-published.
- <sup>35</sup>E. Altman, K. R. Brown, G. Carleo, L. D. Carr, E. Demler, C. Chin, B. DeMarco, S. E. Economou, M. A. Eriksson, K.-M. C. Fu, M. Greiner, K. R. Hazzard, R. G. Hulet, A. J. Kollár, B. L. Lev, M. D. Lukin, R. Ma, X. Mi, S. Misra, C. Monroe, K. Murch, Z. Nazario, K.-K. Ni, A. C. Potter, P. Roushan, M. Saffman, M. Schleier-Smith, I. Siddiqi, R. Simmonds, M. Singh, I. Spielman, K. Temme, D. S. Weiss, J. Vučković, V. Vuletić, J. Ye, and M. Zwierlein, “Quantum Simulators: Architectures and Opportunities”, *PRX Quantum* **2**, 017003 (2021) DOI: 10.1103/PRXQuantum.2.017003.
- <sup>36</sup>A. Keesling, A. Omran, H. Levine, H. Bernien, H. Pichler, S. Choi, R. Samajdar, S. Schwartz, P. Silvi, S. Sachdev, P. Zoller, M. Endres, M. Greiner, V. Vuletić, and M. D. Lukin, “Quantum Kibble-Zurek mechanism and critical dynamics on a programmable Rydberg simulator”, *Nature* **568**, 207–211 (2019) DOI: 10.1038/s41586-019-1070-1.
- <sup>37</sup>P. Hauke, H. G. Katzgraber, W. Lechner, H. Nishimori, and W. D. Oliver, “Perspectives of quantum annealing: methods and implementations”, *Rep. Prog. Phys.* **83**, 054401 (2020) DOI: 10.1088/1361-6633/ab85b8.
- <sup>38</sup>Y. Bando, Y. Susa, H. Oshiyama, N. Shibata, M. Ohzeki, F. J. Gómez-Ruiz, D. A. Lidar, S. Suzuki, A. del Campo, and H. Nishimori, “Probing the universality of topological defect formation in a quantum annealer: Kibble-Zurek mechanism and beyond”, *Phys. Rev. Research* **2**, 033369 (2020) DOI: 10.1103/PhysRevResearch.2.033369.

- <sup>39</sup>A. D. King, S. Suzuki, J. Raymond, A. Zucca, T. Lanting, F. Altomare, A. J. Berkley, S. Ejtemaee, E. Hoskinson, S. Huang, E. Ladizinsky, A. J. R. MacDonald, G. Marsden, T. Oh, G. Poulin-Lamarre, M. Reis, C. Rich, Y. Sato, J. D. Whittaker, J. Yao, R. Harris, D. A. Lidar, H. Nishimori, and M. H. Amin, “Coherent quantum annealing in a programmable 2,000 qubit Ising chain”, *Nat. Phys.* **18**, 1324–1328 (2022) DOI: 10.1038/s41567-022-01741-6.
- <sup>40</sup>B. Gardas, J. Dziarmaga, W. H. Zurek, and M. Zwolak, “Defects in quantum computers”, *Sci. Rep.* **8**, 4539 (2018) DOI: 10.1038/s41598-018-22763-2.
- <sup>41</sup>S. Mathey and S. Diehl, “Activating critical exponent spectra with a slow drive”, *Phys. Rev. Research* **2**, 013150 (2020) DOI: 10.1103/physrevresearch.2.013150.
- <sup>42</sup>B. Ladewig, S. Mathey, and S. Diehl, “Kibble-Zurek mechanism from different angles: The transverse XY model and subleading scalings”, *Phys. Rev. B* **102**, 104306 (2020) DOI: 10.1103/PhysRevB.102.104306.
- <sup>43</sup>J.-M. Cui, Y.-F. Huang, Z. Wang, D.-Y. Cao, J. Wang, W.-M. Lv, L. Luo, A. del Campo, Y.-J. Han, C.-F. Li, and G.-C. Guo, “Experimental Trapped-ion Quantum Simulation of the Kibble-Zurek dynamics in momentum space”, *Sci. Rep.* **6**, 33381 (2016) DOI: 10.1038/srep33381.
- <sup>44</sup>J.-M. Cui, F. J. Gómez-Ruiz, Y.-F. Huang, C.-F. Li, G.-C. Guo, and A. del Campo, “Experimentally testing quantum critical dynamics beyond the Kibble-Zurek mechanism”, *Commun. Phys.* **3**, 44 (2020) DOI: 10.1038/s42005-020-0306-6.
- <sup>45</sup>B. Damski and W. H. Zurek, “Adiabatic-impulse approximation for avoided level crossings: From phase-transition dynamics to Landau-Zener evolutions and back again”, *Phys. Rev. A* **73**, 063405 (2006) DOI: 10.1103/PhysRevA.73.063405.
- <sup>46</sup>C. Zener, “Non-adiabatic crossing of energy levels”, *Proc. Roy. Soc. A* **137**, 696–702 (1932) DOI: 10.1098/rspa.1932.0165.
- <sup>47</sup>E. Majorana, “Atomi orientati in campo magnetico variabile”, *Il Nuovo Cimento* **9**, 43–50 (1932) DOI: 10.1007/978-3-540-48095-2\_7.
- <sup>48</sup>E. C. G. Stückelberg, “Theorie der unelastischen Stösse zwischen Atomen”, *Helv. Phys. Acta* **5**, 369 (1932) DOI: 10.1007/978-3-7643-8878-2\_9.
- <sup>49</sup>B. Damski, “The Simplest Quantum Model Supporting the Kibble-Zurek Mechanism of Topological Defect Production: Landau-Zener Transitions from a New Perspective”, *Phys. Rev. Lett.* **95**, 035701 (2005) DOI: 10.1103/PhysRevLett.95.035701.
- <sup>50</sup>K. Hornberger, “Introduction to Decoherence Theory”, in *Entanglement and Decoherence. Lecture Notes in Physics, vol 768*, edited by A. Buchleitner, C. Viviescas, and M. Tiersch (Springer, Berlin, Heidelberg, 2009), pp. 221–276, DOI: 10.1007/978-3-540-88169-8\_5.
- <sup>51</sup>S. Sarkar, S. Langer, J. Schachenmayer, and A. J. Daley, “Light scattering and dissipative dynamics of many fermionic atoms in an optical lattice”, *Phys. Rev. A* **90**, 023618 (2014) DOI: 10.1103/PhysRevA.90.023618.
- <sup>52</sup>A. Altland and B. D. Simons, *Condensed Matter Field Theory*, 2nd ed. (Cambridge University Press, 2010), DOI: 10.1017/CB09780511789984.

- 
- <sup>53</sup>J. I. Latorre, E. Rico, and G. Vidal, “Ground state entanglement in quantum spin chains”, *Quantum Inf. Comput.* **4**, 48–92 (2004) DOI: 10.26421/qic4.1-4.
- <sup>54</sup>C. Holzhey, F. Larsen, and F. Wilczek, “Geometric and renormalized entropy in conformal field theory”, *Nucl. Phys. B* **424**, 443–467 (1994) DOI: 10.1016/0550-3213(94)90402-2.
- <sup>55</sup>S. Katsura, “Statistical Mechanics of the Anisotropic Linear Heisenberg Model”, *Phys. Rev.* **127**, 1508 (1962) DOI: 10.1103/PhysRev.127.1508.
- <sup>56</sup>E. Lieb, T. Schultz, and D. Mattis, “Two soluble models of an antiferromagnetic chain”, *Ann. Phys. (N. Y.)* **16**, 407–466 (1961) DOI: 10.1016/0003-4916(61)90115-4.
- <sup>57</sup>P. Pfeuty, “The one-dimensional Ising model with a transverse field”, *Ann. Phys. (N. Y.)* **57**, 79–90 (1970) DOI: 10.1016/0003-4916(70)90270-8.
- <sup>58</sup>E. Barouch, B. M. McCoy, and M. Dresden, “Statistical Mechanics of the XY Model. I”, *Phys. Rev. A* **2**, 1075 (1970) DOI: 10.1103/PhysRevA.2.1075.
- <sup>59</sup>E. Barouch and B. M. McCoy, “Statistical Mechanics of the XY Model. II. Spin-Correlation Functions”, *Phys. Rev. A* **3**, 786 (1971) DOI: 10.1103/PhysRevA.3.786.
- <sup>60</sup>J. E. Bunder and R. H. McKenzie, “Effect of disorder on quantum phase transitions in anisotropic XY spin chains in a transverse field”, *Phys. Rev. B* **60**, 344 (1999) DOI: 10.1103/PhysRevB.60.344.
- <sup>61</sup>A. Dutta, G. Aeppli, B. K. Chakrabarti, U. Divakaran, T. F. Rosenbaum, and D. Sen, *Quantum Phase Transitions in Transverse Field Spin Models: From Statistical Physics to Quantum Information* (Cambridge University Press, Cambridge, 2015), DOI: 10.1017/CB09781107706057.
- <sup>62</sup>G. B. Mbeng, A. Russomanno, and G. E. Santoro, “The quantum Ising chain for beginners”, 2020, DOI: 10.48550/ARXIV.2009.09208, arXiv:2009.09208 [quant-ph], pre-published.
- <sup>63</sup>J. Surace and L. Tagliacozzo, “Fermionic Gaussian states: an introduction to numerical approaches”, *SciPost Phys. Lect. Notes*, 54 (2022) DOI: 10.21468/SciPostPhysLectNotes.54.
- <sup>64</sup>N. Goldenfeld, *Lectures On Phase Transitions And The Renormalization Group* (CRC Press, Boca Raton, 1992), DOI: 10.1201/9780429493492.
- <sup>65</sup>J. Cardy, *Scaling and Renormalization in Statistical Physics (Cambridge Lecture Notes in Physics)* (Cambridge University Press, Cambridge, 1996), DOI: 10.1017/CB09781316036440.
- <sup>66</sup>J. M. Deutsch, H. Li, and A. Sharma, “Microscopic origin of thermodynamic entropy in isolated systems”, *Phys. Rev. E* **87**, 042135 (2013) DOI: 10.1103/PhysRevE.87.042135.
- <sup>67</sup>A. M. Kaufman, M. E. Tai, A. Lukin, M. Rispoli, R. Schittko, P. M. Preiss, and M. Greiner, “Quantum thermalization through entanglement in an isolated many-body system”, *Science* **353**, 794–800 (2016) DOI: 10.1126/science.aaf6725.
- <sup>68</sup>L. D’Alessio, Y. Kafri, A. Polkovnikov, and M. Rigol, “From quantum chaos and eigenstate thermalization to statistical mechanics and thermodynamics”, *Adv. Phys.* **65**, 239–362 (2016) DOI: 10.1080/00018732.2016.1198134.

- <sup>69</sup>A. Kamenev, *Field Theory of Non-Equilibrium Systems* (Cambridge University Press, Cambridge, 2011), DOI: 10.1017/CB09781139003667.
- <sup>70</sup>E. Fradkin, *Field Theories of Condensed Matter Physics* (Cambridge University Press, Cambridge, 2013), DOI: 10.1017/CB09781139015509.
- <sup>71</sup>W. H. Zurek, “Cosmic strings in laboratory superfluids and the topological remnants of other phase transitions”, *Acta Phys. Pol. B* **24**, 1301–1311 (1993).
- <sup>72</sup>A. Polkovnikov, “Universal adiabatic dynamics in the vicinity of a quantum critical point”, *Phys. Rev. B* **72**, 161201(R) (2005) DOI: 10.1103/PhysRevB.72.161201.
- <sup>73</sup>C. De Grandi, V. Gritsev, and A. Polkovnikov, “Quench dynamics near a quantum critical point”, *Phys. Rev. B* **81**, 012303 (2010) DOI: 10.1103/PhysRevB.81.012303.
- <sup>74</sup>R. Barankov and A. Polkovnikov, “Optimal Nonlinear Passage Through a Quantum Critical Point”, *Phys. Rev. Lett.* **101**, 076801 (2008) DOI: 10.1103/PhysRevLett.101.076801.
- <sup>75</sup>D. Sen, K. Sengupta, and S. Mondal, “Defect Production in Nonlinear Quench across a Quantum Critical Point”, *Phys. Rev. Lett.* **101**, 016806 (2008) DOI: 10.1103/PhysRevLett.101.016806.
- <sup>76</sup>L.-Y. Qiu, H.-Y. Liang, Y.-B. Yang, H.-X. Yang, T. Tian, Y. Xu, and L.-M. Duan, “Observation of generalized Kibble-Zurek mechanism across a first-order quantum phase transition in a spinor condensate”, *Sci. Adv.* **6**, eaba7292 (2020) DOI: 10.1126/sciadv.aba7292.
- <sup>77</sup>A. Zamora, G. Dagvadorj, P. Comaron, I. Carusotto, N. P. Proukakis, and M. H. Szymańska, “Kibble-Zurek Mechanism in Driven Dissipative Systems Crossing a Nonequilibrium Phase Transition”, *Phys. Rev. Lett.* **125**, 095301 (2020) DOI: 10.1103/PhysRevLett.125.095301.
- <sup>78</sup>C. J. O. Reichhardt, A. del Campo, and C. Reichhardt, “Kibble-Zurek mechanism for nonequilibrium phase transitions in driven systems with quenched disorder”, *Commun. Phys.* **5**, 173 (2022) DOI: 10.1038/s42005-022-00952-w.
- <sup>79</sup>S. Mathey and S. Diehl, “Dynamic renormalization group theory for open Floquet systems”, *Phys. Rev. B* **102**, 134307 (2020) DOI: 10.1103/PhysRevB.102.134307.
- <sup>80</sup>C. De Grandi and A. Polkovnikov, “Adiabatic Perturbation Theory: From Landau–Zener Problem to Quenching Through a Quantum Critical Point”, in *Quantum Quenching, Annealing and Computation. Lecture Notes in Physics, vol 802*, edited by A. K. Chandra, A. Das, and B. K. Chakrabarti (Springer, Berlin, Heidelberg, 2010), pp. 75–114, DOI: 10.1007/978-3-642-11470-0\_4.
- <sup>81</sup>P. Calabrese and J. Cardy, “Evolution of entanglement entropy in one-dimensional systems”, *J. Stat. Mech.*, P04010 (2005) DOI: 10.1088/1742-5468/2005/04/p04010.

- <sup>82</sup>M. Fagotti and P. Calabrese, “Evolution of entanglement entropy following a quantum quench: Analytic results for the XY chain in a transverse magnetic field”, *Phys. Rev. A* **78**, 010306(R) (2008) DOI: 10.1103/PhysRevA.78.010306.
- <sup>83</sup>A. Polkovnikov and V. Gritsev, “Universal Dynamics Near Quantum Critical Points”, in *Understanding Quantum Phase Transitions*, edited by L. Carr (CRC Press, Boca Raton, 2010) Chap. 3, DOI: 10.1201/b10273.
- <sup>84</sup>S. Deng, G. Ortiz, and L. Viola, “Dynamical non-ergodic scaling in continuous finite-order quantum phase transitions”, *EPL* **84**, 67008 (2008) DOI: 10.1209/0295-5075/84/67008.
- <sup>85</sup>J. P. Davis and P. Pechukas, “Nonadiabatic transitions induced by a time-dependent Hamiltonian in the semiclassical/adiabatic limit: The two-state case”, *J. Chem. Phys.* **64**, 3129 (1976) DOI: 10.1063/1.432648.
- <sup>86</sup>A. Joye, “Non-trivial prefactors in adiabatic transition probabilities induced by high-order complex degeneracies”, *J. Phys. A: Math. Gen.* **26**, 6517 (1993) DOI: 10.1088/0305-4470/26/22/045.
- <sup>87</sup>N. V. Vitanov and K.-A. Suominen, “Nonlinear level-crossing models”, *Phys. Rev. A* **59**, 4580 (1999) DOI: 10.1103/PhysRevA.59.4580.
- <sup>88</sup>C. Bäuerle, Y. M. Bunkov, S. N. Fisher, H. Godfrin, and G. R. Pickett, “Laboratory simulation of cosmic string formation in the early Universe using superfluid  $^3\text{He}$ ”, *Nature* **382**, 332–334 (1996) DOI: 10.1038/382332a0.
- <sup>89</sup>V. M. H. Ruutu, V. B. Eltsov, A. J. Gill, T. W. B. Kibble, M. Krusius, Y. G. Makhlin, B. Plaças, G. E. Volovik, and W. Xu, “Vortex formation in neutron-irradiated superfluid  $^3\text{He}$  as an analogue of cosmological defect formation”, *Nature* **382**, 334–336 (1996) DOI: 10.1038/382334a0.
- <sup>90</sup>M. J. Bowick, L. Chandar, E. A. Schiff, and A. M. Srivastava, “The Cosmological Kibble Mechanism in the Laboratory: String Formation in Liquid Crystals”, *Science* **263**, 943–945 (1994) DOI: 10.1126/science.263.5149.943.
- <sup>91</sup>I. Chuang, R. Durrer, N. Turok, and B. Yurke, “Cosmology in the Laboratory: Defect Dynamics in Liquid Crystals”, *Science* **251**, 1336–1342 (1991) DOI: 10.1126/science.251.4999.1336.
- <sup>92</sup>C. N. Weiler, T. W. Neely, D. R. Scherer, A. S. Bradley, M. J. Davis, and B. P. Anderson, “Spontaneous vortices in the formation of Bose-Einstein condensates”, *Nature* **455**, 948–951 (2008) DOI: 10.1038/nature07334.
- <sup>93</sup>G. Lamporesi, S. Donadello, S. Serafini, F. Dalfovo, and G. Ferrari, “Spontaneous creation of Kibble-Zurek solitons in a Bose-Einstein condensate”, *Nat. Phys.* **9**, 656–660 (2013) DOI: 10.1038/nphys2734.
- <sup>94</sup>L. Corman, L. Chomaz, T. Bienaimé, R. Desbuquois, C. Weitenberg, S. Nascimbène, J. Dalibard, and J. Beugnon, “Quench-Induced Supercurrents in an Annular Bose Gas”, *Phys. Rev. Lett.* **113**, 135302 (2014) DOI: 10.1103/PhysRevLett.113.135302.
- <sup>95</sup>L. Chomaz, L. Corman, T. Bienaimé, R. Desbuquois, C. Weitenberg, S. Nascimbène, J. Beugnon, and J. Dalibard, “Emergence of coherence via transverse condensation in a uniform quasi-two-dimensional Bose gas”, *Nat. Commun.* **6**, 6162 (2015) DOI: 10.1038/ncomms7162.

- <sup>96</sup>S. Donadello, S. Serafini, M. Tylutki, L. P. Pitaevskii, F. Dalfovo, G. Lamporesi, and G. Ferrari, “Observation of Solitonic Vortices in Bose-Einstein Condensates”, *Phys. Rev. Lett.* **113**, 065302 (2014) DOI: 10.1103/PhysRevLett.113.065302.
- <sup>97</sup>N. Navon, A. L. Gaunt, R. P. Smith, and Z. Hadzibabic, “Critical dynamics of spontaneous symmetry breaking in a homogeneous Bose gas”, *Science* **347**, 167–170 (2015) DOI: 10.1126/science.1258676.
- <sup>98</sup>V. I. Yukalov, A. N. Novikov, and V. S. Bagnato, “Realization of inverse Kibble-Zurek scenario with trapped Bose gases”, *Phys. Lett. A* **379**, 1366–1371 (2015) DOI: 10.1016/j.physleta.2015.02.033.
- <sup>99</sup>J. Beugnon and N. Navon, “Exploring the Kibble-Zurek mechanism with homogeneous Bose gases”, *J. Phys. B: At. Mol. Opt. Phys.* **50**, 022002 (2017) DOI: 10.1088/1361-6455/50/2/022002.
- <sup>100</sup>L. E. Sadler, J. M. Higbie, S. R. Leslie, M. Vengalattore, and D. M. Stamper-Kurn, “Spontaneous symmetry breaking in a quenched ferromagnetic spinor Bose-Einstein condensate”, *Nature* **443**, 312–315 (2006) DOI: 10.1038/nature05094.
- <sup>101</sup>L. W. Clark, L. Feng, and C. Chin, “Universal space-time scaling symmetry in the dynamics of bosons across a quantum phase transition”, *Science* **354**, 606–610 (2016) DOI: 10.1126/science.aaf9657.
- <sup>102</sup>M. Anquez, B. A. Robbins, H. M. Bharath, M. Boguslawski, T. M. Hoang, and M. S. Chapman, “Kibble-Zurek Mechanism in a Spin-1 Bose-Einstein Condensate”, *Phys. Rev. Lett.* **116**, 155301 (2016) DOI: 10.1103/PhysRevLett.116.155301.
- <sup>103</sup>D. Chen, M. White, C. Borries, and B. DeMarco, “Quantum Quench of an Atomic Mott Insulator”, *Phys. Rev. Lett.* **106**, 235304 (2011) DOI: 10.1103/PhysRevLett.106.235304.
- <sup>104</sup>S. Braun, M. Friesdorf, S. S. Hodgman, M. Schreiber, J. P. Ronzheimer, A. Riera, M. del Rey, I. Bloch, J. Eisert, and U. Schneider, “Emergence of coherence and the dynamics of quantum phase transitions”, *Proc. Natl. Acad. Sci. U. S. A.* **112**, 3641–3646 (2015) DOI: 10.1073/pnas.1408861112.
- <sup>105</sup>C. Meldgin, U. Ray, P. Russ, D. Chen, D. M. Ceperley, and B. DeMarco, “Probing the Bose glass-superfluid transition using quantum quenches of disorder”, *Nat. Phys.* **12**, 646–649 (2016) DOI: 10.1038/nphys3695.
- <sup>106</sup>S. Ulm, J. Roßnagel, G. Jacob, C. Degünther, S. T. Dawkins, U. G. Poschinger, R. Nigmatullin, A. Retzker, M. B. Plenio, F. Schmidt-Kaler, and K. Singer, “Observation of the Kibble-Zurek scaling law for defect formation in ion crystals”, *Nat. Commun.* **4**, 2290 (2013) DOI: 10.1038/ncomms3290.
- <sup>107</sup>K. Pyka, J. Keller, H. L. Partner, R. Nigmatullin, T. Burgermeister, D. M. Meier, K. Kuhlmann, A. Retzker, M. B. Plenio, W. H. Zurek, A. del Campo, and T. E. Mehlstäubler, “Topological defect formation and spontaneous symmetry breaking in ion Coulomb crystals”, *Nat. Commun.* **4**, 2291 (2013) DOI: 10.1038/ncomms3291.
- <sup>108</sup>M. Mielenz, J. Brox, S. Kahra, G. Leschhorn, M. Albert, T. Schaetz, H. Landa, and B. Reznik, “Trapping of Topological-Structural Defects in Coulomb Crystals”, *Phys. Rev. Lett.* **110**, 133004 (2013) DOI: 10.1103/PhysRevLett.110.133004.

- 
- <sup>109</sup>S. C. Chae, N. Lee, Y. Horibe, M. Tanimura, S. Mori, B. Gao, S. Carr, and S.-W. Cheong, “Direct Observation of the Proliferation of Ferroelectric Loop Domains and Vortex-Antivortex Pairs”, *Phys. Rev. Lett.* **108**, 167603 (2012) DOI: 10.1103/PhysRevLett.108.167603.
- <sup>110</sup>S.-Z. Lin, X. Wang, Y. Kamiya, G.-W. Chern, F. Fan, D. Fan, B. Casas, Y. Liu, V. Kiryukhin, W. H. Zurek, C. D. Batista, and S.-W. Cheong, “Topological defects as relics of emergent continuous symmetry and Higgs condensation of disorder in ferroelectrics”, *Nat. Phys.* **10**, 970–977 (2014) DOI: 10.1038/nphys3142.
- <sup>111</sup>S. M. Griffin, M. Lilienblum, K. T. Delaney, Y. Kumagai, M. Fiebig, and N. A. Spaldin, “Scaling Behavior and Beyond Equilibrium in the Hexagonal Manganites”, *Phys. Rev. X* **2**, 041022 (2012) DOI: 10.1103/PhysRevX.2.041022.
- <sup>112</sup>R. Monaco, J. Mygind, and R. J. Rivers, “Zurek-Kibble Domain Structures: The Dynamics of Spontaneous Vortex Formation in Annular Josephson Tunnel Junctions”, *Phys. Rev. Lett.* **89**, 080603 (2002) DOI: 10.1103/PhysRevLett.89.080603.
- <sup>113</sup>A. Maniv, E. Polturak, and G. Koren, “Observation of Magnetic Flux Generated Spontaneously During a Rapid Quench of Superconducting Films”, *Phys. Rev. Lett.* **91**, 197001 (2003) DOI: 10.1103/PhysRevLett.91.197001.
- <sup>114</sup>R. Monaco, J. Mygind, R. J. Rivers, and V. P. Koshelets, “Spontaneous fluxoid formation in superconducting loops”, *Phys. Rev. B* **80**, 180501(R) (2009) DOI: 10.1103/PhysRevB.80.180501.
- <sup>115</sup>D. Golubchik, E. Polturak, and G. Koren, “Evidence for Long-Range Correlations within Arrays of Spontaneously Created Magnetic Vortices in a Nb Thin-Film Superconductor”, *Phys. Rev. Lett.* **104**, 247002 (2010) DOI: 10.1103/PhysRevLett.104.247002.
- <sup>116</sup>S. Deuschländer, P. Dillmann, G. Maret, and P. Keim, “Kibble-Zurek mechanism in colloidal monolayers”, *Proc. Natl. Acad. Sci. U. S. A.* **112**, 6925–6930 (2015) DOI: 10.1073/pnas.1500763112.
- <sup>117</sup>S. Casado, W. González-Viñas, and H. Mancini, “Testing the Kibble-Zurek mechanism in Rayleigh-Bénard convection”, *Phys. Rev. E* **74**, 047101 (2006) DOI: 10.1103/PhysRevE.74.047101.
- <sup>118</sup>M. Gong, X. Wen, G. Sun, D.-W. Zhang, D. Lan, Y. Zhou, Y. Fan, Y. Liu, X. Tan, H. Yu, Y. Yu, S.-L. Zhu, S. Han, and P. Wu, “Simulating the Kibble-Zurek mechanism of the Ising model with a superconducting qubit system”, *Sci. Rep.* **6**, 22667 (2016) DOI: 10.1038/srep22667.
- <sup>119</sup>J. Zhang, F. M. Cucchietti, R. Laflamme, and D. Suter, “Defect production in non-equilibrium phase transitions: experimental investigation of the Kibble-Zurek mechanism in a two-qubit quantum simulator”, *New J. Phys.* **19**, 043001 (2017) DOI: 10.1088/1367-2630/aa6653.
- <sup>120</sup>K. Baumann, R. Mottl, F. Brennecke, and T. Esslinger, “Exploring Symmetry Breaking at the Dicke Quantum Phase Transition”, *Phys. Rev. Lett.* **107**, 140402 (2011) DOI: 10.1103/PhysRevLett.107.140402.
- <sup>121</sup>J. Klinder, H. Keßler, M. Wolke, L. Mathey, and A. Hemmerich, “Dynamical phase transition in the open Dicke model”, *Proc. Natl. Acad. Sci. U. S. A.* **112**, 3290–3295 (2015) DOI: 10.1073/pnas.1417132112.

- <sup>122</sup>W. H. Zurek, U. Dorner, and P. Zoller, “Dynamics of a Quantum Phase Transition”, *Phys. Rev. Lett.* **95**, 105701 (2005) DOI: 10.1103/PhysRevLett.95.105701.
- <sup>123</sup>M. Białończyk and B. Damski, “One-half of the Kibble-Zurek quench followed by free evolution”, *J. Stat. Mech.*, 073105 (2018) DOI: 10.1088/1742-5468/aad3f2.
- <sup>124</sup>A. Francuz, J. Dziarmaga, B. Gardas, and W. H. Zurek, “Space and time renormalization in phase transition dynamics”, *Phys. Rev. B* **93**, 075134 (2016) DOI: 10.1103/PhysRevB.93.075134.
- <sup>125</sup>U. Divakaran, A. Dutta, and D. Sen, “Quenching along a gapless line: A different exponent for defect density”, *Phys. Rev. B* **78**, 144301 (2008) DOI: 10.1103/PhysRevB.78.144301.
- <sup>126</sup>U. Divakaran, V. Mukherjee, A. Dutta, and D. Sen, “Defect Production Due to Quenching Through a Multicritical Point and Along a Gapless Line”, in *Quantum Quenching, Annealing and Computation. Lecture Notes in Physics, vol 802* (Springer, Berlin, Heidelberg, 2010), pp. 57–73, DOI: 10.1007/978-3-642-11470-0\_3.
- <sup>127</sup>S. Deng, G. Ortiz, and L. Viola, “Anomalous nonergodic scaling in adiabatic multicritical quantum quenches”, *Phys. Rev. B* **80**, 241109(R) (2009) DOI: 10.1103/PhysRevB.80.241109.
- <sup>128</sup>V. Mukherjee and A. Dutta, “Adiabatic multicritical quantum quenches: Continuously varying exponents depending on the direction of quenching”, *EPL* **92**, 37004 (2010) DOI: 10.1209/0295-5075/92/37004.
- <sup>129</sup>M. M. Rams, J. Dziarmaga, and W. H. Zurek, “Symmetry Breaking Bias and the Dynamics of a Quantum Phase Transition”, *Phys. Rev. Lett.* **123**, 130603 (2019) DOI: 10.1103/PhysRevLett.123.130603.
- <sup>130</sup>K. Hódsági and M. Kormos, “Kibble–Zurek mechanism in the Ising Field Theory”, *SciPost Phys.* **9**, 055 (2020) DOI: 10.21468/SciPostPhys.9.4.055.
- <sup>131</sup>M. M. Rams and B. Damski, “Scaling of ground-state fidelity in the thermodynamic limit: *XY* model and beyond”, *Phys. Rev. A* **84**, 032324 (2011) DOI: 10.1103/PhysRevA.84.032324.
- <sup>132</sup>S. Mondal, K. Sengupta, and D. Sen, “Theory of defect production in nonlinear quench across a quantum critical point”, *Phys. Rev. B* **79**, 045128 (2009) DOI: 10.1103/PhysRevB.79.045128.
- <sup>133</sup>Á. Bácsi and B. Dóra, “Kibble-Zurek scaling due to environment temperature quench in the transverse field Ising model”, 2022, DOI: 10.48550/ARXIV.2009.09208, arXiv:2203.04029 [cond-mat.str-el], pre-published.
- <sup>134</sup>D. Jaschke, K. Maeda, J. D. Whalen, M. L. Wall, and L. D. Carr, “Critical phenomena and Kibble-Zurek scaling in the long-range quantum Ising chain”, *New J. Phys.* **19**, 033032 (2017) DOI: 10.1088/1367-2630/aa65bc.
- <sup>135</sup>R. Puebla, O. Marty, and M. B. Plenio, “Quantum Kibble-Zurek physics in long-range transverse-field Ising models”, *Phys. Rev. A* **100**, 032115 (2019) DOI: 10.1103/PhysRevA.100.032115.

- 
- <sup>136</sup>A. Chandran, A. Erez, S. S. Gubser, and S. L. Sondhi, “Kibble-Zurek problem: Universality and the scaling limit”, *Phys. Rev. B* **86**, 064304 (2012) DOI: 10.1103/PhysRevB.86.064304.
- <sup>137</sup>D. Sadhukhan, A. Sinha, A. Francuz, J. Stefaniak, M. M. Rams, J. Dziarmaga, and W. H. Zurek, “Sonic horizons and causality in phase transition dynamics”, *Phys. Rev. B* **101**, 144429 (2020) DOI: 10.1103/PhysRevB.101.144429.
- <sup>138</sup>I.-K. Liu, S. Donadello, G. Lamporesi, G. Ferrari, S.-C. Gou, F. Dalfovo, and N. P. Proukakis, “Dynamical equilibration across a quenched phase transition in a trapped quantum gas”, *Commun. Phys.* **1**, 24 (2018) DOI: 10.1038/s42005-018-0023-6.
- <sup>139</sup>N. V. Vitanov, “Transition times in the Landau-Zener model”, *Phys. Rev. A* **59**, 988 (1999) DOI: 10.1103/PhysRevA.59.988.
- <sup>140</sup>K.-A. Suominen, “Parabolic level crossing models”, *Opt. Commun.* **93**, 126–134 (1992) DOI: 10.1016/0030-4018(92)90140-M.
- <sup>141</sup>M. Suzuki, “The dimer problem and the generalized XY-model”, *Phys. Lett. A* **34**, 338–339 (1971) DOI: 10.1016/0375-9601(71)90901-7.
- <sup>142</sup>M. Suzuki, “Relationship among Exactly Soluble Models of Critical Phenomena. I: 2D Ising Model, Dimer Problem and the Generalized XY-Model”, *Prog. Theor. Phys.* **46**, 1337–1359 (1971) DOI: 10.1143/ptp.46.1337.
- <sup>143</sup>K. G. Wilson and J. Kogut, “The renormalization group and the  $\epsilon$  expansion”, *Phys. Rep.* **12**, 75–199 (1974) DOI: 10.1016/0370-1573(74)90023-4.
- <sup>144</sup>T. J. Hollowood, “6 Lectures on QFT, RG and SUSY”, 2009, DOI: 10.48550/ARXIV.0909.0859, arXiv:0909.0859 [hep-th], pre-published.
- <sup>145</sup>M. Kolodrubetz, B. K. Clark, and D. A. Huse, “Nonequilibrium Dynamic Critical Scaling of the Quantum Ising Chain”, *Phys. Rev. Lett.* **109**, 015701 (2012) DOI: 10.1103/PhysRevLett.109.015701.
- <sup>146</sup>M. M. Wolf, F. Verstraete, M. B. Hastings, and J. I. Cirac, “Area Laws in Quantum Systems: Mutual Information and Correlations”, *Phys. Rev. Lett.* **100**, 070502 (2008) DOI: 10.1103/PhysRevLett.100.070502.
- <sup>147</sup>B. Ladewig, S. Diehl, and M. Buchhold, “Monitored open fermion dynamics: Exploring the interplay of measurement, decoherence, and free Hamiltonian evolution”, *Phys. Rev. Research* **4**, 033001 (2022) DOI: 10.1103/PhysRevResearch.4.033001.
- <sup>148</sup>L. Vidmar, L. Hackl, E. Bianchi, and M. Rigol, “Entanglement Entropy of Eigenstates of Quadratic Fermionic Hamiltonians”, *Phys. Rev. Lett.* **119**, 020601 (2017) DOI: 10.1103/PhysRevLett.119.020601.
- <sup>149</sup>L. Vidmar, L. Hackl, E. Bianchi, and M. Rigol, “Volume Law and Quantum Criticality in the Entanglement Entropy of Excited Eigenstates of the Quantum Ising Model”, *Phys. Rev. Lett.* **121**, 220602 (2018) DOI: 10.1103/PhysRevLett.121.220602.
- <sup>150</sup>A. Nahum, S. Vijay, and J. Haah, “Operator spreading in random unitary circuits”, *Phys. Rev. X* **8**, 021014 (2018) DOI: 10.1103/PhysRevX.8.021014.
- <sup>151</sup>T. Zhou and A. Nahum, “Emergent statistical mechanics of entanglement in random unitary circuits”, *Phys. Rev. B* **99**, 174205 (2019) DOI: 10.1103/PhysRevB.99.174205.

- <sup>152</sup>Y. Li, X. Chen, and M. P. A. Fisher, “Quantum Zeno effect and the many-body entanglement transition”, *Phys. Rev. B* **98**, 205136 (2018) DOI: 10.1103/PhysRevB.98.205136.
- <sup>153</sup>Y. Li, X. Chen, and M. P. A. Fisher, “Measurement-driven entanglement transition in hybrid quantum circuits”, *Phys. Rev. B* **100**, 134306 (2019) DOI: 10.1103/PhysRevB.100.134306.
- <sup>154</sup>L. Fidkowski, J. Haah, and M. B. Hastings, “How Dynamical Quantum Memories Forget”, *Quantum* **5**, 382 (2021) DOI: 10.22331/q-2021-01-17-382.
- <sup>155</sup>M. Mezard, G. Parisi, and M. Virasoro, *Spin Glass Theory and Beyond* (World Scientific, Singapore, 1987), DOI: 10.1142/0271.
- <sup>156</sup>P. Calabrese and J. Cardy, “Entanglement entropy and conformal field theory”, *J. Phys. A: Math. Theor.* **42**, 504005 (2009) DOI: 10.1088/1751-8113/42/50/504005.
- <sup>157</sup>T. Castellani and A. Cavagna, “Spin-glass theory for pedestrians”, *J. Stat. Mech.*, P05012 (2005) DOI: 10.1088/1742-5468/2005/05/P05012.
- <sup>158</sup>G. S. Bentsen, S. Sahu, and B. Swingle, “Measurement-induced purification in large- $N$  hybrid Brownian circuits”, *Phys. Rev. B* **104**, 094304 (2021) DOI: 10.1103/PhysRevB.104.094304.
- <sup>159</sup>A. Nahum, S. Roy, B. Skinner, and J. Ruhman, “Measurement and Entanglement Phase Transitions in All-To-All Quantum Circuits, on Quantum Trees, and in Landau-Ginsburg Theory”, *PRX Quantum* **2**, 010352 (2021) DOI: 10.1103/prxquantum.2.010352.
- <sup>160</sup>S.-K. Jian, C. Liu, X. Chen, B. Swingle, and P. Zhang, “Quantum error as an emergent magnetic field”, 2021, DOI: 10.48550/ARXIV.2106.09635, arXiv:2106.09635 [quant-ph], pre-published.
- <sup>161</sup>S.-K. Jian, C. Liu, X. Chen, B. Swingle, and P. Zhang, “Measurement-Induced Phase Transition in the Monitored Sachdev-Ye-Kitaev Model”, *Phys. Rev. Lett.* **127**, 140601 (2021) DOI: 10.1103/PhysRevLett.127.140601.
- <sup>162</sup>F. Barratt, U. Agrawal, S. Gopalakrishnan, D. A. Huse, R. Vasseur, and A. C. Potter, “Field theory of charge sharpening in symmetric monitored quantum circuits”, *Phys. Rev. Lett.* **129**, 120604 (2022) DOI: 10.1103/PhysRevLett.129.120604.
- <sup>163</sup>S.-K. Jian and B. Swingle, “Phase transition in von Neumann entanglement entropy from replica symmetry breaking”, 2021, DOI: 10.48550/ARXIV.2108.11973, arXiv:2108.11973 [quant-ph], pre-published.
- <sup>164</sup>A. Altland, M. Buchhold, S. Diehl, and T. Micklitz, “Dynamics of measured many-body quantum chaotic systems”, *Phys. Rev. Research* **4**, L022066 (2022) DOI: 10.1103/PhysRevResearch.4.L022066.
- <sup>165</sup>M. J. Gullans and D. A. Huse, “Scalable Probes of Measurement-Induced Criticality”, *Phys. Rev. Lett.* **125**, 070606 (2020) DOI: 10.1103/PhysRevLett.125.070606.
- <sup>166</sup>Y. Bao, S. Choi, and E. Altman, “Theory of the phase transition in random unitary circuits with measurements”, *Phys. Rev. B* **101**, 104301 (2020) DOI: 10.1103/PhysRevB.101.104301.

- 
- <sup>167</sup>M. Block, Y. Bao, S. Choi, E. Altman, and N. Y. Yao, “Measurement-Induced Transition in Long-Range Interacting Quantum Circuits”, *Phys. Rev. Lett.* **128**, 010604 (2022) DOI: 10.1103/PhysRevLett.128.010604.
- <sup>168</sup>P. Zhang, C. Liu, S.-K. Jian, and X. Chen, “Universal Entanglement Transitions of Free Fermions with Long-range Non-unitary Dynamics”, *Quantum* **6**, 723 (2022) DOI: 10.22331/q-2022-05-27-723.
- <sup>169</sup>M. Buchhold, T. Müller, and S. Diehl, “Revealing measurement-induced phase transitions by pre-selection”, 2022, DOI: 10.48550/ARXIV.2208.10506, arXiv:2208.10506 [cond-mat.dis-nn], pre-published.
- <sup>170</sup>T. Iadecola, S. Ganeshan, J. H. Pixley, and J. H. Wilson, “Dynamical entanglement transition in the probabilistic control of chaos”, 2022, DOI: 10.48550/ARXIV.2207.12415, arXiv:2207.12415 [cond-mat.dis-nn], pre-published.
- <sup>171</sup>N. O’Dea, A. Morningstar, S. Gopalakrishnan, and V. Khemani, “Entanglement and Absorbing-State Transitions in Interactive Quantum Dynamics”, 2022, DOI: 10.48550/ARXIV.2211.12526, arXiv:2211.12526 [cond-mat.stat-mech], pre-published.
- <sup>172</sup>Y. Li and M. P. A. Fisher, “Statistical mechanics of quantum error correcting codes”, *Phys. Rev. B* **103**, 104306 (2021) DOI: 10.1103/PhysRevB.103.104306.
- <sup>173</sup>Z. Weinstein, Y. Bao, and E. Altman, “Measurement-Induced Power-Law Negativity in an Open Monitored Quantum Circuit”, *Phys. Rev. Lett.* **129**, 080501 (2022) DOI: 10.1103/PhysRevLett.129.080501.
- <sup>174</sup>X. Turkeshi, L. Piroli, and M. Schiró, “Enhanced entanglement negativity in boundary-driven monitored fermionic chains”, *Phys. Rev. B* **106**, 024304 (2022) DOI: 10.1103/PhysRevB.106.024304.
- <sup>175</sup>B. C. Dias, D. Perkovic, M. Haque, P. Ribeiro, and P. A. McClarty, “Quantum Noise as a Symmetry-Breaking Field”, DOI: 10.48550/ARXIV.2208.13861, arXiv:2208.13861 [quant-ph], pre-published.
- <sup>176</sup>X. Turkeshi, A. Biella, R. Fazio, M. Dalmonte, and M. Schiró, “Measurement-induced entanglement transitions in the quantum Ising chain: From infinite to zero clicks”, *Phys. Rev. B* **103**, 224210 (2021) DOI: 10.1103/PhysRevB.103.224210.
- <sup>177</sup>X. Turkeshi, M. Dalmonte, R. Fazio, and M. Schiró, “Entanglement transitions from stochastic resetting of non-Hermitian quasiparticles”, *Phys. Rev. B* **105**, L241114 (2022) DOI: 10.1103/PhysRevB.105.L241114.
- <sup>178</sup>G. Kells, D. Meidan, and A. Romito, “Topological transitions with continuously monitored free fermions”, 2021, DOI: 10.48550/ARXIV.2112.09787, arXiv:2112.09787 [quant-ph], pre-published.
- <sup>179</sup>V. Eisler, “Crossover between ballistic and diffusive transport: the quantum exclusion process”, *J. Stat. Mech.*, P06007 (2011) DOI: 10.1088/1742-5468/2011/06/P06007.
- <sup>180</sup>M. Bauer, D. Bernard, and T. Jin, “Stochastic dissipative quantum spin chains (I): Quantum fluctuating discrete hydrodynamics”, *SciPost Phys.* **3**, 033 (2017) DOI: 10.21468/SciPostPhys.3.5.033.

- <sup>181</sup>D. Bernard and T. Jin, “Open Quantum Symmetric Simple Exclusion Process”, *Phys. Rev. Lett.* **123**, 080601 (2019) DOI: 10.1103/PhysRevLett.123.080601.
- <sup>182</sup>M. Bauer, D. Bernard, and T. Jin, “Equilibrium fluctuations in maximally noisy extended quantum systems”, *SciPost Phys.* **6**, 045 (2019) DOI: 10.21468/SciPostPhys.6.4.045.
- <sup>183</sup>D. Bernard, “Can the macroscopic fluctuation theory be quantized?”, *J. Phys. A: Math. Theor.* **54**, 433001 (2021) DOI: 10.1088/1751-8121/ac2597.
- <sup>184</sup>J. Robertson and F. H. L. Essler, “Exact solution of a quantum asymmetric exclusion process with particle creation and annihilation”, *J. Stat. Mech.*, 103102 (2021) DOI: 10.1088/1742-5468/ac22f8.
- <sup>185</sup>T. Jin, J. S. Ferreira, M. Filippone, and T. Giamarchi, “Exact description of quantum stochastic models as quantum resistors”, *Phys. Rev. Research* **4**, 013109 (2022) DOI: 10.1103/PhysRevResearch.4.013109.
- <sup>186</sup>D. Bernard, F. H. L. Essler, L. Hruza, and M. Medenjak, “Dynamics of fluctuations in quantum simple exclusion processes”, *SciPost Phys.* **12**, 042 (2022) DOI: 10.21468/SciPostPhys.12.1.042.
- <sup>187</sup>M. Knap, “Entanglement production and information scrambling in a noisy spin system”, *Phys. Rev. B* **98**, 184416 (2018) DOI: 10.1103/PhysRevB.98.184416.
- <sup>188</sup>T. Müller, S. Diehl, and M. Buchhold, “Measurement-Induced Dark State Phase Transitions in Long-Ranged Fermion Systems”, *Phys. Rev. Lett.* **128**, 010605 (2022) DOI: 10.1103/PhysRevLett.128.010605.
- <sup>189</sup>T. Minato, K. Sugimoto, T. Kuwahara, and K. Saito, “Fate of Measurement-Induced Phase Transition in Long-Range Interactions”, *Phys. Rev. Lett.* **128**, 010603 (2022) DOI: 10.1103/PhysRevLett.128.010603.
- <sup>190</sup>Y. Fuji and Y. Ashida, “Measurement-induced quantum criticality under continuous monitoring”, *Phys. Rev. B* **102**, 054302 (2020) DOI: 10.1103/PhysRevB.102.054302.
- <sup>191</sup>E. V. H. Doggen, Y. Gefen, I. V. Gornyi, A. D. Mirlin, and D. G. Polyakov, “Generalized quantum measurements with matrix product states: Entanglement phase transition and clusterization”, *Phys. Rev. Research* **4**, 023146 (2022) DOI: 10.1103/PhysRevResearch.4.023146.
- <sup>192</sup>O. Lunt and A. Pal, “Measurement-induced entanglement transitions in many-body localized systems”, *Phys. Rev. Research* **2**, 043072 (2020) DOI: 10.1103/PhysRevResearch.2.043072.
- <sup>193</sup>Y. Minoguchi, P. Rabl, and M. Buchhold, “Continuous gaussian measurements of the free boson CFT: A model for exactly solvable and detectable measurement-induced dynamics”, *SciPost Phys.* **12**, 009 (2022) DOI: 10.21468/SciPostPhys.12.1.009.
- <sup>194</sup>A. Zabalo, M. J. Gullans, J. H. Wilson, S. Gopalakrishnan, D. A. Huse, and J. H. Pixley, “Critical properties of the measurement-induced transition in random quantum circuits”, *Phys. Rev. B* **101**, 060301(R) (2020) DOI: 10.1103/PhysRevB.101.060301.

- 
- <sup>195</sup>C.-M. Jian, Y.-Z. You, R. Vasseur, and A. W. W. Ludwig, “Measurement-induced criticality in random quantum circuits”, *Phys. Rev. B* **101**, 104302 (2020) DOI: 10.1103/PhysRevB.101.104302.
- <sup>196</sup>N. Gisin and I. C. Percival, “The quantum-state diffusion model applied to open systems”, *J. Phys. A: Math. Gen.* **25**, 5677 (1992) DOI: 10.1088/0305-4470/25/21/023.
- <sup>197</sup>N. Gisin and I. C. Percival, “The quantum state diffusion picture of physical processes”, *J. Phys. A: Math. Gen.* **26**, 2245 (1993) DOI: 10.1088/0305-4470/26/9/019.
- <sup>198</sup>X. Chen, Y. Li, M. P. A. Fisher, and A. Lucas, “Emergent conformal symmetry in nonunitary random dynamics of free fermions”, *Phys. Rev. Research* **2**, 033017 (2020) DOI: 10.1103/PhysRevResearch.2.033017.
- <sup>199</sup>M. Coppola, E. Tirrito, D. Karevski, and M. Collura, “Growth of entanglement entropy under local projective measurements”, *Phys. Rev. B* **105**, 094303 (2022) DOI: 10.1103/PhysRevB.105.094303.
- <sup>200</sup>S. Diehl, A. Micheli, A. Kantian, B. Kraus, H. P. Büchler, and P. Zoller, “Quantum states and phases in driven open quantum systems with cold atoms”, *Nat. Phys.* **4**, 878–883 (2008) DOI: 10.1038/nphys1073.
- <sup>201</sup>F. Verstraete, M. M. Wolf, and J. I. Cirac, “Quantum computation and quantum-state engineering driven by dissipation”, *Nat. Phys.* **5**, 633–636 (2009) DOI: 10.1038/nphys1342.
- <sup>202</sup>J. von Delft and H. Schoeller, “Bosonization for beginners — refermionization for experts”, *Ann. Phys. (Berl.)* **510**, 225–305 (1998) DOI: 10.1002/andp.19985100401.
- <sup>203</sup>M. P. A. Fisher and L. I. Glazman, “Transport in a One-Dimensional Luttinger Liquid. NATO ASI Series, vol 345”, in *Mesoscopic Electron Transport*, edited by L. L. Sohn, L. P. Kouwenhoven, and G. Schön (Springer, Dordrecht, 1997), pp. 331–373, DOI: 10.1007/978-94-015-8839-3\_9.
- <sup>204</sup>D. Sénéchal, “An introduction to bosonization”, 1999, DOI: 10.48550/ARXIV.COND-MAT/9908262, arXiv:cond-mat/9908262 [cond-mat.str-el], pre-published.
- <sup>205</sup>T. Giamarchi, *Quantum Physics in One Dimension* (Oxford University Press, Oxford, 2003), DOI: 10.1093/acprof:oso/9780198525004.001.0001.
- <sup>206</sup>H. J. Schulz, G. Cuniberti, and P. Pieri, “Fermi Liquids and Luttinger Liquids”, in *Field Theories for Low-Dimensional Condensed Matter Systems: Spin Systems and Strongly Correlated Electrons*, edited by G. Morandi, P. Sodano, A. Tagliacozzo, and V. Tognetti, Springer Series in Solid-State Sciences, vol 131 (Springer, Berlin, Heidelberg, 2000), pp. 9–81, DOI: 10.1007/978-3-662-04273-1\_2.
- <sup>207</sup>F. H. L. Essler and M. Fagotti, “Quench dynamics and relaxation in isolated integrable quantum spin chains”, *J. Stat. Mech.*, 064002 (2016) DOI: 10.1088/1742-5468/2016/06/064002.
- <sup>208</sup>V. Alba, B. Bertini, M. Fagotti, L. Piroli, and P. Ruggiero, “Generalized-hydrodynamic approach to inhomogeneous quenches: correlations, entanglement and quantum effects”, *J. Stat. Mech.*, 114004 (2021) DOI: 10.1088/1742-5468/ac257d.

- <sup>209</sup>M. Fagotti, “Higher-order generalized hydrodynamics in one dimension: The noninteracting test”, *Phys. Rev. B* **96**, 220302(R) (2017) DOI: 10.1103/PhysRevB.96.220302.
- <sup>210</sup>H. Kim and D. A. Huse, “Ballistic Spreading of Entanglement in a Diffusive Nonintegrable System”, *Phys. Rev. Lett.* **111**, 127205 (2013) DOI: 10.1103/PhysRevLett.111.127205.
- <sup>211</sup>M. Žnidarič, “Entanglement growth in diffusive systems”, *Commun. Phys.* **3**, 100 (2020) DOI: 10.1038/s42005-020-0366-7.
- <sup>212</sup>B. C. Dias, M. Haque, P. Ribeiro, and P. McClarty, “Diffusive Operator Spreading for Random Unitary Free Fermion Circuits”, 2021, DOI: 10.48550/ARXIV.2102.09846, arXiv:2102.09846 [cond-mat.str-el], pre-published.
- <sup>213</sup>M. Žnidarič, “Exact solution for a diffusive nonequilibrium steady state of an open quantum chain”, *J. Stat. Mech.*, L05002 (2010) DOI: 10.1088/1742-5468/2010/05/L05002.
- <sup>214</sup>M. Žnidarič, “Large-deviation statistics of a diffusive quantum spin chain and the additivity principle”, *Phys. Rev. E* **89**, 042140 (2014) DOI: 10.1103/PhysRevE.89.042140.
- <sup>215</sup>M. V. Medvedyeva, F. H. L. Essler, and T. Prosen, “Exact Bethe Ansatz Spectrum of a Tight-Binding Chain with Dephasing Noise”, *Phys. Rev. Lett.* **117**, 137202 (2016) DOI: 10.1103/PhysRevLett.117.137202.
- <sup>216</sup>S. Wolff, J.-S. Bernier, D. Poletti, A. Sheikhan, and C. Kollath, “Evolution of two-time correlations in dissipative quantum spin systems: Aging and hierarchical dynamics”, *Phys. Rev. B* **100**, 165144 (2019) DOI: 10.1103/PhysRevB.100.165144.
- <sup>217</sup>P. E. Dolgirev, J. Marino, D. Sels, and E. Demler, “Non-Gaussian correlations imprinted by local dephasing in fermionic wires”, *Phys. Rev. B* **102**, 100301(R) (2020) DOI: 10.1103/PhysRevB.102.100301.
- <sup>218</sup>J.-S. Bernier, R. Tan, C. Guo, C. Kollath, and D. Poletti, “Melting of the critical behavior of a Tomonaga-Luttinger liquid under dephasing”, *Phys. Rev. B* **102**, 115156 (2020) DOI: 10.1103/PhysRevB.102.115156.
- <sup>219</sup>V. Alba and F. Carollo, “Spreading of correlations in Markovian open quantum systems”, *Phys. Rev. B* **103**, L020302 (2021) DOI: 10.1103/PhysRevB.103.L020302.
- <sup>220</sup>X. Turkeshi and M. Schiró, “Diffusion and thermalization in a boundary-driven dephasing model”, *Phys. Rev. B* **104**, 144301 (2021) DOI: 10.1103/PhysRevB.104.144301.
- <sup>221</sup>Z. Cai and T. Barthel, “Algebraic versus Exponential Decoherence in Dissipative Many-Particle Systems”, *Phys. Rev. Lett.* **111**, 150403 (2013) DOI: 10.1103/PhysRevLett.111.150403.
- <sup>222</sup>D. Poletti, J.-S. Bernier, A. Georges, and C. Kollath, “Interaction-Induced Impeding of Decoherence and Anomalous Diffusion”, *Phys. Rev. Lett.* **109**, 045302 (2012) DOI: 10.1103/PhysRevLett.109.045302.
- <sup>223</sup>D. Poletti, P. Barmettler, A. Georges, and C. Kollath, “Emergence of Glasslike Dynamics for Dissipative and Strongly Interacting Bosons”, *Phys. Rev. Lett.* **111**, 195301 (2013) DOI: 10.1103/PhysRevLett.111.195301.

- 
- <sup>224</sup>E. M. Kessler, “Generalized Schrieffer-Wolff formalism for dissipative systems”, *Phys. Rev. A* **86**, 012126 (2012) DOI: 10.1103/PhysRevA.86.012126.
- <sup>225</sup>H. Spohn, “Approach to equilibrium for completely positive dynamical semigroups of  $N$ -level systems”, *Rep. Math. Phys.* **10**, 189–194 (1976) DOI: 10.1016/0034-4877(76)90040-9.
- <sup>226</sup>H. Spohn, “An algebraic condition for the approach to equilibrium of an open  $N$ -level system”, *Lett. Math. Phys.* **2**, 33–38 (1977) DOI: 10.1007/BF00420668.
- <sup>227</sup>D. Nigro, “On the uniqueness of the steady-state solution of the Lindblad-Gorini-Kossakowski-Sudarshan equation”, *J. Stat. Mech.*, 043202 (2019) DOI: 10.1088/1742-5468/ab0c1c.
- <sup>228</sup>A. Peres, “Separability Criterion for Density Matrices”, *Phys. Rev. Lett.* **77**, 1413 (1996) DOI: 10.1103/PhysRevLett.77.1413.
- <sup>229</sup>M. Horodecki, P. Horodecki, and R. Horodecki, “Separability of mixed states: necessary and sufficient conditions”, *Phys. Lett. A* **223**, 1–8 (1996) DOI: 10.1016/S0375-9601(96)00706-2.
- <sup>230</sup>H. Shapourian, K. Shiozaki, and S. Ryu, “Partial time-reversal transformation and entanglement negativity in fermionic systems”, *Phys. Rev. B* **95**, 165101 (2017) DOI: 10.1103/PhysRevB.95.165101.
- <sup>231</sup>H. Shapourian and S. Ryu, “Entanglement negativity of fermions: Monotonicity, separability criterion, and classification of few-mode states”, *Phys. Rev. A* **99**, 022310 (2019) DOI: 10.1103/PhysRevA.99.022310.
- <sup>232</sup>H. Shapourian, P. Ruggiero, S. Ryu, and P. Calabrese, “Twisted and untwisted negativity spectrum of free fermions”, *SciPost Phys.* **7**, 037 (2019) DOI: 10.21468/SciPostPhys.7.3.037.
- <sup>233</sup>M. B. Plenio, “Logarithmic Negativity: A Full Entanglement Monotone That is not Convex”, *Phys. Rev. Lett.* **95**, 090503 (2005) DOI: 10.1103/PhysRevLett.95.090503.
- <sup>234</sup>H. Maassen and B. Kümmerer, “Purification of quantum trajectories”, *IMS Lecture Notes – Monograph Series* **48**, 252–261 (2006) DOI: 10.1214/074921706000000275.
- <sup>235</sup>S. F. Edwards and P. W. Anderson, “Theory of spin glasses”, *J. Phys. F: Met. Phys.* **5**, 965 (1975) DOI: 10.1088/0305-4608/5/5/017.
- <sup>236</sup>S. Sang and T. H. Hsieh, “Measurement-protected quantum phases”, *Phys. Rev. Research* **3**, 023200 (2021) DOI: 10.1103/PhysRevResearch.3.023200.
- <sup>237</sup>J. Merritt and L. Fidkowski, “Entanglement transitions with free fermions”, 2022, DOI: 10.48550/ARXIV.2210.05681, arXiv:2210.05681 [cond-mat.str-el], pre-published.
- <sup>238</sup>Y. Li, X. Chen, A. W. W. Ludwig, and M. P. A. Fisher, “Conformal invariance and quantum nonlocality in critical hybrid circuits”, *Phys. Rev. B* **104**, 104305 (2021) DOI: 10.1103/PhysRevB.104.104305.
- <sup>239</sup>K. Jacobs, “Wave-function Monte Carlo method for simulating conditional master equations”, *Phys. Rev. A* **81**, 042106 (2010) DOI: 10.1103/PhysRevA.81.042106.

- <sup>240</sup>S. Sang, Y. Li, T. Zhou, X. Chen, T. H. Hsieh, and M. P. A. Fisher, “Entanglement Negativity at Measurement-Induced Criticality”, *PRX Quantum* **2**, 030313 (2021) DOI: 10.1103/prxquantum.2.030313.
- <sup>241</sup>S. Sharma, X. Turkeshi, R. Fazio, and M. Dalmonte, “Measurement-induced criticality in extended and long-range unitary circuits”, *SciPost Phys. Core* **5**, 023 (2022) DOI: 10.21468/SciPostPhysCore.5.2.023.
- <sup>242</sup>J. B. Kogut, “An introduction to lattice gauge theory and spin systems”, *Rev. Mod. Phys.* **51**, 659 (1979) DOI: 10.1103/RevModPhys.51.659.
- <sup>243</sup>M. Buchhold and S. Diehl, “Nonequilibrium universality in the heating dynamics of interacting Luttinger liquids”, *Phys. Rev. A* **92**, 013603 (2015) DOI: 10.1103/PhysRevA.92.013603.
- <sup>244</sup>P. Fendley, H. Saleur, and A. B. Zamolodchikov, “Massless Flows I: The Sine-Gordon and O(n) Models”, *Int. J. Mod. Phys. A* **08**, 5717–5750 (1993) DOI: 10.1142/S0217751X93002265.
- <sup>245</sup>A. J. Daley, “Quantum trajectories and open many-body quantum systems”, *Adv. Phys.* **63**, 77–149 (2014) DOI: 10.1080/00018732.2014.933502.
- <sup>246</sup>A. Nahum, J. Ruhman, S. Vijay, and J. Haah, “Quantum Entanglement Growth under Random Unitary Dynamics”, *Phys. Rev. X* **7**, 031016 (2017) DOI: 10.1103/PhysRevX.7.031016.
- <sup>247</sup>E. V. H. Doggen, Y. Gefen, I. V. Gornyi, A. D. Mirlin, and D. G. Polyakov, “Generalized quantum measurements with matrix product states: Entanglement phase transition and clusterization”, *Phys. Rev. Research* **4**, 023146 (2022) DOI: 10.1103/PhysRevResearch.4.023146.
- <sup>248</sup>S. Wolff, A. Sheikhan, and C. Kollath, “Numerical evaluation of two-time correlation functions in open quantum systems with matrix product state methods: a comparison”, *SciPost Phys. Core* **3**, 010 (2020) DOI: 10.21468/scipostphyscore.3.2.010.
- <sup>249</sup>J. P. Garrahan and I. Lesanovsky, “Thermodynamics of Quantum Jump Trajectories”, *Phys. Rev. Lett.* **104**, 160601 (2010) DOI: 10.1103/PhysRevLett.104.160601.
- <sup>250</sup>C. Ates, B. Olmos, J. P. Garrahan, and I. Lesanovsky, “Dynamical phases and intermittency of the dissipative quantum Ising model”, *Phys. Rev. A* **85**, 043620 (2012) DOI: 10.1103/PhysRevA.85.043620.
- <sup>251</sup>I. Lesanovsky, M. van Horssen, M. Guță, and J. P. Garrahan, “Characterization of Dynamical Phase Transitions in Quantum Jump Trajectories Beyond the Properties of the Stationary State”, *Phys. Rev. Lett.* **110**, 150401 (2013) DOI: 10.1103/PhysRevLett.110.150401.
- <sup>252</sup>V. Ravindranath, Y. Han, Z.-C. Yang, and X. Chen, “Entanglement Steering in Adaptive Circuits with Feedback”, 2022, DOI: 10.48550/ARXIV.2211.05162, arXiv:2211.05162 [cond-mat.stat-mech], pre-published.
- <sup>253</sup>M. Gaudin, “Une démonstration simplifiée du théorème de wick en mécanique statistique”, *Nuclear Physics* **15**, 89–91 (1960) DOI: 10.1016/0029-5582(60)90285-6.
- <sup>254</sup>P. Jordan and E. Wigner, “Über das Paulische Äquivalenzverbot”, *Z. Phys.* **47**, 631–651 (1928) DOI: 10.1007/BF01331938.

- <sup>255</sup>B. Kaufman, “Crystal Statistics. II. Partition Function Evaluated by Spinor Analysis”, *Phys. Rev.* **76**, 1232 (1949) DOI: 10.1103/PhysRev.76.1232.
- <sup>256</sup>Y. Nambu, “A Note on the Eigenvalue Problem in Crystal Statistics”, *Prog. Theor. Phys.* **5**, 1–13 (1950) DOI: 10.1143/ptp/5.1.1.
- <sup>257</sup>E. Fradkin, *Field Theories of Condensed Matter Physics*, 2nd ed. (Cambridge University Press, Cambridge, 2013), DOI: 10.1017/CB09781139015509.
- <sup>258</sup>J. H. H. Perk, “Onsager algebra and cluster XY-models in a transverse magnetic field”, 2017, DOI: 10.48550/ARXIV.1710.03384, arXiv:1710.03384 [cond-mat.stat-mech], pre-published.